Evaluation of the mechanisms of trace elements transport (Pb, Rare Earth Elements,...) and the elemental and isotopic fractionation (Ca and Sr) at the interface water-soil-plant

Sophie Lemarié Gangloff

Université de Strasbourg
Ecole et Observatoire des Sciences de la Terre
Laboratoire d'Hydrologie et de Géochimie de Strasbourg

THÈSE

Présentée par

Sophie LEMARIÉ (GANGLOFF)

Soutenue le 28 janvier 2016

Pour obtenir le grade de : **Docteur de l'Université de Strasbourg**

Discipline/Spécialité : Géochimie - Chimie de l'environnement

Evaluation des mécanismes de transport des éléments traces (Pb, REE, …) et du fractionnement des rapports élémentaires et isotopiques (Ca et Sr) à l'interface eau, sol, plante.

THÈSE dirigée par :

M. STILLE Peter	Directeur de recherche CNRS, UMR 7517
M. CHABAUX François	Professeur, Université de Strasbourg

RAPPORTEURS :

Mme DERENNE Sylvie	Directeur de recherche, CNRS UMR 7619
M. GRUAU Gérard	Directeur de recherche, CNRS UMR 6118

EXAMINATEURS :

M. BRUAND Ary	Professeur, Université d'Orléans
M. BERNASCONI Stefano	Professeur, ETH, Zürich, SUISSE
M. IMFELD Gwenaël	Chargé de Recherche CNRS, UMR7517

A Yves et Romain,

A mes parents

A Delphine, Diane et Claire

REMERCIEMENTS

Je souhaite remercier toutes les personnes qui m'ont apporté leur aide et qui ont contribué à la réussite de cette thèse.

Tout d'abord, je tiens à remercier mes deux directeurs de thèse, Peter Stille et François Chabaux, pour m'avoir fait confiance et m'avoir donné l'opportunité de mener à bien ce travail de recherche. Je les remercie aussi pour leur disponibilité et l'aide qu'ils m'ont apporté lors de la rédaction des différents articles. Je remercie également Anne-Désirée Schmitt pour son soutien et toute l'aide qu'elle m'a apportée durant ce travail de thèse.

Mes remerciements s'adressent également à Mme Sylvie Derenne, Mr Gérard Gruau, Mr Ary Bruand, Mr Stefano Bernasconi et Mr Gwenaël Imfeld qui ont accepté de juger mon travail de thèse.

Je remercie Marie-Claire Pierret, responsable de l'Observatoire d'Hydrogéochimie de l'Environnement, ainsi que Sylvain Benarioumlil de m'avoir aidé, dès que cela était nécessaire, pour accéder au site du Strengbach.

Je tiens également à remercier tous mes collègues de l'équipe GICE (Géochimie isotopique et chimie de l'environnement), tout particulièrement Colin Fourtet, ainsi que tous ceux du LHYGES qui m'ont aidé et soutenu tout au long de cette aventure. Je remercie aussi tous les doctorants que j'ai rencontré au Laboratoire (ils sont très nombreux!), je les remercie tous pour la bonne humeur qu'ils apportent à la vie quotidienne du LHYGES. Encore merci.

Pour finir, je remercie toute ma famille de croire en moi et de m'avoir appris à toujours aller au bout de mes projets. Un très grand merci à Yves et Romain de m'avoir soutenu et surtout encouragé à faire cette thèse. Merci d'avoir été présents tous les jours.

Table des matières

Introduction Générale

Introduction Générale

Les forêts recouvrent près d'un tiers de la superficie terrestre, dont près de 80% se retrouvent en milieu boréal et tropical et environ 10% en milieu tempéré. Elles constituent un enjeu économique et écologique pour la planète. En effet, les arbres agissent comme un puits de CO_2 au cours de leur croissance, ils contribuent ainsi à diminuer l'effet de serre et jouent un rôle sur l'évolution du climat. Il est donc important d'avoir une bonne gestion des écosystèmes forestiers. Pour cela, il est nécessaire de les étudier et plus particulièrement les différents compartiments qui les composent (sol, eau, végétation, atmosphère) ainsi que les différents processus qui influencent leur fonctionnement (altération des minéraux, prélèvement des nutriments par la végétation, impacts des dépôts atmosphériques…).

Les études des écosystèmes forestiers sont possibles par l'intermédiaire de sites expérimentaux à grande échelle comme les bassins versants forestiers. En 1986, le bassin versant du Strengbach (situé dans le Nord-Est de la France) a été mis en place pour suivre l'impact des pluies acides sur le dépérissement forestier dû à un sol carencé en nutriment comme le calcium et le magnésium. Cette carence résulte d'une part d'un sol pauvre en nutriments et d'autre part à son altération par les pluies acides.

Ce site est instrumentalisé pour collecter et suivre des données hydrologiques, météorologiques et géochimiques. Ceci a permis de réaliser de nombreuses études sur les différents compartiments de cet écosystème forestier en milieu tempéré ainsi que de suivre son évolution sur le long terme (trente ans d'existence). Ces études concernent les processus d'altération soumis aux dépôts atmosphériques acides (El Gh'Mari A., 1995, Fichter J., 1997, Aubert D., 2001, Stille et al 2009), la contribution de la matière organique dans les eaux de surface et dans les solutions de sol (Fillion-Guiges N., 1998), les cycles biogéochimiques des nutriments comme le calcium (Schmitt AD 2003, Cenki-Tok et al., 2009) ou le Bore (Cividini D., 2009, 2010), l'étude du fonctionnement de l'écosystème du bassin versant du Strengbach (Prunier J., 2008) ainsi que des études hydrologiques (Viville et al 2010).

Toutes ces études ont répondu à de nombreuses questions scientifiques mais elles en ont engendré de nouvelles. Une d'entre elles se rapporte à la composition de la fraction colloïdale des solutions de sol ainsi que son impact sur le transport des éléments majeurs et traces dans le sol. En effet, l'étude de Cenki-Tok et al. (2009) a mis en évidence la nécessité d'une phase supplémentaire, comme les colloïdes, transportant le calcium pour équilibrer le bilan de masse en calcium. De plus, Stille et al (2009) a également mentionné l'importance d'une phase colloïdale dans le transport des terres rares dans le sol ainsi que son rôle dans le changement du spectre des terres rares en profondeur.

C'est dans ce contexte scientifique que s'inscrit ma thèse qui a débuté en 2010. Pour apporter des éléments de réponse sur l'importance de la fraction colloïdale dans le processus de transport des éléments majeurs et traces dans les solutions de sol, un profil de sol ainsi que les solutions de sol qui lui correspondent ont été échantillonnées. Ils ont été prélevés sur la parcelle expérimentale recouverte d'épicéas VP2, à différentes profondeurs (entre 5 et 60 cm) et saisons (entre 2009 et 2013). Ceci a permis d'avoir des renseignements sur le système dans sa globalité, ainsi que sur son évolution spatiale et temporelle. Afin d'isoler la fraction colloïdale, des expérimentations d'ultrafiltrations ont été réalisées pour ensuite les caractériser chimiquement et isotopiquement.

Cette thèse s'articule autour de 6 chapitres. Le premier présente le site du bassin versant, les échantillons prélevés ainsi que leur préparation et les analyses physico-chimiques et isotopiques effectuées. Le second chapitre présente la caractérisation et l'évolution du carbone organique le long du profile de sol, ainsi que son impact sur la mobilité des éléments majeurs et traces. Il est rédigé sous forme d'article et a été publié à Geochimica et Cosmochimica Acta. Le troisième chapitre décrit les facteurs biotiques et abiotiques qui contrôlent les compositions des fractions colloïdales et dissoutes des solutions de sol. Ce chapitre est rédigé sous forme d'article et a été soumis à Geochimica et Cosmochimica Acta. Le chapitre quatre concerne le comportement des Terres Rares à l'interface sol - solution de sol

pendant le phénomène d'altération ainsi que leur rôle potentiel en tant que traceur pour ce processus. Le chapitre cinq met en évidence les processus de fractionnement isotopique en calcium $\delta^{44/40}Ca$ dans les solutions de sol très influencé par le prélèvement racinaire et la teneur en calcium disponible dans le sol. Ces deux derniers chapitres sont rédigés sous forme d'article en préparation. Le chapitre 6 met en évidence le potentiel du couplage des isotopes de calcium et de strontium pour identifier l'activité des bactéries.

Chapitre 1

Matériels et Méthodes

1. Site d'étude: Le Bassin versant du Strengbach

Le Bassin Versant du Strengbach est un bassin versant forestier de 80 ha situé dans la massif Vosgien au Nord - Est de la France sur la commune de Aubure à une altitude comprise entre 883 m et 1146 m (Figure 1). Ce bassin versant est orienté Est - Ouest et est caractérisé par des pentes plus ou moins fortes en fonction des versants. Ce bassin a été équipé à partir de 1986. En 2007, il a été labellisé en tant qu'Observatoire National par la CNRS sous le nom d'Observatoire Hydro-Géochimique de l'Environnement (OHGE, http://ohge.unistra.fr). Un suivi des paramètres climatologiques, hydrologiques et géochimiques est effectué de façon régulière et continue.

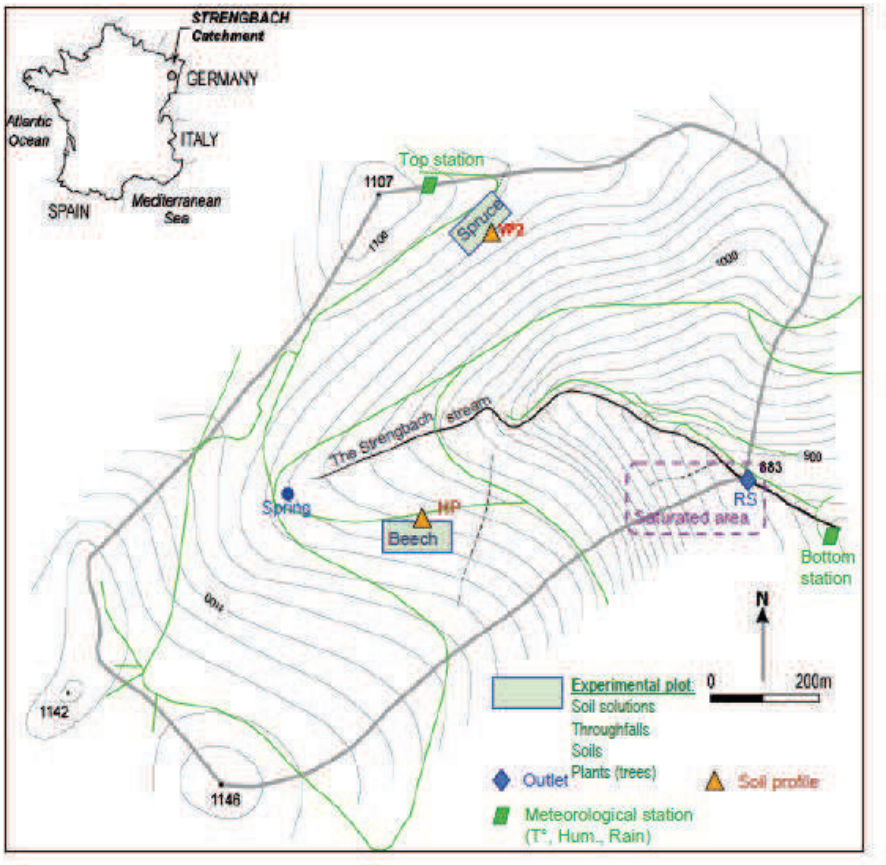

Figure 1: Carte du bassin versant du Strengbach avec les deux parcelles expérimentales (VP: Vieux peuplement sous conifères et HP: la hêtraie)

Le climat est de type océanique-montagnard. La précipitation annuelle est d'environ 1400 mm, 25% sont apportés par de la neige du mois de décembre au mois d'avril. Il y a 20% de précipitation en moins sur le versant sud que sur le versant nord. La température moyenne annuelle est de 6 °C.

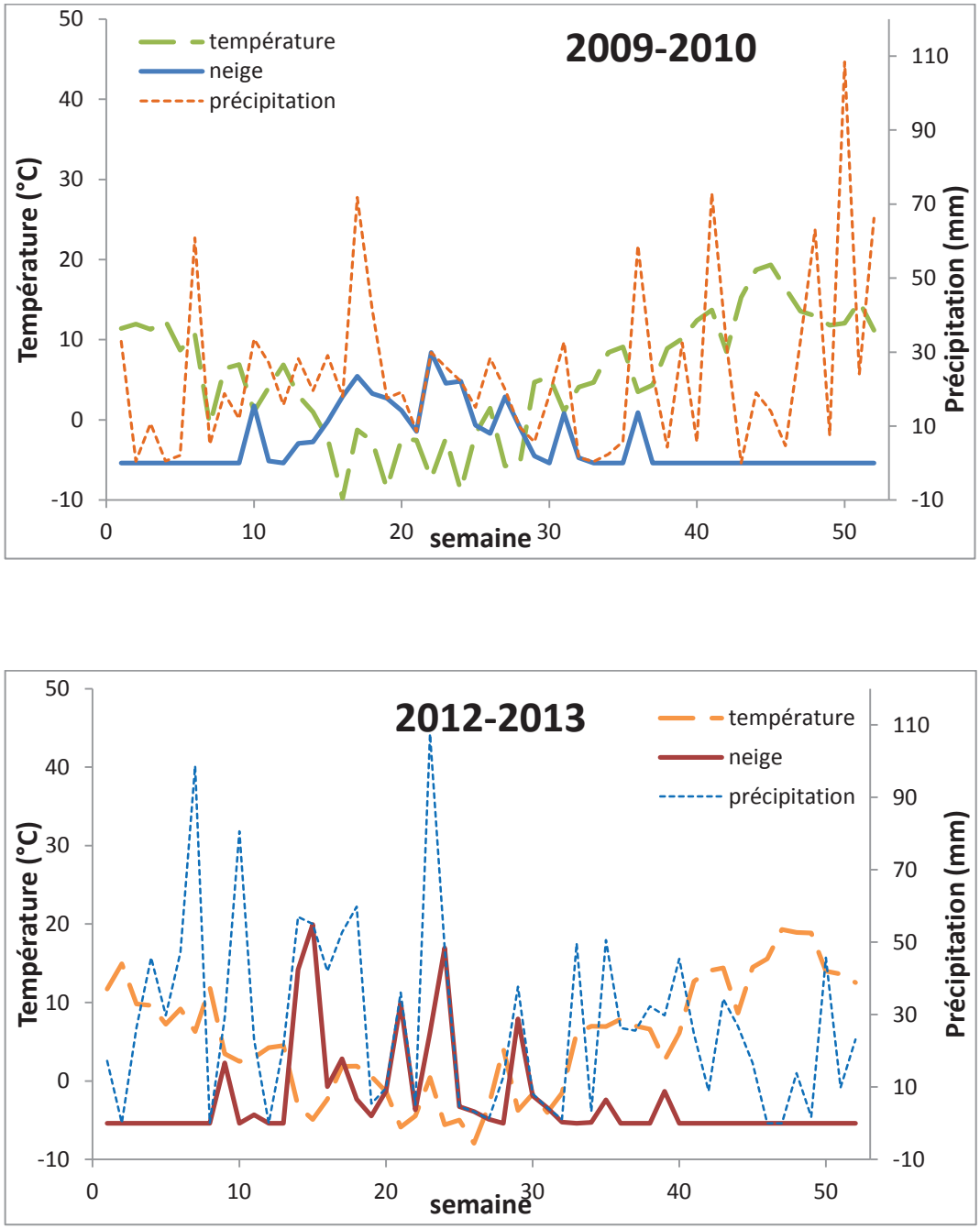

Figure 2: Conditions météorologiques durant les périodes d'échantillonnage

La forêt du bassin versant est dominée à 80% par des conifères et les 20% restant correspondent à des hêtres. Des symptômes de dépérissement forestier ont été observés vers 1980, essentiellement dû à la carence en calcium et en magnésium dans le sol, phénomène observé encore aujourd'hui. Le bassin versant possède deux parcelles expérimentales équipées avec des plaques lysimétriques, des gouttières pour collectées les pluviolessivats, des profils de sol... Une est située sur le versant sud sous couvert de hêtres (HP) et la seconde sur le versant nord sous couvert de conifères (VP) (Figure 1). Tous les échantillons étudiés dans cette thèse proviennent de la parcelle VP sous conifères.

Le sol situé à la parcelle VP est un sol brun acide dont le pH est compris entre 3.7 et 5. L'acidification du sol est dû d'une part à une acidification naturelle par le processus de podzolisation et d'autre part aux dépôts atmosphériques acides. Cette forte acidité accélère l'altération du sol et diminue son pouvoir tampon.

2. Echantillonnage

2.1. **Sol**

Le profil de sol VP2 étudié dans cette thèse a été échantillonné de la surface jusqu'à 1 m de profondeur. Il a été prélevé en Novembre 2010. L'horizon O (humus), dont l'épaisseur est comprise entre 1 et 3 cm, est principalement constitué d'aiguilles de pin plus ou moins décomposées. L'horizon A (10 à 15 cm d'épaisseur) est brun foncé, contient des racines et la teneur en matière organique (MO) est d'environ 100 $g.kg^{-1}$. Sa capacité d'échange cationique (CEC) est comprise entre 20 et 30 $cmol.kg^{-1}$. L'horizon B (50 cm d'épaisseur) est brun rougeâtre avec une densité racinaire plus faible que l'horizon A, la teneur en MO diminue à 10 $g.kg^{-1}$ ainsi que la CEC à 13 $cmol.kg^{-1}$. L'horizon BC (40 cm d'épaisseur) est grisâtre à brun rougeâtre contenant très peu de racines et renfermant des morceaux de granite avec des veines de quartz et d'hématite. La teneur en MO n'est plus que de 3 % et la CEC de l'ordre de 10 $cmol.kg^{-1}$.

La minéralogie de ce sol est constituée d'environ 40 % de quartz, 30 % de feldspath potassique, 10 % de plagioclase, 20% d'argile + micas et 0,5 % d'apatite (Prunier et al., 2015).

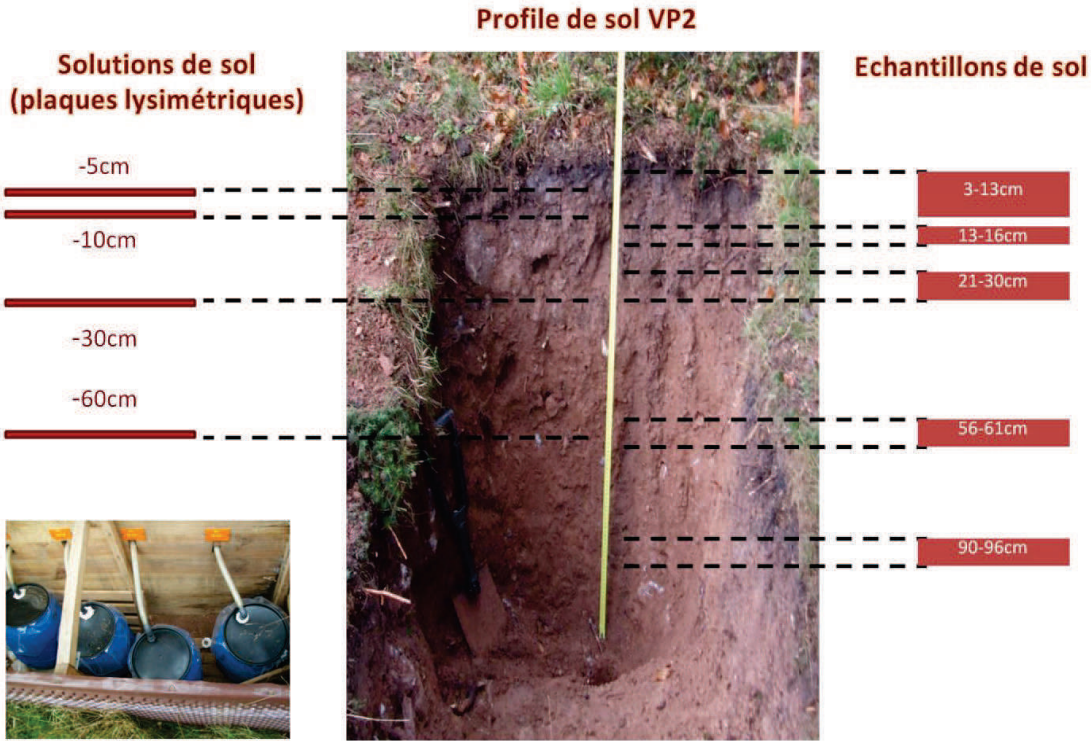

Figure 3: Echantillonnage du profil de sol VP2 et des solutions de sol à 5, 10, 30 et 60 cm de profondeur

2.2. **Solutions de sol**

Seize solutions de sol ont été collectées par l'intermédiaire de plaques lysimétriques sans tension à 5, 10, 30 et 60 cm de profondeur entre le 9 septembre 2009 et le 9 septembre 2010; et 10 entre le 25 septembre 2012 et le 6 août 2013 (Tableau 1).

Période échantillonnage	5cm	10cm	30cm	60cm	0,2µm	UF
09/09/2009 au 12/11/2009	x	x	x	x	x	x
12/11/2009 au 19/03/2010	x	x	x	x	x	x
19/03/2010 au 21/06/2010	x	x	x	x	x	x
21/06/2010 au 08/09/2010	x	x	x	x	x	
25/09/2012 au 20/11/2012	x	x	x	x	x	x
20/11/2012 au 26/03/2013	x			x	x	
22/05/2013 au 06/08/2013	x	x	x	x	x	x

Tableau 1: Périodes d'échantillonnage des solutions de sol (UF : ultra-filtrées)

3. Préparation des échantillons

3.1. **Le profil de sol VP2**

Des expérimentations d'extraction à l'eau ultra-pure (UHP) ont été effectuées sur des échantillons du profile de sol VP2 aux profondeurs 3-13 cm, 13-16 cm, 23-30 cm, 56-60 cm et 90-96 cm. Environ 30 g de chaque échantillon de sol ont été utilisés pour déterminer la teneur en humidité (105° C pendant 48 heures) ; le reste (environ 300 g) a été congelé. La matière organique extractible à l'eau (WEOM) a été obtenue en utilisant une méthode d'extraction avec de l'eau (Kalbitz et al., 2003; Said-Pullicino et al., 2007). Les expérimentations ont été réalisées avec de l'eau UHP pour identifier la MO hydrosoluble et les éléments majeurs et traces qui peuvent être transportés par cette MO hydrosoluble dans les couches supérieures du sol.

À la veille de l'extraction de la MO, le sol a été décongelé au réfrigérateur et tamisé à travers un tamis de 2 mm. Il a été ensuite introduit dans des tubes à centrifuger en polypropylène de 50 ml et mélangé avec de l'eau UHP dans la proportion 1/1,5 (eau/sol sec). Chaque échantillon a été agité pendant 2 heures et ultra-centrifugé à 8000 tr/min pendant 30 minutes à une température de 10° C. Un blanc expérimental a été fait en même temps avec seulement de l'eau UHP dans un tube. Le surnageant est filtré à 0,45 µm avec un filtre en acétate de cellulose. 10 ml du filtrat ont été

immédiatement congelés pour ensuite être lyophylisés pour réaliser un spectre par spectroscopie infrarouge; les 90 ml restant ont été utilisés pour l'analyse chimique (éléments majeurs et traces, titrage, aromaticité) réalisée au "Laboratoire d'Hydrologie et de Géochimie de Strasbourg » (LHyGeS, CNRS, Strasbourg).

Echantillons correspondant aux extractions des échantillons de sol

3.2. **Les solutions de sol**

3.2.1. Procédures de filtrations et ultra-filtrations

Chaque solution de sol a été filtrée à 0,2 µm par des filtres Omnipore® (PTFE hydrophile) (Merck Millipore©). Ensuite, une partie de ces échantillons a été ultra-filtrée (UF) par flux de filtration tangentiel (TFF) par un appareil Labscale TFF de Millipore© dont le protocole est décrit de façon schématique par la figure 4. Les cassettes PelliconXL® (cellulose régénérée) sont directement reliées au réservoir du système. La partie de l'échantillon qui passe au travers de la membrane contient les composés plus petits que le seuil de coupure de la membrane, ils sont collectés dans des bouteilles en polypropylène et correspondent au perméat (P). La partie de l'échantillon qui reste dans le réservoir renferme principalement les composés plus grands que le seuil de coupure de la membrane et correspond au rétentat (R).

Entre chaque ultra-filtration, chaque membrane est nettoyée selon la procédure: 1 litre d'eau UHP (18,2 MΩ.cm), 500 ml de soude à 0,1 M (pour retirer la matière organique), 1 litre d'eau UHP, 500 ml d'un mélange HCl/HNO_3 à 0,1 M (pour retirer les métaux), 1 litre d'eau UHP.

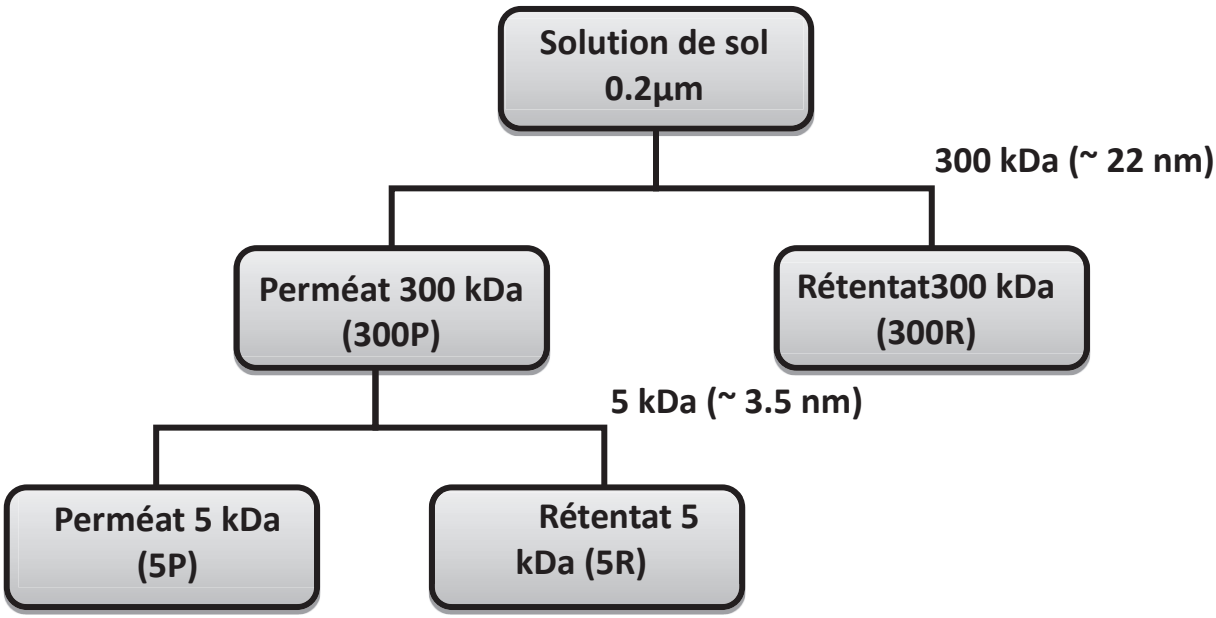

Figure 4: Protocole de filtration et d'ultra-filtration des solutions de sol

Les solutions de sol filtrées à 0,2 µm sont ultra-filtrées à 300 kDa afin d'obtenir le rétentat (300R) correspondant à la fraction colloïdale comprise entre 300 kDa et 0,2 µm (fraction gros colloïde) et le perméat (300P) correspondant à la fraction inférieure à 300 kDa. Ensuite, la fraction 300P est ultra-filtrée à 5 kDa pour obtenir le rétentat (5R) correspondant à la fraction colloïdale comprise entre 5 kDa et 300 kDa (fraction petit colloïde) et le perméat (5P) correspondant à la fraction dissoute dans notre étude (Figure 4). Par manque de volume, deux échantillons prélevés à 60 cm de profondeur ont été ultra-filtrés seulement à 5 kDa.

3.2.2. Paramètres d'ultra-filtrations

Selon Francioso et al. (1996), Ingri et al. (2000), Dahlqvist et al. (2004), Liu and Lead (2006), Schlosser and Croot (2008), Dammshäuser and Croot (2012) and Liu et al. (2013), différents paramètres dus à la procédure d'ultra-filtration tangentielle doivent être considérés pour déterminer

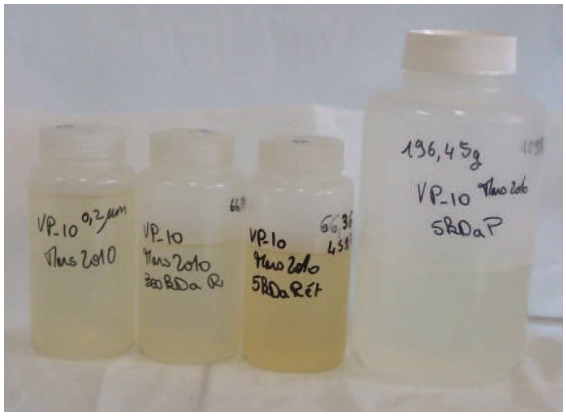

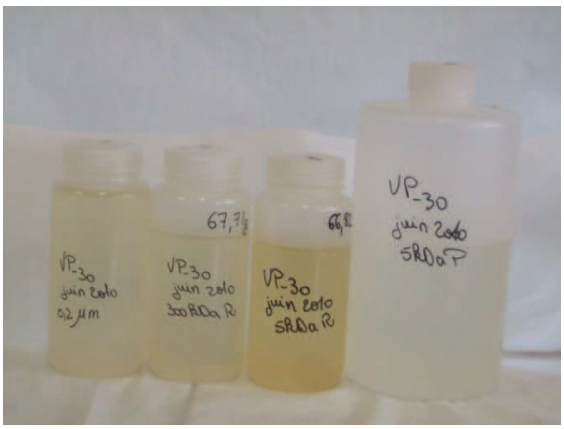

Echantillons correspondant à des solutions de sol ultra-filtrées

correctement les concentrations de chaque fraction ultra-filtrée. Un des paramètres importants est le facteur de concentration volumique du rétentat (VCF_r). Il est déterminé comme suit:

$$VCF_r=(volume\ initial)/(\ volume\ du\ rétentat) \quad (1)$$

Dans cette étude, $VCF_{r(300kDa)}$ est égal à 5.0 ± 0.4 (N=20) et $VCF_{r(5kDa)}$ est égal à 3.6 ± 0.3 (N=20). C'est important d'avoir des valeurs de VCF_r similaires pour chaque seuil de coupure pour pouvoir ensuite comparer les différents échantillons. Les valeurs des concentrations discutées dans les différents chapitres correspondent aux concentrations entre les deux seuils de coupure et sont calculées par:

$$Ci = \frac{(Ci_{rétentat} - Ci_{perméat})}{VCF_{r_i}} \quad (2)$$

où Ci = concentration de l'élément i, VCF_{ri} = facteur de concentration volumique de l'élément i dans le rétentat.

Pour chaque ultra-filtration, il est important de calculer le rendement pour chaque élément pour vérifier qu'il n'y ait pas de phénomène d'adsorption ou de contamination. Le rendement pour chaque composé i correspond à:

$$Rendement\ i = \frac{Quantité\ de\ i\ dans\ le\ rétentat + Quantité\ de\ i\ dans\ le\ perméat}{Quantité\ initiale\ de\ i\ dans\ l'échantillon} \quad (3)$$

Les rendements varient essentiellement entre 99% et 95%.

4. Analyses physicochimiques et isotopiques

4.1. **Le profil de sol**

L'analyse chimique des sols a été faite par le SARM (Service d'Analyse des Roches et des Minéraux de Nancy - France). Les éléments majeurs ont été déterminés par ICP/AES et les éléments traces par ICP/MS. Le carbone organique par un analyseur de carbone utilisant la combustion. La CEC des

sols a été déterminée par l'INRA (Laboratoire des sols d'Arras) en utilisant la méthode de Metson (extraction à l'acétate d'ammonium).

4.2. **Les spectres Infra-rouge des lyophilisats**

Les échantillons lyophylisés ont été mélangés et pressés avec du KBr pour former des pastilles (1mg et 300mg de KBr) et ensuite être analysés par spectroscopie Infra-rouge. Les spectres ont été enregistrés par un spectromètre IR à transformée de Fourier (FTIR) (Brucker-5DXC) à une fréquence comprise entre 4 000 et 450 cm^{-1} avec un intervalle d'acquisition de 1cm^{-1} et une accumulation de 100 scans. Seulement trois échantillons lyophilisés (3-13 cm, 13-16 cm et 23-30 cm) ont donné des signaux suffisants pour fournir des spectres infrarouges. Les deux autres échantillons avaient un signal de bruit de fond trop important pour permettre la détermination des fréquences infrarouges.

4.3. **Les solutions de sol et extraits aqueux**

Le pH est mesuré avec une électrode combinée calibrée par des standards NIST (pH 4.00 et 7.00). Les concentrations des anions (Cl^-, NO_3^-, SO_4^{2-} and PO_4^{3-}) et des cations (Na^+, NH_4^+, K^+, Mg^{2+} and Ca^{2+}) sont déterminés simultanément par chromatographie ionique (DIONEX ICS-3000 - Thermo Fisher Scientific©) (incertitudes< 2 %). Les anions sont analysés par une pré-colonne et colonne AG18-AS18 (Dionex) avec comme éluant de la soude (34 $mmol.L^{-1}$) en mode isocratique à 1$ml.min^{-1}$. Les cations sont analysés par une pré-colonne et colonne CG16-CS16 (Dionex) avec comme éluant de l'acide méthane sulfonique (27 $mmol.L^{-1}$) en mode isocratique à 1$ml.min^{-1}$. Le carbone organique est mesuré par une méthode thermique avec une incertitude de 2% et une limite de détection de 0,3 mg $C.L^{-1}$ (Shimadzu TOC VPH - Shimadzu©). Les concentrations des éléments traces sont déterminées par Inductively Coupled Plasma Atomic Emission Spectrometry (ICP/AES) (Thermo Scientific iCAP 6000 SERIES - Thermo Fisher Scientific©) et Inductively Coupled Plasma Mass Spectrometry

(ICP/MS) (Thermo-Fisher X SerieII - Thermo Fisher Scientific©) par calibration traditionnelle et en utilisant l'Indium comme standard interne. La validité et la reproductibilité des différents paramètres analysés ont été vérifiées par des standards certifiés standards SLRS5, Perade-20, Rain 97 et Big-Moose 02.

L'absorbance UV spécifique à 254 nm ($SUVA_{254}$) a été déterminée par l'absorbance UV à 254 nm normalisée par la concentration en carbone organique (Corga) en mg $C.L^{-1}$. Elle a été mesurée par un spectrophotomètre UV-Vis (SHIMADZU UV-1700). Weishaar et al. (2003) a montré qu'il y avait une relation entre le pourcentage d'aromaticité déterminé par ^{13}C-NMR et la valeur $SUVA_{254}$ (pourcentage d'aromaticité = 6,53 x $SUVA_{254}$ + 3,63).

4.4. **Séparations, purifications chimiques et mesures isotopiques**

4.4.1. Strontium ($^{87}Sr/^{86}Sr$)

La séparation et la purification du strontium (Sr) contenu dans les échantillons ont été menées au LHyGeS suivant une procédure mise au point par (Deniel and Pin, 2001). Ces étapes sont effectuées par chromatographie solide liquide en utilisant une résine échangeuse d'ions Sr-Spec Eichrom©, 50-100 mesh.

La mesure du rapport isotopique $^{87}Sr/^{86}Sr$ des solutions de sol filtrées à 0,2 µm et ultra-filtrées ont été réalisées sur un TIMS Triton (Spectromètre de masse à Thermo-ionisation) (Thermo Fisher Scientific©). Environ 100 ng de Sr sont déposés sur un filament en rhénium (Re) (pureté 99,995%) préalablement dégazé avec du Ta_2O_5 comme activateur. La valeur du rapport isotopique $^{87}Sr/^{86}Sr$ est évaluée par la moyenne statistique de 100 rapports mesurés. La validité et la reproductibilité des mesures sont vérifiées par le standard certifié NBS 987 à chaque séquence analytique ($^{87}Sr/^{86}Sr$ = 0.710250 ± 6 ; 2SD, N=10).

4.4.2. Calcium ($\delta^{44/40}Ca$)

La séparation chimique et la mesure isotopiques du Ca ont été réalisées au LHyGeS. Afin d'éviter tout fractionnement isotopique au cours

de la séparation chimique ou de la mesure, 1µg de double spike $^{42}Ca/^{43}Ca$ est ajouté à une quantité d'échantillon contenant 5 µg de Ca avant d'effectuer la séparation, la purification en Ca et la mesure isotopique. Cette séparation est faite par une chromatographie ionique ICS-3000 (Dionex©) équipée d'un collecteur de fraction. La colonne utilisée est une colonne de type CS16 (Dionex©). Ce protocole expérimental est détaillé dans Schmitt et al. (2009). Une fois purifié, l'échantillon est évaporé à sec et le résidu est dissous dans 1µl d'HNO_3 0,25N pour être déposé sur un filament en Ta (pureté 99,995%) préalablement dégazé et oxydé. La composition isotopique en Ca est mesurée par un TIMS Triton (Thermo Fisher Scientific©) en mode multi-collection dynamique (Schmitt et al., 2009). Entre 150 et 200 cycles de mesures sont collectés. Les valeurs $\delta^{44/40}Ca$ sont corrigées du fractionnement instrumental hors ligne par l'intermédiaire du logiciel Matlab©. Les valeurs isotopiques en Ca sont exprimées en ‰ avec une valeur relative au standard NIST SRM 915a selon l'expression:

$$\delta^{44/40}Ca = (((^{44}Ca/^{40}Ca)_{échantillon}/(^{44}Ca/^{40}Ca)_{SRM\ 915a})-1)*1000$$

La différence de compositions isotopiques en Ca entre deux réservoirs est symbolisé par △ et est définie par:

$\triangle i\text{-}j = \delta^{44/40}Ca_i - \delta^{44/40}Ca_j$ où i et j sont les deux réservoirs à comparer.

Le facteur de fractionnement alpha (α) est défini par la proportion des deux isotopes dans le composé A divisé par la proportion des mêmes isotopes dans le composé B: $\alpha_{A\text{-}B} = R_A/R_B$

La justesse et la reproductibilité des mesures isotopiques sont vérifiées à chaque série analytique par des solutions de référence (Eau de mer : 1,80 ± 0,11 ‰ (2SD, N = 20); CaF2 : 1,45 ± 0,12 ‰ (2SD, N=10)).

4.4.3. Carbone organique ($\delta^{13}C_{orga}$)

Les mesures de $\delta^{13}C_{orga}$ de certains échantillons filtrés et ultra-filtrés ont été faites selon le protocole de Lang et al. (2012) à l'Institut de Géologie de l'ETH à Zürich (Suisse). Tout d'abord, les échantillons sont acidifiés par

de l'acide ortho-phosphorique et le carbone inorganique est éliminé par bullage avec de l'hélium. Ensuite, le C_{orga} est oxydé à chaud. La composition isotopique du CO_2 formé et dégagé est mesurée par un couplage d'équipements composé d'un système d'introduction en ligne GasBench II (Thermo Fisher Scientific©, Bremen, Allemagne), d'un passeur automatique CTC (CTC Analytics AG, Zwingen, Suisse) et d'un couplage de l'interface ConFlo IV avec un Delta V Plus mass spectrometer (les deux ThermoFisher Scientific©).

4.4.4. Validation du protocole d'ultrafiltration appliqué aux mesures isotopiques

Afin de vérifier que les isotopes de Ca ne sont pas fractionnés au cours de l'expérimentation d'ultra-filtration, une solution de Nitrate de Calcium ainsi qu'une eau minérale (Mont-Roucous) ont été ultra-filtrées. Ensuite, la composition isotopique en Ca de l'échantillon initial (filtré à 0,2 µm), des fractions colloïdales et dissoutes ont été mesurées suivant le même protocole que les échantillons. Nous observons que $\delta^{44/40}Ca_{SRM915a}$ = 0,85 ± 0,12 ‰ (2SD, N=3) pour les différentes fractions filtrées et ultra-filtrées de la solution de nitrate de calcium et $\delta^{44/40}Ca_{SRM915a}$ = 1,10 ± 0,12 ‰ (2SD, N=5) pour les différentes fractions de l'eau minérale Mont-Roucous. Ainsi, les signatures isotopiques obtenues sont identiques et montrent que la méthode d'ultra-filtration ne fractionne pas les isotopes de Ca. Aucune variation du rapport isotopique $^{87}Sr/^{86}Sr$ n'a été observée entre les fractions ultra-filtrées et l'échantillon initial (Cf. paragraphe résultats), en accord avec les travaux antérieurs de Sivry et al. (2006) portant sur des eaux de source du Mengong et des eaux de la rivière Nyong . Ceci est également une preuve en faveur de l'absence de fractionnement des isotopes du Sr lors de l'expérimentation d'ultrafiltration.

5. Références

Dahlqvist R., Benedetti M.F., Andersson K., Turner D., Larsson T., Stolpe B. and Ingri J., (2004). Association of calcium with colloidal particles and speciation of calcium in the Kalix and Amazon rivers. *Geochimica et Cosmochimica Acta*, **68** 4059-4075.

Dammshäuser A. and Croot P.L., (2012). Low colloidal associations of aluminium and titanium in surface waters of the tropical Atlantic. *Geochimica et Cosmochimica Acta*, **96** 304-318.

Deniel C. and Pin C., (2001). Single-stage method for the simultaneous isolation of lead and strontium from silicate samples for isotopic measurements. *Analytica Chimica Acta*, **426** 95-103.

Francioso O., Sanchez-Cortes S., Tugnoli V., Ciavatta C., Sitti L. and Gessa C., (1996). Infrared, Raman, and Nuclear Magnetic Resonance (1H, 13C, and 31P) Spectroscopy in the Study of Fractions of Peat Humic Acids. *Appl. Spectrosc.*, **50** 1165-1174.

Ingri J., Widerlund A., Land M., Gustafsson Ö., Andersson P. and Öhlander B., (2000). Temporal variations in the fractionation of the rare earth elements in a boreal river; the role of colloidal particles. *Chemical Geology*, **166** 23-45.

Kalbitz K., Schmerwitz J., Schwesig D. and Matzner E., (2003). Biodegradation of soil-derived dissolved organic matter as related to its properties. *Geoderma*, **113** 273-291.

Lang S.Q., Bernasconi S. and Früh-Green G., (2012). Stable isotope analysis of organic carbon in small (µgC) samples and dissolved organic matter using a GasBench preparation device. *Rapid Communications in Mass Spectrometry*, **1** 9-16.

Liu R. and Lead J.R., (2006). Partial validation of cross flow ultrafiltration by atomic force microscopy. *Anal Chem*, **78** 8105-8112.

Liu R.X., Lead J.R. and Zhang H., (2013). Combining cross flow ultrafiltration and diffusion gradients in thin-films approaches to determine trace metal speciation in freshwaters. *Geochimica et Cosmochimica Acta*, **109** 14-26.

Prunier J., Chabaux F., Stille P., Gangloff S., Pierret M.C., Viville D. and Aubert A., (2015). Geochemical and isotopic (Sr, U) monitoring of soil solutions from the Strengbach catchment (Vosges mountains, France): Evidence for recent weathering evolution. *Chemical Geology*, **417** 289-305.

Said-Pullicino D., Erriquens F.G. and Gigliotti G., (2007). Changes in the chemical characteristics of water-extractable organic matter during composting and their influence on compost stability and maturity. *Bioresour Technol*, **98** 1822-1831.

Schlosser C. and Croot P.L., (2008). Application of cross-flow filtration for determining the solubility of iron species in open ocean seawater. *Limnology and Oceanography: Methods*, **6** 630-642.

Schmitt A.D., Gangloff S., Cobert F., Lemarchand D., Stille P. and Chabaux F., (2009). High performance automated ion chromatography separation for Ca isotope measurements in geological and biological samples. *Journal of Analytical Atomic Spectrometry*, **24** 1089-1097.

Sivry Y., Riotte J. and Dupré B., (2006). Study of exchangeable metal on colloidal humic acids and particulate matter by coupling ultrafiltration and isotopic tracers: Application to natural waters. *Journal of Geochemical Exploration*, **88** 144-147.

Weishaar J.L., Aiken G.R., Bergamaschi B.A., Fram M.S., Fujii R. and Mopper K., (2003). Evaluation of Specific Ultraviolet Absorbance as an Indicator of the Chemical Composition and Reactivity of Dissolved Organic Carbon. *Environmental Science & Technology*, **37** 4702-4708.

Chapitre 2

Characterization and evolution of dissolved organic matter in acidic forest soil and its impact on the mobility of major and trace elements (case of the Strengbach watershed)

Geochimica et Cosmochimica Acta 130 (2014) 21–41

Résumé

Le carbone organique dissous (DOC) joue un rôle important dans le comportement des éléments majeurs et traces dans le sol et influence leur transfert du sol à la solution du sol. Le premier objectif de cette étude est de caractériser les différents groupements fonctionnels organiques pour les extraits aqueux (WEOC) obtenus à partir d'un sol forestier ainsi que leur évolution avec la profondeur. Le second objectif est de préciser l'influence de ces groupements fonctionnels organiques sur la migration des éléments traces dans les fractions WEOC comparée à celle obtenue par les solutions de sol obtenues par des plaques lysimétriques. Toutes les expériences ont été réalisées sur un profil de sol forestier acide (cinq profondeurs dans le premier mètre du sol) de la parcelle expérimentale VP sous épicéas dans le bassin versant de Stengbach.

Les spectres Infra-rouge des fractions WEOC lyophilisées montrent une modification de la structure moléculaire avec la profondeur, soit une diminution des composés polaires tels que les polysaccharides et une augmentation des groupes fonctionnels hydrocarbures moins polaires avec une valeur maximale de l'aromaticité à 30 cm de profondeur. Une Classification ascendante hiérarchique (CAH) de l'évolution des éléments chimiques extractibles à l'eau (WECE) avec l'évolution des groupements fonctionnels organiques dans les compartiments du sol enrichis en matière organique (MO) permet la reconnaissance des relations entre le comportement d'éléments traces et les variations de groupements fonctionnels organiques. Plus précisément, Pb est préférentiellement lié à la fonction acide carboxylique du DOC principalement présente dans le compartiment de la couche supérieure du sol et les terres rares (TR) montrent un comportement similaire au Fe, V et Cr avec une bonne affinité pour les groupements carboxy-phénoliques et phénoliques du DOC. Les résultats expérimentaux montrent que les TR lourdes par rapport aux TR légères sont préférentiellement liées aux groupements fonctionnels aromatiques. Ce comportement différent fractionne le spectre des TR dans les solutions de sol à 30cm de profondeur en raison de l'enrichissement de

l'aromaticité du DOC à cette profondeur. Ces affinités différentes pour les groupes fonctionnels organiques du DOC expliquent certains aspects du comportement des éléments traces dans les solutions du sol et du profil de sol, mais aussi la concurrence entre les éléments traces dans la complexation avec Corga. Les résultats de cette étude sont importants pour la compréhension de la mobilité et la migration des polluants (comme les métaux lourds ou les radionucléides), mais aussi des éléments nutritifs dans les écosystèmes naturels.

Abstract

Dissolved Organic Carbon (DOC) plays an important role in the behavior of major and trace elements in the soil and influences their transfer from soil to soil solution. The first objective of this study is to characterize different organic functional groups for the Water Extracted Organic Carbon (WEOC) fractions of a forest soil as well as their evolution with depth. The second objective is to clarify the influence of these organic functional groups on the migration of the trace elements in WEOC fractions compared to those in the soil solution obtained by lysimeter plates. All experiments have been performed on an acidic forest soil profile (five depths in the first meter) of the experimental spruce parcel in the Stengbach catchment.

The Infra-red spectra of the freeze-dried WEOC fractions show a modification of the molecular structure with depth, i.e. a decrease of the polar compounds such as polysaccharides and an increase of the less polar hydro-carbon functional groups with a maximum value of the aromaticity at 30cm depth. A Hierarchical Ascending Classification (HAC) of the evolution of Water Extractable Chemical Elements (WECE) with the evolution of the organic functional groups in the Organic Matter (OM) enriched soil compartments permits recognition of relationships between trace element behavior and the organic functional group variations. More specifically, Pb is preferentially bound to the carboxylic acid function of DOC mainly present in the upper soil compartment and rare earth elements (REE) show similar behavior to Fe, V and Cr with a good affinity to carboxy-phenolic and

phenolic groups of DOC. The experimental results show that heavy REE compared to light REE are preferentially bound to the aromatic functional group. This different behavior fractionates the REE pattern of soil solutions at 30cm depth due to the here observed aromaticity enrichment of DOC. These different affinities for the organic functional groups of the DOC explain some aspects of the behavior of trace elements in soil solutions and in the soil profile but, also the competition between trace elements in complexation with DOC. The results of this study are important for the understanding of the mobility and the migration of pollutants (as heavy metals or radionucleides) as well as nutrients in natural ecosystems.

1. Introduction

Soil organic matter is a mixture of organic compounds originating from decomposition of plants and animals residues by microorganisms or acidic degradation. In the case of a forest soil, it mainly arises from the degradation of litterfall which controls the quantity of the organic matter (Berg et al., 2000). Leaching by rain, throughfall and then soil solutions allow the soluble organic matter (dissolved organic carbon; DOC) to migrate downwards in the soil (Kalbitz et al., 2000). DOC is a mix of macromolecules of high molecular weight and compounds of low molecular weight which are more mobile in aqueous systems (McCarthy et al., 1996). It consists of a wide range of more or less complex structures and functional groups, which depend on the nature of the litter, the microorganisms and environmental factors such as temperature, moisture or acidic deposition (Prescott et al, 2000; Ussiri et al., 2003; Ohno et al., 2007).

DOC represents only a small proportion of soil organic carbon (SOC) (McGill et al., 1986) but it is also the most active and labile fraction (Kalbitz et al., 2000; Corvasce et al., 2006). Nonetheless, these organic compounds influence the metal transport, the cation exchange capacity (CEC) of the soils (Osher and Buol, 1998; Römkens and Dolfing, 1998), mineral weathering and podzolization (Pohlmann and McColl, 1988; van Hees et al., 2000; Raulund-Ramussen et al., 1998).

According to Zsolnay (1996), DOC corresponds to organic matter (OM) present in soil solution and passing through a filter pore size <0.45 µm. These dissolved organic compounds are situated in different size of the soil pores and are more or less available depending on their size. DOC is mainly located in macropores, contained in gravitational water and can be collected by lysimeter plates; the water extractable organic carbon (WEOC) of soil, which can be obtained by soil shaking with aqueous solution, incorporates DOC localized in macropores and less often in micropores (Zsolnay, 2003; Chantigny, 2003).

Numerous studies characterized the organic functional groups of DOC from forest soil and their evolution with depth (Lorenz et al., 2000; Don and Kalbitz, 2005; Kaiser et al., 2002; Ussiri and Johnson, 2003; 2007) or elucidated the mobility of trace elements in natural waters in function of DOC (Pokrovsky et al, 2005; Pourret et al., 2007; Stolpe et al., 2013). Also experiments have been performed to understand the processes controlling the modification of DOC and related mobility of trace elements (Marsac et al., 2010; Lapouge and Cornard, 2010; Dangleterre and Cornard, 2005; Guan et al., 2006a). The main objective of this study is to characterize the organic functional groups for WEOC fractions of a forest soil as well as their evolution with depth and, also, to elucidate the influence of these organic functional groups on the migration of the trace elements in WEOC fractions compared to those in the soil solution obtained by lysimeter plates. This study has been performed on a soil profile of the previously studied forested Stengbach catchment (Fig1) (Tricca et al., 1999; Riotte et al., 1999; Cenki-Tok et al., 2009; Lemarchand et al, 2010; Rhis et al., 2011; Viville et al., 2012; Lemarchand 2012). The behavior of trace elements, especially of Pb and REE are discussed and compared with results of previously published complementary studies (Aubert et al., 2001; 2002; Stille et al., 2006; 2009; 2011).

2. The sampling site

The catchment covering an area of 80 ha is located in the Vosges mountains (France) at altitudes ranging from 883 m at the outlet to 1146 m at the top (Fig. 1). The bedrock of the catchment is a hydrothermally altered Hercynian leucogranite. The forest is dominated by conifers (80%) and beeches (20%). The catchment has been thoroughly investigated since 1986 and has become a completely equipped environmental observatory with permanent sampling and measuring stations (http://ohge.unistra.fr). The spruce parcel (VP) (Fig.1) is equipped with lysimeter plates situated at 5 cm, 10 cm, 30 cm and 60 cm depth which permit to collect soil solutions.

The climate is oceanic mountainous. An average of 20-25% of the precipitation is snow from December to April. Rainfall occurs over the whole year with an annual average of 1400 mm. The average annual temperature is 6 °C.

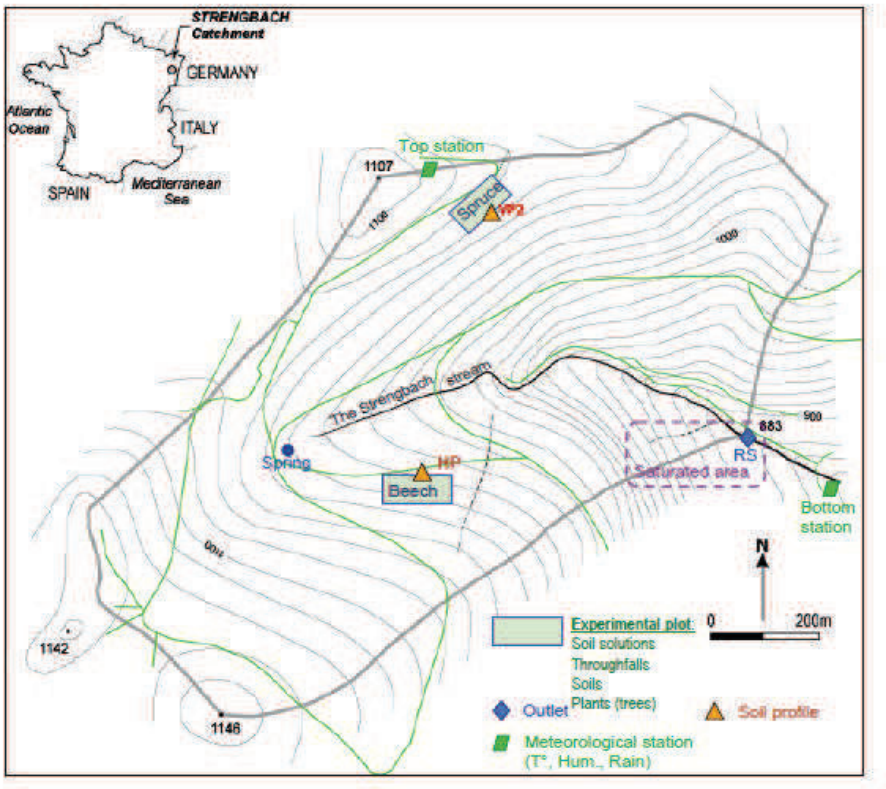

Figure 1: Strengbach catchment with sampling sites.

The investigated VP soil of the spruce parcel at the northern slope is acidic (acid distrochrept type). The pH range is between 3.7 and 5. The acidification of the soil is linked to natural acidification (podzolization process), and to the introduction of acidic atmospheric depositions. The acidity causes the decrease of the buffering capacity of the soil and accelerates weathering.

The O horizon (humus) mainly consists of spruce needles more or less decomposed with a thickness ranging between 1 and 3 cm. The 10-15 cm thick root containing A horizon is dark brown and has an organic matter (OM) content of about 100 $g.kg^{-1}$. The CEC ranges from 20 to 30 $cmol.kg^{-1}$. The about 50 cm thick B horizon is reddish brown and has a lower root density than the upper unit. The OM contents decrease 10 $g.kg^{-1}$. The CEC decreases from 15 to 11.5 $cmol.kg^{-1}$. The BC horizon reaches a depth of about 105 cm. It is greyish to reddish brown, contains only a few roots and encloses granite boulders with quartz and hematite veins. The OM content is about 3 % and the CEC 11.5 to 9.7 $cmol.kg^{-1}$. The mineralogy including the observations of secondary mineral phases in the soil have been previously described (Fichter et al., 1998; Probst et al., 2000; Stille et al., 2009). Different horizons were sampled in November 2010 between the surface and 100cm depth (3-13 cm, 13-16 cm, 23-30 cm, 56-65 cm and 90-96 cm).

3. Materials and methods

3.1. **Water Extraction of Organic Matter (WEOM)**

Approximately 30 g of soil sample were used to determine the moisture content (105°C during 48 hours); the rest of it (approximately 300 g) was frozen. The Water Extractable Organic Matter (WEOM) was obtained by using an extraction method with water (Kalbitz et al., 2003; Said-Pullicino et al., 2007). The experiments were performed with Ultra High Purity (UHP) water to identify the hydro-soluble OM and the major and trace elements that can be transported by this hydro-soluble OM in the upper soil layers.

On the eve of the OM extraction, the soil was thawed in a refrigerator and sieved through a 2 mm sieve. It was then introduced into a 50 ml

polypropylene centrifuge tube and mixed with UHP water in the proportion 1/1.5 (water/dry soil). Each sample was agitated during 2 hours and ultra-centrifuged at 8000 rpm for 30 minutes at a temperature of 10°C. An experimental blank was made at the same time with only UHP water in a tube. The supernatant was filtered at 0.45 µm with a cellulose acetate filter. 10 ml of the filtrate was immediately frozen and freeze-dried for infrared spectroscopy; 90 ml was used for the chemical analysis (major and trace elements, titration, aromaticity) performed at the "Laboratoire d'Hydrologie et de Géochimie de Strasbourg" (LHyGeS, CNRS, Strasbourg).

3.2. **Infrared spectra of the freeze-dried samples**

The dried filtrate samples were prepared as KBr pellets (1 mg with 300 mg of KBr) and then analyzed. Their infrared spectra were recorded and accumulated with a Fourier-transformed infrared (FTIR) spectrophotometer (Brucker-5DXC) at a frequency ranging from 4,000 to 450 cm^{-1} and using a data interval of 1cm-1 and an accumulation of 100 scans. Only three freeze-dried samples (3-13 cm, 13-16 cm and 23-30 cm) yield sufficient signals to provide infrared spectra. The other two deep samples had a too strong background signal to allow for the determination of infrared frequencies.

3.3. **Water Extractable Organic Carbon (WEOC) fraction**

The WEOC (mg $C.g^{-1}$of air dried soil) in the soils corresponds to the Dissolved Organic Carbon (DOC) content in the extracted water, i.e. present in the 0.45 µm filtrate. In order to compare the WEOC of the different depths of the soil profile, it was normalized (WEOCN %) to the amount of Total Organic Carbon (TOC) in the soil. The DOC in the different filtrates was measured by a thermal method (Shimadzu TOC_{VPH}) with an uncertainty of 2% and a detection limit of 0.3 mg C. L^{-1}.

3.4. **Aromaticity of the WEOC fraction**

The Specific Ultraviolet Absorbance at 254nm ($SUVA_{254}$) is defined as the UV absorbance of the extractable samples at 254nm normalized to DOC concentration. $SUVA_{254}$ was measured by an UV-VIS spectrophotometer (SHIMADZU UV-1700). Weishaar et al. (2003) showed that there is a relationship between the percentage of aromaticity determined by ^{13}C-NMR and the $SUVA_{254}$ value (percentage of aromaticity=6.53*$SUVA_{254}$+3.63). This parameter has been determined for the different depths and allows to show the variation of the aromatic character of WEOC with depth.

3.5. **Titration of the WEOC fraction**

The potentiometric titration was performed using the automatic titrator (Titrando 905 Metrohm®) piloted by the software Tiamo® (Vers.2.3). The titrator was equipped with a combined pH electrode and a double burette, filled with NaOH and HCl (Titridose® 0.01 M). The measurements were completed in dynamic mode with an end measurement at fixed pH, after electrode calibration with standard solutions (pH 4.00 and 7.00). 20ml of each WEOC fraction was titrated while stirring, according the following sequence: NaOH (0.01 M) until pH 10, HCl (0.01 M) until pH 2.7 and NaOH (0.01 M) until pH 10. For blank correction, an experimental blank analysis has been performed between each sample (Weber et al., 2006). All potentiometric data were processed by the Nica Donan model to determine the mean proton affinity constant pK_H (Fiol et al., 1999) and the charge density Q_H (Ritchie and Perdue, 2003) which corresponds to the calculated organic charge normalized to the concentration of DOC to obtain Q_H in meq/gC in the WEOC fraction.

3.6. **Physico-chemical analysis of water extraction solutions and lysimeter soil solutions**

The pH has been measured with a combined electrode after calibration with a standard solution NIST (pH 4.00 and 7.00). The concentrations of major anions (Cl^-, NO_3^-, SO_4^{2-} and PO_4^{3-}) and cations (Na^+, NH_4^+, K^+, Mg^{2+}

and Ca^{2+}) were determined simultaneously by ionic chromatography (DIONEX ICS-3000) with an uncertainty below 2%. The trace element concentrations were determined by ICP/AES (JobinYvon – JY124) and ICP/MS (Thermo-Fisher X Série II) with traditional calibration and using Indium as internal standard. The blank for each element was 1 to 5% of the concentration in the sample. The validity and the reproducibility of different parameters have been verified by certified standards SLRS4, Perade-20 and Rain 97.

The Water Extractable Chemical Elements (WECE in mg $X.g^{-1}$ of air dried soil) correspond to the dissolved fractions of major and trace element contents in the extraction water, i.e. present in the 0.45 µm filtrate. In order to compare the WECE of soils from different depths of the profile, it has been normalized ($WECE_N$ %) to the total amount of the element X present in the soil.

3.7. **Chemical concentration and Cation Exchange Capacity (CEC) of soils**

The chemical soil analysis was performed at the SARM (Service d'Analyse des Roches et des Minéraux- Nancy- France). The major elements were determined by using ICP/AES and traces using ICP/MS. The organic carbon content was determined by using an oxygen combustion method with a CS analyzer. The soil CEC was analyzed at INRA (Laboratoire des sols d'Arras) by using the Metson method (extraction with ammonium acetate)

4. Results

4.1. **Chemical compositions of the soil samples**

The major and trace element data of the five soil samples are given in Table 1a. The evolution with depth of the TOC, Al_2O_3, Fe_2O_2, P_2O_5 and MnO concentrations and pH in the soil samples are shown in Fig.2. The 20 cm upper layer is enriched in TOC (100 $g.kg^{-1}$), whereas deeper horizons are depleted (10 $g.kg^{-1}$). The pH increases with depth from 3.9 to 4.7. Most of the elements show increasing concentrations until 30 cm depth, below which the

concentrations remain relatively constant with increasing depth (Table 1a). However, P, S, Pb, As, Cu, Zn, Mn, Sn, Sb, Middle REE (MREE: Gd to Ho), Heavy REE (HREE: Er to Lu) and Y behave differently with depth. To compare these differences in the soil profile, enrichment factors (Table 1b) have been calculated for each element and for each depth relative to Zr (EF_{Zr}) as an immobile element (White et al., 1998; Stille et al., 2011). Fig.3 shows the evolution of EF_{Zr} for TOC, Pb, REE, Fe, P, Sn, As and Sb. TOC and Pb are enriched at the surface down to 60 cm depth. MREE, HREE and P show an accumulation between 20 cm to 60 cm depth. Antimony, Sn, As are slightly enriched in upper horizons and remain rather constant with depth.

4.2. **WEOCN and CEC of soil**

The WEOC and the TOC values of the soils decrease with depth (Table 2). The WEOC variation is not proportional to the TOC of soil. The WEOCN decreases from 0.261 at 3-13 cm depth to 0.106 at 90-96 cm depth. However, at 21-30 cm and 56-60 cm depth, the samples have similar WEOCN values, but they are different from those of the other layers.

The soil CEC values (Table 2) decrease from 25.5 cmol/kg at 3-13 cm depth to 9.75 cmol/kg at 90-96 cm depth. There is a strong correlation (R2=0.98) between WEOC and soil CEC (Fig. 4).

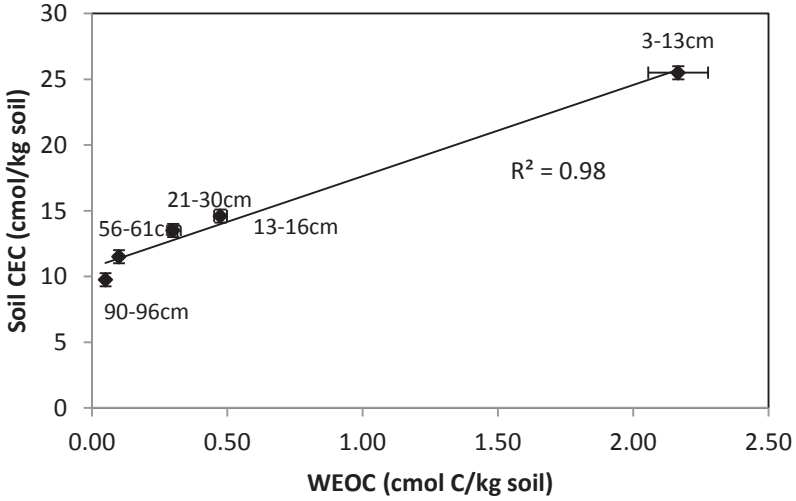

Figure 4: Correlation between WEOC and Soil CEC determined for different depths

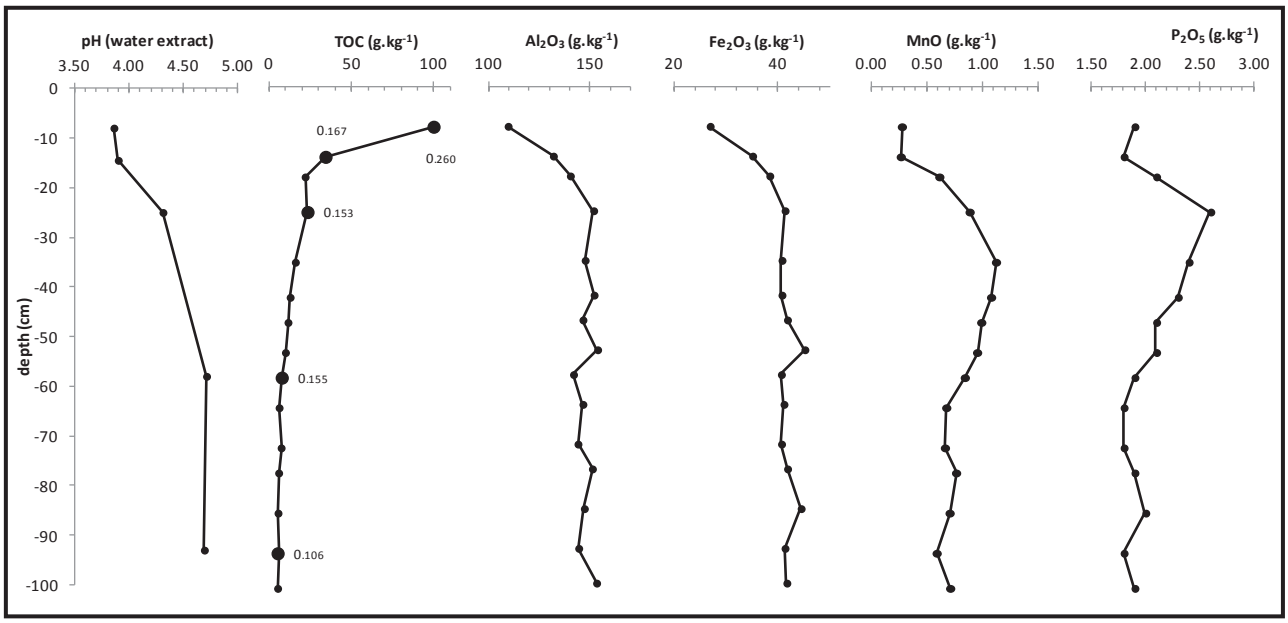

Figure 2: Evolution of pH, organic carbon, Al_2O_3, Fe_2O_3, P_2O_5 and MnO within the soil profile VP2

- $WEOC_N$ (%) for studied samples

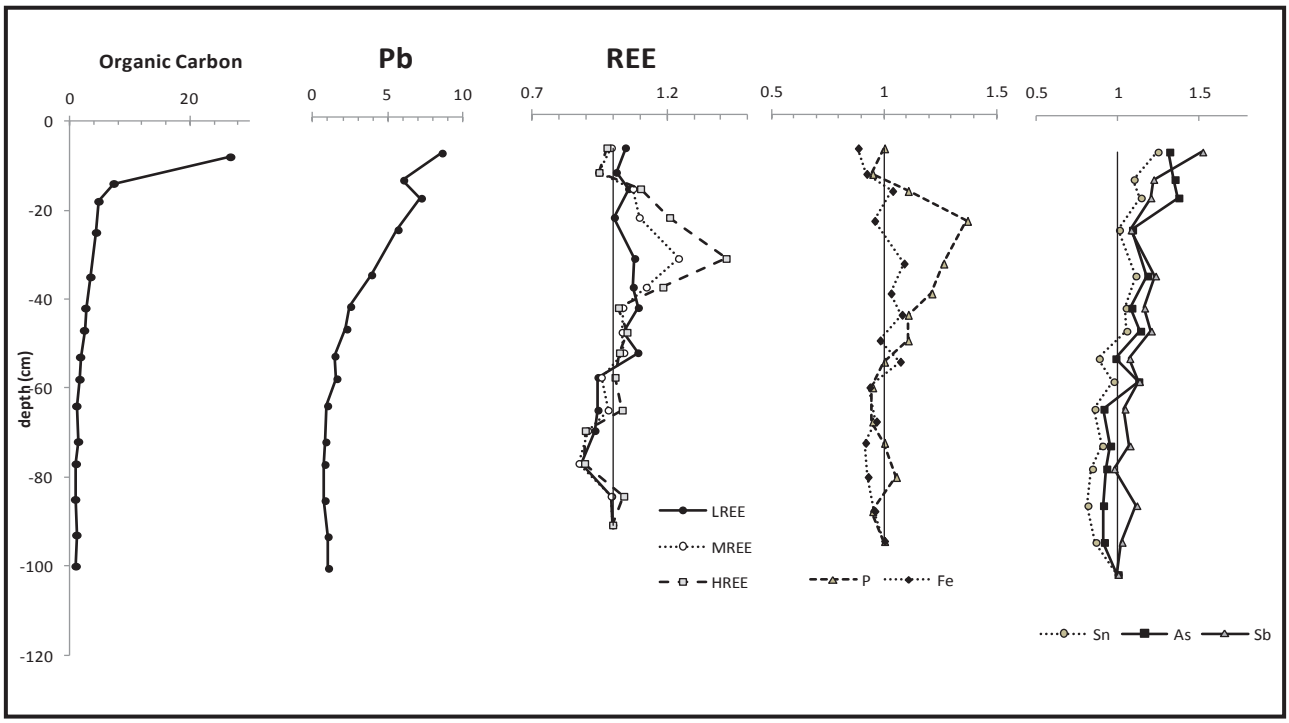

Figure 3: Variation of enrichment factors with depth (see caption and uncertainties of Table 1b)

4.3. **pH, conductivity and titration results**

The physico-chemical characteristics of the water extracts are given in Table 3. The pH corresponding to the water extract at 3-13 cm depth is 3.86. With increasing depth, the pH rises weakly until 56-61cm depth and then, remains relatively constant (4.70). Therefore, the water extracts are differently acidified by organic acids and the H^+ protons coming from the different soil horizons. The mean proton affinity constants (pK_H) and the charge densities (Q_H meq/gC) in Table 3 correspond to the hydrosoluble acidities of the different soils, i.e. to the OM. Only the results for 3-13 cm, 13-16 cm and 23-30 cm depth are given. For the samples deeper than 30 cm, TOC contents were too low to allow for a precise determination of the two parameters. The pK_H values increase and the Q_H values decrease with depth. For the 3-13 cm depth, $pH>pK_H$ means that all active sites are deprotonated. For the 13-16 cm depth, $pH\approx pK_H$ means that 50% of the active sites are deprotonated and 50% are protonated. For the 21-30 cm depth, $pH<pK_H$ means that all active sites are protonated.

The conductivity of the WEOC fractions decreases with depth, which indicates that trace element extracted is more important at close to the surface than at depth. This is confirmed by the rate of the different elements extracted by the $WECE_N$ (Table 4).

Depth (cm)	TOC*	P*	S*	Al*	Si*	Na*	K*	Mg*	Ca*	Ti*	Mn*	Fe*	As**	Rb**	Cs**	Sr**	Ba**	V**	Cr**	Co**	Ni**	Cu**	Zn**
02-13	99.8	0.83	0.5	58.0	273.5	3.2	24.8	2.3	0.36	0.27	0.22	18.8	27.1	239.5	26.59	46.42	203.1	39.05	35.22	2.69	11.18	9.5	27.6
13-16	34.2	0.79	0.1	69.8	313.3	3.5	30.2	0.28	0.35	0.32	0.21	24.5	34.76	292.5	32.51	61.49	240.2	44.36	41.99	3.20	13.42	6.79	23.9
21-30	23.3	1.13	0.1	80.3	304.6	3.8	32.0	0.34	0.35	0.38	0.69	28.8	31.81	331.7	39.18	55.75	261	51.21	45.48	4.52	13.98	7.03	25.14
56-60	7.6	0.83	0.2	75.1	324.1	3.2	30.0	0.31	0.35	0.35	0.65	28.3	28.9	289.4	34.58	51.1	269.8	53.2	48.3	5.04	15.8	7.71	22.8
90-96	5.9	0.79	0.2	76.4	327.7	3.4	30.2	0.31	0.35	0.38	0.46	28.8	26.73	288.7	35.87	50.77	263.4	53.01	46.62	4.75	13.92	14.64	28.38

Depth (cm)	Sn**	Sb**	Y**	Zr**	La**	Ce**	Pr**	Nd**	Sm**	Eu**	Gd**	Tb**	Dy**	Ho**	Er**	Tm**	Yb**	Lu**	Pb**	Th**	U**	Clays <2µm
02-13	15.71	2.96	15.02	154.8	27.76	54.25	6.58	23.64	4.31	0.56	3.1	0.46	2.54	0.49	1.43	0.22	1.49	0.23	61.39	10.69	3.16	5%
13-16	17.34	2.97	17.88	193.7	33.5	65.61	8.01	28.58	5.26	0.66	3.57	0.54	3.11	0.6	1.73	0.26	1.78	0.29	59.4	12.72	3.73	15%
21-30	18.06	2.987	25.21	219.8	37.8	73.53	8.99	32.27	5.89	0.75	4.43	0.69	4.16	0.83	2.47	0.38	2.62	0.41	57.31	14.97	4.4	18%
56-60	15.33	2.75	19	193	36.2	70.28	8.56	30.75	5.73	0.74	4	0.59	3.37	0.64	1.87	0.28	1.96	0.31	13.91	14	4.1	7%
90-96	15.46	2.83	21.62	219.5	37.58	71.74	8.83	31.93	5.89	0.78	4.28	0.64	3.68	0.71	2.12	0.33	2.25	0.35	9.85	14.8	4.37	6%

Table 1a: The chemical composition of the VP2 soil with depth

* in $g.kg^{-1}$ with uncertainty ±2 to 5%

** in $mg.kg^{-1}$ with uncertainty ±5%

Depth (cm)	C	P	S	Al	Si	Na	K	Mg	Ca	Ti	Mn	Fe	As	Rb	Cs	Sr	Ba	V	Cr	Co	Ni	Cu	Zn
03-13	26.80	1.37	3.42	0.979	1.160	1.18	1.04	0.95	0.86	1.01	0.54	0.883	1.316	1.078	0.973	1.163	1.052	1.000	1.015	0.72	0.954	1.63	1.566
13-16	7.34	1.04	0.55	0.942	1.062	1.04	1.01	0.93	0.46	0.95	0.41	0.921	1.349	1.052	0.951	1.231	0.994	0.908	0.967	0.69	0.915	0.93	1.084
21-30	4.40	1.32	0.48	0.955	0.910	1.00	0.95	0.98	0.40	0.99	1.20	0.956	1.088	1.051	1.010	0.984	0.952	0.924	0.923	0.85	0.840	0.85	1.004
56-60	1.64	1.10	0.92	1.016	1.102	0.96	1.01	1.03	0.42	1.04	1.30	1.070	1.126	1.045	1.015	1.027	1.121	1.092	1.117	1.09	0.995	1.06	1.035
90-96	1.12	0.91	0.97	0.910	0.980	0.91	0.90	0.91	0.40	0.98	0.80	0.957	0.916	0.916	0.926	0.897	0.962	0.958	0.948	0.90	0.838	1.77	1.135
uncertainty	*0.08*	*0.08*	*0.09*	*0.001*	*0.001*	*0.02*	*0.002*	*0.01*	*0.01*	*0.01*	*0.10*	*0.002*	*0.003*	*0.001*	*0.002*	*0.002*	*0.001*	*0.002*	*0.002*	*0.01*	*0.004*	*0.01*	*0.003*

Depth (cm)	Sn	Sb	Y	Zr	La	Ce	Pr	Nd	Sm	Eu	Gd	Tb	Dy	Ho	Er	Tm	Yb	Lu	Pb	Th	U
03-13	1.245	1.52	1.011	1.000	1.047	1.072	1.049	1.045	1.03	0.99	1.01	1.0	0.97	1.0	0.98	1.0	0.98	1.0	8.58	1.003	0.98
13-16	1.098	1.22	0.962	1.000	1.010	1.036	1.021	1.010	1.00	0.93	0.93	1.0	0.95	1.0	0.95	0.9	0.94	1.0	6.02	0.954	0.93
21-30	1.008	1.08	1.195	1.000	1.004	1.023	1.010	1.005	0.99	0.94	1.02	1.1	1.13	1.2	1.20	1.2	1.22	1.2	5.64	0.989	0.97
56-60	0.975	1.13	1.027	1.000	1.095	1.113	1.095	1.090	1.10	1.05	1.05	1.1	1.04	1.0	1.03	1.0	1.04	1.0	1.56	1.058	1.02
90-96	0.864	1.02	1.027	1.000	1.000	0.999	0.994	0.995	0.99	0.97	0.99	1.0	1.00	1.0	1.03	1.1	1.04	1.0	0.97	0.979	0.96
uncertainty	*0.004*	*0.03*	*0.004*	*0.001*	*0.002*	*0.001*	*0.009*	*0.003*	*0.01*	*0.09*	*0.02*	*0.1*	*0.02*	*0.1*	*0.04*	*0.3*	*0.04*	*0.2*	*0.02*	*0.005*	*0.02*

Table 1b: Enrichment factors (normalization to Zr and the soil from 100cm depth, i.e. $[(X_i/Zr_i)/(X_{100}/Zr_{100})]$)

depth (cm)	Soil TOC (g C per 100g dried soil)	WEOC (mg C.L-1)	WEOC (mg $C.g^{-1}$ of dried soil)	WEOC (cmol $C.kg^{-1}$ of dried soil)	$WEOC_N$(%) = WEOC/TOC	Soil CEC (cmol.kg-1)
3-13 cm	9.98 ± 0.05	96 ± 1	0.26 ± 0.01	2.2 ± 0.1	0.26 ± 0.01	25.5 ± 0.2
13-16 cm	3.42 ± 0.05	70 ± 1	0.057 ± 0.003	0.48 ± 0.02	0.167 ± 0.009	14.6± 0.2
21-30 cm	2.33 ± 0.05	43 ± 0.9	0.036 ± 0.002	0.30 ± 0.02	0.153 ± 0.008	13.5± 0.2
56-61 cm	0.76 ± 0.05	15 ± 0.3	0.012 ± 0.0005	0.100 ± 0.005	0.15 ± 0.01	11.5± 0.2
90-96 cm	0.59 ± 0.05	8 ± 0.3	0.006± 0.0005	0.050 ± 0.003	0.11 ± 0.01	9.8± 0.2
blanck		0.3				

Table 2: TOC, WEOC, $WEOC_N$ and CEC for different depths (VP2)

depth (cm)	pH	conductivity ($\mu S.cm^{-1}$)	SUVA $_{254nm}$ ($L.mg^{-1}.m^{-1}$)	Aromaticity (%)	pK_H	Qeq (meq/gC)
3-13 cm	3.86	94	2.5	19	1.61	7.5
13-16 cm	3.9	64	4.0	30	4.26	3.0
21-30 cm	4.31	33	4.9	36	6.9	1.6
56-61 cm	4.71	20	1.6	14	n.d.	n.d.
90-96 cm	4.69	37	0.5	8	n.d.	n.d.
blanck	5.49	3				
uncertainty	*0.05*	*2*	*0.05*	*2*	*0.05*	*0.1*

Table 3: pH, Conductivity, $SUVA_{254nm}$, aromaticity, pK_H, Q_H for the water extraction fractions (n.d. non determined)

4.4. **The extractable trace elements**

Table 4 compares the normalized rates of the different water extractable elements ($WECE_N$) with the rate of $WEOC_N$. Sulfur is the most water extractable element at all depths (from 1.6% to 0.5%). The other elements which are also

water extractable are Organic Carbon (0.26% to 0.11%), Mn, Cd, Zn, As, Na, Co, Cu, and Pb. A hierarchical ascending classification (HAC) classifies the elements into two groups (Fig.5). The first group contains elements which are especially extractable at 3-13 cm depth and much less in the other horizons (80% to 30% less than surface horizon) and includes C, P, Co, Cu, Ba, Na, As, Th, Mn, K, Mg, Rb, and Sr. The second group contains $WECE_N$ which progressively decrease with depth. This is the case for Pb, U, Cs, Sn, Si, HREE, V, Cr, Y, Zr, Fe, Light REE (LREE: La, Pr, Nd), Ti, MREE, S, Sb, Al and Ni.

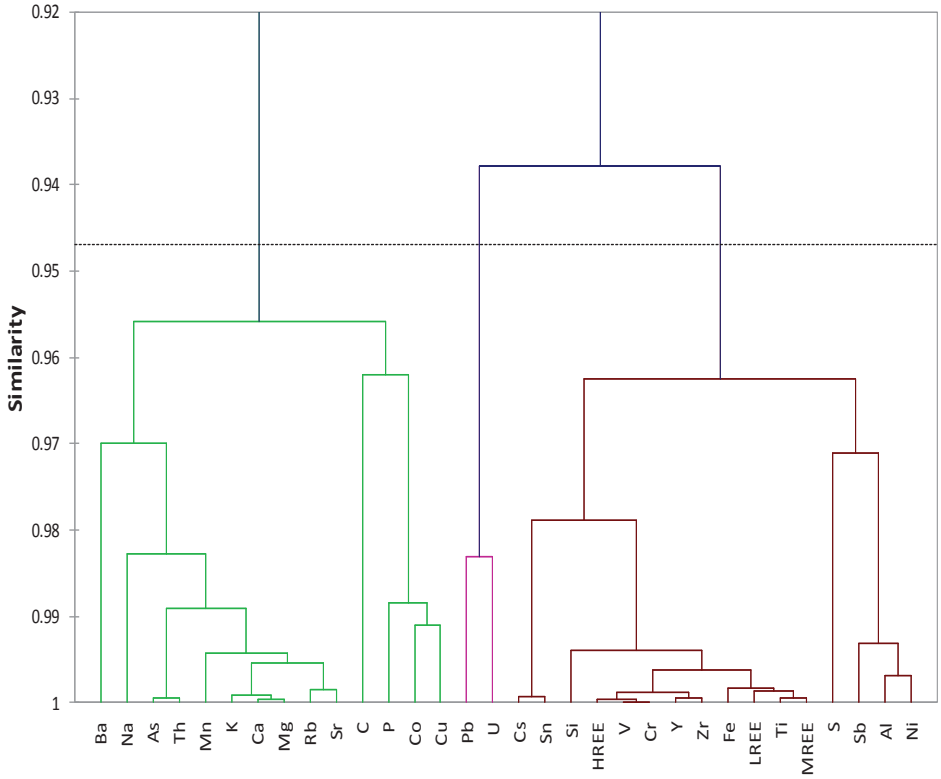

Figure 5: Hierarchical Ascending Classification for WEOCN and WECEN values of samples from all 5 horizons performed by XLSTAT program.

4.5. **Characterization of the Organic Matter (OM)**

The aromaticity of the WEOC fraction is characterized by SUVA254nm (Table 3). The values range from 0.5 to 4.9 (L/mgC.m). They increase from 2.5 to 4.9 with increasing depth but below 30 cm depth they decrease. The surface

values (3-13 cm) match those of humic substances and are of the same order of magnitude as those given by Said-Pullicino et al. (2007) who studied the labile OM evolution during decomposition of plant compost; it is also similar to values found for different dissolved OM (Boyer et al., 2008). Ussiri and Johson (2003) characterized the OM of forest soils by ^{13}C NMR spectroscopy and also observed an increase of aromatic C with depth.

Figure 6 shows the infrared spectra of the three freeze-dried samples (3-13 cm, 13-16 cm and 23-30 cm). The spectra are characterized by the same bands and are similar to those obtained by Haberhauer and Gerzabek (1999) who analyzed powdered forest soils directly without freeze drying; they are also similar to the data set of freeze-dried soil extractions (Kalbitz et al., 1999), to results of experiments on burned soils (Vergnoux et al., 2011) and data collected during composting of vegetal wastes (Van Praagh et al., 2009). The observed principal functional groups are given in Fig.6 and in Table 5. A large band between 3500-3000 cm^{-1} corresponds to the stretching vibration of bonded and not bonded hydroxyl groups. This band presents a shoulder at 3200 cm^{-1} for only the upper layer sample. According to Oh et al. (2005), this points to intermolecular hydrogen binding and hydroxyl groups between different polymers of cellulose, resulting from the decomposition of the needle litter. At 2920 cm^{-1} and 2850 cm^{-1}, two bands are characteristic of the stretching vibration of C-H bonds in the aliphatic groups. The band at 1725 cm^{-1} corresponds to the stretching vibration of C=O bonds in the carboxylic acid function. According to Zhou et al. (2010), this organic function is the result of hydrolysis of the complex cellulose-lignin. The 1650 cm^{-1} band can be attributed to the stretching vibration of C=C bonds in alkene and aromatic groups. According to Demiate et al. (2000) and Vergnoux et al. (2011), 1400 cm^{-1} band might correspond to the bending vibration of the carboxylate ion. The bands between 1265 cm^{-1} and 1200 cm^{-1} correspond to the stretching vibration of the C-O bond in lignin derived arylmethylether (Schwanninger et al., 2004). A large band between 1175 cm^{-1} and 1040 cm^{-1} suggests the presence of polysaccharides.

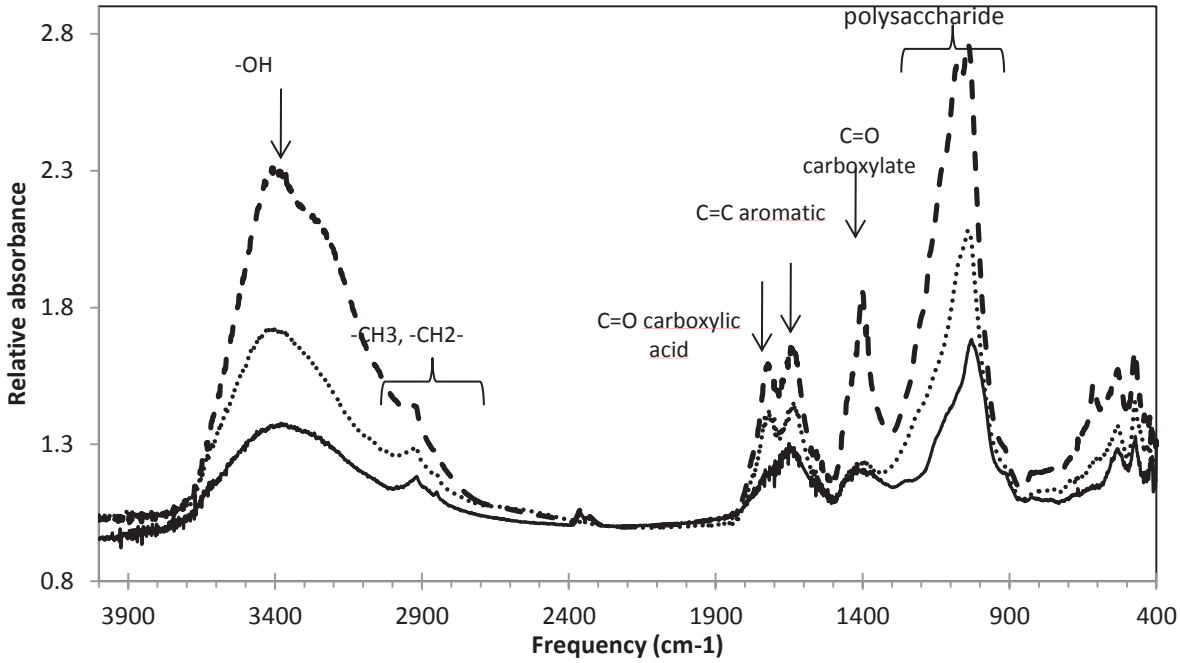

Figure 6: Infrared spectra of different freeze dried samples.

Table 5 shows relative changes of the most important infrared frequencies with depth. The frequencies which decrease with depth are 3400 cm^{-1}, 1400 cm^{-1}, 1170 cm^{-1}, 1140 cm^{-1}, 1075 cm^{-1}, 1040 cm^{-1} and those which increase with depth are 2920 cm^{-1}, 2850 cm^{-1}, 1725 cm^{-1}, 1650 cm^{-1}, 1550 cm^{-1}, 1265 cm^{-1}

Depth (cm)	C	P	S	Al	Si	Na	K	Mg	Ca	Ti	Mn	Fe	As	Rb
03-13	0.260	0.052	1.59	0.019	0.0065	0.201	0.079	0.034	0.57	0.006	0.603	0.042	0.209	0.114
13-16	0.167	0.023	1.24	0.011	0.0057	0.040	0.009	0.006	0.08	0.005	0.094	0.034	0.059	0.026
21-30	0.153	0.018	1.05	0.005	0.0024	0.038	0.004	0.004	0.04	0.002	0.089	0.018	0.028	0.010
56-60	0.155	0.005	0.54	0.001	0.0007	0.034	0.003	0.002	0.02	0.000	0.006	0.002	0.003	0.003
90-96	0.106	0.006	0.66	0.000	0.0004	0.044	0.002	0.002	0.02	0.000	0.005	0.000	0.001	0.001

Depth (cm)	Cs	Sr	Ba	V	Cr	Co	Ni	Cu	Zn	Sn	Sb	Y	Zr	LREE	MREE	HREE	REE
03-13	0.031	0.027	0.017	0.048	0.043	0.156	0.069	0.201	0.296	0.017	0.075	0.005	0.002	0.0038	0.0071	0.006	0.0056
13-16	0.030	0.006	0.009	0.037	0.033	0.062	0.039	0.082	0.087	0.017	0.045	0.004	0.002	0.0032	0.0052	0.0046	0.0043
21-30	0.008	0.003	0.005	0.014	0.013	0.065	0.024	0.064	0.042	0.004	0.030	0.002	0.001	0.0015	0.0026	0.0019	0.002
56-60	0.001	0.002	0.005	0.002	0.003	0.029	0.008	0.038	0.056	0.000	0.010	0.000	0.000	0.0002	0.0005	0.0004	0.0003
90-96	0.0002	0.002	0.004	0.000	0.001	0.018	0.009	0.008	n.d.	0.000	0.003	0.000	0.000	0.0001	0.0001	0.0001	0.0001

Depth (cm)	La	Ce	Pr	Nd	Sm	Eu	Gd	Tb	Dy	Ho	Er	Tm	Yb	Lu	Pb	Th	U
03-13	0.0041	0.0037	0.0035	0.0038	0.0050	0.0086	0.0063	0.0073	0.0068	0.0070	0.0066	0.0059	0.0061	0.0052	0.0847	0.0252	0.0092
13-16	0.0034	0.0031	0.0029	0.0032	0.0037	0.0076	0.0054	0.0052	0.0054	0.0049	0.0049	0.0047	0.0050	0.0040	0.0720	0.0067	0.0098
21-30	0.0017	0.0016	0.0013	0.0015	0.0019	0.0044	0.0027	0.0027	0.0028	0.0024	0.0022	0.0019	0.0018	0.0016	0.0520	0.0039	0.0067
56-60	0.0002	0.0002	0.0002	0.0002	0.0003	0.0007	0.0005	0.0005	0.0006	0.0006	0.0005	0.0005	0.0005	0.0005	0.0028	0.0004	0.0013
90-96	0.0002	0.0001	0.0000	0.0000	0.0001	0.0002	0.0001	0.0001	0.0001	0.0001	0.0001	0.0001	0.0001	0.0001	0.0040	0.0001	0.0002

Table 4: Comparison of the WECEN with the rate of WEOCN(%) (n.d. non determined)

The uncertainties are comprised between 3 and 6%

FTIR frequency (cm^{-1})	3400	2920	2850	1725	1650	1400	1265	1210	1172-1140	1075	1040
Mode	O-H stretching	C-H stretching	C-H stretching	C=O stretching	C=C stretching	COO^- stretching	COC stretching	O-H bending	C-O-C stretching	C-O stretching	C-O stretching
Functional groups	Carboxylic acid, Alcohol, Phenol	Alkyl	Alkyl	Carboxylic acid	Aromatic, alkene	Carboxylate	Phenolic or arylmethyl ether (lignin)	O-H plane deformation	C-O linkage glycosidic	C-O ring	C-O ring and C-O (MeOH)
depth	$RelAbs_{3400}$	$RelAbs_{2920}$	$RelAbs_{2850}$	$RelAbs_{1725}$	$RelAbs_{1650}$	$RelAbs_{1400}$	$RelAbs_{1265}$	$RelAbs_{1170}$	$RelAbs_{1140}$	$RelAbs_{1075}$	$RelAbs_{1040}$
3-13cm	0.1089	0.0678	0.0606	0.0748	0.0766	0.0875	0.0673	0.0940	0.1052	0.1267	0.1301
13-16cm	0.1033	0.0773	0.0717	0.0843	0.0837	0.0739	0.0769	0.0903	0.0960	0.1174	0.1246
21-30cm	0.0955	0.0851	0.0815	0.0857	0.0895	0.0827	0.0822	0.0862	0.0918	0.1037	0.1156

Table 5: Frequencies and vibration modes corresponding to the principal organic functions. $RelAbs_i$ correspond to relative absorbance of each selected band i relative to the sum of the absorbances of all selected bands ($RelAbs_i=Abs_i/\Sigma Abs_i$)

5. Discussion

5.1. **Water Extractable Organic Carbon**

WEOC represents only a small quantity of TOC in the soil (McGill et al., 1986; Corvasce et al., 2006) and influences weathering and heavy metal mobility (Egli et al., 2010) and podzolisation (Buurman and Jongmans, 2005). There are similarities between TOC and WEOC (Kalbitz et al., 2000; Corvasce et al., 2006). The dissolved organic fraction is in equilibrium with solid organic phases and WEOC includes DOC located in macropores and smaller pores (Zsolnay, 1996). Therefore, the WEOC fraction yields informations on the functional groups of TOC_{soil}.

TOC_{soil} and $WEOC_N$ values decrease with depth (Fig.7). The samples from 3 – 30 cm correspond to the OM enriched soil and those from 56 - 96 cm to the OM depleted soil. Similarly, $SUVA_{254nm}$ values are higher for the 13-16 cm and 21-30 cm samples than for those from below 56 cm depth (Table 3). For determination of the mean proton affinity constants (pK_H) and the charge densities (Q_H meq/gC), the signal was insufficient for the 56-60 cm and 90-96 cm samples. The difference between surface samples and those from below 56 cm confirms previous results and interpretations of solid-state ^{13}C NMR spectra of forest soils, suggests that considerable differences exist between deeper and surface soils, points to an increase in the decomposition of OM with depth (Ussiri and Johnson, 2003) and indicates that these changes are accompanied by a modification of the molecular structure. The relative changes of the infrared frequencies further indicate that the changes of the molecular structure of water extractable OM with depth go along with a relative decrease of the polar functional groups and a relative increase of the less polar hydro-carbon functional groups (Table 5). The degradation of the polar functional groups progresses more rapidly than the increase of the aliphatic compounds. Similar observations have been reported for the decomposition of coniferous litter in a catchment in New Hampshire ((Ussiri and Johnson, 2003). Don and Kalbitz (2005), Said-Pullicino et al. (2007) and Jouraiphy et al. (2008) also observed a decrease in carbohydrate compounds, accompanied by an increase in

aromaticity. These variations are due to microbial activities which transform lignin to phenolic compounds and degrades the carbohydrates (Stadler et al., 2006).

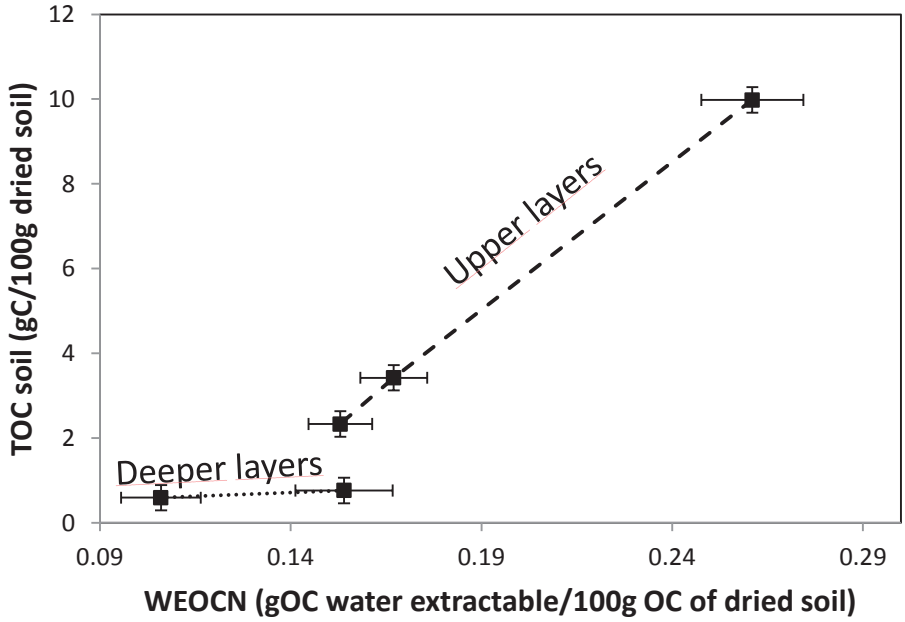

Figure 7: Relation between $WEOC_N$ and TOC_{soil} values for samples from different depths

In this study, one observes an accumulation of aromaticity at depths between 30 and 36 cm. Aromaticity and soil particles (clays) are correlated with each other (R^2=0.85) (Table 1a). McKnight et al (1992) showed that the aromatic compounds are preferentially adsorbed onto soil particles and Murphy and Zachara (1995) observed an increasing adsorption on clays with increasing aromaticity of humic substances. Similarly, Kalbitz et al. (2005) noticed that the sorption of DOC to soil minerals is selective for hydrophobic and aromatic compounds; according to these authors the aromatic carbon is the most stable DOC component which becomes stabilized by sorption to soil minerals.

5.2. **CEC and OM**

Many authors agree that the CEC of soil is strongly linked to the OM (Hunt, 1981; Lin and Chen, 1998; Ruiz Sinoga et al., 2012). Likewise, Oorts et al. (2003) and Bradl (2004) also showed that there is a relationship between CEC, pH and TOC. All these studies explain the good correlation

between WEOC and CEC (Fig.4). At 13-16 cm and 21-30 cm depth samples have large aromaticity (30-36%), but the CEC decreases with depth (Table 2) and is positively correlated to WEOC. This indicates that the CEC is, among others, controlled by the amount of OM rather than the molecular structure of the OM. At the soil surface, pH and pK_H values of the WEOC fraction suggest that the active sites are deprotonated. The 1400 cm^{-1} band infra-red spectrum (3-13 cm) indicates the presence of carboxylate ion. The results also explain the important difference which exists between the CEC values of samples from 3-13 cm and 13-16 cm depth (Table 2) and suggest that exchange between cations and clay-humic complexes decreased. Some cations are more strongly bound with colloids and are not exchangeable. They are complexed and maintained in soil solution. They are thus protected from precipitation and might be transported by soil solutions. The decrease of the Q_H and increase of the pK_H and pH values with depth indicate that there are decreased possibilities for cations to be linked or exchanged with the clay-humic complexes. The co-variations of the WEOC and the soil CEC values support this hypothesis and suggest the depletion of the polar organic functions with depth which can chelate or adsorb different cations (Fig.4).

5.3. **Evolution of trace elements in soil**

Decomposition of needle and leaf litter, partly driven by bacteria (Stadler et al., 2006 ; Sjöberg et al., 2004), causes carbon accumulations in the soils and the formation of low and high molecular-weight organic compounds (Don and Kalbitz, 2005) ; those which are labile and dissolved are transported from the soil litter to the soil by lixiviation due to acidic rain and throughfall (pH=5, http://ohge.unistra.fr). Similarly, trace elements become mobilized during these processes (Kaiser et al., 2002). Some of them have an atmospheric origin: V, Cr, Cu, Zn, Sb, Sn and Pb (Reimann et al., 2007; Guéguen et al., 2012). They become mingled in soil solutions with those coming from mineral weathering. The enrichment factors (Table 1b) indicate that some elements such as Sb, Sn, As, Pb are enriched in the upper soil, or quite constant over the whole soil profile (Fe, Al, U). P generally

decreases with depth. LREE are rather enriched in the upper soil whereas HREE are relatively enriched in the lower soil horizons except the 30cm depth where HREE are enriched. Consequently, all these trace elements manifest different mobilities within the soil profile. Middelburg et al. (1988) and Aiuppa et al. (2000) showed that the relative mobility of different elements (Al, Fe, Mn, Cr, V, U, Sb, As) in soil and soil solution depends on oxidation-reduction reactions which are partly driven by bacteria (Turpeinen et al., 1999; Frohne et al., 2011). Biomethylation reaction transforms As, Sb, Sn and Pb into organometallic volatile compounds which are converted to water-soluble species (Takamatsu et al., 1982; Reimann et al., 2007). In this study, As, Sb, Sn and Pb are the most enriched atmosphere-derived elements in the upper soil layers (Table 1a) and show comparatively high WECEN values (Table 4). In the 19th and 20th century, the mining and industrial activities around the catchment for the production of As (Gabe Gottes <1km), Ag and Pb (Saintes Marie aux Mines <5 km) resulted in important anthropogenic atmospheric deposition and facilitated enrichments in the soil (Stille et al., 2011).

Ultrafiltration experiments with different kinds of waters (from springs, rivers and soil solutions) have shown that there is a direct relationship between DOC and U, REE, Cu, Cr, V concentrations (Pourret et al., 2007; Vasyukova et al., 2010). Fig.5 indicates that WEOC is not a part of the WECE group of U, REE, Cr or V but of the WECE group including Na, K, Rb, Mg, Ba, Sr which are often considered as “dissolved elements” (Pokrovsky and Scott, 2002). Therefore, it is helpful to use the HAC to show that there is a correlation between $WECE_N$ of trace elements and infrared frequencies of WEOC for the OM-rich horizon (3 to 30 cm depth) (Fig. 8). It seems that Fe, V, Cr, REE, Y, Zr, Ti, Pb are correlated with the infrared frequencies (1725 cm^{-1} and 1265 cm^{-1}) corresponding to carboxylic acid and phenolic ether. This is in accordance with the fact that LREE are preferentially bound to carboxylic groups, whereas the HREE are preferentially bound to carboxy-phenolic and phenolic groups (Marsac et al., 2011). Furthermore, Al, Ba, Ni, S and Sb are correlated with the infrared frequencies (1040 cm^{-1},1140 cm^{-1},

1650 cm^{-1}, 2920 cm^{-1} and 3400 cm^{-1}) corresponding to hydroxyl (carboxylic acid, alcohol, phenol), alkyl, aryl and ether functional groups. According to Kummert and Stumm (1980) and Smith D. Scott and Kramer (1998), at acidic pH, the natural OM has multi-sites which can be bound to Al; strong and weak strength binding sites are observed. At low pH, aromatic carboxylic acid forms monodentate inner-sphere complexes with Al; the near presence of phenolic group facilitates the formation of these complexes and, in the case two hydroxyl groups are adjacent or in ortho position to the carboxylic group, the hydroxyl groups participate to the complexation reaction (Cornard and Lapouge, 2007; Guan et al., 2006b). The HAC results also indicate that elements which have important $WECE_N$ in the upper soil compartments and less important values at depth are correlated with WEOCN (labile organic carbon) and with infrared frequency 1400 cm^{-1} corresponding to the carboxylate ion; this is the case for Rb, Mg, K, Na, Cu, P, Sr, Co, Mn (Fig.8). A modelling study on O and B horizons of podzolic soils has demonstrated that most of dissolved major cations were counter-ions, residing in the diffuse layers of DOM (Gustafsson et al., 2000). Consequently, the solubility of these cations depends on the solubility of OM. These results are in accordance with the fact that the dissolved cations (alkaline and alkaline earth) are in the same cluster as DOC (Fig.8). Other elements such as Cu, Co, As, P and Th plot in the same cluster as WEOC. Indeed, Cu and Co form more stable complexes with DOC than other trace elements (Cezikova et al., 2001; Reinmann and de Caritat, 2005; Wang et al., 2008; van Praagh et al., 2009; Egli et al., 2010).

At low pH, Th forms complexes with OM (Reiller et al., 2002); the complexation with carboxylic acid is essentially electrostatic (Bismondo et al, 2003) and might increase the Th mobility in the upper compartment of soil. According to Bauer et al. (2008), As appears mainly in the dissolved form if the molar ratio Fe/C in soil solution is <0.02, which is the case for the Strengbach catchment soil solutions. Microorganisms play an important role in the mobility of As due to the similarity with phosphate (same cluster; Fig.8) which is important in the biological cycles (Caille et al., 2004; Tu et al.,

2003). The HAC also suggests that U, Sn, Si and Cs are related to non-organic functions of WEOC. Experimental studies on U interactions with organic compounds such as humic acid demonstrate that they strongly influence the mobility of this element in soil solutions (Bednar et al 2007). However, at low pH one observes that U is not only controlled by soil OM but also amorphous Fe. Consequently, the linkage possibilities of U with different phases, such as stable organic carbon or both labile and stable organic phases or amorphous Fe causes a complex reaction pattern in the water extracts which remains difficult to interpret.

5.4. **The migration behavior of Iron, Aluminum and DOC**

Iron and Al are not part of the same cluster in the upper OM enriched soil compartment (Fig.8) suggesting that they are bound to DOC with different binding sites (Cabaniss, 1992; Nierop et al., 2002). Additionally, Al and Fe extracted from the VP2 soil profile show very different behavior in the upper OM enriched and in the lower OM depleted soil (Fig.9). Similar to Chorover and Sposito (1995) and Chorover et al. (2004) one observes that Al behaves differently in the Strengbach soil solutions than Fe and DOC; Al concentrations in soil solutions increase from 5 cm (21.6 µmol/L) to 30 cm (29.5 µmol/L) and then decrease similar to Fe and DOC with depth (Table 6). This is in contrast to the $WECE_N$ where $WECE_N$ Al and $WECE_N$ Fe decrease with depth and $WECE_N$Fe is always larger than $WECE_N$Al (Table 4). This can be explained by the different speciations of Al (Al^{3+}) and Fe (oxyhydroxide nano-particulates). Thus, Fe participates in the stabilization of the DOC whereas Al is more mobile with depth. at low pH (3.5 to 4.5), Fe(III) causes strongest flocculation of DOC and, therefore, its immobilization and the formation of the OM rich horizon in the soil profile (Nierop et al., 2002). Consequently, the soil solutions from the upper soil horizons can be considered to be OM-Fe-Al-rich whereas deeper compartments contain rather OM- poor-Al type waters.

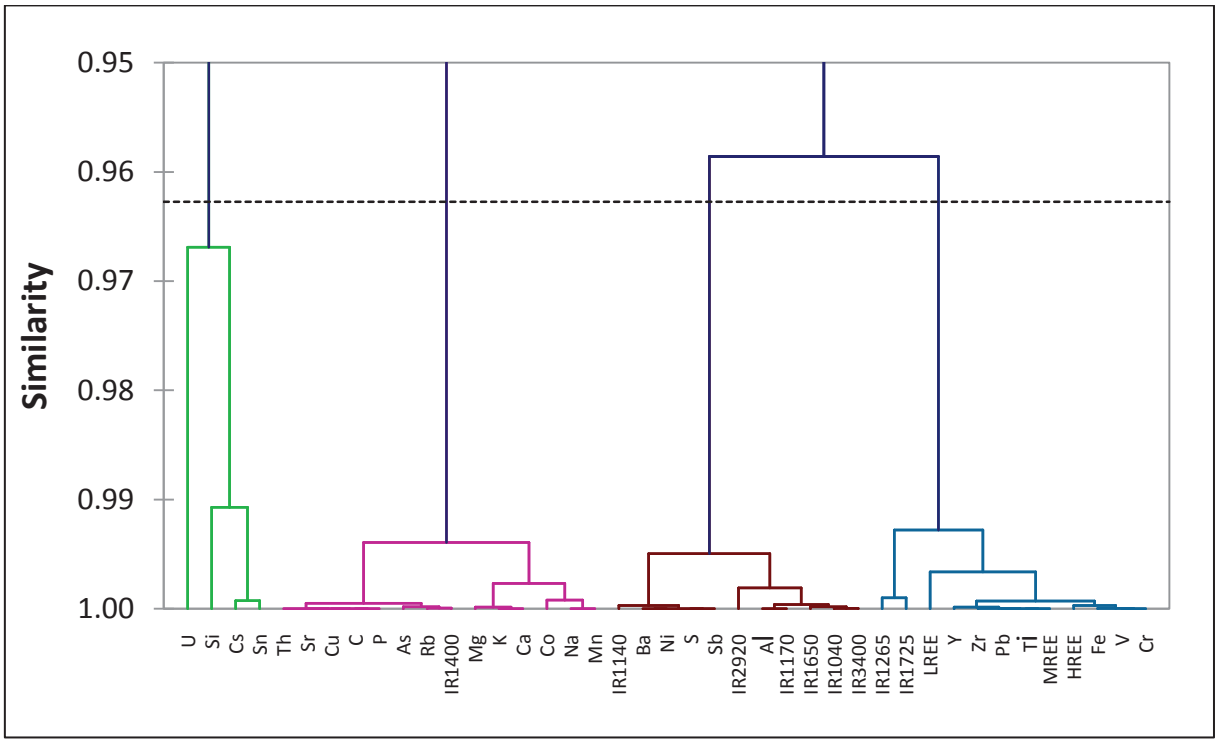

Figure 8: Hierarchical Ascending Classification for WEOCN, WECEN and infrared absorbance of 3 samples from the upper soil profile

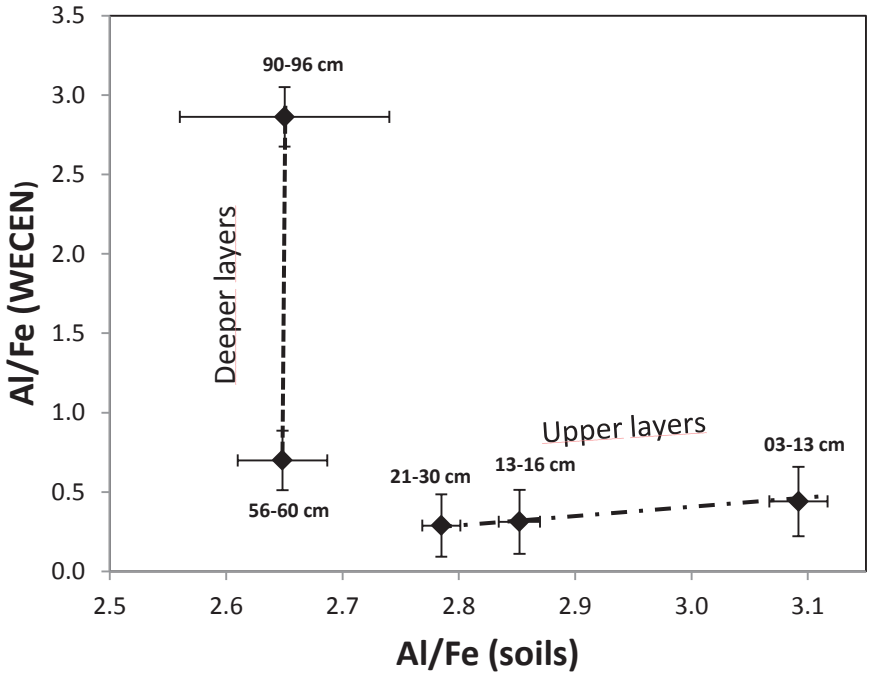

Figure 9: Variation between Al/Fe ($WECE_{N)}$ and Al/Fe (soils) at different depths

5.5. **The migration behavior of Lead**

The upper horizons of French forest soils are enriched in Pb (Hernandez et al., 2003). The Pb concentration of the VP2 topsoil (61 mg.kg^{-1}) is higher than the median value of Pb in European topsoils (22.6 mg.kg-1) (http://weppi.gtk.fi/publ/foregsatlas).

The Pb isotope ratios determined on similar soil profiles in the Strengbach catchment point to the preponderance of atmospheric, anthropogenic Pb until 40 cm depth and the ^{210}Pb activities suggest a migration speed of 0.9 cm.y^{-1} (Stille et al., 2011). The study further suggests that phosphate and iron-rich phases (such as pyromorphite and Fe oxyhydroxides) are primary Pb bearing mineral phases and Pb sinks in these soils

Experiments have shown that when Pb and P are present in the same environnement, pyromorphite formation in soil solution is possible (Zhang et al., 1998); it is stable between pH 4 and 5 and, thus, soil solutions of the Stengbach catchment have appropriate conditions for the pyromorphite formation. The correlations between $WECE_N$ of Pb, P and Fe support the suggestion of the presence of pyromorphite below 16 cm depth (Fig.10). Numerous column experiments with solid humic acids and different metal cations showed that Pb is the most sorbed element during the whole experiment (Cezikova et al., 2001). Lead is easily linked with solid OM and, therefore, Pb and OM show similar depth dependent distributions (Fig.11). The correlations in Figs.10 and 11 also emphasize, in agreement with Sipos et al. (2005), the importance of Fe oxihydroxides and OM for the stabilization of Pb in soils.

The $WECE_N$ values of Pb and the Pb concentrations in soil solutions are comparatively important (Table 4) and suggest that Pb is very labile in this acidic OM enriched soil (discussed above 5.1.). It appears that the pH is an important factor and controls adsorption, complexation and precipitation of Pb (Sauvé et al., 1998; Martinez et al., 2004; Izquierdo et al., 2012); at low pH (<4), the solubility of Pb increases and might form complexes with soluble ligands present in soils (Martinez et al., 2004). It has been shown that there

is a close relationship between Pb and labile OM (Egli et al., 2010; Van Praagh et al., 2009). Other studies indicate that Pb is preferentially coordinated with a carboxylic acid function of DOM (Kurková et al., 2004; Cornard and Lapouge 2007). This organic functional group has been mainly observed in the upper soil compartment where soil solutions are enriched in Pb (Table 6). Park et al. (2011) and Debela et al. (2013) have shown that low molecular weight organic acids, produced from rhizosphere or bacteria, inhibit the precipitation of Pb. These molecules are more mobile than clay-humic complexes and can enhance the lability of Pb. Atmospheric Pb enters the labile soil pool potentially in the soluble form ($PbSO_4$), contributes to the soil-soil solution exchange (Izquierdo et al., 2012) and moves faster than the less soluble Pb oxides or oxihydroxides which form organo-metallic complexes with soil OM or precipitate. Therefore, the lability of Pb strongly depends on the soluble or poorly soluble form of atmospheric deposits, the soil pH and the nature of the molecule of DOM. In function of these parameters, Pb might show different mobilities and speeds of migration in soils, a phenomenon previously observed for atmosphere-derived Pb in soils of the Strengbach catchment (Stille et al., 2011).

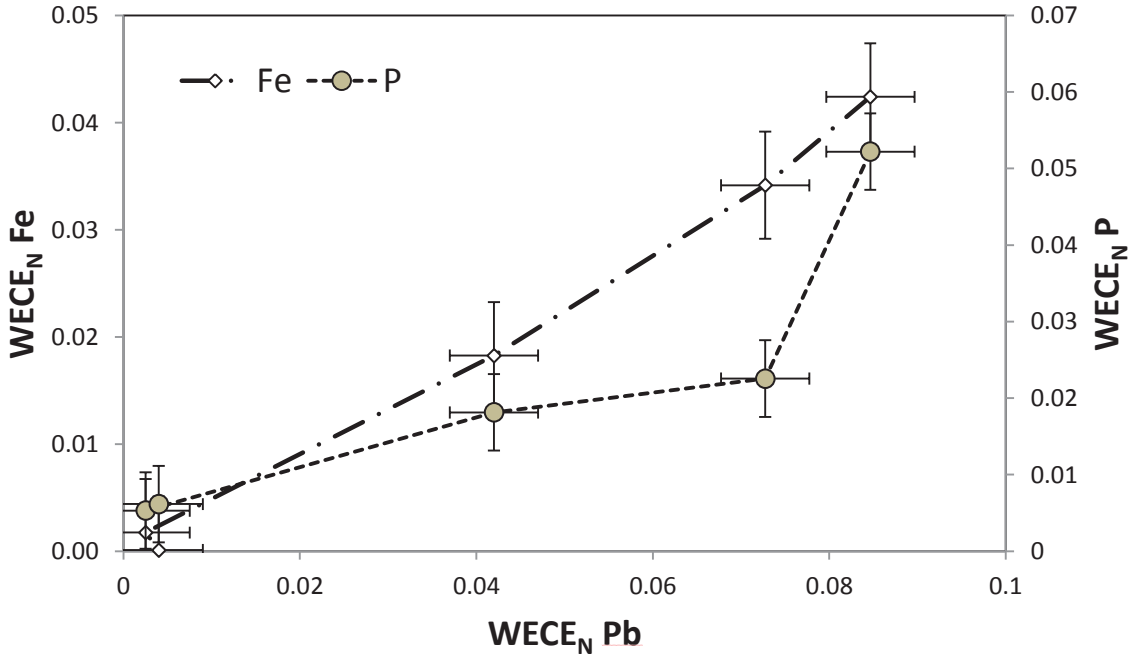

Figure 10 : Relation between WECEN of Pb, Fe and P for different depths

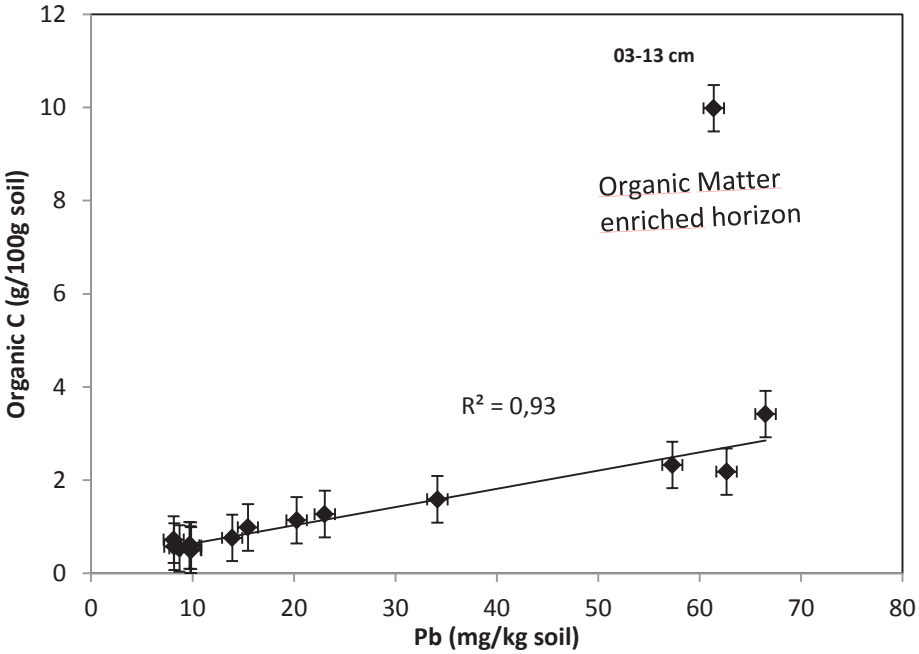

Figure 11 : Correlation between Pb and organic carbon

5.6. **The migration behavior of REE**

Rare earth elements are found together with Pb in the same cluster (Fig.8). Nevertheless, they do not show the same behavior as indicated by the variation of their concentrations in the soil solutions and soil profile; i.e. the REE enrichment profile is different to that of Pb (Fig.3). Lead is especially enriched at the surface while REE manifest specific zones of accumulation. More particularly, between 0 and 10 cm depth, only LREE are slightly enriched (1.1) compared to the HREE and MREE (0.9). This might be the result of vegetation controlled recycling of the LREE (Stille et al., 2006, 2009) or of contributions of fertilizer-derived atmospheric particles enriched in LREE (Aubert et al., 2002). The immobilization of the LREE at close to the surface might be controlled by the precipitation of secondary REE-bearing minerals (Braun and Pagel, 1994) such as florencite or rhabdophane as observed in soils of the Strengbach catchment (Stille et al., 2009). Below 10cm depth, the MREE and especially HREE are enriched than LREE. These enrichments might on one hand be related to increasing presence of primary minerals such as MREE-enriched apatite and HREE-enriched zircon (Aubert

et al., 2001). On the other hand, it might be related to the aromaticity which increases with depth (see below).

Soil solutions (SS) of the Strengbach Catchment

	Pb (µg/L)	Al (µmol/L)	Fe (µmol/L)	DOC (mmolC/L)	Al/(Al+Fe)	Fe/(Al+Fe)
12/11/2009						
5cm	12.4	21.6	8.17	3.42	72.6	27.4
10cm	7.1	26.4	5.77	2.21	82.1	17.9
30cm	4.5	29.5	3.92	2.23	88.3	11.7
60cm	1.1	6.6	0.10	0.92	98.5	1.5
19/03/2010						
5cm	13.9	27.0	9.31	1.74	74.4	25.6
10cm	6.3	29.8	6.27	0.88	82.6	17.4
30cm	2.2	19.4	3.04	0.54	86.5	13.5
60cm	0.2	10.9	0.25	0.20	97.8	2.2
20/11/2012						
5cm	12.5	12.6	6.80	2.17	65.0	35.0
10cm	7.5	21.1	7.70	1.42	73.3	26.7
30cm	2.6	18.1	5.01	1.01	78.3	21.7
60cm	0.3	8.9	0.18	0.24	98.0	2.0
uncertainty	*0.05*	*0.08*	*0.05*	*0.04*	*0.4*	*0.6*

depth	**Soil (S) VP2**	**depth**	**Water extract (WE)**
	S Al/Fe		WE Al/Fe
03-13 cm	3.1	03-13 cm	0.44
13-16 cm	2.9	13-16 cm	0.31
21-30 cm	2.8	21-30 cm	0.29
56-60 cm	2.7	56-60 cm	0.70
90-96 cm	2.7	90-96 cm	2.86
uncertainty	*0.2*	*uncertainty*	*0.02*

Table 6: Pb, Al ,Fe and DOC concentration in different soil solutions, Al/Fe in soil profile and water extracts

The values of $WECE_N$ for REE are similar to those of Si, Y, Zr and Ti (Table 4) and decrease with depth. LREE are less water extractable than MREE. MREE enrichments have been observed when REE have been mixed with humic acids at acidic pH (Pourret et al., 2007) or in waters where REE speciations are dominated by organic colloidal complexes (Tang and Johannesson, 2010).

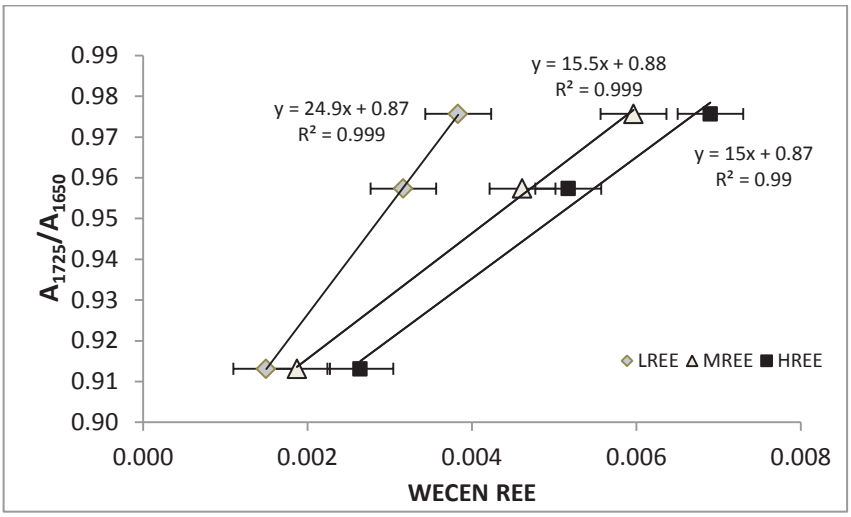

Figure 12 : Correlation between WECEN of REE with A_{1725}/A_{1650} (infrared absorbance)

Figure 12 shows the co-variations between the $WECE_N$ for REE and the ratios of absorbance ($A_{1725cm-1}/A_{1650cm-1}$), corresponding to the evolution of the carboxylic group relative to the aromatic group in the OM enriched soil compartment (Table 5). One observes that the LREE (slope = 24.9) are less water extractable than HREE and MREE (slope = 15) when the carboxylic group decreases relative to the aromaticity. This confirms earlier observations that LREE are preferentially bound to carboxylic groups whereas HREE are preferentially bound to carboxy-phenolic and phenolic groups (Marsac et al., 2012). The DOC and particularly the carboxylic function progressively degrades with depth, while hydrophobic and aromatic compounds are stabilized by sorption to soil minerals (see discussion above 5.1). Thus, LREE are more available for co-precipitation with secondary minerals (e.g. observed rhabdophane in Stille et al. (2009) throughout the soil profile whereas HREE and MREE are preferentially bonded to aromatic compounds; the HREE distribution within the soil profile is similar to that of the aromaticity reaching a maximal value at 30 cm depth (Table3 and Fig3). The ratio of $WECE_NPr/WECE_NYb$ ($WEPr_N/Yb_N$) is constant until 10cm depth, increases at 30 cm depth and, below, becomes constant again. The ratio SPr_N/Yb_N for the soil evolves like that of the water extracts except at 30 cm depth where the ratio decreases (Table 7). This is in accordance with the fact that the HREE are more adsorbed by the soil at this depth than the LREE

because of the enrichment in aromatic compounds at this depth. By comparing the Pr_N/Yb_N ratio of the water extracts with those of different soil solution ratios, one observes some differences but also similarities (Table 7):

*WE Pr_N/Yb_N is constant between 3 and 16 cm depth whereas SS Pr_N/Yb_N slightly decreases from 0.80 at 5 cm depth to 0.74 at 10 cm depth. This results from Pr (LREE) enrichment in the soil solution of the upper soil compartment caused by vegetation controlled LREE recycling and/or atmospheric depositions (see above).

* WE Pr_N/Yb_N and SS Pr_N/Yb_N show similar depth dependent distributions including the enrichment at 30 cm depth. It results from Yb depletion at this depth and enrichment in the deeper soil compartment compared to Pr.

The dotted lines represent extrapolation lines between $WECE_N$HREE or $WECE_N$LREE with $WECE_N$ Al or $WECE_N$ Fe (larger dots for Al and smaller dots for Fe) for samples from soils depleted in OM (40 cm to 96 cm). Similar to Marsac et al. (2012; 2013) one might suggest that there is competition between Fe^{3+}, Al^{3+} and REE for the binding with DOC. They have a high affinity with the same organic functional groups which is confirmed by the classification scheme (Fig.8). The studies of Marsac et al. suggest that at acidic pH and low metal/DOC ratios, Fe^{3+} and Al^{3+} compete more with HREE than LREE; moreover, at high metal/DOC ratios and acidic pH, Al^{3+} competes with LREE. The Fig. 13 showing the variations of WECEN for Al and Fe in function of $WECE_N$ LREE and HREE confirms Marsac et al.'s observations. The slope of the extrapolation line resulting from $WECE_N$ Al and HREE values remains rather unchanged for the OM depleted and enriched soil compartments; thus, the change in the metal/DOC ratio in the soil does not change the extraction behavior of Al and HREE. However, the $WECE_N$ Fe strongly increase compared to the corresponding HREE values in the OM enriched compartment pointing to the competition between Fe and HREE. Alternatively, one observes that the $WECE_N$ Fe and LREE values in the OM enriched compartment plot on the extrapolation line derived from OM depleted soil samples. Thus, in this case, the change in the metal/DOC

ratio does not affect the extraction behavior of Fe and LREE. However, the $WECE_N$ values for Al and corresponding LREE of samples from the OM enriched soil compartment plot below the extrapolation line and point to the competition between Al and LREE. These results are also in agreement with the REE distribution pattern of the soil solutions from the same site which are at greater depth LREE depleted (Stille et al., 2009).

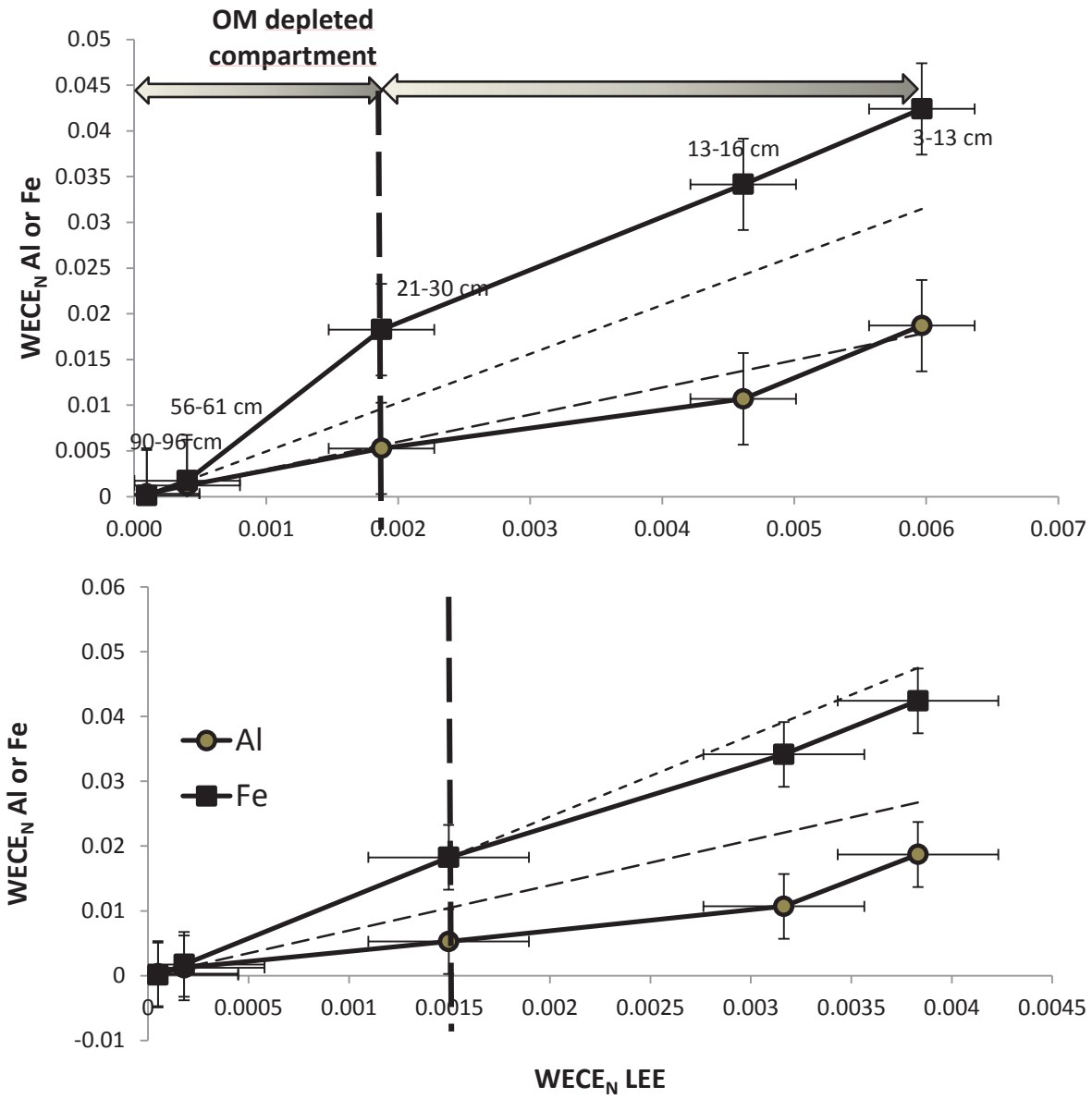

Figure 13: Variation of $WECE_N$ of HREE and LREE with $WECE_N$ of Al and Fe.

	$SS_{\Sigma REE}$ (µg/l)	$SS_{LREE_{UCC}}$	$SS_{MREE_{UCC}}$	$SS_{HREE_{UCC}}$	$SS_{LREE_{UCC}}/SS_{HREE_{UCC}}$	SS_{Pr_N/Yb_N}
12/11/2009						
5cm	0.96	0.006	0.012	0.008	0.73	0.80
10cm	0.76	0.004	0.009	0.006	0.71	0.74
30cm	0.82	0.005	0.008	0.005	0.83	0.94
60cm	0.06	0.000	0.001	0.004	0.09	0.31
19/03/2010						
5cm	1.27	0.008	0.017	0.010	0.78	0.76
10cm	1.04	0.006	0.015	0.013	0.70	0.61
30cm	0.86	0.005	0.010	0.006	0.81	0.84
60cm	0.12	0.001	0.002	0.002	0.48	0.34
20/11/2012						
5cm	0.68	0.004	0.009	0.005	0.75	0.79
10cm	0.76	0.004	0.010	0.006	0.68	0.68
30cm	0.94	0.005	0.011	0.006	0.92	1.01
60cm	0.11	0.001	0.002	0.002	0.27	0.19
uncertainty	*0.02*	*0.001*	*0.0008*	*0.0005*	*0.05*	*0.05*

depth	Soil (S) VP2			depth	Water extract (WE)	
	$S_{\Sigma REE}$ (g.kg-1)	$S_{LREE_{UCC}}/S_{HREE_{UCC}}$	S_{Pr_N/Yb_N}		$WE_{LREE_N/HREE_N}$	WE_{Pr_N/Yb_N}
03-13 cm	127	1.34	1.37	03-13 cm	0.64	0.58
13-16 cm	153	1.34	1.39	13-16 cm	0.69	0.58
21-30 cm	175	1.04	1.06	21-30 cm	0.80	0.73
56-60 cm	165	1.34	1.35	56-60 cm	0.45	0.41
90-96 cm	171	1.19	1.22	90-96 cm	0.52	0.43
uncertainty	*1*	*0.05*	*0.05*	*uncertainty*	*0.05*	0.05

Table 7: REE concentration and Pr/Yb in different soil solutions, soil profile and water extracts

6. Conclusion

The study of WEOC fractions characterized the DOC in the OM enriched compartment of the acidic forest soil in the Strengbach catchment.

More particularly, the infrared spectra showed a modification of the molecular structure with depth, i.e. a decrease of the polar compounds such as polysaccharides and an increase of the less polar hydro-carbon functional groups. This partial modification and degradation permits OM stabilization at 30cm depth with a maximum aromaticity. Moreover, the different structural changes of the DOC have an impact on the ion exchange and the cation complexation and, therefore, on the biodisponibility of nutrients elements such as Ca and Mg in the soil. Consequently, the modification of the DOC is accompanied by a change in the trace elements behavior. Indeed, a HAC of the $WECE_N$ in the OM enriched compartment reveals relationships between trace element behavior and organic functional group variation.

*Lead is preferentially bound to the carboxylic acid function of DOC mainly present in the upper soil compartment. Its mobility strongly depends on the evolution of this organic function but also on its speciation, i.e. soluble or poorly soluble. The less soluble Pb forms organo-metallic complexes with soil OM; the soluble Pb moves more rapidly in soil solutions.

*Rare earth elements behave similarly to Fe, V and Cr with a good affinity to carboxy-phenolic and phenolic groups of DOC. LREE are less water extractable than HREE and the experimental results indicated that HREE are compared to LREE preferentially bound to aromatic functional group. This different behavior fractionates the REE pattern of soil solutions at 30cm depth due to the here observed aromaticity enrichment of DOC.

These different affinities for the organic functional groups of DOC explain some aspects of the behavior of trace elements in soil solutions and in the soil profile, competition between trace elements in the complexation with DOC, preferential trace element adsorption on soil particles, or selective co-precipitation according to pH and redox conditions are important factors controlling trace element fractionation, migration and bioavailability in the soil profile.

The comparison between soil solutions and WEOM fractions highlight similarities and differences in the trace element behaviors. Indeed, the here presented study on the WEOM fractions considers only the horizontal

interlayer of soils; for future studies it would be of interest to perform the same experimentations by using soil solutions instead of UHP water also in order to consider the impact of the gravitational downward water flow.

7. References

Aiuppa A., Allard P., D'Alessandro W., Michel A., Parello F., Treuil M., Valenza M., (2000). Mobility and fluxes of major, minor and trace metals during basalt weathering and groundwater transport at Mt. Etna volcano (Sicily). *Geochimica et Cosmochimica Acta* **64**, 1827-1841.

Aubert D., Stille P., Probst A., Gauthier-Lafaye F., Pourcelot L., Del Nero M., (2002). Characterization and migration of atmospheric REE in soils and surface waters. *Geochimica et Cosmochimica Acta* **66**, 3339-3350.

Aubert D., Stille P., Probst A., (2001). REE fractionation during granite weathering and removal by waters and suspended loads: Sr and Nd isotopic evidence. *Geochimica et Cosmochimica Acta* **65**, 387-406.

Bauer M., Fulda B., Blodau C., (2008). Groundwater derived arsenic in high carbonate wetland soils: Sources, sinks, and mobility. *Science of The Total Environment* **401**, 109-120.

Bednar A. J., Medina V. F., Ulmer-Scholle D. S., Frey B. A., Johnson B. L., Brostoff W. N., Larson S. L., (2007). Effects of organic matter on the distribution of uranium in soil and plant matrices. *Chemosphere* **70**, 237-247.

Berg B., (2000). Litter decomposition and organic matter turnover in northern forest soils. *Forest Ecology and Management* **133**, 13-22.

Bismondo A., Di Bernardo P., Zanonato P., Jiang J., Rao L., (2003). Complexation of thorium(iv) with 2-furoic acid and 2-thenoic acid in aqueous solution. *Dalton Transactions* **0**, 469-474.

Boyer T. H., Miller C. T., Singer P. C., (2008). Modeling the removal of dissolved organic carbon by ion exchange in a completely mixed flow reactor. *Water Research* **42**, 1897-1906.

Bradl H. B., (2004). Adsorption of heavy metal ions on soils and soils constituents. *Journal of Colloid and Interface Science* **277**, 1-18.

Braun J.-J., Pagel M., (1994). Geochemical and mineralogical behavior of REE, Th and U in the Akongo lateritic profile (SW Cameroon). *CATENA* **21**, 173-177.

Buurman P., Jongmans A. G., (2005). Podzolisation and soil organic matter dynamics. *Geoderma* **125**, 71-83.

Cabaniss S. E., (1992). Synchronous Fluorescence Spectra of Metal-Fulvic Acid Complexes. *Environmental Science & Technology* **26**, 1133-1139.

Caille N., Swanwick S., Zhao F. J., McGrath S. P., (2004). Arsenic hyperaccumulation by Pteris vittata from arsenic contaminated soils and the effect of liming and phosphate fertilisation. *Environmental Pollution* **132**, 113-120.

Cenki-Tok B., Chabaux F., Lemarchand D., Schmitt A. D., Pierret M. C., Viville D., Bagard M. L., Stille P., (2009). The impact of water–rock interaction and vegetation on calcium isotope fractionation in soil- and stream waters of a small, forested catchment (the Strengbach case). *Geochimica et Cosmochimica Acta* **73**, 2215-2228.

Čežíková J., Kozler J., Madronová L., Novák J. r., Janoš P., (2001). Humic acids from coals of the North-Bohemian coal field: II. Metal-binding capacity under static conditions. *Reactive and Functional Polymers* **47**, 111-118.

Chantigny M. H., (2003). Dissolved and water-extractable organic matter in soils: a review on the influence of land use and management practices. *Geoderma* **113**, 357-380.

Chorover J., Amistadi M. K., Chadwick O. A., (2004). Surface charge evolution of mineral-organic complexes during pedogenesis in Hawaiian basalt. *Geochimica et Cosmochimica Acta* **68**, 4859-4876.

Chorover J., Sposito G., (1995). Dissolution behavior of kaolinitic tropical soils. *Geochimica et Cosmochimica Acta* **59**, 3109-3121.

Cornard J.-P., Lapouge C., (2007). Modelling of electronic absorption spectrum of Pb(II)–caffeate complex by time-dependent density functional theory. *Chemical Physics Letters* **438**, 41-46.

Corvasce M., Zsolnay A., D'Orazio V., Lopez R., Miano T. M., (2006). Characterization of water extractable organic matter in a deep soil profile. *Chemosphere* **62**, 1583-1590.

Dangleterre L., Cornard J.-P., (2005). Interaction of lead (II) chloride with hydroxyflavones in methanol: A spectroscopic study. *Polyhedron* **24**, 1593-1598.

Debela F., Arocena J. M., Thring R. W., Whitcombe T., (2013). Organic acids inhibit the formation of pyromorphite and Zn-phosphate in phosphorous amended Pb- and Zn-contaminated soil. *Journal of Environmental Management* **116**, 156-162.

Demiate I. M., Dupuy N., Huvenne J. P., Cereda M. P., Wosiacki G., (2000). Relationship between baking behavior of modified cassava starches and starch chemical structure determined by FTIR spectroscopy. *Carbohydrate Polymers* **42**, 149-158.

Don A., Kalbitz K., (2005). Amounts and degradability of dissolved organic carbon from foliar litter at different decomposition stages. *Soil Biol Biochem* **37**, 2171-2179.

Egli M., Sartori G., Mirabella A., Giaccai D., Favilli F., Scherrer D., Krebs R., Delbos E., (2010). The influence of weathering and organic matter on heavy metals lability in silicatic, Alpine soils. *Science of The Total Environment* **408**, 931-946.

Fichter J., Turpault M. P., Dambrine E., Ranger J., (1998). Mineral evolution of acid forest soils in the Strengbach catchment (Vosges mountains, N-E France). *Geoderma* **82**, 315-340.

Fiol S., López R., Ramos A., Antelo J. M., Arce F., (1999). Study of the acid–base properties of three fulvic acids extracted from different horizons of a soil. *Analytica Chimica Acta* **385**, 443-449.

Frohne T., Rinklebe J., Diaz-Bone R. A., Du Laing G., (2011). Controlled variation of redox conditions in a floodplain soil: Impact on metal mobilization and biomethylation of arsenic and antimony. *Geoderma* **160**, 414-424.

Guan X.-H., Chen G.-H., Shang C., (2006a). Combining kinetic investigation with surface spectroscopic examination to study the role of aromatic carboxyl groups in NOM adsorption by aluminum hydroxide. *Journal of Colloid and Interface Science* **301**, 419-427.

Guan X.-H., Shang C., Chen G.-H., (2006b). ATR-FTIR investigation of the role of phenolic groups in the interaction of some NOM model compounds with aluminum hydroxide. *Chemosphere* **65**, 2074-2081.

Guéguen F., Stille P., Dietze V., Gieré R., (2012). Chemical and isotopic properties and origin of coarse airborne particles collected by passive samplers in industrial, urban, and rural environments. *Atmospheric Environment* **62**, 631-645.

Gustafsson J. P., van Hees P., Starr M., Karltun E., Lundström U., (2000). Partitioning of base cations and sulphate between solid and dissolved phases in three podzolised forest soils. *Geoderma* **94**, 311-333.

Haberhauer G., Gerzabek M. H., (1999). Drift and transmission FT-IR spectroscopy of forest soils: an approach to determine decomposition processes of forest litter. *Vibrational Spectroscopy* **19**, 413-417.

Hernandez L., Probst A., Probst J. L., Ulrich E., (2003). Heavy metal distribution in some French forest soils: evidence for atmospheric contamination. *Science of The Total Environment* **312**, 195-219.

Hunt C. D., (1981). Regulation of sedimentary cation exchange capacity by organic matter. *Chemical Geology* **34**, 131-149.

Izquierdo M., Tye A. M., Chenery S. R., (2012). Sources, lability and solubility of Pb in alluvial soils of the River Trent catchment, U.K. *Science of The Total Environment* **433**, 110-122.

Jouraiphy A., Amir S., Winterton P., El Gharous M., Revel J. C., Hafidi M., (2008). Structural study of the fulvic fraction during composting of activated sludge–plant matter: Elemental analysis, FTIR and 13C NMR. *Bioresource Technology* **99**, 1066-1072.

Kaiser K., Guggenberger G., Haumaier L., Zech W., (2002). The composition of dissolved organic matter in forest soil solutions: changes induced by seasons and passage through the mineral soil. *Organic Geochemistry* **33**, 307-318.

Kalbitz K., Schwesig D., Rethemeyer J., Matzner E., (2005). Stabilization of dissolved organic matter by sorption to the mineral soil. *Soil Biology and Biochemistry* **37**, 1319-1331.

Kalbitz K., Schmerwitz J., Schwesig D., Matzner E., (2003). Biodegradation of soil-derived dissolved organic matter as related to its properties. *Geoderma* **113**, 273-291.

Kalbitz K., Geyer S., Geyer W., (2000). A comparative characterization of dissolved organic matter by means of original aqueous samples and isolated humic substances. *Chemosphere* **40**, 1305-1312.

Kalbitz K., Geyer W., Geyer S., (1999). Spectroscopic properties of dissolved humic substances - a reflection of land use history in a fen area. *Biogeochemistry* **47**, 219-238.

Kummert R., Stumm W., (1980). The surface complexation of organic acids on hydrous γ-Al2O3. *Journal of Colloid and Interface Science* **75**, 373-385.

Kurková M., Klika Z., Kliková C., Havel J., (2004). Humic acids from oxidized coals: I. Elemental composition, titration curves, heavy metals in HA samples, nuclear magnetic resonance spectra of HAs and infrared spectroscopy. *Chemosphere* **54**, 1237-1245.

Lapouge C., Cornard J.-P., (2010). Theoretical study of the Pb(II)–catechol system in dilute aqueous solution: Complex structure and metal coordination sphere determination. *Journal of Molecular Structure* **969**, 88-96.

Lemarchand D., Cividini D., Turpault M. P., Chabaux F., (2012). Boron isotopes in different grain size fractions: Exploring past and present water–rock interactions from two soil profiles (Strengbach, Vosges Mountains). *Geochimica et Cosmochimica Acta* **98**, 78-93.

Lemarchand E., Chabaux F., Vigier N., Millot R., Pierret M.-C., (2010). Lithium isotope systematics in a forested granitic catchment (Strengbach, Vosges Mountains, France). *Geochimica et Cosmochimica Acta* **74**, 4612-4628.

Lin J.-G., Chen S.-Y., (1998). The relationship between adsorption of heavy metal and organic matter in river sediments. *Environment International* **24**, 345-352.

Lorenz K., Preston C. M., Raspe S., Morrison I. K., Feger K. H., (2000). Litter decomposition and humus characteristics in Canadian and German spruce ecosystems: information from tannin analysis and 13C CPMAS NMR. *Soil Biology and Biochemistry* **32**, 779-792.

Marsac R., Davranche M., Gruau G., Dia A., Pédrot M., Le Coz-Bouhnik M., Briant N., (2013). Effects of Fe competition on REE binding to humic acid: Origin of REE pattern variability in organic waters. *Chemical Geology* **342**, 119-127.

Marsac R., Davranche M., Gruau G., Dia A., Bouhnik-Le Coz M., (2012). Aluminium competitive effect on rare earth elements binding to humic acid. *Geochimica et Cosmochimica Acta* **89**, 1-9.

Marsac R., Davranche M., Gruau G., Bouhnik-Le Coz M., Dia A., (2011). An improved description of the interactions between rare earth elements and humic acids by modeling: PHREEQC-Model VI coupling. *Geochimica et Cosmochimica Acta* **75**, 5625-5637.

Marsac R., Davranche M., Gruau G., Dia A., (2010). Metal loading effect on rare earth element binding to humic acid: Experimental and modelling evidence. *Geochimica et Cosmochimica Acta* **74**, 1749-1761.

Martínez C. E., Jacobson A. R., McBride M. B., (2004). Lead Phosphate Minerals: Solubility and Dissolution by Model and Natural Ligands. *Environmental Science & Technology* **38**, 5584-5590.

McCarthy J. F., Gu B., Liang L., Mas-Pla J., Williams T. M., Yeh T. C. J., (1996). Field Tracer Tests on the Mobility of Natural Organic Matter in a Sandy Aquifer. *Water Resources Research* **32**, 1223-1238.

McGILL W. B., CANNON K. R., ROBERTSON J. A., COOK F. D., (1986). DYNAMICS OF SOIL MICROBIAL BIOMASS AND WATER-SOLUBLE ORGANIC C IN BRETON L AFTER 50 YEARS OF CROPPING TO TWO ROTATIONS. *Canadian Journal of Soil Science* **66**, 1-19.

McKnight D. M., Wershaw R. L., Bencala K. E., Zellweger G. W., Feder G. L., (1992). Humic substances and trace metals associated with Fe and Al oxides deposited in an acidic mountain stream. *Science of The Total Environment* **117–118**, 485-498.

Middelburg J. J., van der Weijden C. H., Woittiez J. R. W., (1988). Chemical processes affecting the mobility of major, minor and trace elements during weathering of granitic rocks. *Chemical Geology* **68**, 253-273.

Murphy E. M., Zachara J. M., (1995). The role of sorbed humic substances on the distribution of organic and inorganic contaminants in groundwater. *Geoderma* **67**, 103-124.

Nierop K. G. J. J., Jansen B., Verstraten J. M., (2002). Dissolved organic matter, aluminium and iron interactions: precipitation induced by metal/carbon ratio, pH and competition. *Science of The Total Environment* **300**, 201-211.

Oh S. Y., Yoo D. I., Shin Y., Kim H. C., Kim H. Y., Chung Y. S., Park W. H., Youk J. H., (2005). Crystalline structure analysis of cellulose treated with sodium hydroxide and carbon dioxide by means of X-ray diffraction and FTIR spectroscopy. *Carbohydrate Research* **340**, 2376-2391.

Ohno T., Fernandez I. J., Hiradate S., Sherman J. F., (2007). Effects of soil acidification and forest type on water soluble soil organic matter properties. *Geoderma* **140**, 176-187.

Oorts K., Vanlauwe B., Merckx R., (2003). Cation exchange capacities of soil organic matter fractions in a Ferric Lixisol with different organic matter inputs. *Agriculture, Ecosystems & Environment* **100**, 161-171.

Osher L. J., Buol S. W., (1998). Relationship of soil properties to parent material and landscape position in eastern Madre de Dios, Peru. *Geoderma* **83**, 143-166.

Park J. H., Bolan N., Megharaj M., Naidu R., (2011). Concomitant rock phosphate dissolution and lead immobilization by phosphate solubilizing bacteria (Enterobacter sp.). *Journal of Environmental Management* **92**, 1115-1120.

Pohlman A. A., McColl J. G., (1988). Soluble Organics from Forest Litter and their Role in Metal Dissolution. *Soil Sci. Soc. Am. J.* **52**, 265-271.

Pokrovsky O. S., Dupré B., Schott J., (2005). Fe–Al–organic Colloids Control of Trace Elements in Peat Soil Solutions: Results of Ultrafiltration and Dialysis. *Aquatic Geochemistry* **11**, 241-278.

Pokrovsky O. S., Schott J., (2002). Iron colloids/organic matter associated transport of major and trace elements in small boreal rivers and their estuaries (NW Russia). *Chemical Geology* **190**, 141-179.

Pourret O., Davranche M., Gruau G., Dia A., (2007). Organic complexation of rare earth elements in natural waters: Evaluating model calculations from ultrafiltration data. *Geochimica et Cosmochimica Acta* **71**, 2718-2735.

Prescott C. E., Maynard D. G., Laiho R., (2000). Humus in northern forests: friend or foe? *Forest Ecology and Management* **133**, 23-36.

Probst A., El Gh'mari A., Aubert D., Fritz B., McNutt R., (2000). Strontium as a tracer of weathering processes in a silicate catchment polluted by acid atmospheric inputs, Strengbach, France. *Chemical Geology* **170**, 203-219.

Raulund-Rasmussen K., Borggaard O. K., Hansen H. C. B., Olsson M., (1998). Effect of natural organic soil solutes on weathering rates of soil minerals. *European Journal of Soil Science* **49**, 397-406.

Reiller P., Moulin V., Casanova F., Dautel C., (2002). Retention behaviour of humic substances onto mineral surfaces and consequences upon thorium (IV) mobility: case of iron oxides. *Applied Geochemistry* **17**, 1551-1562.

Reimann C., Arnoldussen A., Finne T. E., Koller F., Nordgulen Ø., Englmaier P., (2007). Element contents in mountain birch leaves, bark and wood under different anthropogenic and geogenic conditions. *Applied Geochemistry* **22**, 1549-1566.

Reimann C., de Caritat P., (2005). Distinguishing between natural and anthropogenic sources for elements in the environment: regional geochemical surveys versus enrichment factors. *Science of The Total Environment* **337**, 91-107.

Rihs S., Prunier J., Thien B., Lemarchand D., Pierret M.-C., Chabaux F., (2011). Using short-lived nuclides of the U- and Th-series to probe the kinetics of colloid migration in forested soils. *Geochimica et Cosmochimica Acta* **75**, 7707-7724.

Riotte J., Chabaux F., (1999). (234U/238U) activity ratios in freshwaters as tracers of hydrological processes: the Strengbach watershed (Vosges, France). *Geochimica et Cosmochimica Acta* **63**, 1263-1275.

Ritchie J. D., Perdue E. M., (2003). Proton-binding study of standard and reference fulvic acids, humic acids, and natural organic matter. *Geochimica et Cosmochimica Acta* **67**, 85-96.

Römkens P. F. A. M., Dolfing J., (1998). Effect of Ca on the Solubility and Molecular Size Distribution of DOC and Cu Binding in Soil Solution Samples. *Environmental Science & Technology* **32**, 363-369.

Ruiz Sinoga J. D., Pariente S., Diaz A. R., Martinez Murillo J. F., (2012). Variability of relationships between soil organic carbon and some soil properties in Mediterranean rangelands under different climatic conditions (South of Spain). *CATENA* **94**, 17-25.

Said-Pullicino D., Erriquens F. G., Gigliotti G., (2007). Changes in the chemical characteristics of water-extractable organic matter during composting and their influence on compost stability and maturity. *Bioresour Technol* **98**, 1822-1831.

Sauvé S., McBride M., Hendershot W., (1998). Lead Phosphate Solubility in Water and Soil Suspensions. *Environmental Science & Technology* **32**, 388-393.

Schwanninger M., Rodrigues J. C., Pereira H., Hinterstoisser B., (2004). Effects of short-time vibratory ball milling on the shape of FT-IR spectra of wood and cellulose. *Vibrational Spectroscopy* **36**, 23-40.

Sipos P., Németh T., Mohai I., Dódony I., (2005). Effect of soil composition on adsorption of lead as reflected by a study on a natural forest soil profile. *Geoderma* **124**, 363-374.

Sjöberg G., Nilsson S. I., Persson T., Karlsson P., (2004). Degradation of hemicellulose, cellulose and lignin in decomposing spruce needle litter in relation to N. *Soil Biology and Biochemistry* **36**, 1761-1768.

Smith D. S., Kramer J. R., (1998). Multi-site aluminum speciation with natural organic matter using multiresponse fluorescence data. *Analytica Chimica Acta* **363**, 21-29.

Stadler B., Schramm A., Kalbitz K., (2006). Ant-mediated effects on spruce litter decomposition, solution chemistry, and microbial activity. *Soil Biology and Biochemistry* **38**, 561-572.

Stille P., Pourcelot L., Granet M., Pierret M. C., Guéguen F., Perrone T., Morvan G., Chabaux F., (2011). Deposition and migration of atmospheric Pb in soils from a forested silicate catchment today and in the past (Strengbach case): Evidence from 210Pb activities and Pb isotope ratios. *Chemical Geology* **289**, 140-153.

Stille P., Pierret M. C., Steinmann M., Chabaux F., Boutin R., Aubert D., Pourcelot L., Morvan G., (2009). Impact of atmospheric deposition, biogeochemical cycling and water–mineral interaction on REE fractionation in acidic surface soils and soil water (the Strengbach case). *Chemical Geology* **264**, 173-186.

Stille P., Steinmann M., Pierret M. C., Gauthier-Lafaye F., Chabaux F., Viville D., Pourcelot L., Matera V., Aouad G., Aubert D., (2006). The impact of vegetation on REE fractionation in stream waters of a small forested catchment (the Strengbach case). *Geochimica et Cosmochimica Acta* **70**, 3217-3230.

Stolpe B., Guo L., Shiller A. M., Aiken G. R., (2013). Abundance, size distributions and trace-element binding of organic and iron-rich nanocolloids in Alaskan rivers, as revealed by field-flow fractionation and ICP-MS. *Geochimica et Cosmochimica Acta* **105**, 221-239.

TAKAMATSU T., AOKI H., YOSHIDA T., (1982). Determination of Arsenate, Arsenite, Monomethylarsonate, and Dimethylarsinate in Soil Polluted With Arsenic. *Soil Science* **133**, 239-246.

Tang J., Johannesson K. H., (2010). Ligand extraction of rare earth elements from aquifer sediments: Implications for rare earth element complexation with organic matter in natural waters. *Geochimica et Cosmochimica Acta* **74**, 6690-6705.

Tricca A., Stille P., Steinmann M., Kiefel B., Samuel J., Eikenberg J., (1999). Rare earth elements and Sr and Nd isotopic compositions of dissolved and suspended loads from small river systems in the Vosges mountains (France), the river Rhine and groundwater. *Chemical Geology* **160**, 139-158.

Tu C., Ma L. Q., Zhang W., Cai Y., Harris W. G., (2003). Arsenic species and leachability in the fronds of the hyperaccumulator Chinese brake (Pteris vittata L.). *Environmental Pollution* **124**, 223-230.

Turpeinen R., Pantsar-Kallio M., Häggblom M., Kairesalo T., (1999). Influence of microbes on the mobilization, toxicity and biomethylation of arsenic in soil. *Science of The Total Environment* **236**, 173-180.

Ussiri D. A. N., Johnson C. E., (2007). Organic matter composition and dynamics in a northern hardwood forest ecosystem 15 years after clear-cutting. *Forest Ecology and Management* **240**, 131-142.

Ussiri D. A. N., Johnson C. E., (2003). Characterization of organic matter in a northern hardwood forest soil by 13C NMR spectroscopy and chemical methods. *Geoderma* **111**, 123-149.

van Hees P. A. W., Lundström U. S., Giesler R., (2000). Low molecular weight organic acids and their Al-complexes in soil solution—composition, distribution and seasonal variation in three podzolized soils. *Geoderma* **94**, 173-200.

van Praagh M., Heerenklage J., Smidt E., Modin H., Stegmann R., Persson K. M., (2009). Potential emissions from two mechanically–biologically pretreated (MBT) wastes. *Waste Management* **29**, 859-868.

Vasyukova E. V., Pokrovsky O. S., Viers J., Oliva P., Dupré B., Martin F., Candaudap F., (2010). Trace elements in organic- and iron-rich surficial fluids of the boreal zone: Assessing colloidal forms via dialysis and ultrafiltration. *Geochimica et Cosmochimica Acta* **74**, 449-468.

Vergnoux A., Guiliano M., Di Rocco R., Domeizel M., Théraulaz F., Doumenq P., (2011). Quantitative and mid-infrared changes of humic substances from burned soils. *Environmental Research* **111**, 205-214.

Viville D., Chabaux F., Stille P., Pierret M. C., Gangloff S., (2012). Erosion and weathering fluxes in granitic basins: The example of the Strengbach catchment (Vosges massif, eastern France). *CATENA* **92**, 122-129.

Wang S., Terdkiatburana T., Tadé M. O., (2008). Adsorption of Cu(II), Pb(II) and humic acid on natural zeolite tuff in single and binary systems. *Separation and Purification Technology* **62**, 64-70.

Weber T., Allard T., Tipping E., Benedetti M. F., (2006). Modeling Iron Binding to Organic Matter†. *Environmental Science & Technology* **40**, 7488-7493.

Weishaar J. L., Aiken G. R., Bergamaschi B. A., Fram M. S., Fujii R., Mopper K., (2003). Evaluation of Specific Ultraviolet Absorbance as an Indicator of the Chemical Composition and Reactivity of Dissolved Organic Carbon. *Environmental Science & Technology* **37**, 4702-4708.

White A. F., Blum A. E., Schulz M. S., Vivit D. V., Stonestrom D. A., Larsen M., Murphy S. F., Eberl D., (1998). Chemical Weathering in a Tropical Watershed, Luquillo Mountains, Puerto Rico: I. Long-Term Versus Short-Term Weathering Fluxes. *Geochimica et Cosmochimica Acta* **62**, 209-226.

Zhang P., Ryan J. A., Yang J., (1998). In Vitro Soil Pb Solubility in the Presence of Hydroxyapatite. *Environmental Science & Technology* **32**, 2763-2768.

Zhou Y., Stuart-Williams H., Farquhar G. D., Hocart C. H., (2010). The use of natural abundance stable isotopic ratios to indicate the presence of oxygen-containing chemical linkages between cellulose and lignin in plant cell walls. *Phytochemistry* **71**, 982-993.

Zsolnay Á., (2003). Dissolved organic matter: artefacts, definitions, and functions. *Geoderma* **113**, 187-209.

Zsolnay A., 1996. Chapter 4 - Dissolved Humus in Soil Waters, in: Alessandro P. (Ed.), Humic Substances in Terrestrial Ecosystems. Elsevier Science B.V., Amsterdam, pp. 171-223

.

Chapitre 3

Factors controlling the chemical composition of colloidal and dissolved fractions in soil solutions and the mobility of trace elements in soils.

Article soumis à Geochimica et Cosmochimica Acta le 5 juin 2015

Résumé

Les fractions colloïdales et dissoutes de solutions de sol jouent des rôles différents dans le transport des éléments majeurs et traces dans les sols. L'un des objectifs de cette étude est de déterminer les processus et les conditions physico-chimiques qui influencent la composition des solutions de sol d'un sol forestier et le second d'élucider leur impact sur le transport d'éléments majeurs et traces à travers la fraction colloïdale (0,2 µm à 5 kDa) et la fraction dissoute (<5 kDa) dans le premier mètre du sol. Toutes les expériences ont été réalisées avec les solutions de sol obtenues par des plaques lysimétriques situées sur une parcelle expérimentale du bassin versant du Strengbach sous couvert d'épicéas. Les échantillons de surface filtrée à 0,2 µm ont permis de mettre en évidence l'influence de la décomposition de la litière sur la composition chimique des solutions de sol en surface ainsi que l'impact des conditions bio-géochimiques du sol (pH, humidité, température, oxique ou anoxique) sur la décomposition de la litière. Ainsi, dans les conditions anoxiques, la décomposition de la litière est plus importante et les solutions de sol sont enrichies en calcium, phosphore, manganèse et cuivre tandis que les autres le sont en aluminium et en fer. Les conditions physico-chimiques dans les horizons plus profonds du sol sont moins dépendants des conditions de surface et donc plus stables. Les fractions colloïdales et dissoutes des solutions du sol ont été obtenues par ultrafiltration tangentielles. Les résultats expérimentaux montrent que les éléments nutritifs comme les nitrates ou phosphates sont principalement dans la fraction dissoute et par conséquent plus bio-disponibles, révèlent que les minéraux secondaires peuvent être dissous et/ou précipités dans la fraction colloïdale comme pyromorphite ($Pb_5(PO_4)_3X$) et que l'activité bactérienne influence la composition des fractions colloïdales et dissoutes. L'activité bactérienne sélective peut enrichir la fraction colloïdale en Ca, Mn, Cu et P, diminuer les quantités V, Cr, Pb et Fe dans la fraction dissoute ou modifier les structures des molécules organiques. Les résultats sont importants pour une meilleure compréhension du rôle des fractions

colloïdales et dissoutes (< 5 kDa) dans le transport des éléments majeurs et traces dans la solution du sol et, plus particulièrement, dans la mobilité des polluants et la bio-disponibilité des nutriments pour un écosystème forestier.

Abstract

Colloidal and dissolved fractions of soil solutions play different roles in the transport of major and trace elements in soils. Therefore, one objective of this study was to determine the processes and physico-chemical conditions which affect the composition of the soil solutions of a forest soil and the second one to elucidate their impact on the major and trace element transport through the colloidal (0.2 µm to 5 kDa) and the dissolved (< 5 kDa) fractions in the first meter of the soil. All experiments have been performed with soil solutions obtained by lysimeter plates situated on an experimental spruce parcel of the Strengbach catchment. The surface samples filtered at 0.2 µm allowed to highlight the influence of the litter decomposition on the chemical composition of the upper soil solutions; and also, the impact of the soil bio-geochemical conditions (pH, moisture, temperature, oxic or anoxic, bacterial community) on the litter decomposition. Thus, in anoxic conditions, the litter decay is more important and the soil solutions are Ca, P, Mn and Zn enriched while others are Al and Fe enriched. The physico-chemical conditions in deeper soil horizons are less season dependent and thus more stable. The colloidal and dissolved fractions of the soil solutions have been obtained by tangential flow ultra-filtration. The experimental results show that nutrients like NO_3^- or P are principally in the dissolved fraction and consequently more bio-available, reveal that secondary minerals may be dissolved and/or precipitated in the colloidal fraction like pyromorphite ($Pb_5(PO_4)_3X$) and that bacterial activity influences the composition of the colloidal and dissolved fractions. Selective bacterial activity can enrich the colloidal fraction in Ca, Mn and P, diminish Pb, V, Cr and Fe amounts in the dissolved fraction or change of the organic carbon (OC) structures. The results are important for a better understanding of the role of the colloidal

and dissolved (<5 kDa) fractions in the transport of the major and trace elements in soil solutions and, more particularly, the mobility of the polluant and the bio-availability of nutrients for a forested ecosystem.

1. Introduction

The mobilization of major and trace elements in soils begins with the leaching of the soils surface by rain and/or throughfall. The resulting soil solution carries elements originating from litterfall decomposition, soil alteration and atmospheric deposition. It gravitates through the soil and allows the transport of metals, nutrients or pollutants towards deeper soil horizons. Therefore, it is important to understand the transport processes of these different components in soil solutions which control the availability of nutrients for the vegetation and the composition of surface waters (Aiuppa et al., 2000; Gustafsson et al., 2000; Bauer et al., 2008; Egli et al., 2010; Fraysse et al., 2010; Clarholm and Skyllberg, 2013).

The composition of soil solutions can be affected by various processes such as the adsorption of metals on soil organic matter or clays that delay migration but they continue to move after desorption (Bradl, 2004; Sipos et al., 2005; Meng et al., 2009; Wu et al., 2011; Filella and Williams, 2012). The seasonal alternation of wet and dry cycles changes the redox conditions of soil and soil solutions involving the changes in the mobility of their components due to different solubilities of e.g. Fe, Cu, Cr, Mn (Fuss et al., 2011; Miller et al., 2012; Fulda et al., 2013; Shaheen et al., 2014). These alternations of oxic and anoxic events govern also the bacterial activities that influence the composition of soil solutions by e.g. dissolution of soil particles in a selective manner to get specific nutrient elements required for their growth (Blum et al., 2002; Aouad et al., 2006; Gabor et al., 2014; Gangloff et al., 2014a; Kleber et al., 2015). The vegetation influences also the composition of soil solutions taking up nutrients by absorption or adsorption (Clarholm and Skyllberg, 2013) or by recycling after degradation of litterfall (Stille et al., 2006). Thus, the biochemical processes influence the composition of the soil solutions and more particularly the concentration of

dissolved or particulate OC which complexes cations as a function of the molecular size, the organic functional groups (Gangloff et al., 2014b) and its structural evolution with depth (Lorenz et al., 2000; Kaiser et al., 2002; Ussiri and Johnson, 2003; Don and Kalbitz, 2005; Ussiri and Johnson, 2007). These parameters influence the kind of the colloidal or dissolved phases in the soil solutions, and consequently the transport at the soil / soil solution interface.

Numerous ultra-filtration experiments have been performed with sea-water or surface waters (Ingri et al., 2000; Dahlqvist et al., 2004; Andersson et al., 2006; Singhal et al., 2006; Waeles et al., 2008; Liu et al., 2013) but only a few with soil solutions (van Hees et al., 2001; Pokrovsky et al., 2005; Pédrot et al., 2009) in order to better understand the transport mechanisms of major and trace elements. The main objective of this study was to elucidate the transport by the colloidal and dissolved phases in the first meter of the soil. It has been performed on soil solutions obtained by lysimeter plates installed in the previously studied forested Strengbach catchment (Riotte and Chabaux, 1999; Tricca et al., 1999; Schmitt et al., 2003; Stille et al., 2006; Cenki-Tok et al., 2009; Stille et al., 2009; Lemarchand et al., 2010; Rihs et al., 2011; Stille et al., 2011; Lemarchand et al., 2012; Viville et al., 2012; Gangloff et al., 2014b; Gangloff et al., 2014a; Pierret et al., 2014). The samples were collected during two different periods and have been ultra-filtered to determine the composition of the colloidal and dissolved phases according to the season and the depth and, thus, to better understand the spatial and temporal displacement of major and trace elements in a soil of a forested ecosystem.

2. Sampling site

The forested Strengbach catchment covering an area of 80 ha is located in the eastern part of the Vosges mountains (northeastern France) at altitudes ranging from 883 m at the outlet to 1146 m at the top (Fig. 1). The forest is dominated by conifers (80%) and beeches (20%). The climate of the

Strengbach catchment is oceanic mountainous. 20-25% of the precipitation is snow which falls between December and April. Rainfall occurs over the whole year with an annual average of 1400 mm. The average annual temperature is 6°C. The particular weather conditions recorded during the sampling periods are given in Electronic Annex E.A.T1. The catchment has been thoroughly investigated since 1986 and has become a completely equipped environmental observatory with permanent sampling and measuring stations (http://ohge.unistra.fr).

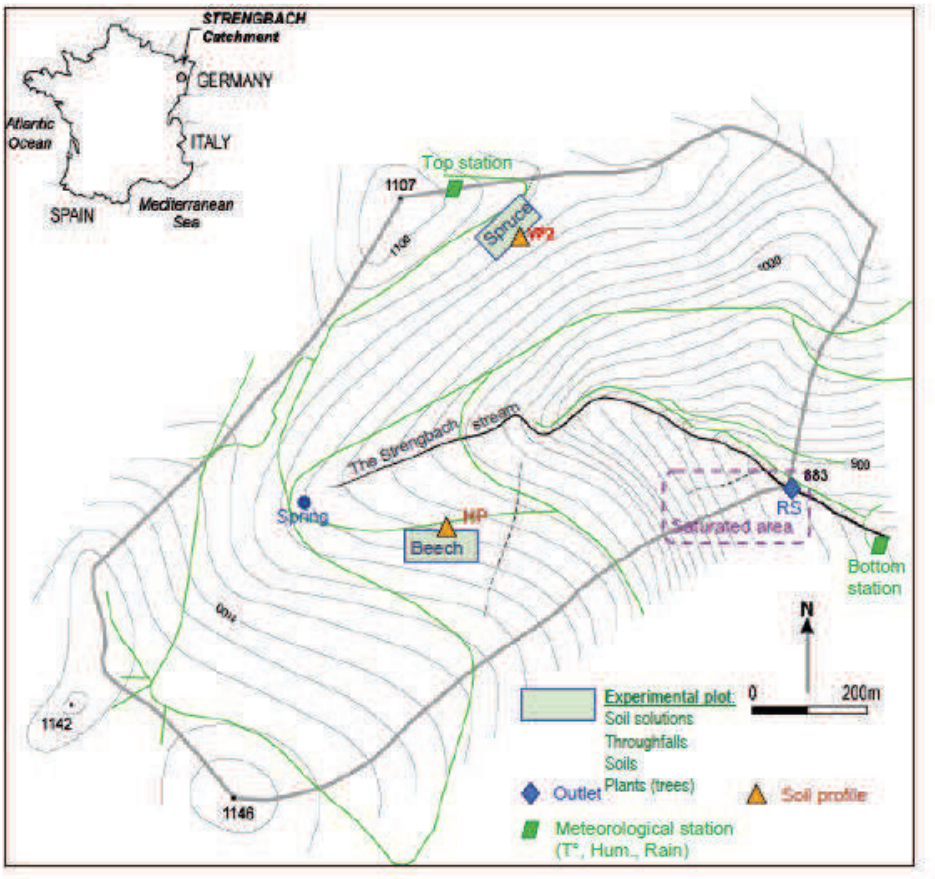

Figure 1: Strengbach catchment with sampling sites

The bedrock of the catchment is a hydrothermally altered Hercynian leucogranite. In addition small microgranite and gneiss bodies occur. The soils are brown acidic to ochreous podzolic. The acidification of soils is linked on the one hand to natural acidification (podzolization process), and on the other hand to the introduction of anthropogenic acidic atmospheric depositions in the 1990th.

The experimental parcel VP2 is situated under spruces at the northern slope of the catchment and the soil is brown acidic (acid dystrochrept type). The pH range is between 3.7 and 5. This acidity accelerates weathering and podzolization including leaching and illuviation processes in the soil (Lundström et al., 2000). The acidity causes the decrease of the buffering capacity of the soil and accelerates weathering. The O horizon (humus) consists of spruce needles more or less decomposed with a thickness ranging between 1 and 3 cm. The A horizon (10–15 cm thick) is dark brown and has an organic matter (OM) content of about 100 $g.kg^{-1}$. The B horizon (50 cm thick) is reddish brown. The OM contents decrease 10 $g.kg^{-1}$. The BC horizon reaches a depth of about 105 cm. It is greyish to reddish brown. The soil profile including its mineralogical composition has been described previously (Fichter et al., 1998; Probst et al., 2000; Stille et al., 2009; Gangloff et al., 2014b). This study focalizes more particularly on soil solutions originating from this parcel which are collected through zero tension lysimeter plates situated at 5, 10, 30 and 60 cm depth. Sixteen soil solutions have been sampled between 09/09/2009 and 09/09/2010; and 10 between 09/25/2012 and 08/06/2013 (Electronic Annex E.A.T2).

3. Materials and methods

3.1. **Filtrations and ultra-filtrations**

Each soil solution was filtered to 0.2 µm in a frontal way on Omnipore® membrane filters (hydrophilic PTFE) (Merck Millipore©, Billerica, MA). Then, a portion of these samples was ultra-filtered (UF) (Electronic Annex E.A.T2) with a Tangential Flow Filtration (TFF) by a Labscale TFF device of Millipore© (Merck Millipore©, Billerica, MA) as described schematically in Fig.2. The PelliconXL® cassettes (regenerated cellulose) were directly connected to the reservoir of the system. The portion of the sample which passed through the membrane containing compounds smaller than the cut-off size was collected in a polypropylene bottle and corresponds to the permeate (P). The part of the sample which remained in the reservoir

contains mainly compounds larger than the cut-off size and corresponds to the retentate (R). UHP water is ultra-filtered instead of the sample and corresponds to the blank. The concentration of each element represents approximately 2% of the concentrations in the sample.

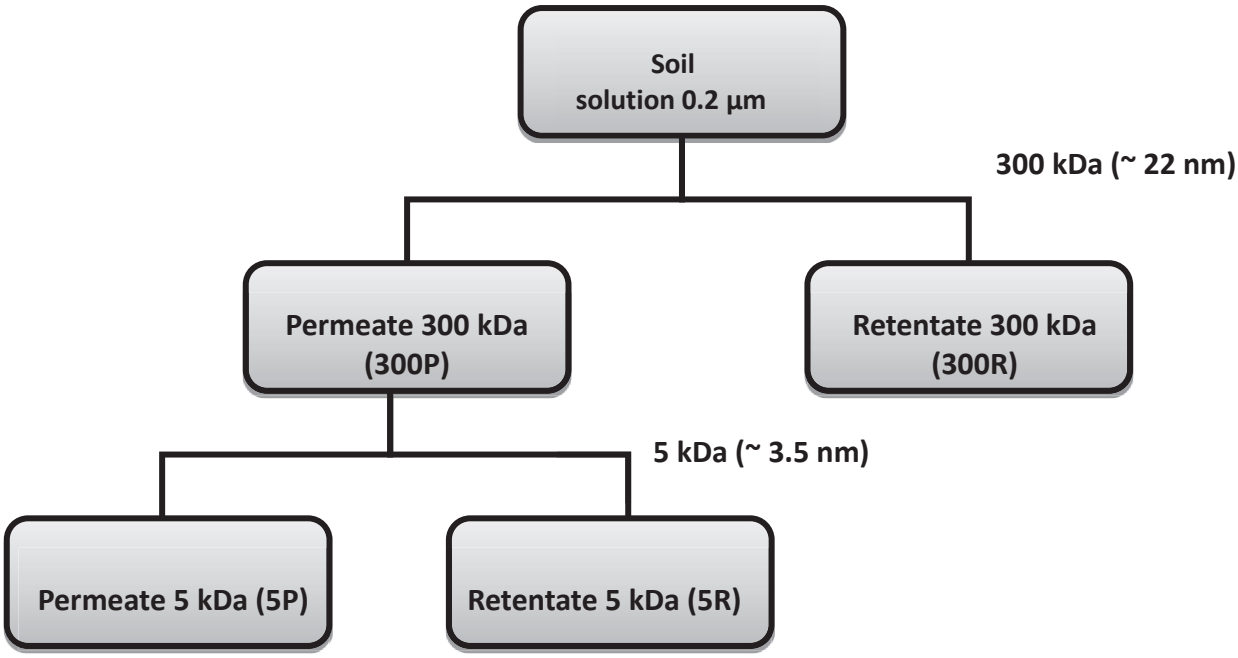

Figure 2: Ultrafiltration procedure followed for soil solutions

The Labscale device was equipped with a retentate back pressure valve, feed and retentate pressure indicators. This equipment permits reproducible ultra-filtrations with feed and retentate pressures at 20 psi and 10 psi, respectively. Between each ultra-filtration, every membrane was rinsed according the following procedure: 1 liter of ultra-high purity (UHP) water (18.2 MΩ.cm), 500 ml of a NaOH 0.1 M solution (to remove organic matter), 1 liter of UHP water, 500 ml of a HCl/HNO_3 0.1 M solution (to remove metals), 1 liter of UHP water. The rinsing steps and their importance have been previously described (Ingri et al., 2000; Dahlqvist et al., 2007; Schlosser and Croot, 2008; Dammshäuser and Croot, 2012).

3.2. **The ultra-filtration parameters**

In this study, the 0.2 µm soil solutions were ultra-filtered at the 300 kDa cut-off size to obtain the retentate (300R) containing the colloidal fraction between 0.2 µm and 300 kDa (large-size colloidal fraction) and the permeate (300P) corresponding to the fraction < 300 kDa (Fig.2). Then, the 300P fraction was ultra-filtered at the 5 kDa cut-off size to obtain the retentate (5R) containing the colloidal fraction between 300 kDa and 5 kDa (small size colloidal fraction) and the permeate (5P) corresponding to the dissolved fraction in this study. Therefore, the 0.2 µm soil solutions have been divided in three different size fractions (Fig.2). Due to shortage of volume, two samples were only ultra-filtered at the 5 kDa cut-off size (Electronic Annex E.A.T2).

According to Francioso et al. (1996), Ingri et al. (2000), Dahlqvist et al. (2004), Liu and Lead (2006), Schlosser and Croot (2008), Dammshäuser and Croot (2012) and Liu et al. (2013) different parameters resulting from the TFF procedure have to be considered and included in equations in order to determine the concentrations of each ultra-filtered fraction. One important parameter is the retentate volumic concentration factor (VCF_r) which has to be determined as:

$$VCF_r=(initial\ volume)/(retentate\ volume) \qquad (1)$$

In this study, $VCF_{r(300kDa)}$ is 5.0 ± 0.4 (N=20) and $VCF_{r(5kDa)}$ is 3.6 ± 0.3 (N=20). It is very important to have similar volume concentration factors for each size cut off to compare the different colloidal fractions. Then, in this study, all uncertainties correspond to 2SD and the concentrations discussed to the concentration between two cut-off sizes and can be calculated by:

$$Ci = \frac{(Ci_{retentate} - Ci_{permeate})}{VCF_{r_i}} \qquad (2)$$

where Ci = concentration of the element i and VCF_{ri} = retentate volumic concentration factor of the element i. For each ultra-filtration, it is important to calculate the recovery to check if there is an experimental deviation such

as adsorption or contamination. This recovery for the component i corresponds to:

$$Recovery\ i = \frac{Quantity\ of\ i\ in\ colloidal\ fraction + Quantity\ of\ i\ in\ permeate\ fraction}{Quantity\ of\ i\ in\ initial\ fraction} \quad (3)$$

Recoveries mainly varied between 99% and 95%.

3.3. **Analytical methods**

An aliquot of each soil solution was analyzed for elemental parameters. The pH was measured with a combined electrode after a calibration with standard solutions NIST (at pH 4.00 and 7.00). The concentrations of the major anions (Cl^-, NO_3^-, SO_4^{2-} and PO_4^{3-}) and cations (Na^+, NH_4^+, K^+, Mg^{2+} and Ca^{2+}) were determined simultaneously by an ionic chromatography (DIONEX ICS-3000 - Thermo Fisher Scientific©, Waltham, MA) (uncertainty < 2 %). The anions were analyzed by the AS18 column and CG18 guard column (Dionex - Thermo Fisher Scientific©, Waltham, MA) with sodium hydroxide (34 $mmol.L^{-1}$) as eluent according to an isocratic method (1 $ml.min^{-1}$). The cations were analyzed by the CS16 column and CG16 guard column (Dionex - Thermo Fisher Scientific©, Waltham, MA) with methan-sulfonic acid (27 $mmol.L^{-1}$) as eluent according to an isocratic method (1 $ml.min^{-1}$). The organic carbon (OC) in the different samples was measured by thermal method (Shimadzu TOC VPH - Shimadzu©, Kyoto, Japan) with an uncertainty of 2 % and a detection limit of 0.3 mg $C.L^{-1}$. The trace element concentrations were determined by Inductively Coupled Plasma Atomic Emission Spectrometry (ICP/AES) (Thermo Scientific iCAP 6000 SERIES - Thermo Fisher Scientific©, Waltham, MA) and Inductively Coupled Plasma Mass Spectrometry (ICP/MS) (Thermo-Fisher X SerieII - Thermo Fisher Scientific©, Waltham, MA) with traditional calibration and using Indium as internal standard. The validity and the reproducibility of different analyzed parameters have been verified by the certified standards SLRS5, Perade-20, Rain 97 and Big-Moose 02.

3.4. **Aromaticity**

The Specific Ultraviolet Absorbance at 254nm ($SUVA_{254}$) is determined by UV absorbance of the soil solutions samples at 254nm normalized to the OC concentration in mg $C.L^{-1}$. $SUVA_{254}$ were measured by an UV-VIS spectrophotometer (SHIMADZU UV-1700, Shimadzu©, Kyoto, Japan). Weishaar et al. (2003) showed that there is a relationship between the percentage of aromaticity determined by ^{13}C-NMR and the $SUVA_{254}$ value (percentage of aromaticity=6.53*$SUVA_{254}$+3.63). This parameter has been determined for the different samples and allows to show the variation of the aromatic character for all colloidal and dissolved fractions.

4. Results

4.1. **Organic carbon, aromaticity and pH variations in the soil solutions**

The pH values of the soil solutions filtered at 0.2 µm show no season dependent variations. The average pH at 5 cm depth is 4.24 (± 0.40) (N=7). The pH values increase with depth and reach 5.20 (± 0.66) (N=7) at 60 cm. Only the samples collected in June 2010 and August 2013 show an even higher value of 6.1 (Electronic Annex E.A.T3). Figures 3A and 3B show the variation of the pH as a function of OC for the 0.2 µm samples and Figure 3C that of the H^+ concentration as a function of the OC for some UF samples. It appears that variation of pH is correlated with OC for 4 profiles (Fig 3A) but not for two sampling dates (Fig 3B). The protons are correlated with OC for only the UF upper samples of November 2012 and August 2013 (Fig 3C).

E.A. T3: Concentrations for the 0.2 µm, colloidal and dissolved fractions calculated with Eq.(2) for each sampling date at different depth

(<D.L.: below to the detection limit and n.d.: no determined)

Sampling period	depth	Colloidal size	Date	pH (measured)	H+ (mmol/L)	Aromaticity (%)	DOC (mmol/l)	NO2 (mmol/l)	NH4 (mmol/l)	NO3 (mmol/l)	Si (mmol/l)	P (µmol/l)	Ca (µmol/l)	Mn (µmol/l)	Al (µmol/l)	Fe (µmol/l)	Mo (nmol/l)	V (nmol/l)	Cr (nmol/l)	Cu (nmol/l)	Zn (nmol/l)	Cd (nmol/l)	Pb (nmol/l)
09/09/2009 to 11/12/2009	**5cm**	0.2µm	11/12/09	4.08	0.083	30.7	3.51	*<D.L.*	0.096	0.076	0.146	35.81	42.00	22.00	21.48	8.17	1.04	24.75	18.65	55.39	623.9	1.09	59.00
		0.2 µm to 300kDa		n.d.	n.d.	31.4	0.02	*<D.L.*	0.000	0.000	0.000	0.00	0.00	0.02	0.70	0.22	0.02	0.00	0.16	1.70	0.0	0.01	2.19
		300kDa to 5kDa		n.d.	n.d.	31.8	1.58	*<D.L.*	0.015	0.000	0.000	3.55	14.00	7.00	8.99	3.91	0.47	8.36	7.92	22.91	186.4	0.21	35.00
		<5kDa		n.d.	n.d.	24.3	1.85	*<D.L.*	0.081	0.076	0.146	32.26	28.00	15.00	12.02	4.04	0.52	17.40	11.15	30.93	436.7	0.98	24.89
11/12/2009 to 03/19/2010	**5cm**	0.2µm	03/19/10	4.05	0.089	36.7	1.79	*<D.L.*	0.015	0.043	0.084	20.65	16.75	7.58	18.97	7.42	0.73	20.83	17.31	33.04	168.2	0.48	63.22
		0.2 µm to 300kDa		4.00	0.000	37.0	0.00	*<D.L.*	0.000	0.000	0.000	0.32	0.00	0.00	0.07	0.22	0.00	0.03	0.00	0.78	0.0	0.01	0.58
		300kDa to 5kDa		3.70	0.037	37.2	1.05	*<D.L.*	0.004	0.001	0.000	2.81	4.83	1.49	9.20	4.27	0.21	8.43	6.88	16.73	33.6	0.04	34.07
		<5kDa		4.21	0.065	31.9	0.74	*<D.L.*	0.011	0.042	0.084	17.61	12.00	6.11	9.70	2.93	0.52	12.36	10.76	15.53	134.6	0.43	28.57
03/19/2010 to 06/21/2010	**5cm**	0.2µm	06/21/10	5.10	0.008	35.4	4.08	0.160	0.444	0.064	0.173	56.77	53.25	28.47	30.19	14.93	5.63	35.95	34.62	297.40	1085.6	1.96	83.01
		0.2 µm to 300kDa		5.06	0.000	37.8	0.47	0.000	0.013	0.000	0.000	1.68	4.93	2.52	3.76	2.29	0.31	2.68	3.92	39.72	122.3	0.10	12.48
		300kDa to 5kDa		5.30	0.002	40.4	2.29	0.018	0.075	0.000	0.000	5.55	24.58	12.26	19.09	10.15	2.19	14.97	19.61	190.70	581.0	0.41	49.66
		<5kDa		4.95	0.006	30.2	1.32	0.142	0.356	0.065	0.173	49.68	23.75	13.68	7.33	2.49	3.13	18.30	11.09	66.98	382.3	1.44	20.87
06/21/2010 to 09/08/2010	**5cm**	0.2µm	08/09/10	3.97	0.107	34.0	3.33	*<D.L.*	0.043	0.017	0.136	20.00	21.75	9.87	35.78	19.34	1.04	28.88	25.00	43.27	275.2	0.66	79.63
09/25/2012 to 11/20/2012	**5cm**	0.2µm	11/20/12	4.40	0.040	38.3	2.17	*<D.L.*	0.016	0.010	0.049	8.39	10.30	4.50	13.48	7.26	1.15	19.65	15.35	45.32	422.0	0.36	62.74
		0.2µm to 300kDa		4.13	0.008	38.0	0.35	*<D.L.*	0.001	0.000	0.000	0.35	1.15	0.39	2.04	1.52	n.d.	2.38	2.25	6.68	22.9	0.04	12.28
		300kDa to 5kDa		4.05	0.021	35.2	1.17	*<D.L.*	0.006	0.000	0.000	1.61	5.03	2.07	6.99	3.88	n.d.	9.68	6.74	23.25	188.1	0.18	35.45
		<5kDa		4.60	0.011	27.0	0.65	*<D.L.*	0.009	0.010	0.049	6.29	4.13	2.04	4.45	1.86	n.d.	7.59	6.35	15.39	211.0	0.14	15.00
11/20/2012 to 03/26/2013	**5cm**	0.2µm	03/26/13	4.10	0.079	34.0	2.11	*<D.L.*	0.006	0.032	0.066	7.81	15.73	8.56	17.33	8.19	0.63	16.90	17.31	40.91	565.7	0.49	52.12
05/22/2013 to 08/06/2013	**5cm**	0.2µm	08/06/13	4.00	0.100	38.3	3.96	*<D.L.*	0.015	0.006	0.111	8.68	18.65	9.38	34.26	18.51	1.04	33.40	31.35	67.03	275.2	0.62	101.35
		0.2 µm to 300kDa		3.64	0.024	43.3	0.86	*<D.L.*	0.003	0.000	0.000	0.84	2.95	1.14	6.98	5.57	0.21	5.15	6.05	14.41	30.6	0.08	27.36
		300kDa to 5kDa		3.72	0.048	37.8	2.08	*<D.L.*	0.006	0.000	0.000	3.55	10.33	4.79	16.60	9.33	0.42	13.92	13.25	31.01	122.3	0.32	48.45
		<5kDa		4.50	0.028	31.3	1.01	*<D.L.*	0.006	0.006	0.111	4.29	5.38	3.45	10.68	3.61	0.31	14.32	12.04	21.61	122.3	0.23	25.54
09/09/2009 to 11/12/2009	**10cm**	0.2µm	11/12/09	4.60	0.025	28.1	2.27	<D.L.	0.134	0.125	0.078	30.00	33.00	13.68	26.63	5.63	0.52	10.41	25.90	39.81	420.5	0.97	34.27
		0.2 µm to 300kDa		n.d.	n.d.	28.4	0.05	<D.L.	0.000	0.000	0.000	0.00	0.00	0.00	1.39	0.31	n.d.	0.05	0.22	2.55	3.8	0.02	1.20
		300kDa to 5kDa		n.d.	n.d.	30.2	1.23	<D.L.	0.023	0.000	0.000	5.70	9.50	2.52	14.06	3.83	n.d.	3.56	11.50	18.65	122.4	0.19	20.10
		<5kDa		n.d.	n.d.	23.3	1.01	<D.L.	0.109	0.125	0.078	24.30	22.50	11.40	11.19	1.56	n.d.	6.80	13.20	18.92	294.2	0.85	12.96
11/12/2009 to 03/19/2010	**10cm**	0.2µm	03/19/10	4.30	0.050	32.0	1.03	<D.L.	0.003	0.030	0.066	9.35	12.25	5.69	21.33	5.41	0.42	6.48	14.04	17.94	122.3	0.45	27.03
		0.2µm to 300kDa		4.25	0.000	32.9	0.00	<D.L.	0.000	0.000	0.000	0.00	0.00	0.00	0.12	0.03	0.00	0.04	0.23	0.00	0.0	0.00	0.17
		300kDa to 5kDa		4.00	0.018	32.2	0.61	<D.L.	0.001	0.000	0.000	1.81	3.68	1.23	8.29	2.11	0.10	1.97	4.49	9.54	30.6	0.10	13.39
		<5kDa		4.40	0.037	29.8	0.43	<D.L.	0.002	0.030	0.066	7.55	8.63	4.46	12.92	3.27	0.31	4.48	9.31	8.40	91.7	0.35	13.44
03/19/2010 to 06/21/2010	**10cm**	0.2µm	06/21/10	5.50	0.008	31.9	1.85	0.106	0.320	0.064	0.079	34.52	31.50	12.90	23.70	7.53	1.98	10.61	19.23	173.09	626.9	1.78	31.70
		0.2µm to 300kDa		5.10	0.000	31.1	0.02	0.000	0.001	0.000	0.000	0.00	0.05	-0.01	0.45	0.26	0.10	0.00	0.39	0.96	0.0	0.00	0.62
		300kDa to 5kDa		5.03	0.002	33.8	1.28	0.000	0.078	0.000	0.000	4.20	10.80	4.59	16.14	5.79	0.63	4.13	12.69	124.14	244.6	0.70	23.62
		<5kDa		5.33	0.006	28.0	0.55	0.106	0.241	0.068	0.079	30.30	20.65	8.31	7.11	1.47	1.25	6.48	6.15	47.99	382.3	1.09	7.46
06/21/2010 to 09/08/2010	**10cm**	0.2µm	08/09/10	4.44	0.036	33.3	1.79	*<D.L.*	0.045	0.015	0.070	18.32	14.23	5.46	23.78	10.72	0.73	11.20	19.23	28.32	244.6	0.53	41.89
09/25/2012 to 11/20/2012	**10cm**	0.2µm	11/20/12	4.46	0.035	33.5	1.43	*<D.L.*	*<D.L.*	0.045	0.040	12.90	11.83	5.94	23.56	8.46	1.04	11.20	17.31	25.96	244.6	0.62	35.23
		0.2 µm to 300kDa		4.42	0.001	34.0	0.02	*<D.L.*	*<D.L.*	0.001	0.000	0.10	0.10	0.00	0.54	0.18	0.00	0.00	0.00	1.26	15.3	0.00	0.76
		300kDa to 5kDa		4.17	0.016	31.6	0.89	*<D.L.*	*<D.L.*	0.000	0.000	2.71	3.95	1.55	11.08	4.47	0.10	2.26	8.21	14.88	79.5	0.12	20.27
		<5kDa		4.73	0.018	29.2	0.52	*<D.L.*	*<D.L.*	0.044	0.040	10.10	7.78	4.39	11.94	3.81	0.94	8.94	9.10	9.82	148.3	0.51	14.20
05/22/2013 to 08/06/2013	**10cm**	0.2µm	08/06/13	4.12	0.076	34.0	1.68	*<D.L.*	0.003	0.015	0.049	11.03	7.95	4.50	23.11	9.98	0.42	15.72	19.23	19.67	152.9	0.44	38.03
		0.2µm to 300kDa		3.94	0.011	34.0	0.34	*<D.L.*	0.001	0.000	0.000	0.97	0.95	0.38	3.93	2.59	0.05	1.13	2.77	3.72	13.7	0.04	8.71
		300kDa to 5kDa		3.92	0.025	33.9	0.78	*<D.L.*	0.002	0.000	0.000	2.19	3.85	1.71	9.05	4.04	0.14	2.68	5.92	9.01	55.9	0.17	17.31
		<5kDa		4.54	0.040	30.9	0.55	*<D.L.*	0.001	0.015	0.049	7.87	3.15	2.41	10.13	3.35	0.23	11.91	10.54	6.94	80.6	0.23	12.02
09/09/2009 to 11/12/2009	**30cm**	0.2µm	11/12/09	4.30	0.050	28.8	2.22	*<D.L.*	0.036	0.095	0.025	4.84	33.00	13.17	28.78	3.94	0.52	11.00	10.58	38.24	267.58	0.71	21.48
		0.2 µm to 300kDa		n.d.	n.d.	28.4	0.05	*<D.L.*	0.001	0.000	0.000	0.00	0.00	-0.04	1.48	0.21	n.d.	0.00	0.07	1.98	0.00	0.00	1.41
		300kDa to 5kDa		n.d.	n.d.	31.6	0.79	*<D.L.*	0.000	0.000	0.000	1.29	7.25	1.13	12.59	1.49	n.d.	2.92	3.46	16.23	51.99	0.17	8.13
		<5kDa		n.d.	n.d.	22.9	1.38	*<D.L.*	0.035	0.095	0.025	3.55	25.75	12.41	14.81	2.22	n.d.	8.48	6.86	21.13	169.72	0.60	12.42
11/12/2009 to 03/19/2010	**30cm**	0.2µm	03/19/10	4.80	0.018	33.7	0.55	*<D.L.*	0.011	0.010	0.026	3.23	8.50	3.08	17.04	2.97	0.52	4.91	10.77	17.31	70.34	0.30	10.28
		0.2 µm to 300kDa		4.72	0.000	34.9	0.01	*<D.L.*	0.000	0.000	0.000	0.00	0.00	0.00	0.27	0.10	0.00	0.11	0.00	0.29	0.00	0.00	0.29
		300kDa to 5kDa		4.30	0.003	33.7	0.26	*<D.L.*	0.003	0.000	0.000	0.81	1.73	0.81	6.89	1.24	0.10	1.41	2.81	7.53	25.99	0.07	4.49
		<5kDa		4.88	0.015	27.3	0.28	*<D.L.*	0.008	0.010	0.026	2.32	6.75	2.27	9.88	1.64	0.42	3.39	7.96	9.50	44.34	0.22	5.50
03/19/2010 to 06/21/2010	**30cm**	0.2µm	06/21/10	4.43	0.037	31.7	0.92	*<D.L.*	0.012	0.041	0.069	4.19	9.75	4.30	21.78	3.84	0.63	6.48	15.38	17.62	168.20	0.60	12.89
		0.2 µm to 300kDa		4.40	0.000	30.7	0.02	*<D.L.*	0.000	0.000	0.000	0.00	0.10	0.00	0.09	0.01	0.00	0.04	0.00	0.09	0.00	0.00	0.26
		300kDa to 5kDa		4.13	0.011	31.9	0.49	*<D.L.*	0.003	0.000	0.000	0.68	2.55	0.97	7.97	1.40	0.21	2.84	6.23	7.18	65.75	0.16	5.88
		<5kDa		4.55	0.026	26.5	0.40	*<D.L.*	0.009	0.041	0.069	3.58	7.10	3.33	13.72	2.42	0.42	3.61	9.15	10.36	100.92	0.45	6.74
06/21/2010 to 09/08/2010	**30cm**	0.2µm	08/09/10	4.59	0.026	30.6	1.25	*<D.L.*	0.025	0.029	0.045	4.97	13.80	6.14	19.07	6.36	0.42	7.47	15.38	16.99	183.49	0.55	15.16
09/25/2012 to 11/20/2012	**30cm**	0.2µm	11/20/12	4.59	0.026	31.6	1.00	*<D.L.*	*<D.L.*	0.010	0.036	4.19	4.60	2.15	16.63	4.28	0.52	5.50	12.31	18.41	149.85	0.20	12.93
		0.2µm to 300kDa		4.54	0.001	30.3	0.03	*<D.L.*	*<D.L.*	0.000	0.000	0.06	0.05	0.00	0.43	0.17	n.d.	0.10	0.37	0.00	0.00	0.00	0.46
		300kDa to 5kDa		4.20	0.013	31.7	0.67	*<D.L.*	*<D.L.*	0.000	0.000	1.39	2.88	1.03	8.96	2.48	n.d.	2.71	5.37	11.37	88.69	0.09	9.14
		<5kDa		4.92	0.012	26.9	0.30	*<D.L.*	*<D.L.*	0.010	0.036	2.77	1.68	1.12	7.23	1.63	n.d.	2.70	6.57	7.04	58.10	0.11	3.33
05/22/2013 to 08/06/2013	**30cm**	0.2µm	08/06/13	4.70	0.020	34.3	0.83	*<D.L.*	0.008	0.006	0.070	3.23	2.90	1.64	17.78	4.48	0.31	4.52	14.62	11.64	65.75	0.58	7.48
		0.2µm to 300kDa		4.55	0.001	33.8	0.02	*<D.L.*	0.000	0.000	0.000	0.06	0.03	0.04	0.57	0.33	0.02	0.04	0.15	0.14	n.d.	0.01	0.25
		300kDa to 5kDa		4.38	0.008	32.0	0.46	*<D.L.*	0.003	0.001	0.000	1.39	1.38	0.81	8.39	2.59	0.06	0.84	5.54	5.74	n.d.	0.30	4.57
		<5kDa		5.00	0.010	28.6	0.35	*<D.L.*	0.005	0.005	0.070	2.77	1.50	0.79	8.82	1.56	0.24	3.64	8.93	5.77	n.d.	0.28	2.66
09/09/2009 to 11/12/2009	**60cm**	0.2µm	11/12/09	4.90	0.025	16.0	0.92	*<D.L.*	0.079	0.118	0.039	30.32	10.75	2.24	6.59	0.47	0.63	8.06	7.69	23.76	321.1	0.44	4.54
		0.2µm to 5kDa		n.d.	n.d.	16.0	0.41	*<D.L.*	0.008	0.009	0.000	12.90	1.50	0.25	3.93	0.18	n.d.	2.43	2.80	22.65	192.7	0.11	1.93
		<5kDa		n.d.	n.d.	15.5	0.51	*<D.L.*	0.071	0.166	0.039	17.42	9.50	1.99	2.67	0.28	n.d.	5.63	4.90	1.11	128.4	0.33	2.59
11/12/2009 to 03/19/2010	**60cm**	0.2µm	03/19/10	4.80	0.018	15.5	0.20	*<D.L.*	0.004	0.005	0.052	4.84	10.00	3.89	6.26	0.17	1.04	1.63	5.58	3.59	168.2	0.61	0.84
		0.2µm to 300kDa		4.90	0.000	16	0.00	*<D.L.*	0.000	0.000	0.000	0.00	0.00	0.00	0.07	0.01	0.00	0.01	0.09	1.32	0.0	0.01	0.01
		300kDa to 5kDa		4.34	0.003	14	0.05	*<D.L.*	0.001	0.000	0.000	0.32	2.75	0.88	1.22	0.07	0.10	0.08	0.33	0.22	30.6	0.12	0.18
		<5kDa		5.13	0.015	10.5	0.15	*<D.L.*	0.003	0.005	0.052	4.52	7.25	3.03	4.96	0.10	0.94	1.54	5.16	2.04	134.6	0.48	0.65
03/19/2010 to 06/21/2010	**60cm**	0.2µm	06/21/10	6.09	0.001	15.7	0.23	*<D.L.*	0.094	0.045	0.051	0.35	10.58	4.55	1.33	0.03	1.04	1.57	2.50	7.87	275.2	0.29	0.34
		0.2 µm to 300kDa		6.08	0.000	16.4	0.00	*<D.L.*	0.000	0.000	0.000	0.03	0.00	0.01	0.07	0.00	0.00	0.00	0.08	0.00	0.0	0.00	0.02
		300kDa to 5kDa		6.03	0.000	18.2	0.11	*<D.L.*	0.028	0.002	0.000	0.10	5.18	1.97	0.64	0.01	0.68	0.24	0.63	2.83	110.1	0.12	0.06
		<5kDa		5.94	0.001	14.0	0.12	*<D.L.*	0.065	0.043	0.051	0.23	5.35	2.57	0.63	0.02	0.35	1.34	1.79	5.04	165.1	0.17	0.26
06/21/2010 to 09/08/2010	**60cm**	0.2µm	08/09/10	4.9	0.013	18.1	0.42	*<D.L.*	0.011	0.010	0.039	1.19	9.08	3.04	3.26	0.07	5.21	10.41	15.38	13.22	535.2	0.60	1.73
09/25/2012 to 11/20/2012	**60cm**	0.2µm	11/20/12	4.86	0.014	18.4	0.26	*<D.L.*	*<D.L.*	*<D.L.*	0.031	0.39	3.05	1.26	8.15	0.11	0.31	5.89	5.38	7.88	1804.3	0.16	1.35
		0.2 µm to 300kDa		4.80	0.000	15.7	0.01	*<D.L.*	*<D.L.*	*<D.L.*	0.000	0.03	0.00	0.00	0.39	0.01	n.d.	0.00	0.00	0.53	0.0	0.01	0.05
		300kDa to 5kDa		4.50	0.008	18	0.09	*<D.L.*	*<D.L.*	*<D.L.*	0.000	0.10	0.83	0.38	2.04	0.01	n.d.	0.97	0.82	2.80	535.2	0.07	0.62
		<5kDa		4.97	0.008	18.9	0.16	*<D.L.*	*<D.L.*	*<D.L.*	0.031	0.23	2.23	0.87	5.71	0.08	n.d.	4.93	4.56	4.55	1269.1	0.08	0.69
11/20/2012 to 03/26/2014	**60cm**	0.2µm	03/26/2013	4.95	0.011	17.2	0.23	*<D.L.*	0.001	0.001	0.046	0.68	2.43	0.71	6.81	0.13	*<D.L.*	0.98	5.77	5.82	111.6	0.11	1.16
05/22/2013 to 08/06/2013	**60cm**	0.2µm	08/06/13	6.20	0.001	21.1	0.28	*<D.L.*	0.019	0.005	0.045	5.48	27.00	0.46	2.96	0.14	0.10	1.06	7.31	18.25	1727.8	0.11	0.36
		0.2µm to 5kDa		6.47	0.000	21.0	0.18	*<D.L.*	0.010	0.000	0.000	2.26	16.00	0.24	1.55	0.09	0.02	0.36	1.56	11.34	n.d.	0.06	0.30
		<5kDa		6.30	0.001	22.0	0.10	*<D.L.*	0.009	0.005	0.045	3.23	11.00	0.21	1.41	0.06	0.08	0.70	5.75	6.91	n.d.	0.04	0.07

E.A. T4: Proportion of each element in the different fractions against 0.2 µm content for each sampling date at different depth

(<D.L.: below to the detection limit and n.d.: no determined)

Sampling period	depth	Colloidal size	Date	pH (measured)	H+	Aromaticity (%)	DOC	NO2	NH4	NO3	Si	P	Ca	Mn	Al	Fe	Mo	V	Cr	Cu	Zn	Cd	Pb
09/09/2009 to 11/12/2009	**5cm**	0.2µm	11/12/09	4.08	1.00	30.7	1.00	<D.L.	1.00	1.00	1.00	1.00	1.00	1.00	1.00	1.00	1.00	1.00	1.00	1.00	1.00	1.00	1.00
		0.2 µm to 300kDa		n.d.	n.d.	31.4	0.00	<D.L.	0.00	0.00	0.00	0.00	0.00	0.00	0.00	0.03	0.03	0.02	0.00	0.01	0.03	0.00	0.01	0.03
		300kDa to 5kDa		n.d.	n.d.	31.8	0.45	<D.L.	0.16	0.00	0.00	0.10	0.33	0.31	0.42	0.48	0.45	0.34	0.42	0.41	0.30	0.19	0.71
		<5kDa		n.d.	n.d.	24.3	0.53	<D.L.	0.84	1.00	1.00	0.90	0.67	0.69	0.56	0.49	0.50	0.70	0.60	0.56	0.70	0.90	0.38
11/12/2009 to 03/19/2010	**5cm**	0.2µm	03/19/10	4.05	1.00	36.7	1.00	<D.L.	1.00	1.00	1.00	1.00	1.00	1.00	1.00	1.00	1.00	1.00	1.00	1.00	1.00	1.00	1.00
		0.2 µm to 300kDa		4.00	0.00	37.0	0.00	<D.L.	0.01	0.00	0.00	0.02	0.00	0.00	0.00	0.03	0.00	0.00	0.00	0.02	0.00	0.03	0.01
		300kDa to 5kDa		3.70	0.42	37.2	0.59	<D.L.	0.26	0.02	0.00	0.14	0.29	0.20	0.48	0.58	0.29	0.40	0.40	0.51	0.20	0.09	0.54
		<5kDa		4.21	0.73	31.9	0.41	<D.L.	0.72	0.98	1.00	0.85	0.72	0.81	0.51	0.39	0.71	0.59	0.62	0.47	0.80	0.89	0.45
03/19/2010 to 06/21/2010	**5cm**	0.2µm	06/21/10	5.10	1.00	35.4	1.00	1.00	1.00	1.00	1.00	1.00	1.00	1.00	1.00	1.00	1.00	1.00	1.00	1.00	1.00	1.00	1.00
		0.2 µm to 300kDa		5.06	0.00	37.8	0.11	0.00	0.03	0.00	0.00	0.03	0.09	0.09	0.12	0.15	0.06	0.07	0.11	0.13	0.11	0.05	0.15
		300kDa to 5kDa		5.30	0.25	40.4	0.56	0.11	0.17	0.00	0.00	0.10	0.46	0.43	0.63	0.68	0.39	0.42	0.57	0.64	0.54	0.21	0.60
		<5kDa		4.95	0.76	30.2	0.32	0.89	0.80	1.02	1.00	0.88	0.45	0.48	0.24	0.17	0.56	0.51	0.32	0.23	0.35	0.74	0.25
06/21/2010 to 09/08/2010	**5cm**	0.2µm	08/09/10	3.97	1.00	34.0	1.00	<D.L.	1.00	1.00	1.00	1.00	1.00	1.00	1.00	1.00	1.00	1.00	1.00	1.00	1.00	1.00	1.00
09/25/2012 to 11/20/2012	**5cm**	0.2µm	11/20/12	4.40	1.00	38.3	1.00	<D.L.	1.00	1.00	1.00	1.00	1.00	1.00	1.00	1.00	1.00	1.00	1.00	1.00	1.00	1.00	1.00
		0.2µm to 300kDa		4.13	0.20	38.0	0.16	<D.L.	0.06	0.00	0.00	0.04	0.11	0.09	0.15	0.21	n.d.	0.12	0.15	0.15	0.05	0.10	0.20
		300kDa to 5kDa		4.05	0.53	35.2	0.54	<D.L.	0.36	0.00	0.00	0.19	0.49	0.46	0.52	0.53	n.d.	0.49	0.44	0.51	0.45	0.50	0.57
		<5kDa		4.60	0.28	27.0	0.30	<D.L.	0.57	1.04	1.00	0.75	0.40	0.45	0.33	0.26	n.d.	0.39	0.41	0.34	0.50	0.40	0.24
11/20/2012 to 03/26/2013	**5cm**	0.2µm	03/26/13	4.10	1.00	34.0	1.00	<D.L.	1.00	1.00	1.00	1.00	1.00	1.00	1.00	1.00	1.00	1.00	1.00	1.00	1.00	1.00	1.00
05/22/2013 to 08/06/2013	**5cm**	0.2µm	08/06/13	4.00	1.00	38.3	1.00	<D.L.	1.00	1.00	1.00	1.00	1.00	1.00	1.00	1.00	1.00	1.00	1.00	1.00	1.00	1.00	1.00
		0.2 µm to 300kDa		3.64	0.24	43.3	0.22	<D.L.	0.22	0.00	0.00	0.10	0.16	0.12	0.20	0.30	0.20	0.15	0.19	0.22	0.11	0.12	0.27
		300kDa to 5kDa		3.72	0.48	37.8	0.53	<D.L.	0.40	0.00	0.00	0.12	0.55	0.51	0.48	0.50	0.40	0.42	0.42	0.46	0.44	0.51	0.48
		<5kDa		4.50	0.28	31.3	0.26	<D.L.	0.39	1.00	1.00	0.78	0.29	0.37	0.31	0.20	0.30	0.43	0.38	0.32	0.44	0.36	0.25
09/09/2009 to 11/12/2009	**10cm**	0.2µm	11/12/09	4.60	1.00	28.1	1.00	<D.L.	1.00	1.00	1.00	1.00	1.00	1.00	1.00	1.00	1.00	1.00	1.00	1.00	1.00	1.00	1.00
		0.2 µm to 300kDa		n.d.	n.d.	28.4	0.02	<D.L.	0.00	0.00	0.00	0.00	0.00	0.00	0.05	0.05	n.d.	0.01	0.01	0.06	0.01	0.02	0.04
		300kDa to 5kDa		n.d.	n.d.	30.2	0.54	<D.L.	0.17	0.00	0.00	0.24	0.29	0.18	0.53	0.68	n.d.	0.34	0.46	0.47	0.29	0.20	0.59
		<5kDa		n.d.	n.d.	23.3	0.44	<D.L.	0.81	1.00	1.00	0.82	0.68	0.83	0.42	0.28	n.d.	0.65	0.54	0.48	0.70	0.88	0.38
11/12/2009 to 03/19/2010	**10cm**	0.2µm	03/19/10	4.30	1.00	32.0	1.00	<D.L.	1.00	1.00	1.00	1.00	1.00	1.00	1.00	1.00	1.00	1.00	1.00	1.00	1.00	1.00	1.00
		0.2µm to 300kDa		4.25	0.00	32.9	0.00	<D.L.	0.00	0.01	0.00	0.00	0.00	0.00	0.01	0.01	0.00	0.01	0.02	0.00	0.00	0.01	0.01
		300kDa to 5kDa		4.00	0.36	32.2	0.59	<D.L.	0.35	0.00	0.00	0.19	0.30	0.22	0.39	0.39	0.25	0.30	0.32	0.53	0.25	0.23	0.50
		<5kDa		4.40	0.74	29.8	0.41	<D.L.	0.65	1.00	1.00	0.81	0.70	0.78	0.61	0.60	0.75	0.69	0.66	0.47	0.75	0.77	0.50
03/19/2010 to 06/21/2010	**10cm**	0.2µm	06/21/10	5.50	1.00	31.9	1.00	<D.L.	1.00	1.00	1.00	1.00	1.00	1.00	1.00	1.00	1.00	1.00	1.00	1.00	1.00	1.00	1.00
		0.2µm to 300kDa		5.10	0.00	31.1	0.01	<D.L.	0.00	0.00	0.00	0.00	0.00	0.00	0.02	0.03	0.05	0.00	0.02	0.01	0.00	0.00	0.02
		300kDa to 5kDa		5.03	0.25	33.8	0.69	<D.L.	0.24	0.00	0.00	0.23	0.34	0.36	0.68	0.77	0.32	0.39	0.66	0.72	0.39	0.39	0.75
		<5kDa		5.33	0.76	28.0	0.30	<D.L.	0.75	1.06	1.00	0.76	0.66	0.64	0.30	0.20	0.63	0.61	0.32	0.28	0.61	0.61	0.24
06/21/2010 to 09/08/2010	**10cm**	0.2µm	08/09/10	4.44	1.00	33.3	1.00	<D.L.	1.00	1.00	1.00	1.00	1.00	1.00	1.00	1.00	1.00	1.00	1.00	1.00	1.00	1.00	1.00
09/25/2012 to 11/20/2012	**10cm**	0.2µm	11/20/12	4.46	1.00	33.5	1.00	<D.L.	<D.L.	1.00	1.00	1.00	1.00	1.00	1.00	1.00	1.00	1.00	1.00	1.00	1.00	1.00	1.00
		0.2 µm to 300kDa		4.42	0.03	34.0	0.01	<D.L.	<D.L.	0.00	0.00	0.01	0.01	0.00	0.02	0.02	0.00	0.00	0.00	0.05	0.06	0.00	0.02
		300kDa to 5kDa		4.17	0.46	31.6	0.62	<D.L.	<D.L.	0.00	0.00	0.21	0.33	0.26	0.47	0.53	0.10	0.20	0.47	0.57	0.33	0.19	0.58
		<5kDa		4.73	0.51	29.2	0.36	<D.L.	<D.L.	1.00	1.00	0.78	0.66	0.74	0.51	0.45	0.90	0.80	0.53	0.38	0.61	0.81	0.40
05/22/2013 to 08/06/2013	**10cm**	0.2µm to 300kDa	08/06/13	4.12	1.00	34.0	1.00	<D.L.	1.00	1.00	1.00	1.00	1.00	1.00	1.00	1.00	1.00	1.00	1.00	1.00	1.00	1.00	1.00
		0.2µm to 300kDa		3.94	0.15	34.0	0.21	<D.L.	0.19	0.00	0.00	0.09	0.12	0.08	0.17	0.26	0.13	0.07	0.14	0.19	0.09	0.10	0.23
		300kDa to 5kDa		3.92	0.33	33.9	0.46	<D.L.	0.45	0.00	0.00	0.20	0.48	0.38	0.39	0.41	0.35	0.17	0.31	0.46	0.37	0.38	0.46
		<5kDa		4.54	0.53	30.9	0.33	<D.L.	0.36	1.00	1.00	0.71	0.40	0.54	0.44	0.34	0.56	0.76	0.55	0.35	0.53	0.52	0.32
09/09/2009 to 11/12/2009	**30cm**	0.2µm	11/12/09	4.30	1.00	28.8	1.00	<D.L.	1.00	1.00	1.00	1.00	1.00	1.00	1.00	1.00	1.00	1.00	1.00	1.00	1.00	1.00	1.00
		0.2 µm to 300kDa		n.d.	n.d.	28.4	0.02	<D.L.	0.03	0.00	0.00	0.00	0.00	0.00	0.05	0.05	n.d.	0.00	0.01	0.05	0.00	0.00	0.07
		300kDa to 5kDa		n.d.	n.d.	31.6	0.36	<D.L.	0.00	0.00	0.00	0.27	0.22	0.09	0.44	0.38	n.d.	0.27	0.33	0.42	0.19	0.23	0.38
		<5kDa		n.d.	n.d.	22.9	0.62	<D.L.	0.97	1.00	1.00	0.73	0.78	0.94	0.51	0.56	n.d.	0.77	0.65	0.55	0.63	0.84	0.58
11/12/2009 to 03/19/2010	**30cm**	0.2µm	03/19/10	4.80	1.00	33.7	1.00	<D.L.	1.00	1.00	1.00	1.00	1.00	1.00	1.00	1.00	1.00	1.00	1.00	1.00	1.00	1.00	1.00
		0.2 µm to 300kDa		4.72	0.00	34.9	0.01	<D.L.	0.00	0.00	0.00	0.00	0.00	0.00	0.02	0.03	0.00	0.02	0.00	0.02	0.00	0.00	0.03
		300kDa to 5kDa		4.30	0.17	33.7	0.48	<D.L.	0.28	0.03	0.00	0.25	0.20	0.26	0.40	0.42	0.20	0.29	0.26	0.43	0.37	0.25	0.44
		<5kDa		4.88	0.83	27.3	0.51	<D.L.	0.72	0.97	1.00	0.72	0.79	0.74	0.58	0.55	0.80	0.69	0.74	0.55	0.63	0.75	0.54
03/19/2010 to 06/21/2010	**30cm**	0.2µm	06/21/10	4.43	1.00	31.7	1.00	<D.L.	1.00	1.00	1.00	1.00	1.00	1.00	1.00	1.00	1.00	1.00	1.00	1.00	1.00	1.00	1.00
		0.2 µm to 300kDa		4.40	0.00	30.7	0.03	<D.L.	0.00	0.00	0.00	0.00	0.01	0.00	0.00	0.00	0.00	0.01	0.00	0.01	0.00	0.00	0.02
		300kDa to 5kDa		4.13	0.30	31.9	0.53	<D.L.	0.23	0.00	0.00	0.16	0.26	0.22	0.37	0.36	0.33	0.44	0.41	0.41	0.39	0.26	0.46
		<5kDa		4.55	0.70	26.5	0.44	<D.L.	0.77	1.00	1.00	0.85	0.73	0.78	0.63	0.63	0.67	0.56	0.59	0.59	0.60	0.74	0.52
06/21/2010 to 09/08/2010	**30cm**	0.2µm	08/09/10	4.59	1.00	30.6	1.00	<D.L.	1.00	1.00	1.00	1.00	1.00	1.00	1.00	1.00	1.00	1.00	1.00	1.00	1.00	1.00	1.00
09/25/2012 to 11/20/2012	**30cm**	0.2µm	11/20/12	4.59	1.00	31.6	1.00	<D.L.	<D.L.	1.00	1.00	1.00	1.00	1.00	1.00	1.00	1.00	1.00	1.00	1.00	1.00	1.00	1.00
		0.2µm to 300kDa		4.54	0.04	30.3	0.03	<D.L.	<D.L.	0.00	0.00	0.02	0.01	0.00	0.03	0.04	n.d.	0.02	0.03	0.00	0.00	0.00	0.04
		300kDa to 5kDa		4.20	0.50	31.7	0.67	<D.L.	<D.L.	0.00	0.00	0.33	0.63	0.48	0.54	0.58	n.d.	0.49	0.44	0.62	0.59	0.46	0.71
		<5kDa		4.92	0.46	26.9	0.30	<D.L.	<D.L.	1.01	1.00	0.66	0.36	0.52	0.44	0.38	n.d.	0.49	0.53	0.38	0.39	0.54	0.26
05/22/2013 to 08/06/2013	**30cm**	0.2µm to 300kDa	08/06/13	4.70	1.00	34.3	1.00	<D.L.	1.00	1.00	1.00	1.00	1.00	1.00	1.00	1.00	1.00	1.00	1.00	1.00	1.00	1.00	1.00
		0.2µm to 300kDa		4.55	0.05	33.8	0.02	<D.L.	0.02	0.00	0.00	0.02	0.01	0.02	0.03	0.07	0.06	0.01	0.01	0.01	n.d.	0.01	0.03
		300kDa to 5kDa		4.38	0.40	32.0	0.55	<D.L.	0.33	0.09	0.00	0.43	0.47	0.49	0.47	0.58	0.18	0.19	0.38	0.49	n.d.	0.52	0.61
		<5kDa		5.00	0.50	28.6	0.42	<D.L.	0.64	0.91	1.00	0.86	0.52	0.48	0.50	0.35	0.76	0.81	0.61	0.50	n.d.	0.48	0.36
09/09/2009 to 11/12/2009	**60cm**	0.2µm	11/12/09	4.90	1.00	16.0	1.00	<D.L.	1.00	1.00	1.00	1.00	1.00	1.00	1.00	1.00	1.00	1.00	1.00	1.00	1.00	1.00	1.00
		0.2µm to 5kDa		n.d.	n.d.	16.0	0.44	<D.L.	0.10	0.08	0.00	0.43	0.14	0.11	0.60	0.39	n.d.	0.30	0.36	0.95	0.60	0.25	0.43
		<5kDa		n.d.	n.d.	15.5	0.56	<D.L.	0.90	1.41	1.00	0.57	0.88	0.89	0.40	0.61	n.d.	0.70	0.64	0.05	0.40	0.75	0.57
11/12/2009 to 03/19/2010	**60cm**	0.2µm to 300kDa	03/19/10	4.80	1.00	15.5	1.00	<D.L.	1.00	1.00	1.00	1.00	1.00	1.00	1.00	1.00	1.00	1.00	1.00	1.00	1.00	1.00	1.00
		0.2µm to 300kDa		4.90	0.00	16	0.02	<D.L.	0.00	0.00	0.00	0.00	0.00	0.00	0.01	0.03	0.00	0.00	0.02	0.37	0.00	0.02	0.02
		300kDa to 5kDa		4.34	0.17	14	0.27	<D.L.	0.29	0.00	0.00	0.07	0.28	0.23	0.20	0.40	0.10	0.05	0.06	0.06	0.18	0.20	0.21
		<5kDa		5.13	0.83	10.5	0.71	<D.L.	0.71	1.02	1.00	0.93	0.73	0.78	0.79	0.57	0.90	0.94	0.92	0.57	0.80	0.78	0.77
03/19/2010 to 06/21/2010	**60cm**	0.2µm	06/21/10	6.09	1.00	15.7	1.00	<D.L.	1.00	1.00	1.00	1.00	1.00	1.00	1.00	1.00	1.00	1.00	1.00	1.00	1.00	1.00	1.00
		0.2 µm to 300kDa		6.08	0.00	16.4	0.00	<D.L.	0.00	0.00	0.00	0.09	0.00	0.00	0.05	0.01	0.00	0.00	0.03	0.00	0.00	0.01	0.06
		300kDa to 5kDa		6.03	0.00	18.2	0.49	<D.L.	0.30	0.05	0.00	0.27	0.49	0.43	0.48	0.35	0.65	0.15	0.25	0.36	0.40	0.41	0.19
		<5kDa		5.94	1.00	14.0	0.51	<D.L.	0.69	0.95	1.00	0.64	0.51	0.56	0.47	0.64	0.34	0.85	0.71	0.64	0.60	0.58	0.76
06/21/2010 to 09/08/2010	**60cm**	0.2µm	08/09/10	4.9	1.00	18.1	1.00	<D.L.	1.00	1.00	1.00	1.00	1.00	1.00	1.00	1.00	1.00	1.00	1.00	1.00	1.00	1.00	1.00
09/25/2012 to 11/20/2012	**60cm**	0.2µm	11/20/12	4.86	1.00	18.4	1.00	<D.L.	<D.L.	<D.L.	1.00	1.00	1.00	1.00	1.00	1.00	1.00	1.00	1.00	1.00	1.00	1.00	1.00
		0.2 µm to 300kDa		4.80	0.00	15.7	0.05	<D.L.	<D.L.	<D.L.	0.00	0.08	0.00	0.00	0.05	0.10	n.d.	0.00	0.00	0.07	0.00	0.05	0.03
		300kDa to 5kDa		4.50	0.57	18	0.34	<D.L.	<D.L.	<D.L.	0.00	0.25	0.27	0.30	0.25	0.11	n.d.	0.16	0.15	0.36	0.30	0.42	0.46
		<5kDa		4.97	0.57	18.9	0.61	<D.L.	<D.L.	<D.L.	1.00	0.58	0.73	0.70	0.70	0.79	n.d.	0.84	0.85	0.58	0.70	0.53	0.51
11/20/2012 to 03/26/2014	**60cm**	0.2µm	03/26/2013	4.95	1.00	17.2	1.00	<D.L.	1.00	1.00	1.00	1.00	1.00	1.00	1.00	1.00	n.d.	1.00	1.00	1.00	1.00	1.00	1.00
05/22/2013 to 08/06/2013	**60cm**	0.2µm	08/06/13	6.20	1.00	21.1	1.00	<D.L.	1.00	1.00	1.00	1.00	1.00	1.00	1.00	1.00	1.00	1.00	1.00	1.00	1.00	1.00	1.00
		0.2µm to 5kDa		6.47	0.00	21.0	0.64	<D.L.	0.50	0.00	0.00	0.41	0.59	0.53	0.52	0.62	0.20	0.34	0.21	0.62	n.d.	0.58	0.82
		<5kDa		6.30	1.00	22.0	0.36	<D.L.	0.50	1.00	1.00	0.59	0.41	0.47	0.48	0.38	0.80	0.66	0.79	0.38	n.d.	0.42	0.18

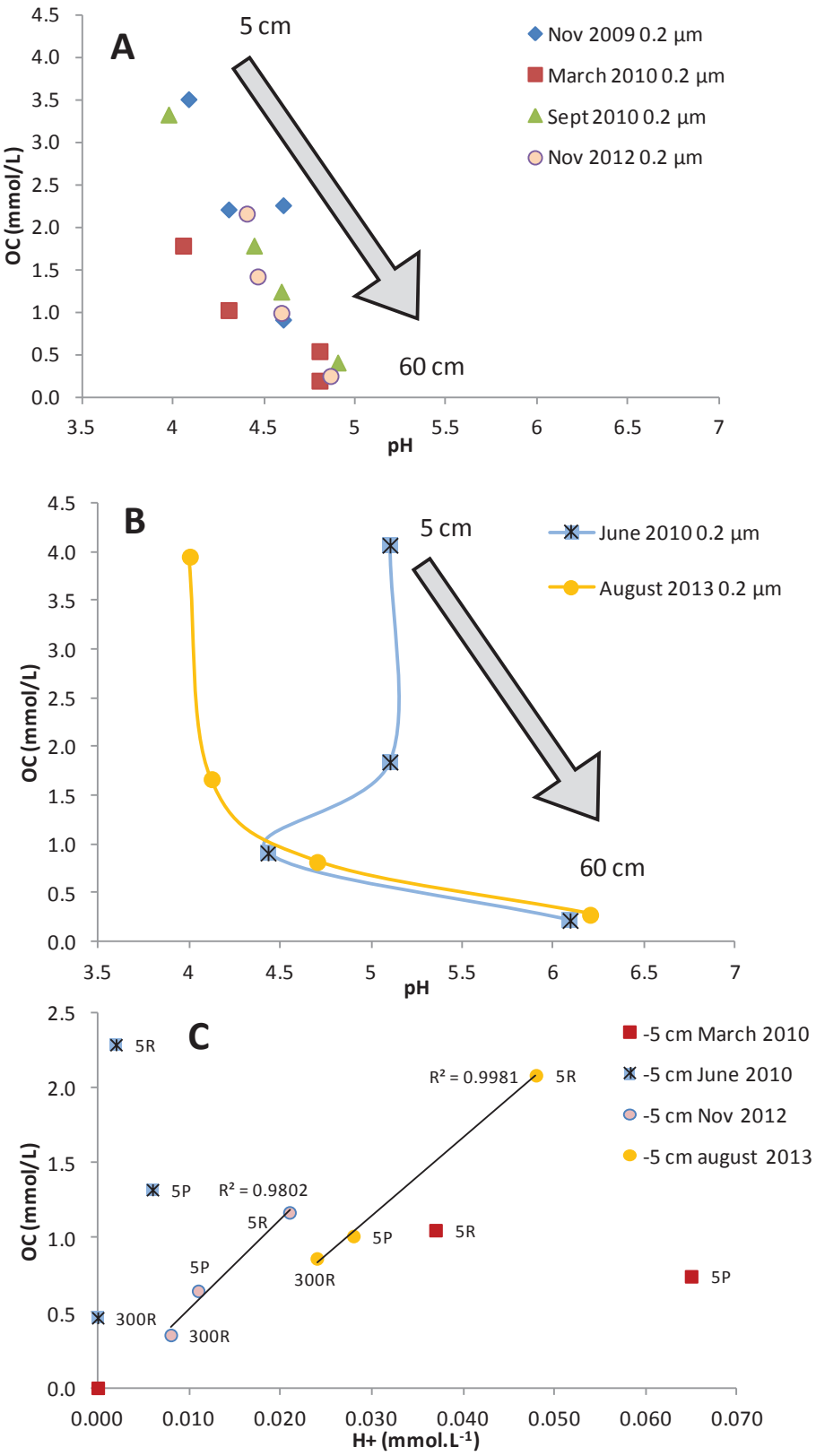

Figure 3: Variation of pH with OC for the 0.2 µm samples (A and B) and variation of H^+ concentration with OC for some UF samples (C)

The OC content of the 0.2 µm filtered soil solutions from 5 to 60 cm depth are 2.95 (±0.94) mmol.L^{-1} (N=7) and 0.36 (± 0.26) mmol.L^{-1} (N=7), respectively (Electronic Annex E.A.T3). The corresponding aromaticities are 35 (± 3) % (N=7) and 17 (± 2) % (N=7), respectively. Aromaticities and OC have the same magnitude as those observed by Kalbitz et al. (1999) , Weishaar et al. (2003), Gabor et al. (2014) and Verstraeten et al. (2014) for soil solutions from coniferous forest soils. They fluctuate as a function of the season in the upper soil compartment and diminish with depth (Electronic Annex E.A.T3 and Fig 4) as observed previously (Kaiser et al., 2001; Verstraeten et al., 2014)

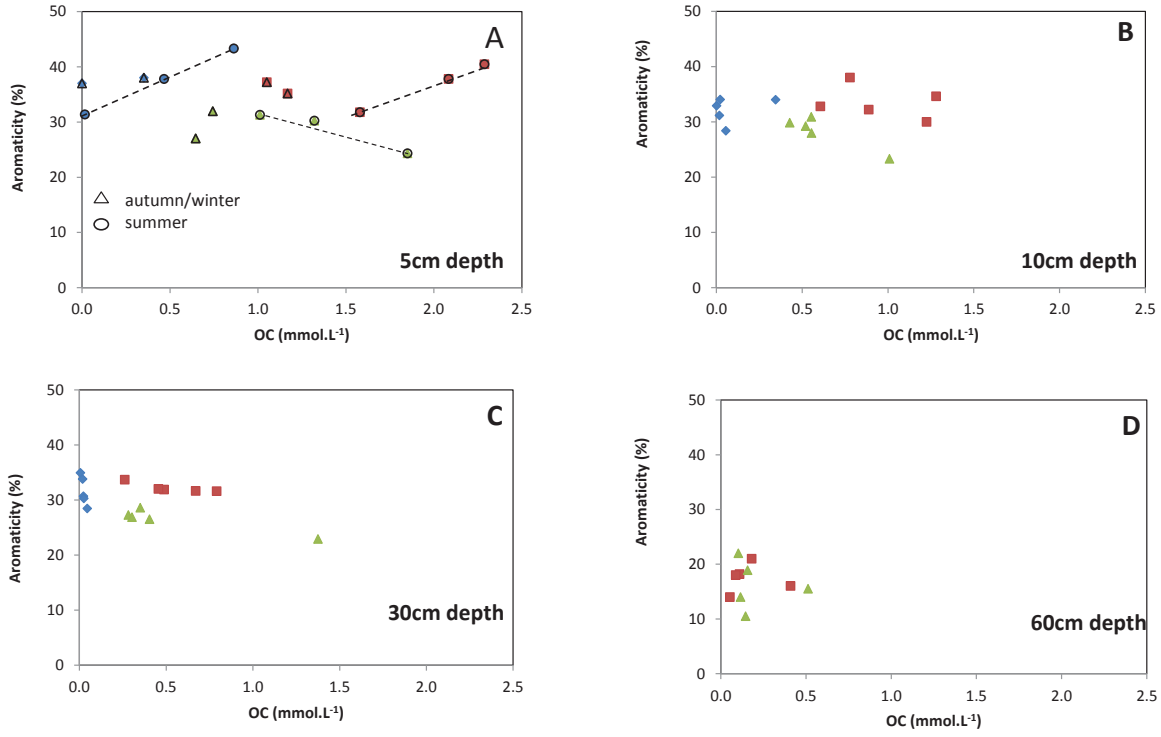

Figure 4: Variation of aromaticity with OC for the UF samples as function of depth (◆ 0,2 µm to 300kDa ■300 kDa to 5 kDa ▲ <5 kDa)

date	Sep-09	Oct-09	Nov-09	Dec-09	Jan-10	Feb-10	Mar-10	Apr-10	May-10	Jun-10	Jul-10	Aug-10	Sep-10
P_{rain} (mm)	44.7	87.0	116.4	172.8	79.0	90.8	60.6	36.0	124.0	123.7	95.8	231.2	65.1
P_{snow} (mm)	0.0	0.0	21.4	70.1	74.0	61.2	34.4	14.0	13.6	0.0	0.0	0.0	0.0
P_{rain} (mm per day)	1.5	2.8	3.9	5.6	2.5	3.2	2.0	1.2	4.0	4.1	3.1	7.5	2.2
P_{snow} (mm per day)	0.0	0.0	0.7	2.3	2.4	2.2	1.1	0.5	0.4	0.0	0.0	0.0	0.0
T (°C) mean	11.7	6.1	4.0	-2.5	-5.3	-3.1	-0.1	5.7	6.6	12.9	16.1	12.5	9.1
T (°C) Max	18.0	17.5	10.9	5.4	0.0	2.6	8.8	16.4	17.5	19.2	23.8	19.2	14.1
T (°C) Min	6.2	-3.1	-0.7	-15.1	-10.6	-11.5	-10.6	-1.6	0.3	6.1	9.3	5.2	2.5

date	Sep-12	Oct-12	Nov-12	Dec-12	Jan-13	Feb-13	Mar-13	Apr-13	May-13	Jun-13	Jul-13	Aug-13
P_{rain} (mm)	111.3	175.4	168.4	223.1	89.0	132.1	63.0	109.7	151.1	97.9	30.8	93.5
P_{snow} (mm)	0.0	16.7	35.3	98.8	47.8	82.4	40.7	7.0	8.8	0.0	0.0	0.0
P_{rain} (mm per day)	3.7	5.7	5.6	7.2	2.9	4.7	2.0	3.7	4.9	3.3	1.0	3.0
P_{snow} (mm per day)	0.0	0.5	1.2	3.2	1.5	2.9	1.3	0.2	0.3	0.0	0.0	0.0
T (°C) mean	10.5	7.2	3.1	-1.3	-2.2	-5.2	-1.4	4.4	6.0	11.9	16.8	14.3
T (°C) Max	18.1	15.4	7.4	8.8	5.2	2.3	6.5	13.8	10.9	23.6	24.6	24.4
T (°C) Min	5.6	-4.7	-4.8	-10.3	-9.5	-11.2	-7.7	-3.8	0.3	5.7	10.7	9.9

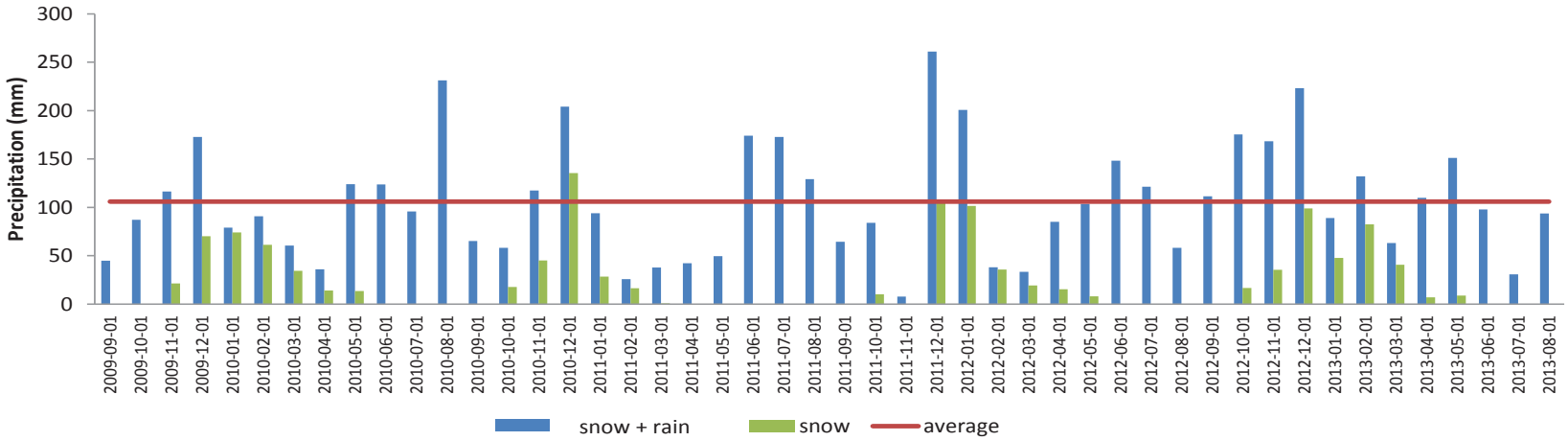

Electronic Annex T1: weather conditions recorded at the top station during the sampling periods

Sampling period	depth	Sample name
09/09/2009 to 11/12/2009	5 cm	VP-5 Nov-09*
	10 cm	VP-10 Nov-09*
	30 cm	VP-30 Nov-09*
	60 cm	VP-60 Nov-09**
11/12/2009 to 03/19/2010	5 cm	VP-5 March-10*
	10 cm	VP-10 March-10*
	30 cm	VP-30 March-10*
	60 cm	VP-60 March-10*
03/19/2010 to 06/21/2010	5 cm	VP-5 June-10*
	10 cm	VP-10 June-10*
	30 cm	VP-30 June-10*
	60 cm	VP-60 June-10*

Sampling period	depth	Sample name
06/21/2010 to 09/08/2010	5 cm	VP-5 Sept-10
	10 cm	VP-10 Sept-10
	30 cm	VP-30 Sept-10
	60 cm	VP-60 Sept-10
09/25/2012 to 11/20/2012	5 cm	VP-5 Nov-12*
	10 cm	VP-10 Nov-12*
	30 cm	VP-30 Nov-12*
	60 cm	VP-60 Nov-12*
11/20/2012 to 03/26/2013	5 cm	VP-5 March-13
	60 cm	VP-60 March-13
05/22/2013 to 08/06/2013	5 cm	VP-5 Aug-13*
	10 cm	VP-10 Aug-13*
	30 cm	VP-30 Aug-13*
	60 cm	VP-60 Aug-13**

Electronic Annex T2: Dates of sampling periods and corresponding names of soil solutions
*ultra- filtered samples
** ultra-filtered samples only at 5 kDa cut off size

Figure 4 shows the variations of the OC with the aromaticity at different depths. In general, whatever the fraction, the OC and aromaticity values show large variabilities in samples from the upper soil horizons which diminish with depth. Only the UF samples from upper soil solutions have 10 and 20% of OC in the 300R colloidal fraction with the strongest aromaticity (40%) (Electronic Annexes E.A.T3). For nearly all soil solutions, the OC is strongly enriched in the 5R colloidal fraction (40 to 70%) whereas the aromaticity is relatively constant until 30 cm depth (i.e. 36% to 32%) and decreases substantially to 17% at 60 cm depth. The proportion of the OC in the dissolved 5P fraction increases with depth and the aromaticity is less important i.e. 29% for the 5 and 10 cm depth, 26% for the 30 cm depth and 16% for the deepest samples (Electronic Annex E.A.T3).

4.2. **Variations of concentrations of Nitrogen (NO_3^-, NO_2^-, NH_4^+), P, Ca, Mn and trace elements (Cd, Zn) in the soil solutions**

In the upper soil solutions (filtered at 0.2 µm), the concentration patterns for NH_4^+, NO_2^-, P, Ca, Mn and trace elements (Cd, Zn) fluctuate in the same way (Fig 5A, 5E and Electronic Annex E.A.T3). The samples collected in June 2010 show five to ten time higher concentrations than those collected in other periods. Below 30 cm depth, they decrease substantially and show no season dependent variation. Nitrite anions are only detectable in soil solutions collected in June 2010 at 5 and 10 cm depth. The nitrate contents show different behaviour than the other major elements and fluctuate in the same way whatever the sampling depth (Electronic Annex E.A.T3).

Proportions for all these elements in colloidal and dissolved fractions are given in the Electronic Annex E.A.T4. This distribution is of the same order of magnitude as previously noticed by van Hees et al. (2001), Pokrovsky and Schott (2002), Pourret et al. (2007b), Waeles et al. (2008) and Pokrovsky et al. (2010).

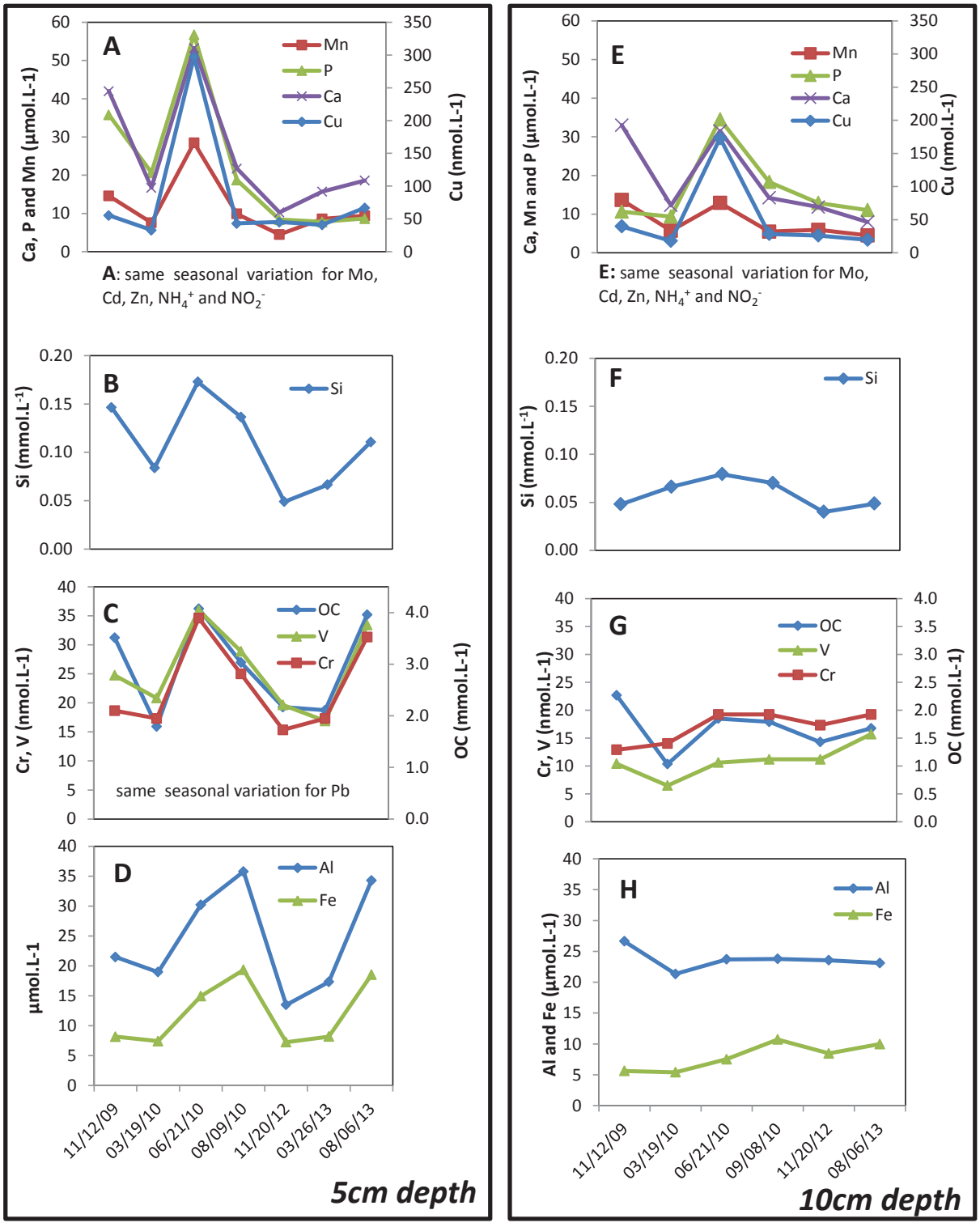

Figure 5: Seasonal variations of concentrations for the soil solutions filtered at 0.2 µm

4.3. **Variation of the concentrations of Si, Al and Fe in the soil solutions**

The concentrations of Al, Fe and Si are given in the Electronic Annex E.A.T3. The concentration patterns for Al and Fe fluctuate in the similar way with a different magnitude (Fig 5D and 5H). Aluminum content is of the same order of magnitude with depth and season (20 ± 3 $\mu mol.L^{-1}$), and decreases only at 60 cm depth (6 ± 3 $\mu mol.L^{-1}$) whereas Fe decrease from (12 ± 5 $\mu mol.L^{-1}$) at 5 cm depth until low concentrations at 60 cm depth (0.16 ± 0.09 $\mu mol.L^{-1}$). Aluminum and Fe are more enriched in the colloidal fractions with always a larger proportion for Fe (Electronic Annex E.A. T4). Iron is one of the most enriched elements in the colloidal 300R fraction whereas Al appears, as previously observed, more in the dissolved fraction (van Hees et al., 2000).

Silicon varies only seasonally in 0.2 µm soil solutions from 5 cm depth (Fig 5B and 5F). Below 10 cm depth, its amount remains relatively constant whatever the season and the depth (0.05 ± 0.01 $mmol.L^{-1}$). In the case of all UF samples, Si is entirely found in the dissolved 5P fraction.

4.4. **V, Cr, Pb concentrations in soil solutions**

Lead, V and Cr contents fluctuate seasonally in the upper and deeper 0.2 µm soil solutions in the same way as OC (Fig 5C, 5G and Electronic Annex E.A.T3). They decrease with depth for Pb from 71 (± 14) $nmol.L^{-1}$ to 1.5 (± 0.9) $nmol.L^{-1}$, for Cr from 22.8 (± 6.5) $nmol.L^{-1}$ to 7 (± 2) $nmol.L^{-1}$ and for V from 26 (± 6) $nmol.L^{-1}$ to 4 (± 3) $nmol.L^{-1}$. The molar ratio V:Cr is 1:1 for all 0.2 µm soil solutions from 5 cm depth and 1:2 for samples from other depths.

For the upper UF samples, Cr and V are similarly distributed in different fractions, i.e. nearly 60% in the colloidal fraction and 40% in the dissolved fraction. In the colloidal 5R fractions, these proportions vary with depth whereas they increase in the dissolved 5P fraction. Lead shows a distribution in the UF soil solutions similar to that of Fe. The distribution of

these trace elements in the colloidal fractions is of the same order of magnitude as found by Pokrovsky and Schott (2002), Waeles et al. (2008), Pokrovsky et al. (2010) and Pourret et al. (2012).

5. Discussion

Geochemical studies on soil solutions has illustrated that their chemical compositions are controlled by several sources (e.g., Stille et al., 2009; Kraepiel et al., 2015; Prunier et al., 2015). In addition to atmospheric deposition and recycling by vegetation, including the degradation of litter, the chemical elements can also have a lithologic origin, which results from the interactions of water with minerals of the soil. These studies also suggest that the OM, as well as its evolution, plays an important role in the chemical composition of soil solutions (Kaiser et al., 2001; Craine et al., 2007; Pourret et al 2007; Kleber et al., 2015). This last parameter is rarely taken into account when the spatial and temporal chemical variations of soil solutions are discussed. It is one of the objectives of the discussion below to provide further information on the origin of the chemical variation of soil solutions linked to the evolution of litter degradation and the variation of the OM in the soil profile.

5.1. Impact of litter degradation on major and trace elements in surface soil solutions

The degradation of the litter creates a significant OM flux but also a flux in all biogenic chemical elements that it contains, as well illustrated, for instance, for Ca (e.g., Poszwa et al., 2000; Dijkstra et al., 2002; Cenki-tok et al 2009; Clarholm et al., 2013). High concentrations of Ca in the most superficial soil solutions, and their decrease with depth are classically interpreted such as a signature of the recycling of the Ca by vegetation with a Ca input by litter degradation in the surface soil horizons, and a loss in the deeper horizons by root uptake. In our study, one observes a positive correlation between Ca and P, Mn, Zn, Cd concentrations in the uppermost

soil solutions filtered at 0.2 µm (Table 1A), which suggests a common main origin for all these elements, namely in the present case the needle litter degradation. This hypothesis is reinforced for Ca, P and Mn by the similar Ca/P and Ca/Mn molar ratios analyzed in the spruce needles and in soil solutions (Table 1B). Moreover, the chemical composition of the upper 0.2 µm soil solutions varies over time, with for instance, OC enrichments observed at four sampling periods (Fig. 5B and 5C). Among these four samples, those collected in November 2009 and June 2010 are also enriched in reduced nitrogen compounds like NH_4^+ or NO_2^- (Fig.5A) with NO_3^- and pH high values (Electronic Annex E.A.T3). The presence of NH_4^+, NO_2^- and high pH values is classical for anoxic or oxygen poor environments (Philippot and Hallin, 2005) marked by the occurrence of denitrification process, which reduces NO_3^- to NO_2^- and consumes H^+ causing a pH increase (Grybos et al., 2009; Frohne et al., 2011; Buettner et al., 2014). It is a respiratory process for microorganisms where NO_3^- and NO_2^- are the final electron acceptors instead of O_2 during the oxidation of organic matter (OM) (Levy-Booth et al., 2014). Thus, in anoxic environment enriched in OM, the denitrifying bacteria reduce NO_3^- to NH_4^+ (Jorgensen, 1989; Takaya, 2002; Canfield et al., 2010), whereas in oxic environments, the nitrification process involves two steps: nitritation ($NH_4^+ \rightarrow NO_2^-$) and nitratation ($NO_2^- \rightarrow NO_3^-$) with a decrease of pH and a fast oxidation of NO_2^- (Allison and Prosser, 1993; Canfield et al., 2010; González-Blanco et al., 2012). The occurrence of different steps of the nitrogen cycle according to the anoxic or oxic character of the environment thus easily explains the variations of the concentrations of nitrogen species in the upper soil solutions of the Strengbach watershed.

In addition to the increase of nitrogen compounds in samples filtered at 0.2 µm and collected in November 2009 and June 2010, these samples show also an increase of P, Ca, Mn, Zn and Cd concentrations (Figures 5A and 5E). This is linked to the fact that in anoxic events microorganisms transform recalcitrant OC to reach N necessary to form NO_3^- or NO_2^- as terminal electron acceptors (Craine et al., 2007). The OC transformation may be more important than for the other sampling periods and hence may cause

a more important Ca, P, Mn, Zn and Cd release. Such an interpretation is consistent with Berg (2000)'s observation that the litter decay degree is inversely correlated with Mn and Ca contents in the residual litter.

A

Soil solutions (0.2 µm and 5 cm depth)	With Mn			With (OC+N)/Ar		
	slope	R^2	p-Value	slope	R^2	p-Value
Si ($\mu mol.L^{-1}$)	4.5	0.750	0.012	1401	0.870	0.020
P ($\mu mol.L^{-1}$)	1.9	0.892	0.001	1250	0.890	0.030
Ca ($\mu mol.L^{-1}$)	1.8	0.995	< 0,0001	1028	0.957	0.022
Mn ($\mu mol.L^{-1}$)	1.0	1.000	0.000	589	0.975	0.013
Zn ($nmol.L^{-1}$)	39.8	0.971	0.017	24036	0.970	0.015
Cd ($nmol.L^{-1}$)	0.061	0.966	0.000	38	0.929	0.036

B

Spruce needles (summer 2011)	Al	Ca	Fe	Mn	P	Ca/P (molar)	Ca/Mn (molar)
(µg.g-1)	125	1885	70	1355	1636	0.89	1.91

Table 1: (A) Slopes, correlation coefficients and p-values for the variations of Si, P, Ca, Mn, Zn and Cd concentrations with the Ca concentrations for the soil solutions filtered at 0.2 µm at 5 cm depth . (B) Chemical composition of spruce needles.

It is therefore proposed based on the above observations, that the chemical dynamics of OC, nitrogen compounds but also of Ca, Mn, P, Zn and Cd of upper soil solutions (filtered at 0.2µm) are related to the context of litter degradation, which differs in oxic and anoxic conditions by the involvement of two different respiratory ways for soil microorganisms, with probably different bacterial communities in each conditions, as observed by López-Mondéjar et al. (2015) in some forest soils. Development of bacterial communities and their activity are indeed regulated by seasonal parameters (temperature, rainfall) (Tack et al., 2006; McMahon and Chapelle, 2008; Backnäs et al., 2012; Shaheen et al., 2014), but also, and maybe more importantly, by the soil water filling pore space (WFPS), which influences the O_2 rate in the soil microenvironment (Chen et al., 2015; Ge et al., 2015).

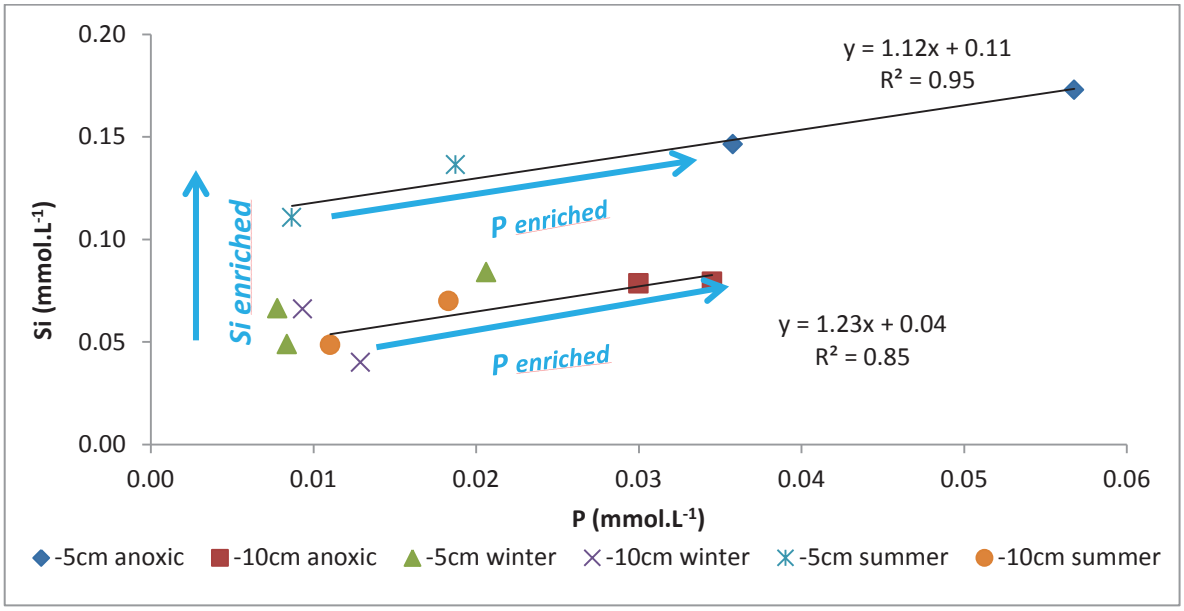

Figure 6: Covariations of Si and P for soil solutions filtered at 0.2 µm at 5 cm and 10 cm depth

An enrichment of Si is also observed in the surface soil solutions from the Strengbach watershed in spring and summer (Fig. 5B). This increase of Si can be explained by a release of Si from aluminosilicate minerals and/or by a biogenic Si flux, due to phytolithe dissolution (Ehrlich et al., 2010). The phytolithes represent biogenic Si in the soil, which correspond to a recent rapidly dissolved and recycled Si (Alexandre et al., 2011). Moreover, P is positively correlated with Si in soil solutions collected in spring and summer close to the surface and filtered at 0.2 µm (Fig. 6). Such a correlation indicates a parallel evolution of Si and P in soils or soil solutions, which has most likely to be linked to the litter decomposition, as the latter has been invoked to explain the P concentration variations in the soil solutions (see above). In the soils, the most important part of P_{orga} is represented by the phosphate inositols [$C_6H_6(OH)_3(OPO_3H_2)_3$ and $C_6H_6(OPO_3H_2)_6$], commonly named phytates, which result from degradation of the cell walls. Phytates are very stable molecules, which are not bio-available (Rodríguez and Fraga, 1999; Courty et al., 2010; Fuentes et al., 2014). The correlation between Si and P could thus indicate a parallel dissolution of phytates and phytolithes, co-occurring with litterfall degradation, which is consistent with the

observation that P and Si vary similarly during plant biodegradation (Ehrlich et al., 2010). However P, similarly to Si, can also have a lithological origin, particularly in the Strengbach site, where the granitic bedrocks contain apatites (Aubert et al., 2001; Fischer et al., 1998) and surface soils secondary phosphate minerals, such as rhabdophanes ($LREE(PO_4)$) (Stille et al., 2009) or pyromorphites ($Pb_5(PO4)_3X$) (Stille et al., 2011; Gangloff et al., 2014). In the upper soil solutions, it is thus possible to have a mixture of Si and P originating from secondary minerals and from the degradation of the litter. Based only on chemical concentration analyses, it is however difficult to characterize the exact place of such lithogenic fluxes relative to the biogenic ones. The only firm conclusions that can be proposed at this stage from the correlation between P, Si and OC are either that the biogenic contribution linked to the litter decomposition is much more intense than the lithogenic ones in the OC enriched samples, or either, if the lithogenic contribution is still significant (e.g., Prunier et al., 2015) that the latter is itself controlled or modulated by the intensity of litter degradation.

The atmospheric derived trace elements, like Pb, V and Cr, which are deposited on litterfall are likely or can be theoretically mobilized during needle litter decomposition (Reimann et al., 2007; Stille et al., 2011; Guéguen et al., 2012; Hidemori et al., 2014). This probably explains why the concentrations of these trace elements in the uppermost soil solution (5cm depth) show the same seasonal variation as OC concentrations (Fig5C and 5G). Another reason is their affinity for soil OC (Čežíková et al., 2001; Wällstedt et al., 2010; Pourret et al., 2012; Shaheen et al., 2014). However in the Strengbach case, lead is more enriched in the upper soil solutions than V or Cr (respective averages: 75 $nmol.L^{-1}$, 26 $nmol.L^{-1}$ and 23 $nmol.L^{-1}$), with soil solutions Pb/V or Pb/Cr concentration ratios 15 times higher than those of recent or present-day atmospheric dusts (Guéguen et al., 2012). This difference can be related to the important enrichment of Pb in the upper soil originating from the mining and industrial activities near the catchment during the 19^{th} and the beginning of the 20^{th} century (Stille et al., 2011). Consequently, it can be proposed that V and Cr in the here studied soil

solutions principally originate from recent atmospheric dusts, while Pb concentrations record older soil enrichments. The Atmospheric origin of Cr and V is confirmed by the similar Cr/V values analyzed in soil solution and in atmospheric deposits (Guéguen et al., 2012).

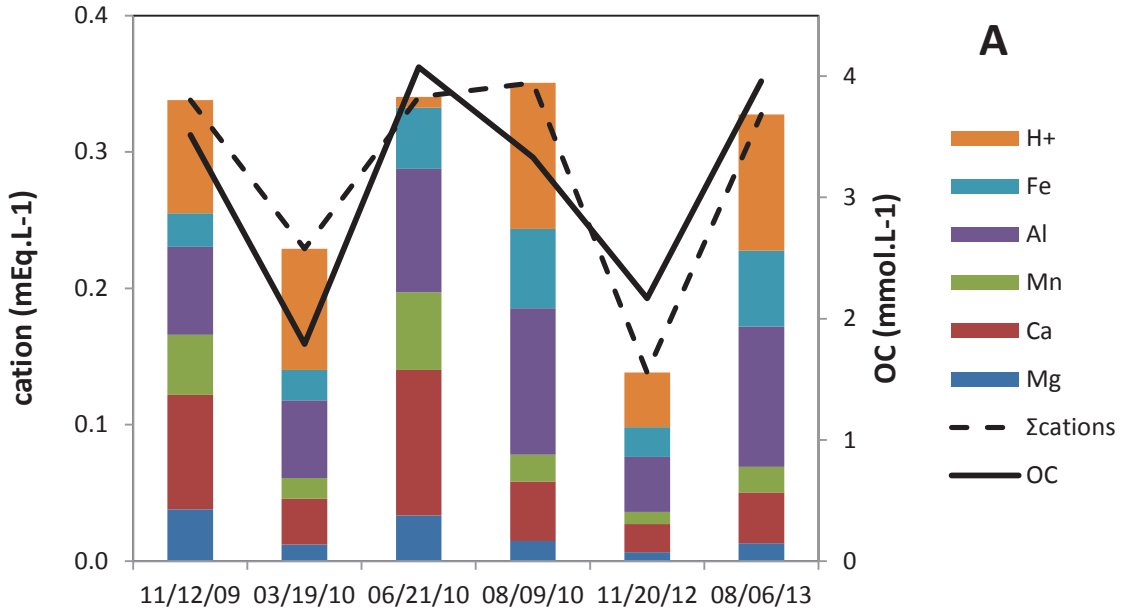

B

fraction - depth	R^2	p-Value
0.2µm - 5cm	**0.85**	**0.015**
0.2µm - 10cm	**0.90**	**0.015**
0.2µm - 30cm	**0.94**	**0.005**
0.2µm - 60cm	0.62	0.14
300R - 5cm	**0.99**	**0.001**
300R - 10cm	**1.00**	**<0,0001**
300R - 30cm	0.74	0.15
5R - 5cm	**0.97**	**0.007**
5R - 10cm	**0.98**	**0.003**
5R - 30cm	**0.99**	**0.002**
5R - 60cm	0.38	0.5
5P - 5cm	0.70	0.18
5P - 10cm	0.83	0.081
5P - 30cm	**0.91**	**0.03**
5P - 60cm	0.50	0.4

Figure 7: (A) Distribution of major cations in the 0.2 µm samples at 5 cm depth and (B) Correlation coefficients and p-values corresponding to the variation of OC with Σcations in different sample

Compared to the above elements (Mn, P, Ca, Cd, Zn), which are enriched in the soil solution of November 2009 and June 2010, Fe and Al are rather impoverished (Fig.5A and 5D). As suggested by Kraepiel et al. (2015), Al and Fe would be much more influenced by geochemical than biological processes in the upper soil layers. Especially, their solubility in soil solutions depends on the pH, the presence of organic complexes and for Fe the redox conditions (Kleber et al., 2015). Thus, it can be anticipated that during the passage of the soil solution through the soil, the concentrations of those metals in soil solutions will be modified. It is important to note here that when comparing the soil solution composition between 5 and 30 cm (Fig. 7A and 7B) concentrations of the major cations and OC significantly vary. The OC enriched samples are also cations enriched and OC is significantly correlated with (H^++Σcations) in the organic horizon soil solutions filtered at 0.2 µm and in 5R colloidal fractions (Fig.7B) (see also § 5.3). It may be proposed that in surface soil solutions, Al and Fe contents vary to equilibrate the charge of OC as a function of the other major cations that originate from litter degradation. Their amounts are lower during the anoxic events because Ca and Mn are more important or because the pH value, which is weakly higher, may also decrease their solubility. Consequently, it is important to characterize the evolution of OC in the different fractions with depth (colloidal and dissolved) for having a better understanding of the soil solution compositions.

5.2. **Organic carbon transformation during the litter decomposition and its evolution with depth**

The OC enrichment in the upper soil solutions filtered at 0.2 µm results from an increase of formation of hydrophilic molecules whose aromaticity is not systematically larger than that of the other samples (Electronic Annex E.A.T3). For the corresponding UF samples, one observes that the OC in the colloidal fractions (300R and 5R) increases with aromaticity whereas it decreases in the dissolved fraction (5P) (Fig 4A). In

contrast, the samples with smaller OC contents are collected during winter, their aromaticity and OC contents are almost similar for the 5R and 5P fractions and below the detection limit for the 300R fraction (Fig. 4A). This OC distribution might be explained by litter decomposition. The resulting structural organic components are principally cellulose, pectin, hemicellulose, lignin and structural proteins (Berg, 2000; Sjöberg et al., 2004; Craine et al., 2007). During the litter decay, the organic macro-molecules are transformed along a continuum in smaller organic molecules like carbohydrates and novel aromatic recalcitrant compounds (Kaiser et al., 2002; Kalbitz and Geyer, 2002; Prescott, 2010). These organic molecules are modified by hydrolysis or oxidation-reduction reactions catalyzed by enzymatic systems (Ussiri and Johnson, 2003; Don and Kalbitz, 2005; Klotzbücher et al., 2013). The different upper UF samples show a variation of OC structure as a function of the season (Fig. 4A). This is in accord with the conclusion of (Kaiser et al., 2001) who suggested that in winter, OC seems to be mainly controlled by soil leaching with soil solutions and, in summer, by the decomposition processes resulting in the production of water-soluble aromatic compounds.

The aromaticity of soil solutions filtered at 0.2 µm and collected in November 2009 is smaller and their OC values are larger than those observed for the other samples from different depths (Electronic Annex E.A.T3). This signifies that OC is more hydrophilic and, consequently, more mobile for this period. In the particular case of the samples collected during the anoxic events (November 2009 and June 2010), the aromaticity/OC ratio is lower for these different fractions compared to the other samples (not shown). Moreover, OC content is very low or below detection limit as observed for the 300R fraction. These differences attest an organic molecular structure different for OC corresponding to the samples collected during anoxic events, with less aromaticity and a less macromolecular structural organization. Such variations probably point out a higher evolution degree of the OC derived from the needles litter degradation during the anoxic events. Simultaneously, the soil microorganisms need NO_3^- or NO_2^- as final electron

acceptor for their respiration (see section 5.1.). Numerous studies showed that the microorganisms use N_{orga} as potential N source at low N availability rather than N_{inorg} (Craine et al., 2007; Hayatsu et al., 2008; Nannipieri and Eldor, 2009; Chen et al., 2015). Other studies dealing with litter decomposition determined a two steps decay process. The first one concerns compounds which are easily mineralized (cellulose and hemicellulose) and its decay rate is fast and proportional to the N content; the second one concerns the transformation of the recalcitrant compounds (lignin) and its decay rate is slower and inversely proportional to N (Melillo et al., 1982; Berg, 2000; Lorenz et al., 2000; Craine et al., 2007; Prescott, 2010; Walela et al., 2014). Moreover, according to Lorenz et al. (2000) and Craine et al. (2007), the lignin-derived compounds may sequester N and the soil microorganisms may degrade this recalcitrant OC to reach N. Altogether, these different data and information confirm that the OC and N composition of the upper soil solutions reflects the decomposition of the litter and indirectly depends on biotic processes controlled by the soil microorganisms.

Once the litter is decomposed and leached by rain or throughfall, the water-soluble compounds are dissolved and transported by the soil solution along the profile (Kalbitz et al., 2003; Corvasce et al., 2006; Gangloff et al., 2014). The organic functional groups of OC in the upper soil solutions vary as a function of the degree of litter decomposition and the biochemical processes involved (see above). This variability induces a change in the mobility of the water soluble compounds along the soil profile and consequently in the nutrient and trace element transport (Kaiser et al., 2001; Stadler et al., 2006; Gangloff et al., 2014). For the sampling periods (without November 2009), the OC values in 0.2 µm filtered soil solutions decrease with depth. The 300R fraction, below 10 cm depth, does not contain detectable amounts of OC either because the macromolecules are disassembled or adsorbed on the soil particles through organic aromatic rings (Kalbitz et al., 2005). Organic carbon is principally found in the colloidal 5R fraction with a weak variation in the aromaticity along the soil profile whereas the amounts of OC contained in the dissolved 5P fraction

decreases and remain relatively constant until 30 cm depth (Fig 4). Organic carbon is more rapidly modified in the 300R and 5P fractions while the OC transformations are less substantial in the 5R fraction along the soil profile. The OC content and aromaticity variation between 5cm and 10 cm depth samples attest a transformation with a molecular deconstruction (Fig. 4A). According to Ussiri and Johnson (2003), the OC molecular structure changes considerably with depth. The polar functional groups decrease and the aliphatic compounds increase with depth (Gangloff et al., 2014). The depletion of polar functional groups with depth might be related to the bio-degradation of OC by microorganisms in the upper soil solutions (Kaiser et al., 2002; Stadler et al., 2006).

The 60 cm depth samples were collected below the rhizosphere (30-40 cm depth). The colloidal and the dissolved fractions of these samples have lower OC contents and aromaticities (Electronic Annex E.A.T3). This OC could be provided by microbial metabolites from the rhizosphere or secreted by the soil microorganisms (Pédrot et al., 2010), and hence has probably no more direct genetic relationship with OC coming from litter degradation.

5.3. **Evolution of major and trace element concentrations with depth and in the different soil solution fractions**

The co-variation of the soil solution pH as a function of OC concentrations in some samples along the soil profile (Figure 3A) confirms that OC is a proton source for soil solutions (Fujii et al., 2008; Clarholm and Skyllberg, 2013). Gangloff et al. (2014) determined the mean proton affinity constant (pK_H) and the charge density (Q_H mEq/gC) for OC in water extracts of another soil profile of the same experimental parcel. The respective values for the 3-13 cm soil sample were 1.6 and 7.5 mEq/gC and 4.3 and 3 mEq/gC for the 13-16 cm soil sample. The charge density and the pH values of the soil solutions (Electronic Annex E.A.T3) suggest that OC protons are more exchangeable with soil cations at the surface than below 13 cm depth.

This phenomenon certainly explains the decrease of soil solution acidity between 5 cm and 10 cm depth (Electronic Annex E.A.T3). In the particular case of the upper UF samples collected in November 2012 and August 2013, the correlation between protons and OC points out that the carboxylic functional groups are protonated indicating that protons equilibrate the ionic balance between cations and OC in these samples (Fig. 3C). However, such correlation is not systematic, and does not exist, for the two upper UF samples collected in June 2010 and March 2010 (Fig 3C). More particularly, for the samples of June 2010, OC might be saturated by the cations like Ca^{2+}, Mn^{2+}, Al^{3+} and Fe^{3+} (Clarholm and Skyllberg, 2013) and the protons might be used for the microorganisms respiratory processes. For March 2010 samples, the excess protons are probably originating from rain or throughfalls.

According to Clarholm and Skyllberg (2013), and in agreement with the significant correlation between the OC and (H^+ + Σcations) concentrations (Fig. 7B) in the samples filtered at 0.2 µm and in the 5R colloidal fraction, the cations participate in the regulation of the pH and equilibrate the negative charges of OC. In our study, the most abundant cations that balance the anionic sites of OC are Ca and Al with a contribution of Mn, and Fe (Table 2). Na and K are known to be not involved directly in the equilibration of the OC charges of soil solutions (Pourret et al., 2007; Clarholm et al., 2013).

depth	Date	0.2 µm filtered					5R fraction					5P fraction				
		H+ (%)	Ca (%)	Mn (%)	Al (%)	Fe (%)	H+ (%)	Ca (%)	Mn (%)	Al (%)	Fe (%)	H+ (%)	Ca (%)	Mn (%)	Al (%)	Fe (%)
5 cm	11/12/09	47	24	12	12	5	46	22	11	15	6	14	41	22	17	6
5 cm	03/19/10	64	12	5	14	5	65	8	3	16	8	68	13	6	10	3
5 cm	06/21/10	6	40	21	22	11	0	37	19	29	16	11	45	26	14	5
5 cm	08/09/10	55	11	5	18	10										
5 cm	11/20/12	53	14	6	18	10	26	20	8	29	17	47	18	9	19	8
5 cm	03/26/13	61	12	7	13	6										
5 cm	08/06/13	55	10	5	19	10	29	16	7	29	18	55	11	7	21	7
	Mean	49	18	9	17	8	33	21	9	24	13	39	25	14	16	6
10 cm	11/12/09	24	32	13	26	5	44	17	4	27	7	35	31	16	16	2
10 cm	03/19/10	53	13	6	23	6	54	11	4	25	6	56	13	7	19	5
10 cm	06/21/10	10	38	15	28	9	5	27	11	41	15	14	47	19	16	3
10 cm	08/09/10	40	16	6	26	12										
10 cm	11/20/12	41	14	7	28	10	42	11	4	31	12	39	17	10	26	8
10 cm	08/06/13	62	7	4	19	8	49	9	4	25	13	68	5	4	17	6
	Mean	38	20	9	25	8	39	15	6	30	11	42	23	11	19	5
30 cm	11/12/09	39	26	10	22	3	31	22	3	39	5	15	39	19	23	3
30 cm	03/19/10	36	17	6	34	6	22	13	6	50	9	42	19	6	28	5
30 cm	06/21/10	48	13	6	28	5	46	11	4	33	6	49	14	6	26	5
30 cm	08/09/10	36	19	9	27	9										
30 cm	11/20/12	48	9	4	31	8	46	10	4	32	9	51	7	5	31	7
30 cm	08/06/13	43	6	4	38	10	38	6	4	40	12	44	7	3	39	7
	Mean	42	15	6	30	7	36	12	4	39	8	40	17	8	29	5
60 cm	11/12/09	55	24	5	15	1	82	5	1	12	1	36	42	9	12	1
60 cm	03/19/10	47	26	10	16	0	38	35	11	15	1	49	24	10	16	0
60 cm	06/21/10	5	61	26	8	0	0	66	25	8	0	10	56	27	7	0
60 cm	08/09/10	45	32	11	12	0										
60 cm	11/20/12	53	11	5	31	0	71	7	3	18	0	47	13	5	34	1
60 cm	03/26/13	53	11	3	32	1										
60 cm	08/06/13	2	87	1	9	0	0	89	1	9	0	7	80	2	10	0
	Mean	37	36	9	17	0	38	41	8	13	0	30	43	10	16	1

Table 2: Proportions of major cations in different soil solutions filtered at 0.2µm and in the 5R and 5P fractions

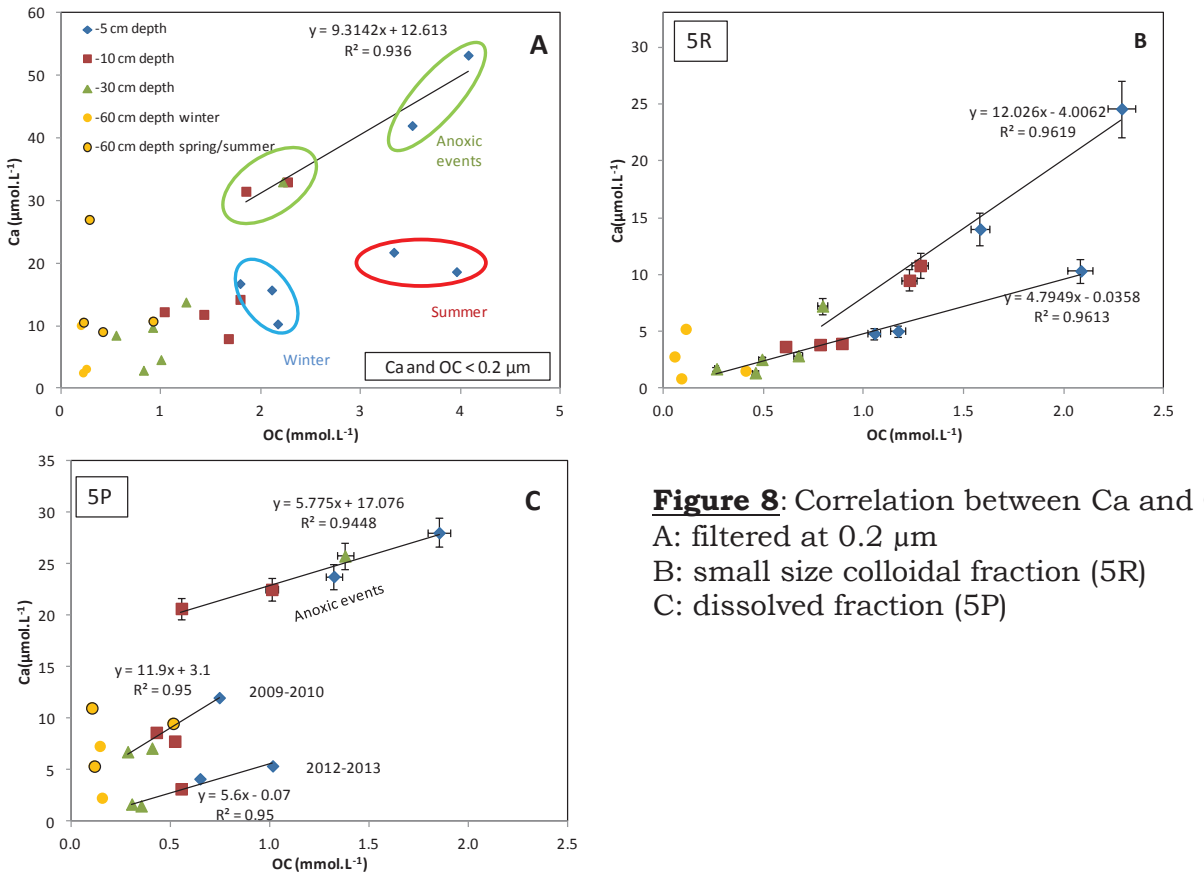

Figure 8: Correlation between Ca and OC in soil solutions
A: filtered at 0.2 µm
B: small size colloidal fraction (5R)
C: dissolved fraction (5P)

	0.2 µm filtered		5R		5P	
	Slope	R^2	Slope	R^2	Slope	R^2
5 cm	1.80	0.995	1.86	0.997	1.81	0.992
10 cm	2.63	0.984	2.26	0.984	2.30	0.947
30 cm	2.55	0.984	2.00	0.969	2.06	0.990
60 cm	2.34	0.959	2.40	0.953	1.96	0.949

Table 3: Correlation between Ca and Mn for all samples at different depth

In our study, the soil solution data show that Ca and Mn have a very similar behavior in all fractions (Table 3). Systematically, their concentrations are higher in the anoxic samples (Electronic Annex E.A.T3). The co-variations between Ca and OC concentrations in different fractions and at different depth, as illustrated in Figure 8, indicate that Ca and Mn are complexed with OC, most likely to equilibrate the negative charges of OC (Dahlqvist et al., 2004; Pokrovsky et al., 2010) especially those of the carboxylate functional group (Gangloff et al., 2014). In the 5R colloidal fractions, Ca and Mn are complexed with OC according two trends as a function of the oxic or anoxic conditions (Fig. 8B) and in the 5P dissolved fractions, according three trends (Fig. 8C). All these trends signify that Ca and Mn are firstly complexed with OC in the 5R colloidal fraction and differently in the anoxic condition, on the one hand because there is more Ca and Mn originating from the litter decomposition or, on the other hand, due to a larger density of carboxylate functional group of OC. In the 5P dissolved fraction, the linear relationship representing the variation of Ca and Mn as a function of OC intercepts the Ca and Mn axis for the anoxic samples and for those collected in 2009-2010, while not for those collected in 2012-2013 which are less enriched in Ca and Mn (Electronic Annex E.A.T3). The different correlations imply that Ca and Mn are complexed with OC. For the anoxic samples and those collected in 2009-2010, the observation that OC concentrations tend to zero before Ca and Mn, certainly indicates that in addition of Ca and Mn complexed with OC a part of these elements is still

under free species like $Ca^{2+}_{(H2O)}$ and $Mn^{2+}_{(H2O)}$ in soil solutions. Consequently, the relative proportion of Ca and Mn in the 5P dissolved fraction is less important for the more depleted samples. This phenomenon has been also observed by Pokrovsky et al. (2010) for Ca in the study of the Severnaya Dvina river. More the sample was depleted in Ca, more the proportion of Ca in the colloidal fraction was important. Moreover, in this study, the Ca and Mn proportions decrease in the 5R colloidal fraction between 5 cm and 10 cm depth and in the 5P dissolved fraction between 10 cm and 30 cm depth (Table 2). This may indicate that Ca and Mn are weakly complexed with OC and may be exchangeable between the colloidal and dissolved fractions and between dissolved fraction and the vegetation, which the rhizosphere is situated at 30 cm depth. Once in the dissolved fraction, Ca and Mn may be used as nutrients in the biotic processes (Dijkstra and Smits, 2002; Schmitt et al., 2013).

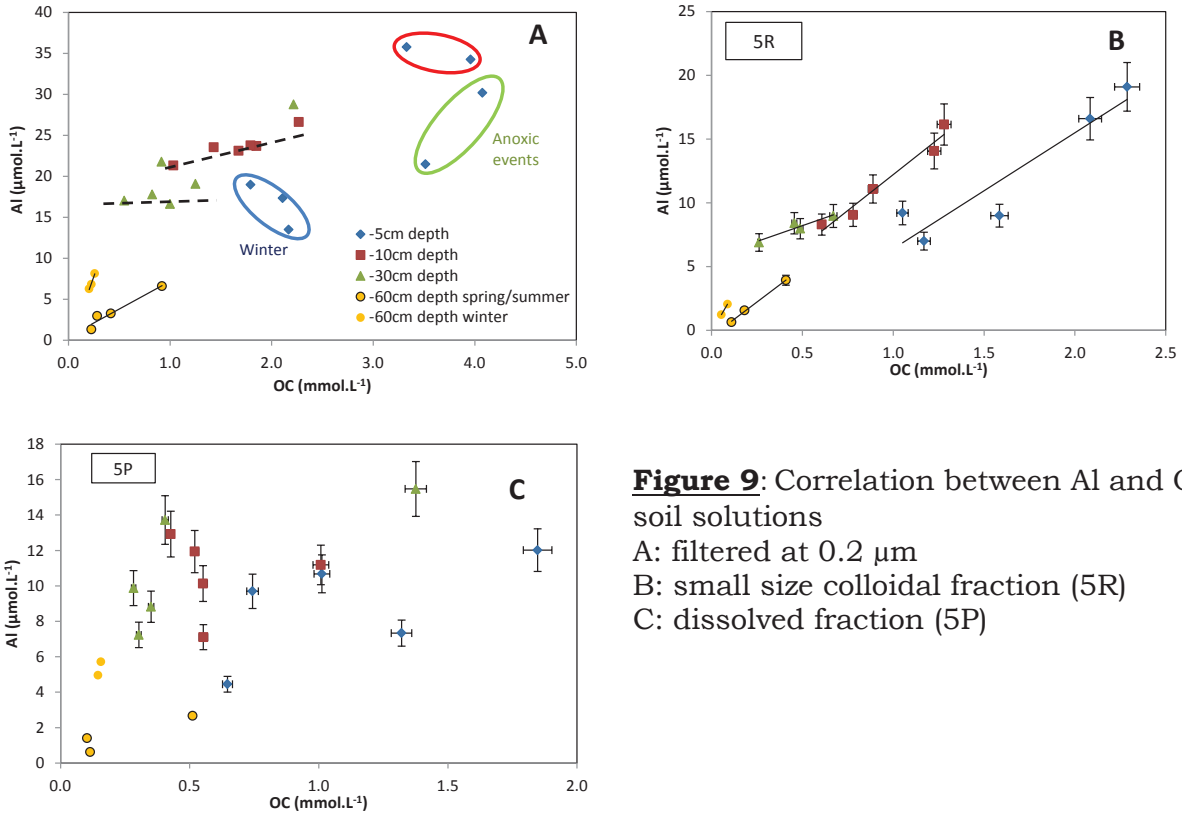

Figure 9: Correlation between Al and OC in soil solutions
A: filtered at 0.2 µm
B: small size colloidal fraction (5R)
C: dissolved fraction (5P)

The variation of Al concentrations in soil solutions as a function of OC at different depths and in the different fractions (0.2 µm, 5R and 5P) is shown in Figure 9. Aluminum is correlated with OC in the colloidal 5R fraction. Its proportion in the 5R colloidal fraction increases with depth as well as the Al/OC ratio (Table 2 and Fig. 9B). This highlights Al enrichment in the colloidal fraction. In this study, the pH values of the soil solutions are below 4.5 and, thus, induce the dissolution of Al hydroxides in the soil. Released Al is complexed with OC as a function of the contents of other cations. High proportions of more exchangeable cations such as Ca or H^+, decrease the proportion of Al complexed with OC. Dijkstra and Fitzhugh (2003) observed the same behavior of Al in soil solutions from a forest soil. The type of the organic functional groups and the binding strength between Al and OC are different compared to Ca, Mn and Fe (Clarholm and Skyllberg, 2013; Gangloff et al., 2014). This explains the Al enrichment in the colloidal fraction causing OC stabilization. The concentrations of Al increase between 5 and 10 cm depth for the winter samples while they are constant for samples impacted by micro-organisms activity releasing sufficient other cations like Ca or Mn to stabilize OC (Electronic Annex E.A.T3, Fig. 8 and Fig. 10B). A study of ultra-filtered forest soil solutions also points to a seasonal variation of the Al concentration in the <1 kDa fraction (Umemura et al., 2003). Below 30 cm depth, the concentrations of Al increase in the dissolved 5P fraction whereas those of other cations decrease due to absorption by roots or adsorption on oxyhydroxides (Dijkstra and Fitzhugh, 2003). Thus, Al substitutes the other cations coming either from colloidal or dissolved fraction or from dissolution of soil particles (Clarholm and Skyllberg, 2013). That Al can be transferred from the colloidal to the dissolved fraction at 30 cm depth is indicated by the variation of Al concentrations (Fig. 10 A, B and C). During such a transfer, Al might replace soil depleted nutrient cations like Ca or Mn and thus become a phyto-toxic risk.

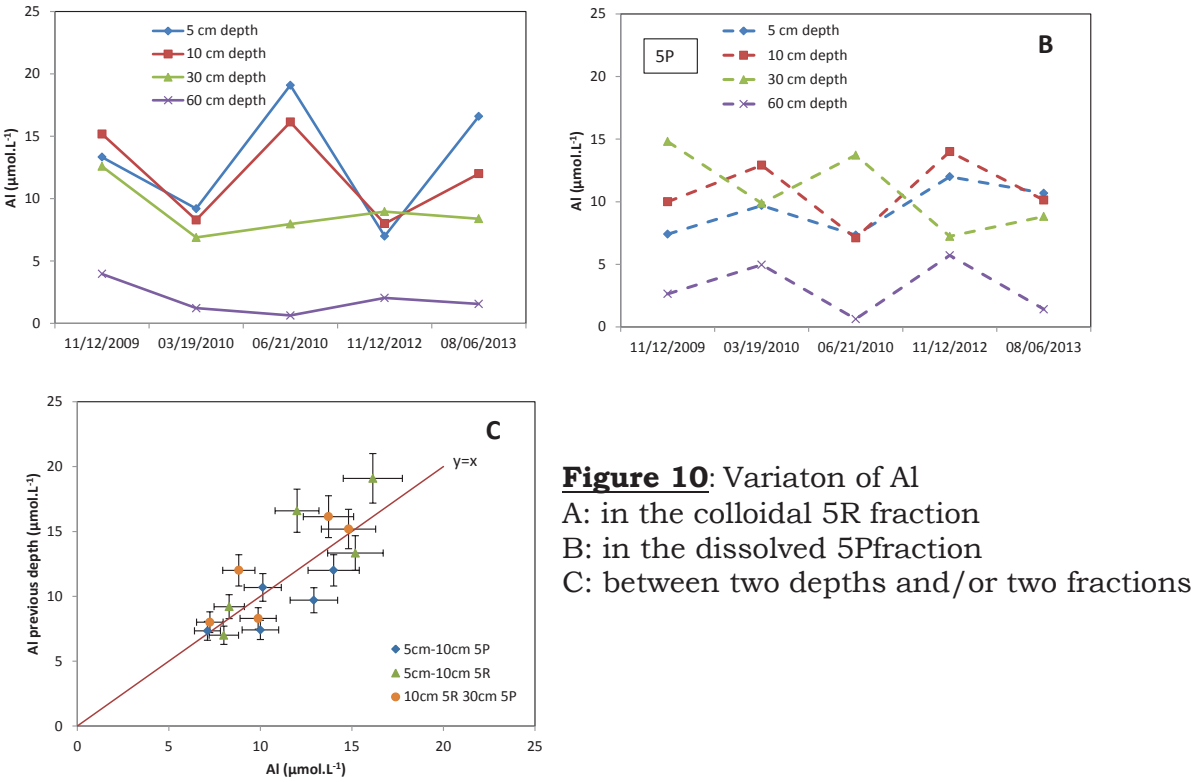

Figure 10: Variaton of Al
A: in the colloidal 5R fraction
B: in the dissolved 5Pfraction
C: between two depths and/or two fractions

The variation of Fe concentrations in soil solutions as a function of OC at different depths and in the different fractions (0.2 µm, 5R and 5P) is shown in Figure 8. In this study, the pH values of the soil solutions are below 4.5 and, thus, induce the dissolution of the soil Fe hydroxides. Once released Fe is complexed with OC as a function of the contents of other cations. Iron is correlated with OC in the colloidal 5R fraction according to the same trend along the soil profile (Electronic Annex E.A. Fig.1B), which suggests they follow the same evolution in the 5R colloidal fraction with depth. The relative proportions of Fe are always larger than those of Al and OC in the colloidal fractions compared to the 0.2 µm filtered samples (Electronic Annex E.A.T4). These different distributions are due to their different affinity for the organic functional groups of OC (Cabaniss, 1992; Nierop et al., 2002; Gangloff et al., 2014). Similarly to Pédrot et al. (2009), Stolpe et al. (2013) and Buettner et al. (2014), we observe that Fe has more affinities for aromaticity enriched OC in the colloidal 300R and 5R fractions (not shown). Kalbitz et al. (2005) pointed out that the aromatic carbon is the most stable component which stabilizes OC by sorption to soil minerals.

Consequently, Fe may be adsorbed to the soil particles at the same time as OC stabilization through aromatic compounds. Moreover, a comparison between Al and Fe behaviors in soil water extracts obtained with a soil profile of the same experimental parcel showed that Fe was present in the micro and macro-pores while Al was more mobile and present in the macro-pores (Gangloff et al 2014). This comparison consolidates the hypothesis that Fe is probably adsorbed to the soil particles while Al is more present in gravity soil solutions. The behavior of Fe as a function of OC is different in the dissolved 5P fraction (Electronic Annex E.A. Fig.1C). Whatever the OC concentrations, those of Fe are relatively constant (2.53 ± 0.25 µmol/L ; 2SE; N=15) between 5 and 30 cm depth. This stable value might correspond to the steady state for Fe in the 5P dissolved fractions beyond which Fe precipitates. Indeed, it has been observed that there is a steady state from which Fe precipitates in the dissolved fraction that is achieved with less Fe in the presence of microorganisms (Thuróczy et al., 2011).

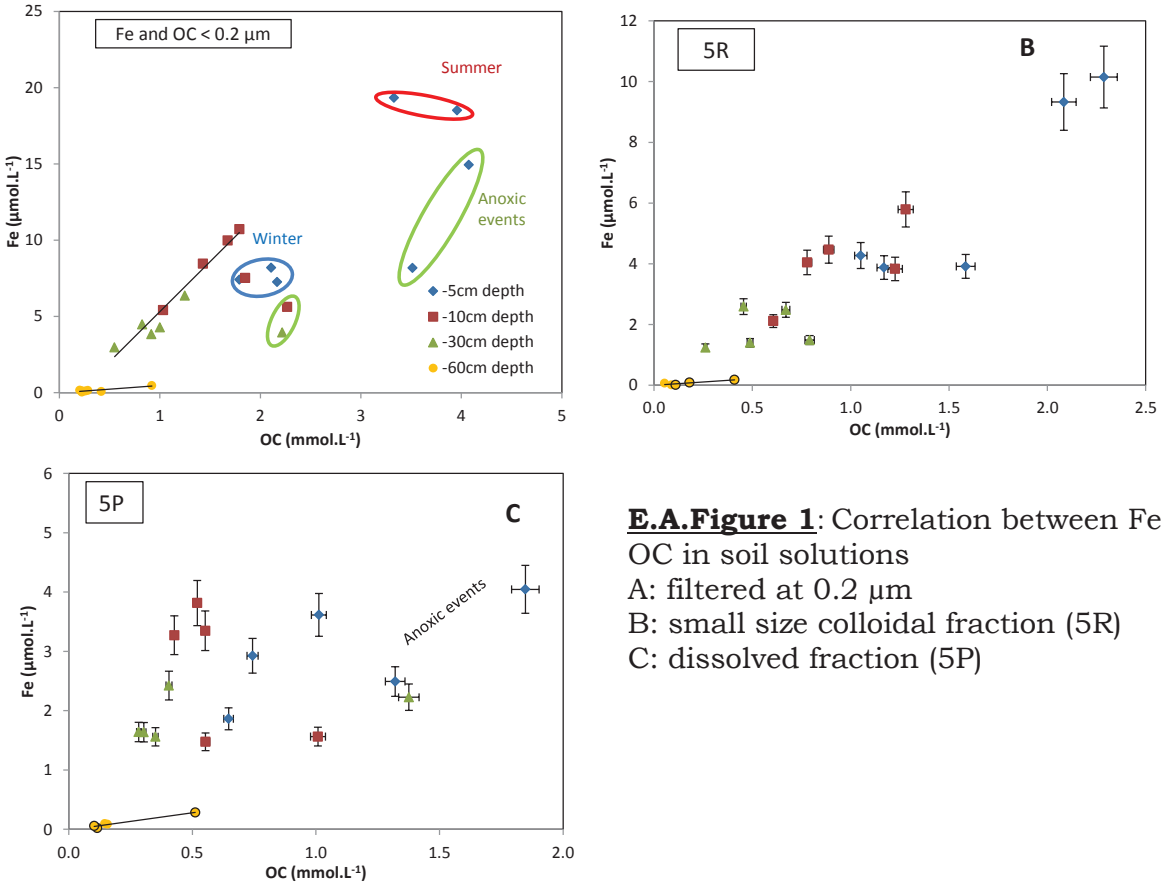

E.A.Figure 1: Correlation between Fe and OC in soil solutions
A: filtered at 0.2 µm
B: small size colloidal fraction (5R)
C: dissolved fraction (5P)

Lead shows the same distribution as Fe in all fractions of the UF soil solutions (Electronic Annex E.A.T4) suggesting that they have affinities for the same organic functional groups of OC or are part of a same phase which evolves between soil and soil solutions. The Pb concentrations of the colloidal 5R fractions are as a function of depth individually correlated with those of OC (Electronic Annex E.A. Fig.2). The Pb/OC ratio decreases with increasing depth. The intersections of each line with the Pb axis indicate that some of the Pb is not complexed with OC but mobilized with another phase (Electronic Annex E.A. Fig.2B). The correlation between Pb and P in the colloidal 5R fraction points to the dissolution and/or precipitation of pyromorphite ($Pb_5(PO_4)_3X$) as suggested previously (Stille et al., 2011; Gangloff et al., 2014) for the same experimental parcel (Fig.11). Numerous previous studies suggested that soil OC, phosphate and iron-rich phases (pyromorphite and Fe-oxyhydroxides) stabilize Pb in the soil (Nriagu, 1974; Lee and Touray, 1998; Zhang et al., 1998; Čežíková et al., 2001; Sipos et al., 2005; Stille et al., 2011; Pourret et al., 2012; Gangloff et al., 2014), explaining that a large part of Pb carried by the Strengbach watershed soil and the colloidal fraction of the soil solution can be, as proposed in § 5-1, an old Pb originating from the mining and industrial activities near the catchment during the 19th and the beginning of the 20th century (Stille et al., 2011).

According to Shaheen et al. (2014), V and Cr show different mobility dynamics in the soil solutions due to the different kinetic redox reactions. However, in this study, they manifest same variations in the 0.2 µm samples from 5 and 10 cm depth (Fig. 5C and Electronic Annex E.A.T3). This suggests that redox reactions had the same impact on Cr and V and that the difference in their behavior below 10 cm depth might be due to other processes like preferential precipitation. The oxidized form of Cr is more soluble and mobile than the reduced one and is stabilized by OC in soil

solutions (Kotaś and Stasicka, 2000; Wu et al., 2011). The dynamics of Cr

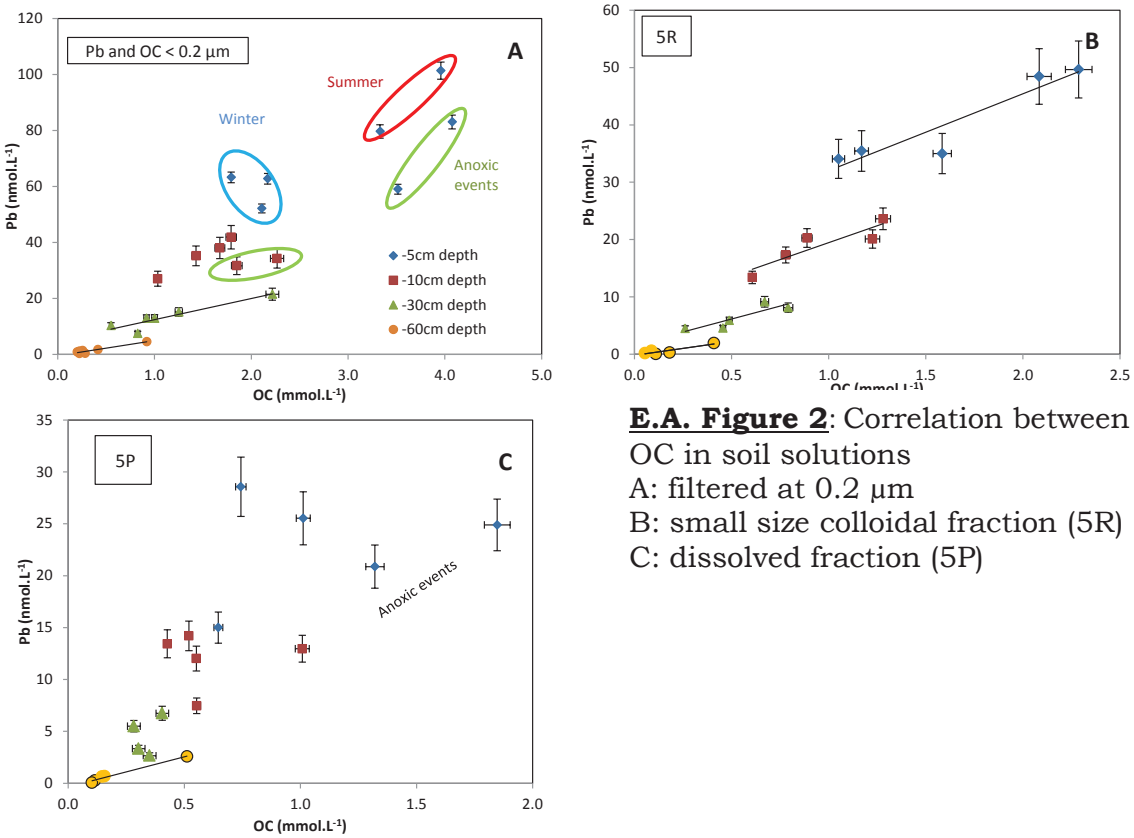

E.A. Figure 2: Correlation between Pb and OC in soil solutions
A: filtered at 0.2 µm
B: small size colloidal fraction (5R)
C: dissolved fraction (5P)

between soil and soil solutions is governed by the presence of Fe and OC (Shaheen et al., 2014). The same enrichment factors for Fe and Cr and affinity for the same organic functional groups have been observed in a neighboring soil profile of the same experimental parcel (Gangloff et al., 2014). Concentrations of Cr are correlated with those of OC in the colloidal 5R fraction from 5 cm until 60 cm depth (Electronic Annex E.A. Fig. 3). Thus, during the mineralization of OC with increasing depth, Fe and Cr might evolve in the same way in the colloidal fraction. Below 60 cm depth, there is a continuous correlation between Cr and OC in the colloidal 5R fraction while there is almost no Fe. Consequently, OC can transport Cr along the whole soil profile.

Lead, V and Cr vary with OC in the dissolved 5P fractions in the same way with the particularity that the concentrations of the metals are lower for the anoxic events (Electronic Annex E.A.Fig2C, E.A.Fig3C and E.A.Fig4C). For the majority of oxic samples, low molecular weight organic molecules

(LMWOM) are produced from bacteria or rhizosphere and are part of OC in the dissolved 5P fraction. These organic molecules complex the trace elements and enhance their mobility in the soil (Park et al., 2011; Debela et al., 2013). In the anoxic cases, the difference of trace element concentrations can be explained by a difference of the organic functional groups that less chelate trace elements like Pb, V or Cr. Another reason can be the formation of a biofilm which traps the toxic metals that are less available in soil solutions (Aouad et al., 2008).

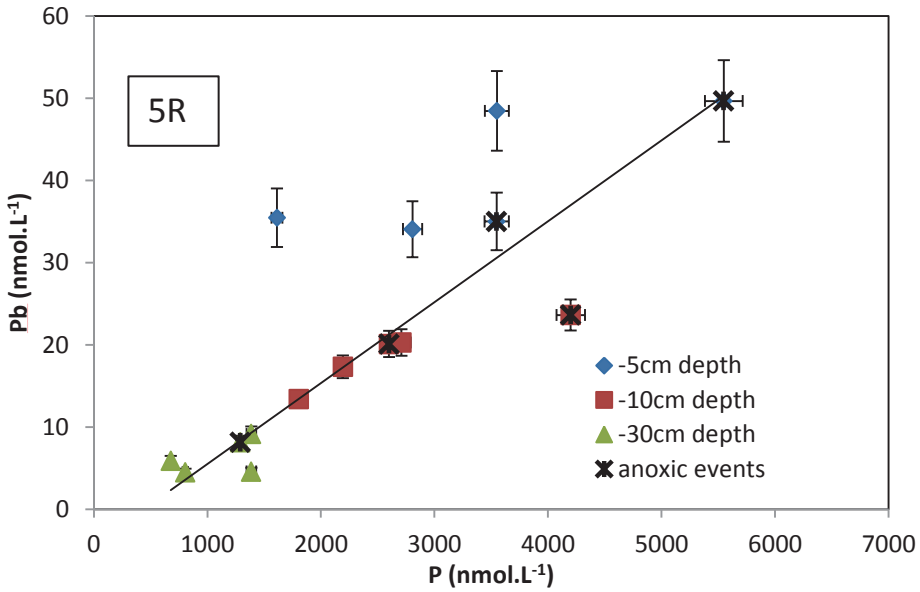

Figure 11: Correlation between Pb and P in small size colloidal fractions (5R)

.

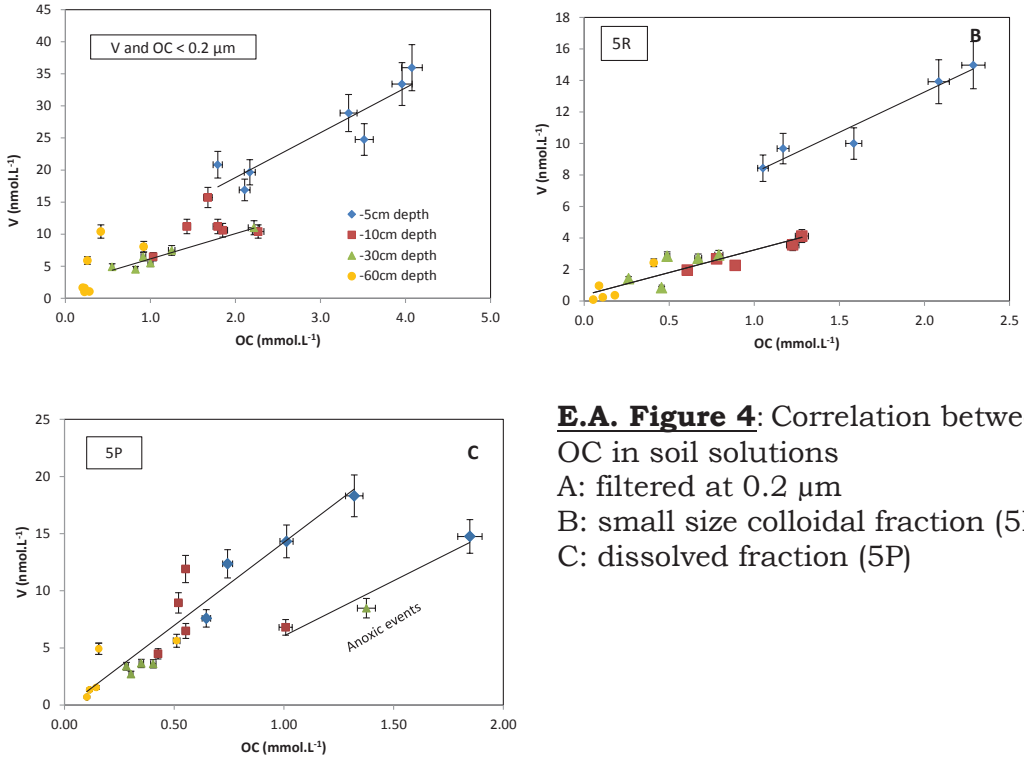

E.A. Figure 4: Correlation between V and OC in soil solutions
A: filtered at 0.2 µm
B: small size colloidal fraction (5R)
C: dissolved fraction (5P)

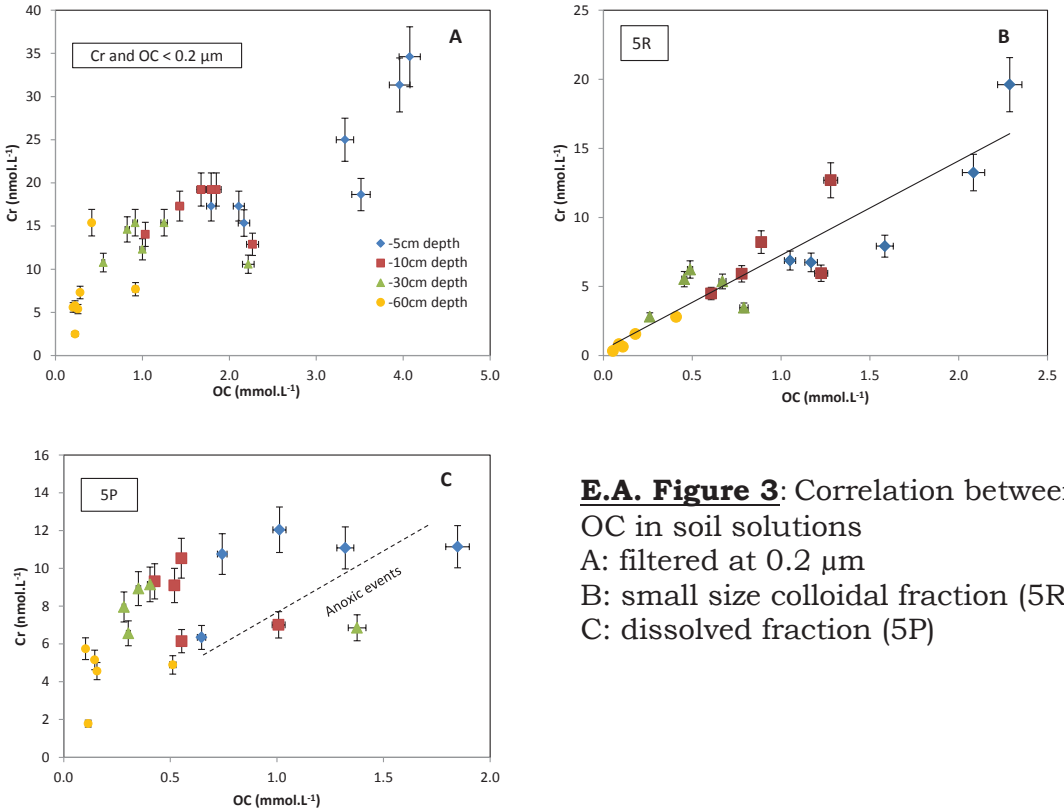

E.A. Figure 3: Correlation between Cr and OC in soil solutions
A: filtered at 0.2 µm
B: small size colloidal fraction (5R)
C: dissolved fraction (5P)

6. Conclusions

The data present in this study, confirm therefore that major and trace elements in soils may be transported by OC in soil solutions during organic matter degradation. The alternation of wet and dry seasons causes important changes in the soils redox conditions and consequently the bacterial activities. As a function of these changing conditions different bacterial communities with different nutrient needs may develop and, thus, degrade the needle and leaf litter. Along with the different stages of decomposition, OC and mineral derived elements are released. Our study shows that this decomposition plays an important role in the chemical composition of the uppermost soil solutions. Once dissolved, the major and trace elements are transported by OC in the soil solutions and are redistributed between the colloidal and dissolved fractions. The UF experiments highlight this repartition in the different fractions and their seasonal evolution with depth. They also show the existence of different OC structures, which evolve as a function of depth and oxic or anoxic events. The study of the UF soil solutions equally permits to describe more precisely the material balance, gives additional information on the bio-geochemical evolution in soil solutions filtered at 0.2 µm and more particularly on the joint evolution of cations and OC in different fractions and with depth. Our study also show (1) that all nutrients are principally in the dissolved fraction and are hence easily bio-available for microorganisms and roots, except maybe P and (2) that Al in the colloidal fraction can become a phyto-toxic risk when it passes to the dissolved fraction to replace soil depleted nutrient cations like Ca or Mn.

7. References

Aiuppa A., Allard P., D'alessandro W., Michel A., Parello F., Treuil M. and Valenza M., (2000). Mobility and fluxes of major, minor and trace metals during basalt weathering and groundwater transport at Mt. Etna volcano (Sicily). *Geochimica et Cosmochimica Acta*, **64** 1827-1841.

Alexandre A., Bouvet M. and Abbadie L., (2011). The role of savannas in the terrestrial Si cycle: A case-study from Lamto, Ivory Coast. *Global and Planetary Change*, **78** 162-169.

Allison S.M. and Prosser J.I., (1993). Ammonia oxidation at low pH by attached populations of nitrifying bacteria. *Soil Biology and Biochemistry*, **25** 935-941.

Andersson K., Dahlqvist R., Turner D., Stolpe B., Larsson T., Ingri J. and Andersson P., (2006). Colloidal rare earth elements in a boreal river: Changing sources and distributions during the spring flood. *Geochimica et Cosmochimica Acta*, **70** 3261-3274.

Aouad G., Crovisier J.L., Geoffroy V.A., Meyer J.M. and Stille P., (2006a). Microbially-mediated glass dissolution and sorption of metals by Pseudomonas aeruginosa cells and biofilm. *Journal of Hazardous Materials*, **136** 889-895.

Aouad G., Stille P., Crovisier J.L., Geoffroy V.A., Meyer J.M. and Lahd-Geagea M., (2006b). Influence of bacteria on lanthanide and actinide transfer from specific soil components (humus, soil minerals and vitrified municipal solid waste incinerator bottom ash) to corn plants: Sr-Nd isotope evidence. *The Science of the total environment*, **370** 545-551.

Aouad G., Crovisier J.L., Damidot D., Stille P., Hutchens E., Mutterer J., Meyer J.M. and Geoffroy V.A., (2008). Interactions between municipal solid waste incinerator bottom ash and bacteria (Pseudomonas aeruginosa). *The Science of the total environment*, **393** 385-393.

Backnäs S., Laine-Kaulio H. and Kløve B., (2012). Phosphorus forms and related soil chemistry in preferential flowpaths and the soil matrix of a forested podzolic till soil profile. *Geoderma*, **189–190** 50-64.

Bauer M., Fulda B. and Blodau C., (2008). Groundwater derived arsenic in high carbonate wetland soils: Sources, sinks, and mobility. *Science of The Total Environment*, **401** 109-120.

Baumann B., Snozzi M., Van Der Meer J.R. and Zehnder A.J.B., (1997). Development of stable denitrifying cultures during repeated aerobic-anaerobic transient periods. *Water Research*, **31** 1947-1954.

Berg B., (2000). Litter decomposition and organic matter turnover in northern forest soils. *Forest Ecology and Management*, **133** 13-22.

Blum J.D., Klaue A., Nezat C.A., Driscoll C.T., Johnson C.E., Siccama T.G., Eagar C., Fahey T.J. and Likens G.E., (2002). Mycorrhizal weathering of apatite as an important calcium source in base-poor forest ecosystems. *Nature*, **417** 729-731.

Bradl H.B., (2004). Adsorption of heavy metal ions on soils and soils constituents. *Journal of Colloid and Interface Science*, **277** 1-18.

Buettner S.W., Kramer M.G., Chadwick O.A. and Thompson A., (2014). Mobilization of colloidal carbon during iron reduction in basaltic soils. *Geoderma*, **221–222** 139-145.

Cabaniss S.E., (1992). Synchronous Fluorescence Spectra of Metal-Fulvic Acid Complexes. *Environmental Science & Technology*, **26** 1133-1139.

Canfield D.E., Glazer A.N. and Falkowski P.G., (2010). The Evolution and Future of Earth's Nitrogen Cycle. *Science*, **330** 192-196.

Cenki-Tok B., Chabaux F., Lemarchand D., Schmitt A.D., Pierret M.C., Viville D., Bagard M.L. and Stille P., (2009). The impact of water–rock interaction and vegetation on calcium isotope fractionation in soil- and stream waters of a small, forested catchment (the Strengbach case). *Geochimica et Cosmochimica Acta*, **73** 2215-2228.

ČežíKová J., Kozler J., Madronová L., Novák J.R. and Janoš P., (2001). Humic acids from coals of the North-Bohemian coal field: II. Metal-binding capacity under static conditions. *Reactive and Functional Polymers*, **47** 111-118.

Chen L., Zhang J.-B., Zhao B.-Z., Xin X.-L., Zhou G.-X., Tan J.-F. and Zhao J.-H., (2014). Carbon Mineralization and Microbial Attributes in Straw-Amended Soils as Affected by Moisture Levels. *Pedosphere*, **24** 167-177.

Chen Z., Ding W., Xu Y., Müller C., Rütting T., Yu H., Fan J., Zhang J. and Zhu T., (2015). Importance of heterotrophic nitrification and dissimilatory nitrate reduction to ammonium in a cropland soil: Evidences from a 15N tracing study to literature synthesis. *Soil Biology and Biochemistry*, **91** 65-75.

Clarholm M. and Skyllberg U., (2013). Translocation of metals by trees and fungi regulates pH, soil organic matter turnover and nitrogen availability in acidic forest soils. *Soil Biology and Biochemistry*, **63** 142-153.

Corvasce M., Zsolnay A., D'orazio V., Lopez R. and Miano T.M., (2006). Characterization of water extractable organic matter in a deep soil profile. *Chemosphere*, **62** 1583-1590.

Courty P.-E., Buée M., Diedhiou A.G., Frey-Klett P., Le Tacon F., Rineau F., Turpault M.-P., Uroz S. and Garbaye J., (2010). The role of ectomycorrhizal communities in forest ecosystem processes: New perspectives and emerging concepts. *Soil Biology and Biochemistry*, **42** 679-698.

Craine J.M., Morrow C. and Fierer N., (2007). MICROBIAL NITROGEN LIMITATION INCREASES DECOMPOSITION. *Ecology*, **88** 2105-2113.

Dahlqvist R., Andersson K., Ingri J., Larsson T., Stolpe B. and Turner D., (2007). Temporal variations of colloidal carrier phases and associated trace elements in a boreal river. *Geochimica et Cosmochimica Acta*, **71** 5339-5354.

Dahlqvist R., Benedetti M.F., Andersson K., Turner D., Larsson T., Stolpe B. and Ingri J., (2004). Association of calcium with colloidal particles and speciation of calcium in the Kalix and Amazon rivers. *Geochimica et Cosmochimica Acta*, **68** 4059-4075.

Dammshäuser A. and Croot P.L., (2012). Low colloidal associations of aluminium and titanium in surface waters of the tropical Atlantic. *Geochimica et Cosmochimica Acta*, **96** 304-318.

Debela F., Arocena J.M., Thring R.W. and Whitcombe T., (2013). Organic acids inhibit the formation of pyromorphite and Zn-phosphate in phosphorous amended Pb- and Zn-contaminated soil. *Journal of Environmental Management*, **116** 156-162.

Dijkstra F.A. and Smits M.M., (2002). Tree Species Effects on Calcium Cycling: The Role of Calcium Uptake in Deep Soils. *Ecosystems*, **5** 385-398.

Dijkstra F.A. and Fitzhugh R.D., (2003). Aluminum solubility and mobility in relation to organic carbon in surface soils affected by six tree species of the northeastern United States. *Geoderma*, **114** 33-47.

Don A. and Kalbitz K., (2005). Amounts and degradability of dissolved organic carbon from foliar litter at different decomposition stages. *Soil Biol Biochem*, **37** 2171-2179.

Egli M., Sartori G., Mirabella A., Giaccai D., Favilli F., Scherrer D., Krebs R. and Delbos E., (2010). The influence of weathering and organic matter on heavy metals lability in silicatic, Alpine soils. *Science of The Total Environment*, **408** 931-946.

Ehrlich H., Demadis K.D., Pokrovsky O.S. and Koutsoukos P.G., (2010). Modern Views on Desilicification: Biosilica and Abiotic Silica Dissolution in Natural and Artificial Environments. *Chemical Reviews*, **110** 4656-4689.

Falkowski P.G., Fenchel T. and Delong E.F., (2008). The Microbial Engines That Drive Earth's Biogeochemical Cycles. *Science*, **320** 1034-1039.

Fichter J., Turpault M.P., Dambrine E. and Ranger J., (1998). Mineral evolution of acid forest soils in the Strengbach catchment (Vosges mountains, N-E France). *Geoderma*, **82** 315-340.

Filella M. and Williams P.A., (2012). Antimony interactions with heterogeneous complexants in waters, sediments and soils: A review of binding data for homologous compounds. *Chem Erde-Geochem*, **72** 49-65.

Fimmen R., Richter D., Jr., Vasudevan D., Williams M. and West L., (2008). Rhizogenic Fe–C redox cycling: a hypothetical biogeochemical mechanism that drives crustal weathering in upland soils. *Biogeochemistry*, **87** 127-141.

Francioso O., Sanchez-Cortes S., Tugnoli V., Ciavatta C., Sitti L. and Gessa C., (1996). Infrared, Raman, and Nuclear Magnetic Resonance (1H, 13C, and 31P) Spectroscopy in the Study of Fractions of Peat Humic Acids. *Appl. Spectrosc.*, **50** 1165-1174.

Fraysse F., Pokrovsky O.S. and Meunier J.D., (2010). Experimental study of terrestrial plant litter interaction with aqueous solutions. *Geochimica et Cosmochimica Acta*, **74** 70-84.

Frohne T., Rinklebe J., Diaz-Bone R.A. and Du Laing G., (2011). Controlled variation of redox conditions in a floodplain soil: Impact on metal mobilization and biomethylation of arsenic and antimony. *Geoderma*, **160** 414-424.

Fuentes B., Mora M.D.L.L., Bol R., San Martin F., Pérez E. and Cartes P., (2014). Sorption of inositol hexaphosphate on desert soils. *Geoderma*, **232–234** 573-580.

Fujii K., Funakawa S., Hayakawa C. and Kosaki T., (2008). Contribution of different proton sources to pedogenetic soil acidification in forested ecosystems in Japan. *Geoderma*, **144** 478-490.

Fulda B., Voegelin A., Ehlert K. and Kretzschmar R., (2013). Redox transformation, solid phase speciation and solution dynamics of copper during soil reduction and reoxidation as affected by sulfate availability. *Geochimica et Cosmochimica Acta*, **123** 385-402.

Fuss C., Driscoll C., Johnson C., Petras R. and Fahey T., (2011). Dynamics of oxidized and reduced iron in a northern hardwood forest. *Biogeochemistry*, **104** 103-119.

Gabor R.S., Eilers K., Mcknight D.M., Fierer N. and Anderson S.P., (2014). From the litter layer to the saprolite: Chemical changes in water-soluble soil organic matter and their correlation to microbial community composition. *Soil Biology and Biochemistry*, **68** 166-176.

Gangloff S., Stille P., Schmitt A.-D. and Chabaux F., (2014a). Impact of Bacterial Activity on Sr and Ca Isotopic Compositions (87Sr/86Sr and δ44/40Ca) in Soil Solutions (the StrengbachCZO). *Procedia Earth and Planetary Science*, **10** 109-113.

Gangloff S., Stille P., Pierret M.-C., Weber T. and Chabaux F., (2014b). Characterization and evolution of dissolved organic matter in acidic forest soil and its impact on the mobility of major and trace elements (case of the Strengbach watershed). *Geochimica et Cosmochimica Acta*, **130** 21-41.

Ge S., Jiang Y. and Wei S., (2015). Gross Nitrification Rates and Nitrous Oxide Emissions in an Apple Orchard Soil in Northeast China. *Pedosphere*, **25** 622-630.

Gilliam F.S., Yurish B.M. and Adams M.B., (2001). Temporal and spatial variation of nitrogen transformations in nitrogen-saturated soils of a central Appalachian hardwood forest. *Canadian Journal of Forest Research*, **31** 1768-1785.

González-Blanco G., Beristain-Cardoso R., Cuervo-López F., Cervantes F.J. and Gómez J., (2012). Simultaneous oxidation of ammonium and p-cresol linked to nitrite reduction by denitrifying sludge. *Bioresource Technology*, **103** 48-55.

Grybos M., Davranche M., Gruau G., Petitjean P. and Pédrot M., (2009). Increasing pH drives organic matter solubilization from wetland soils under reducing conditions. *Geoderma*, **154** 13-19.

Guéguen F., Stille P., Dietze V. and Gieré R., (2012). Chemical and isotopic properties and origin of coarse airborne particles collected by passive samplers in industrial, urban, and rural environments. *Atmospheric Environment*, **62** 631-645.

Gustafsson J.P., Van Hees P., Starr M., Karltun E. and Lundström U., (2000). Partitioning of base cations and sulphate between solid and dissolved phases in three podzolised forest soils. *Geoderma*, **94** 311-333.

Hayatsu M., Tago K. and Saito M., (2008). Various players in the nitrogen cycle: Diversity and functions of the microorganisms involved in nitrification and denitrification. *Soil Science & Plant Nutrition*, **54** 33-45.

Hidemori T., Nakayama T., Matsumi Y., Kinugawa T., Yabushita A., Ohashi M., Miyoshi T., Irei S., Takami A., Kaneyasu N., Yoshino A., Suzuki R., Yumoto Y. and Hatakeyama S., (2014). Characteristics of atmospheric aerosols containing heavy metals measured on Fukue Island, Japan. *Atmospheric Environment*, **97** 447-455.

Ingri J., Widerlund A., Land M., Gustafsson Ö., Andersson P. and Öhlander B., (2000). Temporal variations in the fractionation of the rare earth elements in a boreal river; the role of colloidal particles. *Chemical Geology*, **166** 23-45.

Jorgensen K.S., (1989). Annual Pattern of Denitrification and Nitrate Ammonification in Estuarine Sediment. *Applied and Environmental Microbiology*, **55** 1841-1847.

Kaiser K., Guggenberger G., Haumaier L. and Zech W., (2001). Seasonal variations in the chemical composition of dissolved organic matter in organic forest floor layer leachates of old-growth Scots pine (Pinus sylvestris L.) and European beech (Fagus sylvatica L.) stands in northeastern Bavaria, Germany. *Biogeochemistry*, **55** 103-143.

Kaiser K., Guggenberger G., Haumaier L. and Zech W., (2002). The composition of dissolved organic matter in forest soil solutions: changes induced by seasons and passage through the mineral soil. *Organic Geochemistry*, **33** 307-318.

Kalbitz K. and Geyer S., (2002). Different effects of peat degradation on dissolved organic carbon and nitrogen. *Organic Geochemistry*, **33** 319-326.

Kalbitz K., Geyer W. and Geyer S., (1999). Spectroscopic properties of dissolved humic substances - a reflection of land use history in a fen area. *Biogeochemistry*, **47** 219-238.

Kalbitz K., Schmerwitz J., Schwesig D. and Matzner E., (2003). Biodegradation of soil-derived dissolved organic matter as related to its properties. *Geoderma*, **113** 273-291.

Kalbitz K., Schwesig D., Rethemeyer J. and Matzner E., (2005). Stabilization of dissolved organic matter by sorption to the mineral soil. *Soil Biol Biochem*, **37** 1319-1331.

Kleber M., Eusterhues K., Keiluweit M., Mikutta C., Mikutta R. and Nico P.S. (2015) Chapter One - Mineral–Organic Associations: Formation, Properties, and Relevance in Soil Environments, in: Donald L.S. (Ed.), Advances in Agronomy. Academic Press, pp. 1-140.

Klotzbücher T., Kaiser K., Filley T.R. and Kalbitz K., (2013). Processes controlling the production of aromatic water-soluble organic matter during litter decomposition. *Soil Biology and Biochemistry*, **67** 133-139.

Kotaś J. and Stasicka Z., (2000). Chromium occurrence in the environment and methods of its speciation. *Environmental Pollution*, **107** 263-283.

Kraepiel A.M.L., Dere A.L., Herndon E.M. and Brantley S.L., (2015). Natural and anthropogenic processes contributing to metal enrichment in surface soils of central Pennsylvania. *Biogeochemistry*, **123** 265-283.

Lee P.-K. and Touray J.-C., (1998). Characteristics of a polluted artificial soil located along a motorway and effects of acidification on the leaching behavior of heavy metals (Pb, Zn, Cd). *Water Research*, **32** 3425-3435.

Lemarchand D., Cividini D., Turpault M.P. and Chabaux F., (2012). Boron isotopes in different grain size fractions: Exploring past and present water–rock interactions from two soil profiles (Strengbach, Vosges Mountains). *Geochimica et Cosmochimica Acta*, **98** 78-93.

Lemarchand E., Chabaux F., Vigier N., Millot R. and Pierret M.-C., (2010). Lithium isotope systematics in a forested granitic catchment (Strengbach, Vosges Mountains, France). *Geochimica et Cosmochimica Acta*, **74** 4612-4628.

Levy-Booth D.J., Prescott C.E. and Grayston S.J., (2014). Microbial functional genes involved in nitrogen fixation, nitrification and denitrification in forest ecosystems. *Soil Biology and Biochemistry*, **75** 11-25.

Liu R. and Lead J.R., (2006). Partial validation of cross flow ultrafiltration by atomic force microscopy. *Anal Chem*, **78** 8105-8112.

Liu R.X., Lead J.R. and Zhang H., (2013). Combining cross flow ultrafiltration and diffusion gradients in thin-films approaches to determine trace metal speciation in freshwaters. *Geochimica et Cosmochimica Acta*, **109** 14-26.

López-Mondéjar R., Voříšková J., Větrovský T. and Baldrian P., (2015). The bacterial community inhabiting temperate deciduous forests is vertically stratified and undergoes seasonal dynamics. *Soil Biology and Biochemistry*, **87** 43-50.

Lorenz K., Preston C.M., Raspe S., Morrison I.K. and Feger K.H., (2000). Litter decomposition and humus characteristics in Canadian and German spruce ecosystems: information from tannin analysis and 13C CPMAS NMR. *Soil Biology and Biochemistry*, **32** 779-792.

Lundström U.S., Van Breemen N. and Bain D., (2000). The podzolization process. A review. *Geoderma*, **94** 91-107.

Maougal R.T., Brauman A., Plassard C., Abadie J., Djekoun A. and Drevon J.J., (2014). Bacterial capacities to mineralize phytate increase in the rhizosphere of nodulated common bean (Phaseolus vulgaris) under P deficiency. *European Journal of Soil Biology*, **62** 8-14.

Mcmahon P.B. and Chapelle F.H., (2008). Redox Processes and Water Quality of Selected Principal Aquifer Systems. *Ground Water*, **46** 259-271.

Melillo J.M., Aber J.D. and Muratore J.F., (1982). Nitrogen and Lignin Control of Hardwood Leaf Litter Decomposition Dynamics. *Ecology*, **63** 621-626.

Meng Y.-T., Zheng Y.-M., Zhang L.-M. and He J.-Z., (2009). Biogenic Mn oxides for effective adsorption of Cd from aquatic environment. *Environmental Pollution*, **157** 2577-2583.

Miller A.Z., Dionísio A., Sequeira Braga M.A., Hernández-Mariné M., Afonso M.J., Muralha V.S.F., Herrera L.K., Raabe J., Fernandez-Cortes A., Cuezva S., Hermosin B., Sanchez-Moral S., Chaminé H. and Saiz-Jimenez C., (2012). Biogenic Mn oxide minerals coating in a subsurface granite environment. *Chemical Geology*, **322–323** 181-191.

Nannipieri P. and Eldor P., (2009). The chemical and functional characterization of soil N and its biotic components. *Soil Biology and Biochemistry*, **41** 2357-2369.

Nierop K.G.J.J., Jansen B. and Verstraten J.M., (2002). Dissolved organic matter, aluminium and iron interactions: precipitation induced by metal/carbon ratio, pH and competition. *Science of The Total Environment*, **300** 201-211.

Nriagu J.O., (1974). Lead orthophosphates—IV Formation and stability in the environment. *Geochimica et Cosmochimica Acta*, **38** 887-898.

Park J.H., Bolan N., Megharaj M. and Naidu R., (2011). Concomitant rock phosphate dissolution and lead immobilization by phosphate solubilizing bacteria (Enterobacter sp.). *Journal of Environmental Management*, **92** 1115-1120.

Patel K.J., Singh A.K., Nareshkumar G. and Archana G., (2010). Organic-acid-producing, phytate-mineralizing rhizobacteria and their effect on growth of pigeon pea (Cajanus cajan). *Applied Soil Ecology*, **44** 252-261.

Pédrot M., Dia A. and Davranche M., (2009). Double pH control on humic substance-borne trace elements distribution in soil waters as inferred from ultrafiltration. *Journal of Colloid and Interface Science*, **339** 390-403.

Pédrot M., Dia A. and Davranche M., (2010). Dynamic structure of humic substances: Rare earth elements as a fingerprint. *Journal of Colloid and Interface Science*, **345** 206-213.

Perdrial J.N., Warr L.N., Perdrial N., Lett M.-C. and Elsass F., (2009). Interaction between smectite and bacteria: Implications for bentonite as backfill material in the disposal of nuclear waste. *Chemical Geology*, **264** 281-294.

Philippot L. and Hallin S., (2005). Finding the missing link between diversity and activity using denitrifying bacteria as a model functional community. *Current Opinion in Microbiology*, **8** 234-239.

Pierret M.C., Stille P., Prunier J., Viville D. and Chabaux F., (2014). Chemical and U–Sr isotopic variations in stream and source waters of the Strengbach watershed (Vosges mountains, France). *Hydrol. Earth Syst. Sci.*, **18** 3969-3985.

Pokrovsky O.S. and Schott J., (2002). Iron colloids/organic matter associated transport of major and trace elements in small boreal rivers and their estuaries (NW Russia). *Chemical Geology*, **190** 141-179.

Pokrovsky O.S., Dupré B. and Schott J., (2005). Fe–Al–organic Colloids Control of Trace Elements in Peat Soil Solutions: Results of Ultrafiltration and Dialysis. *Aquatic Geochemistry*, **11** 241-278.

Pokrovsky O.S., Viers J., Shirokova L.S., Shevchenko V.P., Filipov A.S. and Dupré B., (2010). Dissolved, suspended, and colloidal fluxes of organic carbon, major and trace elements in the Severnaya Dvina River and its tributary. *Chemical Geology*, **273** 136-149.

Pourret O., Dia A., Gruau G., Davranche M. and Bouhnik-Le Coz M., (2012). Assessment of vanadium distribution in shallow groundwaters. *Chemical Geology*, **294** 89-102.

Pourret O., Dia A., Davranche M., Gruau G., Henin O. and Angee M., (2007). Organo-colloidal control on major- and trace-element partitioning in shallow groundwaters: Confronting ultrafiltration and modelling. *Applied Geochemistry*, **22** 1568-1582.

Prescott C., (2010). Litter decomposition: what controls it and how can we alter it to sequester more carbon in forest soils? *Biogeochemistry*, **101** 133-149.

Probst A., El Gh'mari A., Aubert D., Fritz B. and Mcnutt R., (2000). Strontium as a tracer of weathering processes in a silicate catchment polluted by acid atmospheric inputs, Strengbach, France. *Chemical Geology*, **170** 203-219.

Reimann C., Arnoldussen A., Finne T.E., Koller F., Nordgulen Ø. and Englmaier P., (2007). Element contents in mountain birch leaves, bark and wood under different anthropogenic and geogenic conditions. *Applied Geochemistry*, **22** 1549-1566.

Rihs S., Prunier J., Thien B., Lemarchand D., Pierret M.-C. and Chabaux F., (2011). Using short-lived nuclides of the U- and Th-series to probe the kinetics of colloid migration in forested soils. *Geochimica et Cosmochimica Acta*, **75** 7707-7724.

Riotte J. and Chabaux F., (1999). (234U/238U) activity ratios in freshwaters as tracers of hydrological processes: the Strengbach watershed (Vosges, France). *Geochimica et Cosmochimica Acta*, **63** 1263-1275.

RodríGuez H. and Fraga R., (1999). Phosphate solubilizing bacteria and their role in plant growth promotion. *Biotechnology Advances*, **17** 319-339.

Schlosser C. and Croot P.L., (2008). Application of cross-flow filtration for determining the solubility of iron species in open ocean seawater. *Limnology and Oceanography: Methods*, **6** 630-642.

Schmitt A.-D., Chabaux F. and Stille P., (2003). The calcium riverine and hydrothermal isotopic fluxes and the oceanic calcium mass balance. *Earth and Planetary Science Letters*, **213** 503-518.

Schmitt A.-D., Cobert F., Bourgeade P., Ertlen D., Labolle F., Gangloff S., Badot P.-M., Chabaux F. and Stille P., (2013). Calcium isotope fractionation during plant growth under a limited nutrient supply. *Geochimica et Cosmochimica Acta*, **110** 70-83.

Shaheen S.M., Rinklebe J., Rupp H. and Meissner R., (2014). Lysimeter trials to assess the impact of different flood–dry-cycles on the dynamics of pore water concentrations of As, Cr, Mo and V in a contaminated floodplain soil. *Geoderma*, **228–229** 5-13.

Singhal R.K., Preetha J., Karpe R., Tirumalesh K., Kumar S.C. and Hegde A.G., (2006). The use of ultra filtration in trace metal speciation studies in sea water. *Environment International*, **32** 224-228.

Sipos P., Németh T., Mohai I. and Dódony I., (2005). Effect of soil composition on adsorption of lead as reflected by a study on a natural forest soil profile. *Geoderma*, **124** 363-374.

Sjöberg G., Nilsson S.I., Persson T. and Karlsson P., (2004). Degradation of hemicellulose, cellulose and lignin in decomposing spruce needle litter in relation to N. *Soil Biology and Biochemistry*, **36** 1761-1768.

Stadler B., Schramm A. and Kalbitz K., (2006). Ant-mediated effects on spruce litter decomposition, solution chemistry, and microbial activity. *Soil Biology and Biochemistry*, **38** 561-572.

Stille P., Pierret M.C., Steinmann M., Chabaux F., Boutin R., Aubert D., Pourcelot L. and Morvan G., (2009). Impact of atmospheric deposition, biogeochemical cycling and water–mineral interaction on REE fractionation in acidic surface soils and soil water (the Strengbach case). *Chemical Geology*, **264** 173-186.

Stille P., Pourcelot L., Granet M., Pierret M.C., Guéguen F., Perrone T., Morvan G. and Chabaux F., (2011). Deposition and migration of atmospheric Pb in soils from a forested silicate catchment today and in the past (Strengbach case): Evidence from 210Pb activities and Pb isotope ratios. *Chemical Geology*, **289** 140-153.

Stille P., Steinmann M., Pierret M.C., Gauthier-Lafaye F., Chabaux F., Viville D., Pourcelot L., Matera V., Aouad G. and Aubert D., (2006). The impact of vegetation on REE fractionation in stream waters of a small forested catchment (the Strengbach case). *Geochimica et Cosmochimica Acta*, **70** 3217-3230.

Stolpe B., Guo L., Shiller A.M. and Aiken G.R., (2013). Abundance, size distributions and trace-element binding of organic and iron-rich nanocolloids in Alaskan rivers, as revealed by field-flow fractionation and ICP-MS. *Geochimica et Cosmochimica Acta*, **105** 221-239.

Sundermeyer-Klinger H., Meyer W., Warninghoff B. and Bock E., (1984). Membrane-bound nitrite oxidoreductase of Nitrobacter: evidence for a nitrate reductase system. *Arch. Microbiol.*, **140** 153-158.

Tack F.M.G., Van Ranst E., Lievens C. and Vandenberghe R.E., (2006). Soil solution Cd, Cu and Zn concentrations as affected by short-time drying or wetting: The role of hydrous oxides of Fe and Mn. *Geoderma*, **137** 83-89.

Takaya N., (2002). Dissimilatory nitrate reduction metabolisms and their control in fungi. *Journal of Bioscience and Bioengineering*, **94** 506-510.

Thuróczy C.E., Gerringa L.J.A., Klunder M.B., Laan P. and De Baar H.J.W., (2011). Observation of consistent trends in the organic complexation of dissolved iron in the Atlantic sector of the Southern Ocean. *Deep Sea Research Part II: Topical Studies in Oceanography*, **58** 2695-2706.

Tricca A., Stille P., Steinmann M., Kiefel B., Samuel J. and Eikenberg J., (1999). Rare earth elements and Sr and Nd isotopic compositions of dissolved and suspended loads from small river systems in the Vosges mountains (France), the river Rhine and groundwater. *Chemical Geology*, **160** 139-158.

Umemura T., Usami Y., Aizawa S.-I., Tsunoda K.-I. and Satake K.-I., (2003). Seasonal change in the level and the chemical forms of aluminum in soil solution under a Japanese cedar forest. *Science of The Total Environment*, **317** 149-157.

Ussiri D.a.N. and Johnson C.E., (2003). Characterization of organic matter in a northern hardwood forest soil by 13C NMR spectroscopy and chemical methods. *Geoderma*, **111** 123-149.

Ussiri D.a.N. and Johnson C.E., (2007). Organic matter composition and dynamics in a northern hardwood forest ecosystem 15 years after clear-cutting. *Forest Ecology and Management*, **240** 131-142.

Van Hees P.a.W., Lundström U.S. and Giesler R., (2000). Low molecular weight organic acids and their Al-complexes in soil solution—composition, distribution and seasonal variation in three podzolized soils. *Geoderma*, **94** 173-200.

Van Hees P.a.W., Van Hees A.M.T. and Lundström U.S., (2001). Determination of aluminium complexes of low molecular organic acids in soil solution from forest soils using ultrafiltration. *Soil Biology and Biochemistry*, **33** 867-874.

Verstraeten A., De Vos B., Neirynck J., Roskams P. and Hens M., (2014). Impact of air-borne or canopy-derived dissolved organic carbon (DOC) on forest soil solution DOC in Flanders, Belgium. *Atmospheric Environment*, **83** 155-165.

Viville D., Chabaux F., Stille P., Pierret M.C. and Gangloff S., (2012). Erosion and weathering fluxes in granitic basins: The example of the Strengbach catchment (Vosges massif, eastern France). *CATENA*, **92** 122-129.

Waeles M., Tanguy V., Lespes G. and Riso R.D., (2008). Behaviour of colloidal trace metals (Cu, Pb and Cd) in estuarine waters: An approach using frontal ultrafiltration (UF) and stripping chronopotentiometric methods (SCP). *Estuarine, Coastal and Shelf Science*, **80** 538-544.

Walela C., Daniel H., Wilson B., Lockwood P., Cowie A. and Harden S., (2014). The initial lignin:nitrogen ratio of litter from above and below ground sources strongly and negatively influenced decay rates of slowly decomposing litter carbon pools. *Soil Biology and Biochemistry*, **77** 268-275.

Wällstedt T., Björkvald L. and Gustafsson J.P., (2010). Increasing concentrations of arsenic and vanadium in (southern) Swedish streams. *Applied Geochemistry*, **25** 1162-1175.

Weishaar J.L., Aiken G.R., Bergamaschi B.A., Fram M.S., Fujii R. and Mopper K., (2003). Evaluation of Specific Ultraviolet Absorbance as an Indicator of the Chemical Composition and Reactivity of Dissolved Organic Carbon. *Environmental Science & Technology*, **37** 4702-4708.

Wu P., Zhang Q., Dai Y., Zhu N., Dang Z., Li P., Wu J. and Wang X., (2011). Adsorption of Cu(II), Cd(II) and Cr(III) ions from aqueous solutions on humic acid modified Ca-montmorillonite. *Geoderma*, **164** 215-219.

Zhang P., Ryan J.A. and Yang J., (1998). In Vitro Soil Pb Solubility in the Presence of Hydroxyapatite. *Environmental Science & Technology*, **32** 2763-2768.

Chapitre 4

Weathering behavior of REE-Y in a granitic soil profile (Case of Strengbach watershed)

Résumé

Les éléments terres rares et yttrium (REE-Y) peuvent servir comme traceurs du processus d'altération des roches et de la formation des sols. Un des objectifs de cette étude est de mieux comprendre les différents phénomènes qui impacte la mobilisation de REE-Y et modifie le spectre de REE-Y le long d'un profil de sol. Notre étude a été réalisée sur un profil de sol granitique et sur les solutions de sol correspondantes, échantillonnés dans la parcelle de forêt VP2 recouverte d'épicéas du bassin versant du Strengbach. Les comportements des spectres de REE-Y sont discutés et comparés avec des résultats précédemment publiés. Les échantillons ont été recueillis entre 2009 et 2013 et ultra-filtrés afin de déterminer l'influence spatiale et temporelle ainsi que celle des fractions colloïdales et dissoutes sur l'évolution des spectres de REE-Y. Le Facteur d'enrichissement EF_{Ti} du sol indique qu'au cours du processus d'altération, le zircon et les minéraux de phosphates pourraient être dissous et induisent la formation des phases minérales secondaires comme le xénotime dans les horizons du sol plus profonds. Les solutions de sol ultra-filtrées, provenant de l'horizon humique, montrent que les REE-Y sont principalement enrichis dans la fraction colloïdale qui contrôle la dynamique des REE-Y, alors que dans les solutions de sol plus profondes les fractions colloïdales et dissoutes influencent les REE-Y. La mobilité des REE-Y est contrôlée par la dissolution des minéraux comme le zircon et les phosphates, la précipitation des REE-Y(PO4) et l'évolution du Carbone organique avec la profondeur. Une étude comparative du profil de sol, des extraits aqueux du sol et des solutions de sol montre que l'anomalie $(Eu^*/Eu)_{DS}$ reflète l'altération du plagioclase dans les micropores et la migration du Eu libéré vers les macropores, l'anomalie $(Ce^*/Ce)_{DS}$ est stabilisée par le transfert d'électron de l'acide humique (aromaticité) et fournit des informations sur les conditions d'oxydo-réduction seulement pour les horizons du sol les plus profonds appauvris en acides humiques et enfin l'enrichissement des HREE dans les solutions de sol les plus profondes résulte de la dissolution partielle des minéraux secondaires dans les horizons supérieurs du sol (au-dessus de 30 cm de profondeur).

Abstract

Rare earth elements and yttrium (REE-Y) can be used as tracers of bedrock weathering and soil formation. One of the aims of this study is to better understand the different phenomena which impact the REE-Y mobilization and modify the REE-Y pattern along a soil profile. Our study has been performed on a granitic soil profile and soil solutions corresponding, sampled in the VP2 forest parcel covered with spruces from the Strengbach catchment. The behavior of the REE-Y pattern are discussed and compared with previously published results. The samples were collected from 2009 to 2013 and ultra-filtered to determine the spatial and temporal influence as well as that of the colloidal and dissolved fractions on the evolution of the REE-Y patterns. The EF_{Ti} of the soil indicates that during alteration process, phosphate minerals and zircon might be dissolved and induce the formation of secondary mineral phase like xenotime in the deeper soil horizons. The ultra-filtered soil solutions from humic horizon show that the REE-Y are principally enriched in the colloidal fraction controlling the REE-Y dynamic while in the deeper soil solutions colloidal and dissolved fractions influence the REE-Y. The mobility of REE-Y is controlled by the dissolution of the zircon and phosphate minerals, the precipitation of the REE-Y(PO_4) and the evolution of OC with depth. The comparative study of the soil profile, soil water extracts and soil solutions show that $(Eu^*/Eu)_{DS}$ anomaly reflects weathering of plagioclase in the micropores and the migration of the released Eu to the macropores, the $(Ce^*/Ce)_{DS}$ anomaly, is stabilized by the electron shuttling of the humic acid (aromaticity) and provides information on the redox conditions only in the deeper soil horizons depleted in humic acid and finally the HREE enrichment in the deeper soil solutions results from the partial dissolution of secondary minerals in the upper soil horizons (above 30 cm depth).

1. Introduction

During bedrock weathering and soil formation, dissolution of primary minerals occurs (Probst et al., 2000; Harlavan and Erel, 2002; Sanematsu et al., 2015) allowing the release of the dissolved constituents into soil solutions. Rare earths elements and yttrium (REE-Y) are present in many minerals and can thus be used as tracers of such processes (Laveuf and Cornu, 2009).

According to (Aubert et al., 2001; Aubert et al., 2002; Aubert et al., 2004; Laveuf and Cornu, 2009; Stille et al., 2009), zircon and phosphate minerals are important phases controlling the REE concentrations in the soil. Zircon is enriched in Heavy Rare Earth Elements (HREE: Er, Tm, Yb, Lu) and comparatively stable during weathering (Balan et al., 2001; Taboada et al., 2006; Nardi et al., 2013). However, Du et al. (2012) have shown that under certain conditions zircon might be weakly dissolved and release REE in soil solution. Phosphate minerals are Light Rare Earth Elements (LREE: La, Ce, Pr, Nd) (Laveuf and Cornu, 2009) or Middle Rare Earth Element (MREE: Gd, Tb, Dy, Ho) enriched (Aubert et al., 2001; Hannigan and Sholkovitz, 2001). These minerals are more soluble than zircon and release more REE with phosphate (PO_4^{3-}) to the soil solution. Silicate minerals like feldspar are particularly enriched in Europium (Eu). Their dissolution releases a high content of Eu in the soil solution.

Once released REE are transported by the soil solutions and migrate along the soil profile. During their transport, they might precipitate in secondary phases immobilizing REE-Y according to their solubility and the composition of the soil solutions. Dissolved organic carbon (DOC) which chelates REE permits their mobilization (Goyne et al., 2010; Marsac et al., 2010; Pédrot et al., 2010; Marsac et al., 2013; Gangloff et al., 2014b) and inhibits other processes like adsorption/coprecipitation with Mn or Fe oxides (Dia et al., 2000; Davranche et al., 2005; Davranche et al., 2008). The PO_4^{3-} precipitates with REE-Y to form secondary mineral phases like xenotime and florencite (Braun and Pagel, 1994; Stille et al., 2009; Sanematsu et al., 2015; Santana et al., 2015) according to their solubility constants (Liu and Byrne,

1997). The seasonal alternation of the wet and dry cycles in the soil imposes the pH and redox conditions of the soil solutions and, might induce the formation of REE-Y$(OH)_3$ or CeO_2 (Davranche et al., 2008; Laveuf et al., 2012; Davranche et al., 2015; Vázquez-Ortega et al., 2015). The newly formed secondary minerals might also dissolve and release REE-Y again. All these processes which mobilize and immobilize REE-Y in the soil profile generate REE fractionations or enrichments/depletions (Ce* and/or Eu*) in the soil and soil solutions compared to the parent material. Thus, the study of the evolution of the REE-Y patterns along the soil profile and in the corresponding soil solutions permits to obtain indications concerning weathering processes of the bedrock and the soil formation.

The aim of this study is to better understand the different phenomena which impact the REE-Y mobilization and modify the REE-Y pattern along a soil profile. Our study has been performed on a granitic soil profile sampled in the VP2 forest parcel covered with spruces from the Strengbach catchment. The behavior of the REE-Y pattern are discussed and compared with previously published results of soils (Aubert et al., 2001; Stille et al., 2006), soil solutions (Stille et al., 2009) and soil water extracts (Gangloff et al., 2014b). We complete the comparison with soil solutions sampled from 2009 to 2013 and ultra-filtered to determine the influence of the season as well as that of the colloidal and dissolved fractions on the evolution of the REE-Y patterns.

2. Sampling site

The forested Strengbach catchment covering an area of 80 ha is located in the eastern part of the Vosges mountains (northeastern France) at altitudes ranging from 883 m at the outlet to 1146 m at the top (Fig. 1). The forest is dominated by conifers (80%) and beeches (20%). This catchment site has been thoroughly investigated since 1986 and has become a completely

equipped environmental observatory with permanent sampling and measuring stations (http://ohge.unistra.fr).

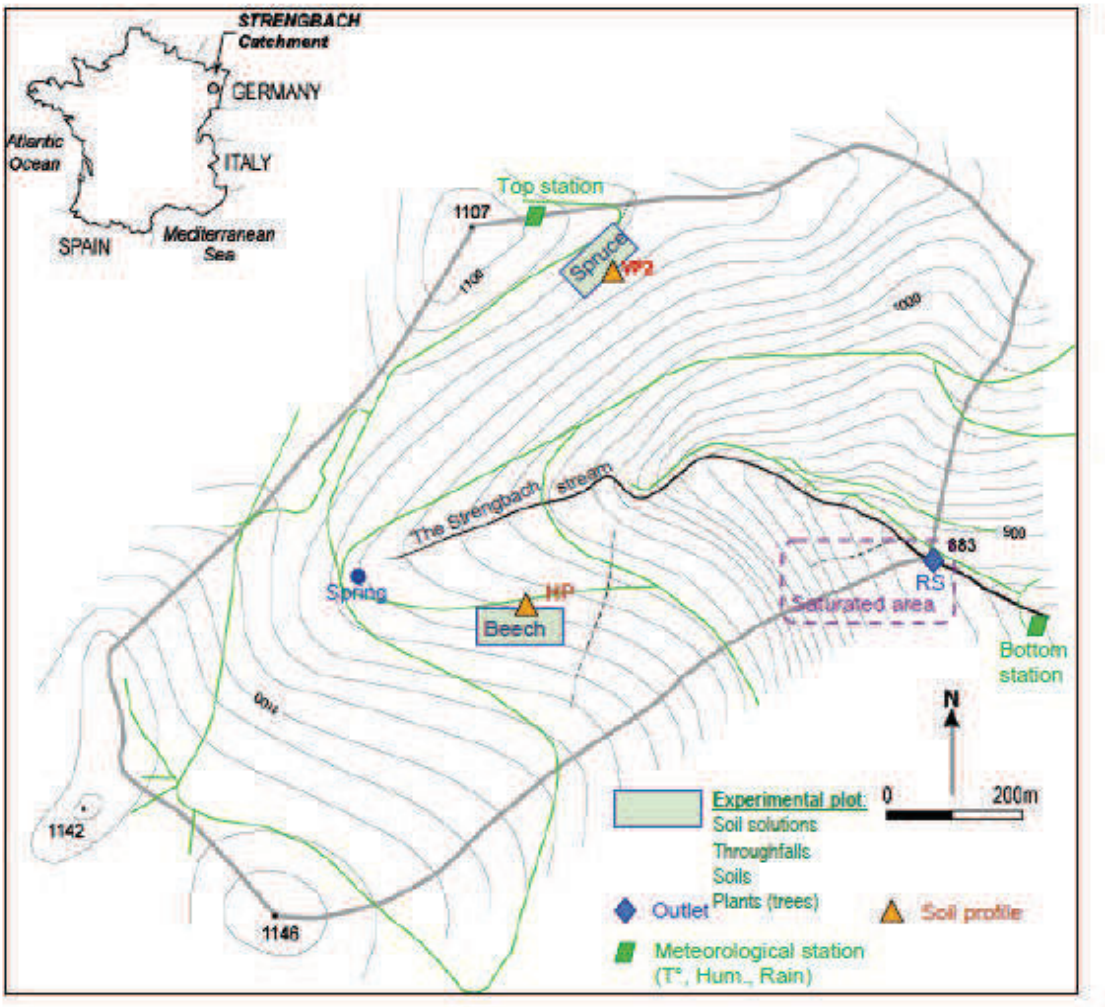

Figure 1: Strengbach catchment with sampling sites

The bedrock of the catchment is a hydrothermally altered Hercynian leucogranite. In addition small microgranite and gneiss bodies occur. The soils are brown acidic to ochreous podzolic. The acidification of soils is linked on the one hand to natural acidification (podzolization process), and on the other hand to the introduction of acidic atmospheric depositions. The climate of the Strengbach catchment is oceanic mountainous. An average of 20-25% of the precipitations is snow which falls between December and April. Rainfall occurs over the whole year with an annual average of 1400 mm. The average annual temperature is 6°C.

The experimental parcel VP2 is situated under spruces at the northern slope of the catchment (Fig.1). The soils are brown acidic and have a pH ranging between 3.7 and 5. This acidity accelerates weathering and podzolization including leaching and illuviation processes in the soil (Lundström et al., 2000). The soil profile VP2 has been described previously (Gangloff et al., 2014b). The 1 to 3 cm thick O horizon mainly consists of more or less decomposed spruce needles litter. The 10-15 cm thick root containing A horizon is dark brown and has an organic matter (OM) content of about 100 g kg^{-1}. The about 50 cm thick B horizon is reddish brown and has a lower root density than the upper unit. The OM contents decrease to 10 g kg^{-1}. The BC horizon reaches a depth of about 105 cm. It is greyish to reddish brown, contains only a few roots and encloses granite boulders with quartz and hematite veins. Mineralogy observations of secondary mineral phases in the soil of the Strengbach catchment have been previously described (Fichter et al., 1998; Probst et al., 2000; Aubert et al., 2001; Stille et al., 2009)

This study focalizes more particularly on the rare earth element (REE) behavior in soil solutions and soil profile VP2 originating from this parcel. Sixteen soil solutions have been collected through zero tension lysimeter plates situated at 5, 10, 30 and 60 cm depth between 09/09/2009 and 09/09/2010; and 10 between 09/25/2012 and 08/06/2013 (Table 1). The soil profile VP2 has been sampled in November 2010 down to a depth of 100 cm.

3. Materials and methods

3.1. **Soil profile and water extraction of soils**

3.1.1. Soil profile

The chemical soil analysis was performed at the SARM (Service d'Analyse Des Roches et des Minéraux - Nancy - France), the major elements were determined by using ICP/AES and trace elements using ICP/MS. To

compare the behavior of the REE in the soil profile VP2, enrichment factors have been calculated for each depth relative to Ti (EFTi) (Fig. 2).

3.1.2. Water extract

The soils were mixed with Ultra-High Purity (UHP) water in the proportion 1:1.5 (UHP water: soil). Each sample was shaken during 2 hours and ultra-centrifuged at 8000 rpm for 30 min at 10 °C. The supernatant was filtered at 0.45 µm and the filtrate was used for chemical analysis. The Water Extractable Chemical Elements (WECE in mg X g^{-1} of air dried soil) correspond to the dissolved fraction of REE contents in the extraction water, i.e. in the 0.45 µm filtrate. To compare the WECE of soils from different depths of the profile, it has been normalized ($WECE_N$ %) to the total amount of the element X present in the soil. The protocol is more detailed in Gangloff et al. (2014b).

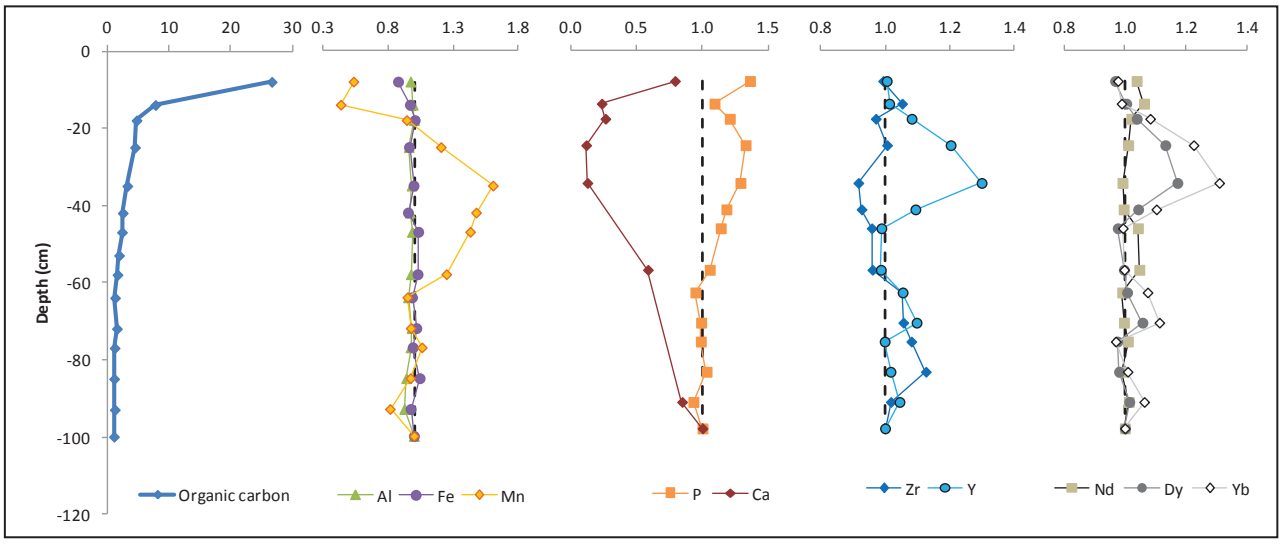

Figure 2: Enrichment factors (normalization to Ti and the soil from 100cm depth, i.e. $[(X_i/Ti_i)/(X_{100}/Ti_{100})]$)

3.2. **Filtrations and ultra-filtrations of soil solutions**

Each soil solution was filtered to 0.2 µm in a frontal way on Omnipore® membrane filters (hydrophilic PTFE). Then, a part of these samples have been ultra-filtered with a Tangential Flow Filtration (TFF) by a Labscale TFF device of Millipore© (Table 1). The filtration membranes used are in regenerated cellulose (PelliconXL©). The part of the sample which passed through the membrane containing compounds smaller than the cut-off size corresponds to the permeate (P). The part of the sample which remained in the reservoir contains mainly compounds larger than the cut-off size and corresponds to the retentate (R). The ultra-filtrations and washing membrane protocols were described in more details in Gangloff et al. (2016) (in review).

3.3. **The ultra-filtration parameters**

The 0.2 µm soil solutions were ultra-filtered at the 300 kDa cut-off size to obtain the retentate (300R) containing the colloidal fraction between 0.2 µm and 300 kDa (large-size colloidal fraction) and the permeate (300P) corresponding to the <300 kDa fraction. The 300P fraction was ultra-filtered at the 5 kDa cut-off size to obtain the retentate (5R) containing the colloidal fraction between 300 kDa and 5 kDa (small size colloidal fraction) and the permeate (5P) corresponding to the dissolved fraction. By shortage of volume, two samples were only ultra-filtered at the 5kDa cut-off size (Table 1).

According to Francioso et al. (1996), Ingri et al. (2000), Dahlqvist et al. (2004), Liu and Lead (2006), Schlosser and Croot (2008), Dammshäuser and Croot (2012) and Liu et al. (2013), TFF procedure necessitates the determination of the retentate volumic concentration factor (VCFr):

$$VCF_r = (initial\ volume)/(retentate\ volume) \qquad (1)$$

In this study, VCF_r(300 kDa) is 5.0 ± 0.4 (N = 20) and VCF_r (5kDa) is 3.6 ± 0.3 (N=20). The VCF_r have to be similar for each size cut off to compare the different colloidal fractions. The colloidal concentration between two cut-off sizes can be calculated:

$$Ci_{colloidal} = \frac{(Ci_{retentate} - Ci_{permeate})}{VCFri} \qquad (2)$$

For each ultra-filtration, it is important to calculate the recovery to check if there is an experimental deviation such as adsorption or contamination (Gangloff et al., 2016)(in review). All recoveries varied mainly between 99% and 95% except for the heavy rare earth elements (HREE) which varied between 95% and 90%.

3.4. **Analytical methods**

An aliquot of each water extract and soil solution were analyzed. The pH was measured with a combined electrode after a calibration with standard solution NIST (pH 4.00 and 7.00). The concentrations of the PO_4^{3-} were determined by an ionic chromatography (DIONEX ICS-3000) (uncertainty < 2 %). The organic carbon (OC) in the different samples was measured by thermal method (Shimadzu TOC $_{VPH}$) with an uncertainty of 2 % and a detection limit of 0.3 mg $C.L^{-1}$. The trace element concentrations were determined by ICP/AES (Thermo Scientific iCAP 6000 SERIES) and ICP/MS (Thermo-Fisher X SerieII) (uncertainty between 5 to 10%).The validity and the reproducibility of different parameters have been verified by the certified standards SLRS5, Perade-20, Rain 97 and Big-Moose 02.

3.5. **Aromaticity of the water extracts and soil solutions**

The Specific Ultraviolet Absorbance at 254nm ($SUVA_{254}$) has been defined by UV absorbance of the water extracts and the soil solutions samples at 254nm normalized to the OC concentration in mg $C.L^{-1}$. $SUVA_{254}$ were measured by an UV-VIS spectrophotometer (SHIMADZU UV-1700). Weishaar et al. (2003) showed that there is a relationship between the percentage of aromaticity determined by ^{13}C-NMR and the $SUVA_{254}$ value

(percentage of aromaticity=6.53*$SUVA_{254}$+3.63). This parameter has been determined for the different samples and allows to show the variation of the aromatic character.

3.6. **Concentration of REE for soil solutions at 60cm depth**

The soil solutions filtered at 0.2 µm and the 5P fractions originating from the 60 cm depth and whose REE concentrations were below detection limit, have been concentrated nearly fourteen times by partial evaporation in a PTFE vessel with nitric acid.

4. Results

4.1. **Chemical composition and Rare Earth Elements (REE) distribution pattern in the soil profile VP2**

The major and trace element data of the soil samples are given in Table 2. The upper 20 cm soil layer is most enriched in TOC (100 g kg^{-1}), whereas deeper horizons are depleted (10 g kg^{-1}). The pH increases with depth from 3.9 to 4.7. Clays and the aromaticity of the soil organic matter are enriched at 30 cm depth (Gangloff et al., 2014b). Most of the elements show increasing concentrations until 30 cm depth, below which the concentrations remain relatively constant with increasing depth (Table 2). However, TOC, Mn, P, Ca, Y, Middle REE (MREE: Gd to Ho) and Heavy REE (HREE: Er to Lu) behave differently with depth. To compare these differences in the soil profile, enrichment factors (Table 3) have been calculated for each element and each depth relative to the immobile Ti (EF_{Ti}) (White et al., 1998; Stille et al., 2011; Vázquez-Ortega et al., 2015). Figure 2 shows the evolution of EF_{Ti} for TOC, Al, Fe, Mn, P, Ca, Y, Zr and REE. Iron and Al are weakly whereas Ca is strongly depleted until 40 cm depth. Phosphorus and Mn are enriched between 20 and 60 cm depth while Zr is weakly depleted until 60 cm depth and enriched below. Dysprosium (MREE), Yb (HREE) and Y show accumulations at 35 cm and 70 cm depth while Nd (LREE) is accumulated in the surface soil and at 50 cm depth.

Table 1: Concentrations for the 0.2µm and colloidal fractions calculated with Eq.(2) for each sampling date at different depth

(<D.L.: below to the detection limit and n.d.: no determined)

Sampling period	sample type	depth	Colloidal size	Date	pH (measured)	H+ (mmol/L)	Aromaticity (%)	DOC (mmol/l)	P (µmol/l)	Mn (µmol/l)	Al (µmol/l)	Fe (µmol/l)	Y (nmol/l)	Zr (nmol/l)	ΣREE (nmol/l)	La (nmol/l)	Ce (nmol/l)	Pr (nmol/l)	Nd (nmol/l)	Sm (nmol/l)	Eu (nmol/l)	Gd (nmol/l)	Tb (nmol/l)	Dy (nmol/l)	Ho (nmol/l)	Er (nmol/l)	Tm (nmol/l)	Yb (nmol/l)	Lu (nmol/l)	Eu*/Eu DS	Ce*/Ce DS
09/09/2009 to 11/12/2009	**soil solution**	**5cm**	0.2µm	11/12/09	4.08	0.083	30.7	3.51	35.81	14.57	21.48	8.17	2.82	2.43	8.71	1.82	3.24	0.37	1.57	0.42	0.09	0.44	0.06	0.34	0.06	0.14	0.02	0.12	0.02	1.23	0.93
09/09/2009 to 11/12/2009	**soil solution**	**5cm**	0.2 µm to 300kDa		n.d.	n.d.	31.4	0.02	0.00	0.02	0.70	0.22	0.04	0.08	0.13	0.02	0.06	0.006	0.03	0.004	0.001	0.01	0.000	0.006	0.001	0.001	0.000	0.002	0.000	1.63	1.55
09/09/2009 to 11/12/2009	**soil solution**	**5cm**	300kDa to 5kDa		n.d.	n.d.	31.8	1.58	3.55	4.50	8.99	3.91	1.69	1.86	4.17	0.93	1.56	0.173	0.73	0.195	0.040	0.20	0.031	0.156	0.026	0.066	0.009	0.051	0.007	1.25	0.90
09/09/2009 to 11/12/2009	**soil solution**	**5cm**	<5kDa		n.d.	n.d.	24.3	1.85	32.26	10.05	12.02	4.04	1.01	0.44	4.52	0.92	1.66	0.194	0.85	0.202	0.045	0.23	0.036	0.177	0.031	0.084	0.011	0.072	0.009	1.28	0.92
11/12/2009 to 03/19/2010	**soil solution**	**5cm**	0.2µm	03/19/10	4.05	0.089	36.7	1.79	20.65	7.58	18.97	7.42	2.25	2.40	7.14	1.76	2.72	0.303	1.15	0.306	0.062	0.26	0.055	0.234	0.046	0.111	0.017	0.090	0.015	1.35	0.87
11/12/2009 to 03/19/2010	**soil solution**	**5cm**	0.2 µm to 300kDa		4.00	0.000	37.0	0.00	0.32	-0.02	0.07	0.22	0.02	0.00	0.07	0.02	0.02	0.003	0.01	0.006	0.000	0.01	0.000	0.002	0.000	0.001	0.000	0.000	0.000	0.12	0.77
11/12/2009 to 03/19/2010	**soil solution**	**5cm**	300kDa to 5kDa		3.70	0.037	37.2	1.05	2.81	1.49	9.20	4.27	1.05	1.54	3.69	0.95	1.39	0.151	0.58	0.154	0.032	0.15	0.026	0.123	0.022	0.054	0.008	0.043	0.006	1.30	0.84
11/12/2009 to 03/19/2010	**soil solution**	**5cm**	<5kDa		4.21	0.065	31.9	0.74	17.61	6.11	9.70	2.93	1.18	0.86	3.38	0.79	1.31	0.149	0.56	0.146	0.030	0.11	0.028	0.110	0.024	0.057	0.008	0.046	0.008	1.47	0.92
03/19/2010 to 06/21/2010	**soil solution**	**5cm**	0.2µm	06/21/10	5.10	0.008	35.4	4.08	56.77	28.47	30.19	14.93	3.49	4.89	9.60	1.64	3.97	0.428	1.69	0.445	0.086	0.45	0.080	0.388	0.073	0.172	0.024	0.141	0.020	1.18	1.18
03/19/2010 to 06/21/2010	**soil solution**	**5cm**	0.2 µm to 300kDa		5.06	0.000	37.8	0.47	1.68	2.52	3.76	2.29	0.39	0.64	1.24	0.24	0.51	0.054	0.20	0.053	0.011	0.06	0.010	0.049	0.009	0.022	0.003	0.016	0.002	1.22	1.11
03/19/2010 to 06/21/2010	**soil solution**	**5cm**	300kDa to 5kDa		5.30	0.002	40.4	2.29	5.55	12.26	19.09	10.15	2.23	3.46	6.17	0.97	2.58	0.283	1.10	0.291	0.056	0.30	0.053	0.258	0.047	0.116	0.016	0.089	0.013	1.18	1.25
03/19/2010 to 06/21/2010	**soil solution**	**5cm**	<5kDa		4.95	0.006	30.2	1.32	49.68	13.68	7.33	2.49	0.87	0.79	2.19	0.43	0.87	0.091	0.38	0.101	0.018	0.09	0.018	0.081	0.017	0.034	0.006	0.036	0.005	1.16	1.04
06/21/2010 to 09/08/2010	**soil solution**	**5cm**	0.2µm	08/09/10	3.97	0.107	34.0	3.33	18.74	9.87	35.78	19.34	2.98	4.28	8.93	1.49	3.67	0.390	1.62	0.432	0.092	0.43	0.069	0.357	0.061	0.149	0.018	0.127	0.017	1.31	1.17
09/25/2012 to 11/20/2012	**soil solution**	**5cm**	0.2µm	11/20/12	4.40	0.040	38.3	2.17	8.39	4.50	13.48	7.26	1.51	2.30	4.57	0.78	1.91	0.199	0.83	0.193	0.053	0.22	0.031	0.172	0.030	0.078	0.010	0.064	0.010	1.57	1.18
09/25/2012 to 11/20/2012	**soil solution**	**5cm**	0.2µm to 300kDa		4.13	0.008	38.0	0.35	0.35	0.39	2.04	1.52	0.25	0.48	0.84	0.17	0.35	0.038	0.14	0.031	0.008	0.04	0.006	0.031	0.004	0.013	0.003	0.010	0.002	1.46	1.09
09/25/2012 to 11/20/2012	**soil solution**	**5cm**	300kDa to 5kDa		4.05	0.021	35.2	1.17	1.61	2.07	6.99	3.88	0.81	1.46	2.50	0.41	1.07	0.112	0.45	0.109	0.026	0.12	0.019	0.095	0.016	0.041	0.004	0.032	0.004	1.39	1.24
09/25/2012 to 11/20/2012	**soil solution**	**5cm**	<5kDa		4.60	0.011	27.0	0.65	6.29	2.04	4.45	1.86	0.45	0.37	1.23	0.20	0.49	0.049	0.24	0.053	0.019	0.06	0.007	0.046	0.010	0.023	0.004	0.022	0.004	1.98	1.14
11/20/2012 to 03/26/2013	**soil solution**	**5cm**	0.2µm	03/26/13	4.10	0.079	34.0	2.11	7.81	8.56	17.33	8.19	1.55	2.41	4.50	0.68	1.87	0.199	0.85	0.213	0.046	0.22	0.031	0.178	0.030	0.084	0.012	0.068	0.011	1.30	1.23
05/22/2013 to 08/06/2013	**soil solution**	**5cm**	0.2µm	08/06/13	4.00	0.100	38.3	3.96	8.68	9.38	34.26	18.51	3.01	5.82	9.07	1.37	3.78	0.416	1.68	0.439	0.093	0.44	0.069	0.369	0.067	0.167	0.024	0.132	0.023	1.30	1.25
05/22/2013 to 08/06/2013	**soil solution**	**5cm**	0.2 µm to 300kDa		3.64	0.024	43.3	0.86	0.84	1.14	6.98	5.57	0.62	1.55	2.02	0.34	0.86	0.092	0.37	0.085	0.019	0.09	0.016	0.079	0.013	0.032	0.004	0.025	0.003	1.35	1.20
05/22/2013 to 08/06/2013	**soil solution**	**5cm**	300kDa to 5kDa		3.72	0.048	37.8	2.08	1.03	4.79	16.60	9.33	1.40	3.24	4.22	0.66	1.75	0.203	0.79	0.200	0.043	0.20	0.032	0.161	0.029	0.074	0.010	0.061	0.010	1.32	1.22
05/22/2013 to 08/06/2013	**soil solution**	**5cm**	<5kDa		4.50	0.028	31.3	1.01	6.81	3.45	10.68	3.61	1.00	1.03	2.82	0.37	1.18	0.121	0.52	0.154	0.030	0.15	0.021	0.129	0.024	0.061	0.010	0.045	0.010	1.25	1.36
09/09/2009 to 11/12/2009	**soil solution**	**10cm**	0.2µm	11/12/09	4.60	0.025	28.1	2.27	10.65	13.68	26.63	5.63	2.05	1.87	7.50	1.17	2.81	0.377	1.21	0.402	0.160	0.38	0.116	0.298	0.108	0.167	0.080	0.158	0.073	1.49	1.17
09/09/2009 to 11/12/2009	**soil solution**	**10cm**	0.2 µm to 300kDa		n.d.	n.d.	28.4	0.05	0.00	0.00	1.39	0.31	0.02	0.01	0.12	0.04	0.04	0.005	0.01	0.007	0.003	0.00	0.002	0.005	0.002	0.004	0.001	0.002	0.000	0.80	0.75
09/09/2009 to 11/12/2009	**soil solution**	**10cm**	300kDa to 5kDa		n.d.	n.d.	30.2	1.23	2.58	2.52	14.06	3.83	1.35	1.21	4.39	0.67	1.68	0.219	0.70	0.217	0.093	0.23	0.067	0.181	0.064	0.098	0.045	0.083	0.040	1.45	1.22
09/09/2009 to 11/12/2009	**soil solution**	**10cm**	<5kDa		n.d.	n.d.	23.3	1.01	8.71	11.40	11.19	1.56	0.67	0.66	3.08	0.47	1.11	0.159	0.51	0.170	0.069	0.15	0.049	0.117	0.045	0.076	0.037	0.075	0.035	1.47	1.12
11/12/2009 to 03/19/2010	**soil solution**	**10cm**	0.2µm	03/19/10	4.30	0.050	32.0	1.03	9.35	5.69	21.33	5.41	1.57	1.70	4.86	0.79	2.14	0.207	0.82	0.219	0.051	0.21	0.035	0.174	0.033	0.081	0.011	0.075	0.010	1.48	1.31
11/12/2009 to 03/19/2010	**soil solution**	**10cm**	0.2µm to 300kDa		4.25	0.000	32.9	0.00	0.00	0.00	0.12	0.03	0.00	0.00	0.02	0.01	0.01	0.000	0.00	0.001	0.001	0.00	0.000	0.001	0.000	0.000	0.000	-0.001	0.000	1.95	0.93
11/12/2009 to 03/19/2010	**soil solution**	**10cm**	300kDa to 5kDa		4.00	0.018	32.2	0.61	1.81	1.23	8.29	2.11	0.61	1.01	2.08	0.36	0.92	0.087	0.34	0.095	0.021	0.09	0.015	0.073	0.014	0.033	0.004	0.029	0.004	1.43	1.29
11/12/2009 to 03/19/2010	**soil solution**	**10cm**	<5kDa		4.40	0.037	29.8	0.43	7.55	4.46	12.92	3.27	0.96	0.69	2.76	0.43	1.21	0.120	0.48	0.123	0.030	0.12	0.020	0.101	0.019	0.048	0.007	0.047	0.006	1.51	1.34
03/19/2010 to 06/21/2010	**soil solution**	**10cm**	0.2µm	06/21/10	5.50	0.008	31.9	1.85	34.52	12.90	23.70	7.53	2.02	3.69	6.10	0.94	2.57	0.248	1.09	0.293	0.071	0.30	0.050	0.249	0.048	0.119	0.018	0.102	0.014	1.48	1.27
03/19/2010 to 06/21/2010	**soil solution**	**10cm**	0.2µm to 300kDa		5.10	0.000	31.1	0.02	0.00	-0.01	0.45	0.26	0.05	0.04	0.06	0.01	0.04	0.007	0.00	-0.001	0.000	0.00	0.001	0.001	0.002	0.001	0.001	0.001	0.001	0.79	2.05
03/19/2010 to 06/21/2010	**soil solution**	**10cm**	300kDa to 5kDa		5.03	0.002	33.8	1.28	8.00	4.59	16.14	5.79	1.42	3.29	4.37	0.67	1.89	0.196	0.75	0.201	0.050	0.21	0.036	0.173	0.032	0.081	0.012	0.069	0.009	1.48	1.33
03/19/2010 to 06/21/2010	**soil solution**	**10cm**	<5kDa		5.33	0.006	28.0	0.55	26.32	8.31	7.11	1.47	0.56	0.37	1.67	0.26	0.64	0.046	0.34	0.092	0.021	0.09	0.013	0.075	0.014	0.037	0.005	0.032	0.004	1.46	1.10
06/21/2010 to 09/08/2010	**soil solution**	**10cm**	0.2µm	08/09/10	4.44	0.036	33.3	1.79	18.32	5.46	23.78	10.72	2.62	4.17	8.45	1.37	3.70	0.334	1.44	0.372	0.099	0.39	0.057	0.320	0.055	0.143	0.018	0.125	0.017	1.57	1.31
09/25/2012 to 11/20/2012	**soil solution**	**10cm**	0.2µm	11/20/12	4.46	0.035	33.5	1.43	12.90	5.94	23.56	8.46	1.68	2.85	5.15	0.76	2.28	0.213	0.91	0.233	0.053	0.25	0.031	0.191	0.030	0.090	0.012	0.081	0.011	1.34	1.38
09/25/2012 to 11/20/2012	**soil solution**	**10cm**	0.2 µm to 300kDa		4.42	0.001	34.0	0.02	0.10	0.00	0.54	0.18	0.03	0.03	0.08	0.00	0.04	0.005	0.02	0.003	0.002	0.00	0.002	0.004	0.000	0.003	0.000	0.003	0.000	4.39	2.93
09/25/2012 to 11/20/2012	**soil solution**	**10cm**	300kDa to 5kDa		4.17	0.016	31.6	0.89	2.71	1.55	11.08	4.47	0.93	2.05	2.97	0.47	1.32	0.124	0.51	0.129	0.030	0.14	0.021	0.111	0.020	0.051	0.006	0.044	0.006	1.39	1.35
09/25/2012 to 11/20/2012	**soil solution**	**10cm**	<5kDa		4.73	0.018	29.2	0.52	10.10	4.39	11.94	3.81	0.72	0.77	2.10	0.30	0.92	0.084	0.38	0.101	0.021	0.11	0.009	0.075	0.010	0.036	0.006	0.034	0.006	1.21	1.37
05/22/2013 to 08/06/2013	**soil solution**	**10cm**	0.2µm to 300kDa	08/06/13	4.12	0.076	34.0	1.68	11.03	4.50	23.11	9.98	1.69	3.76	5.54	0.80	2.45	0.231	0.98	0.266	0.064	0.26	0.036	0.215	0.036	0.096	0.015	0.080	0.012	1.49	1.39
05/22/2013 to 08/06/2013	**soil solution**	**10cm**	0.2µm to 300kDa		3.94	0.011	34.0	0.34	0.97	0.38	3.93	2.59	0.28	0.89	0.98	0.16	0.44	0.041	0.17	0.038	0.010	0.04	0.007	0.035	0.007	0.017	0.002	0.014	0.001	1.63	1.34
05/22/2013 to 08/06/2013	**soil solution**	**10cm**	300kDa to 5kDa		3.92	0.025	33.9	0.78	2.19	1.71	9.05	4.04	0.70	1.85	2.35	0.35	1.05	0.100	0.41	0.103	0.027	0.10	0.017	0.091	0.018	0.040	0.006	0.036	0.006	1.64	1.38
05/22/2013 to 08/06/2013	**soil solution**	**10cm**	<5kDa		4.54	0.040	30.9	0.55	7.87	2.41	10.13	3.35	0.70	1.03	2.20	0.29	0.96	0.090	0.40	0.124	0.026	0.12	0.012	0.089	0.011	0.039	0.006	0.030	0.005	1.32	1.43
09/09/2009 to 11/12/2009	**soil solution**	**30cm**	0.2µm	11/12/09	4.30	0.050	28.8	2.22	4.84	13.17	28.78	3.94	1.72	1.43	5.85	0.94	2.67	0.241	1.01	0.240	0.059	0.25	0.038	0.191	0.034	0.087	0.012	0.065	0.009	1.46	1.36
09/09/2009 to 11/12/2009	**soil solution**	**30cm**	0.2 µm to 300kDa		n.d.	n.d.	28.4	0.05	0.00	-0.04	1.48	0.21	0.03	-0.02	0.14	0.00	0.09	0.006	0.02	0.006	0.002	0.01	0.001	0.005	0.001	0.002	0.000	0.002	0.000	2.75	5.36
09/09/2009 to 11/12/2009	**soil solution**	**30cm**	300kDa to 5kDa		n.d.	n.d.	31.6	0.79	1.29	1.13	12.59	1.49	1.01	0.88	2.50	0.46	1.13	0.091	0.41	0.100	0.023	0.10	0.016	0.085	0.014	0.035	0.005	0.025	0.003	1.40	1.27
09/09/2009 to 11/12/2009	**soil solution**	**30cm**	<5kDa		n.d.	n.d.	22.9	1.38	3.55	12.41	14.81	2.22	0.79	0.55	3.43	0.61	1.51	0.144	0.59	0.137	0.032	0.14	0.022	0.109	0.021	0.051	0.007	0.039	0.006	1.40	1.23
11/12/2009 to 03/19/2010	**soil solution**	**30cm**	0.2µm	03/19/10	4.80	0.018	33.7	0.55	3.23	3.08	17.04	2.97	1.57	1.51	5.48	0.86	2.56	0.243	0.92	0.233	0.055	0.22	0.035	0.172	0.035	0.078	0.015	0.060	0.013	1.50	1.43
11/12/2009 to 03/19/2010	**soil solution**	**30cm**	0.2 µm to 300kDa		4.72	0.000	34.9	0.01	0.00	0.00	0.27	0.10	0.02	0.00	0.08	0.01	0.02	0.002	0.02	0.007	0.004	0.01	0.001	0.006	0.002	0.002	0.001	0.002	0.001	3.45	0.96
11/12/2009 to 03/19/2010	**soil solution**	**30cm**	300kDa to 5kDa		4.30	0.003	33.7	0.26	0.81	0.81	6.89	1.24	0.69	0.87	2.34	0.38	1.12	0.097	0.37	0.088	0.023	0.09	0.015	0.072	0.014	0.033	0.006	0.025	0.006	1.52	1.48
11/12/2009 to 03/19/2010	**soil solution**	**30cm**	<5kDa		4.88	0.015	27.3	0.28	2.32	2.27	9.88	1.64	0.87	0.65	3.06	0.47	1.41	0.144	0.53	0.137	0.028	0.12	0.019	0.095	0.019	0.042	0.008	0.033	0.006	1.39	1.41
03/19/2010 to 06/21/2010	**soil solution**	**30cm**	0.2µm	06/21/10	4.43	0.037	31.7	0.92	4.19	4.30	21.78	3.84	2.25	2.20	8.05	1.14	3.85	0.334	1.36	0.332	0.084	0.33	0.052	0.271	0.046	0.126	0.015	0.092	0.012	1.55	1.55
03/19/2010 to 06/21/2010	**soil solution**	**30cm**	0.2 µm to 300kDa		4.40	0.000	30.7	0.02	0.00	0.00	0.09	0.01	0.02	0.01	0.07	0.01	0.03	0.001	0.02	0.001	0.001	0.01	0.000	0.001	0.000	0.000	0.000	0.000	0.000	1.51	0.86
03/19/2010 to 06/21/2010	**soil solution**	**30cm**	300kDa to 5kDa		4.13	0.011	31.9	0.49	0.68	0.97	7.97	1.40	1.01	1.60	3.69	0.56	1.76	0.150	0.62	0.146	0.038	0.15	0.023	0.121	0.020	0.052	0.006	0.037	0.005	1.55	1.49
03/19/2010 to 06/21/2010	**soil solution**	**30cm**	<5kDa		4.55	0.026	26.5	0.40	3.58	3.33	13.72	2.42	1.22	0.60	4.28	0.57	2.07	0.182	0.72	0.185	0.045	0.17	0.028	0.148	0.026	0.073	0.009	0.055	0.007	1.55	1.63
06/21/2010 to 09/08/2010	**soil solution**	**30cm**	0.2µm	08/09/10	4.59	0.026	30.6	1.25	4.97	6.14	19.07	6.36	2.45	3.07	8.32	1.25	4.00	0.334	1.37	0.332	0.079	0.33	0.050	0.283	0.048	0.126	0.018	0.095	0.011	1.46	1.52
09/25/2012 to 11/20/2012	**soil solution**	**30cm**	0.2µm	11/20/12	4.59	0.026	31.6	1.00	4.19	2.15	16.63	4.28	1.59	1.79	5.87	0.88	2.86	0.234	0.96	0.226	0.057	0.23	0.035	0.191	0.032	0.084	0.009	0.064	0.007	1.54	1.54
09/25/2012 to 11/20/2012	**soil solution**	**30cm**	0.2µm to 300kDa		4.54	0.001	30.3	0.03	0.06	0.00	0.43	0.17	0.02	0.10	0.11	0.02	0.05	0.007	0.01	0.002	0.001	0.01	0.001	0.004	0.001	0.000	0.000	0.003	0.000	1.13	1.46
09/25/2012 to 11/20/2012	**soil solution**	**30cm**	300kDa to 5kDa		4.20	0.013	31.7	0.67	1.39	1.03	8.96	2.48	0.99	1.44	3.83	0.60	1.88	0.149	0.61	0.144	0.036	0.15	0.023	0.117	0.020	0.051	0.006	0.036	0.005	1.46	1.53
09/25/2012 to 11/20/2012	**soil solution**	**30cm**	<5kDa		4.92	0.012	26.9	0.30	2.77	1.12	7.23	1.63	0.57	0.25	1.92	0.25	0.93	0.078	0.34	0.080	0.021	0.07	0.011	0.069	0.012	0.033	0.003	0.025	0.003	1.75	1.59
05/22/2013 to 08/06/2013	**soil solution**	**30cm**	0.2µm to 300kDa	08/06/13	4.70	0.020	34.3	0.83	3.23	1.64	17.78	4.48	1.50	3.07	5.66	0.80	2.70	0.227	0.96	0.233	0.059	0.25	0.036	0.191	0.032	0.085	0.012	0.069	0.008	1.51	1.54
05/22/2013 to 08/06/2013	**soil solution**	**30cm**	0.2µm to 300kDa		4.55	0.001	33.8	0.02	0.06	0.04	0.57	0.33	0.03	0.08	0.15	0.03	0.07	0.005	0.03	0.006	0.001	0.01	0.001	0.005	0.000	0.002	0.000	0.001	0.000	0.67	1.16
05/22/2013 to 08/06/2013	**soil solution**	**30cm**	300kDa to 5kDa		4.38	0.008	32.0	0.46	1.39	0.81	8.39	2.59	0.81	1.84	3.02	0.43	1.48	0.121	0.50	0.115	0.030	0.13	0.019	0.100	0.017	0.043	0.005	0.034	0.004	1.51	1.60
05/22/2013 to 08/06/2013	**soil solution**	**30cm**	<5kDa		5.00	0.010	28.6	0.35	2.77	0.79	8.82	1.56	0.66	1.15	2.49	0.35	1.15	0.101	0.44	0.111	0.029	0.12	0.017	0.086	0.015	0.040	0.006	0.034	0.004	1.55	1.48
09/09/2009 to 11/12/2009	**soil solution**	**60cm**	0.2µm	11/12/09	4.90	0.025	16.0	0.92	30.32	2.24	6.59	0.47	0.30	1.10	0.71	0.14	0.23	0.031	0.13	0.037	0.010	0.04	0.006	0.036	0.007	0.020	0.004	0.023	0.004	1.35	0.75
09/09/2009 to 11/12/2009	**soil solution**	**60cm**	0.2µm to 5kDa		n.d.	n.d.	16.0	0.41	12.90	0.25	3.93	0.18	0.23	0.46	0.08	0.02	0.02	0.003	0.02	0.003	0.006	0.00	0.001	0.002	0.000	0.001	0.000	0.002	0.000	2.01	0.54
09/09/2009 to 11/12/2009	**soil solution**	**60cm**	<5kDa		n.d.	n.d.	15.5	0.51	17.42	1.99	2.67	0.28	0.08	0.66	0.45	0.07	0.04	0.018	0.11	0.021	0.040	0.03	0.016	0.021	0.016	0.020	0.019	0.018	0.016	2.63	0.75
11/12/2009 to 03/19/2010	**soil solution**	**60cm**	0.2µm	03/19/10	4.80	0.018	15.5	0.20	4.84	3.89	6.26	0.17	0.07	0.45	0.20	0.048	0.069	0.009	0.035	0.009	0.002	0.008	0.001	0.007	0.001	0.005	0.001	0.006	0.001	1.34	0.78
11/12/2009 to 03/19/2010	**soil solution**	**60cm**	0.2µm to 5kDa		4.34	0.003	14	0.05	0.32	0.88	1.22	0.07	0.01	0.08	0.10	0.023	0.033	0.004	0.017	0.004	0.001	0.004	0.001	0.003	0.001	0.002	0.000	0.003	0.000	1.38	0.78
11/12/2009 to 03/19/2010	**soil solution**	**60cm**	<5kDa		5.13	0.015	10.5	0.15	4.52	3.03	4.96	0.10	0.05	0.38	0.11	0.025	0.036	0.004	0.018	0.004	0.001	0.005	0.001	0.004	0.001	0.003	0.001	0.004	0.001	1.30	0.79
03/19/2010 to 06/21/2010	**soil solution**	**60cm**	0.2µm	06/21/10	6.09	0.001	15.7	0.23	0.35	4.55	1.33	0.03	0.04	0.29	0.13	0.022	0.044	0.006	0.025	0.006	0.001	0.005	0.001	0.005	0.001	0.004	0.001	0.006	0.001	1.53	0.96
03/19/2010 to 06/21/2010	**soil solution**	**60cm**	0.2µm to 5kDa		6.03	0.000	18.2	0.11	0.10	1.97	0.64	0.01	0.03	0.20	0.09	0.016	0.034	0.005	0.020	0.004	0.001	0.004	0.001	0.004	0.001	0.002	0.000	0.004	0.001	1.53	0.95
03/19/2010 to 06/21/2010	**soil solution**	**60cm**	<5kDa		5.94	0.001	14.0	0.12	0.23	2.57	0.63	0.02	0.01	0.08	0.03	0.005	0.009	0.001	0.004	0.001	0.000	0.001	0.000	0.001	0.000	0.001	0.000	0.002	0.000	1.55	0.97
06/21/2010 to 09/08/2010	**soil solution**	**60cm**	0.2µm	08/09/10	4.9	0.013	18.1	0.42	1.19	3.04	3.26	0.07	0.19	0.32	0.63	0.08	0.27	0.032	0.14	0.028	0.007	0.03	0.003	0.018	0.003	0.010	0.001	0.012	0.002	1.52	1.31
09/25/2012 to 11/20/2012	**soil solution**	**60cm**	0.2µm	11/20/12	4.86	0.014	18.4	0.26	0.39	1.26	8.15	0.11	0.09	0.58	0.28	0.0720	0.0957	0.0112	0.0514	0.0121	0.0021	0.0125	0.0017	0.0087	0.0017	0.0054	0.0009	0.0073	0.0012	1.03	0.73
09/25/2012 to 11/20/2012	soil solution	60cm	0.2µm to 5kDa		4.50	0.008	18	0.09	0.10	0.38	2.04	0.01	0.04	0.17	0.13	0.0411	0.0469	0.0047	0.0182	0.0044	0.0006	0.0050	0.0005	0.0024	0.0005	0.0019	0.0003	0.0023	0.0003	0.84	0.71
09/25/2012 to 11/20/2012	soil solution	60cm	<5kDa		4.97	0.008	18.9	0.16	0.23	0.87	5.71	0.08	0.05	0.40	0.16	0.0342	0.0517	0.0074	0.0339	0.0068	0.0012	0.0068	0.0010	0.0056	0.0012	0.0032	0.0005	0.0044	0.0008	1.06	0.75
11/20/2012 to 03/26/2014	**soil solution**	**60cm**	0.2µm	03/26/13	4.95	0.011	17.2	0.23	0.68	0.71	6.81	0.13	0.17	0.44	0.43	0.058	0.162	0.021	0.096	0.023	0.004	0.019	0.003	0.015	0.003	0.009	0.001	0.0115	0.002	1.31	1.10
05/22/2013 to 08/06/2013	**soil solution**	**60cm**	0.2µm	08/06/13	6.20	0.001	21.1	0.28	5.48	0.46	2.96	0.14	0.11	0.54	0.24	0.01	0.08	0.013	0.06	0.016	0.003	0.01	0.002	0.012	0.002	0.008	0.001	0.011	0.002	1.34	1.27
05/22/2013 to 08/06/2013	**soil solution**	**60cm**	0.2µm to 5kDa		6.47	0.000	21.0	0.18	2.26	0.24	1.55	0.09	0.06	0.35	0.18	0.01	0.07	0.011	0.05	0.012	0.002	0.01	0.001	0.008	0.001	0.005	0.001	0.006	0.001	1.48	1.39
05/22/2013 to 08/06/2013	**soil solution**	**60cm**	<5kDa		6.30	0.001	22.0	0.10	3.23	0.21	1.41	0.06	0.05	0.18	0.06	0.00	0.01	0.002	0.02	0.004	0.001	0.00	0.001	0.004	0.001	0.003	0.000	0.005	0.001	1.04	0.85

Depth (cm)	La*	Ce*	Pr*	Nd*	Sm*	Eu*	Gd*	Tb*	Dy*	Ho*	Er*	Tm*	Yb*	Lu*	Y*	Zr*	Al**	Fe**	Mn**	Ti**	P**	$(Ce^*/Ce)_{DS}$	$(Eu^*/Eu)_{DS}$	$(Nd/Yb)_{DS}$
-8	27.76	54.25	6.6	23.64	4.31	0.56	3.10	0.46	2.54	0.49	1.43	0.22	1.49	0.23	15.0	154.8	5.80	1.88	0.02	0.27	0.08	1.02	0.98	1.06
-14	33.5	65.61	8.0	28.58	5.26	0.66	3.57	0.54	3.11	0.60	1.73	0.26	1.78	0.29	17.9	193.7	6.98	2.45	0.02	0.32	0.08	1.03	0.96	1.07
-18	34.22	66.82	8.1	28.95	5.28	0.70	3.90	0.59	3.39	0.68	1.96	0.30	2.06	0.32	20.1	188.4	7.43	2.68	0.05	0.34	0.09	1.03	0.97	0.94
-25	37.8	73.53	9.0	32.27	5.89	0.75	4.43	0.69	4.16	0.83	2.47	0.38	2.62	0.41	25.2	219.8	8.04	2.88	0.07	0.38	0.11	1.02	0.99	0.82
-35	35.26	68.49	8.4	30.13	5.59	0.76	4.18	0.67	4.10	0.85	2.54	0.39	2.66	0.41	25.9	190.6	7.81	2.84	0.09	0.36	0.10	1.02	0.99	0.76
-42	37.12	71.84	8.8	31.6	5.76	0.78	4.30	0.65	3.81	0.76	2.25	0.34	2.35	0.37	22.8	201.3	8.05	2.84	0.08	0.38	0.10	1.01	0.99	0.90
-47	37.21	71.97	8.7	31.35	5.85	0.76	4.11	0.60	3.38	0.65	1.88	0.29	2.00	0.31	19.5	197.2	7.76	2.92	0.08	0.36	0.09	1.02	0.98	1.05
-53	41.68	80.72	9.8	35.4	6.57	0.86	4.73	0.70	4.11	0.79	2.34	0.35	2.43	0.38	24.3	234.2	8.14	3.15	0.07	0.39	0.09	1.02	0.97	0.98
-58	36.19	70.28	8.6	30.75	5.73	0.74	4.00	0.59	3.37	0.64	1.87	0.28	1.96	0.31	19.0	193	7.51	2.83	0.07	0.35	0.08	1.02	0.98	1.05
-64	36.35	70.22	8.6	30.75	5.71	0.75	4.15	0.62	3.60	0.71	2.09	0.32	2.23	0.35	21.5	223.7	7.75	2.87	0.05	0.37	0.08	1.01	0.98	0.92
-72	34.93	66.96	8.2	29.57	5.48	0.73	4.05	0.61	3.61	0.69	2.04	0.31	2.21	0.35	21.4	214.4	7.63	2.84	0.05	0.35	0.08	1.01	0.98	0.90
-77	37.33	71.33	8.7	31.68	5.87	0.78	4.16	0.62	3.52	0.68	1.96	0.30	2.04	0.32	20.6	232.1	8.00	2.92	0.06	0.37	0.08	1.00	0.99	1.04
-85	37.06	70.67	8.7	31.29	5.79	0.79	4.20	0.63	3.57	0.69	2.02	0.32	2.14	0.34	21.1	243.7	7.79	3.10	0.05	0.38	0.09	1.00	1.01	0.98
-93	37.58	71.74	8.8	31.93	5.89	0.78	4.28	0.64	3.68	0.71	2.12	0.33	2.25	0.35	21.6	219.5	7.64	2.88	0.05	0.38	0.08	1.00	0.98	0.95
-100	36.29	69.3	8.6	30.97	5.74	0.78	4.19	0.62	3.56	0.68	1.99	0.30	2.08	0.33	20.3	211.9	8.11	2.91	0.06	0.37	0.08	1.00	1.00	1.00

Table 2: The chemical composition, Ce*, Eu* and Nd/Yb ratio of the VP_2 soil with depth (* corresponds to $mg.kg^{-1}$ and ** to $g.kg^{-1}$)

Depth (cm)	La	Ce	Pr	Nd	Sm	Eu	Gd	Tb	Dy	Ho	Er	Tm	Yb	Lu	Y	Zr	Al	Fe	Mn	Ti	P
-8	1.04	1.07	1.04	1.04	1.02	0.99	1.01	1.01	0.97	0.97	0.97	0.99	0.98	0.95	1.01	0.99	0.97	0.88	0.54	1.00	0.31
-14	1.06	1.09	1.08	1.06	1.06	0.98	0.98	1.00	1.00	1.01	1.00	0.99	0.99	1.02	1.01	1.05	0.99	0.97	0.44	1.00	0.25
-18	1.03	1.05	1.03	1.02	1.00	0.98	1.02	1.04	1.04	1.08	1.07	1.07	1.08	1.06	1.08	0.97	1.00	1.01	0.94	1.00	0.27
-25	1.01	1.03	1.02	1.01	0.99	0.94	1.03	1.09	1.13	1.18	1.20	1.22	1.23	1.22	1.20	1.01	0.96	0.96	1.21	1.00	0.30
-35	0.99	1.01	0.99	0.99	0.99	1.00	1.02	1.11	1.17	1.26	1.30	1.31	1.31	1.29	1.30	0.92	0.98	1.00	1.61	1.00	0.29
-42	1.00	1.01	1.00	1.00	0.98	0.98	1.00	1.03	1.04	1.09	1.10	1.10	1.10	1.10	1.09	0.93	0.97	0.95	1.48	1.00	0.27
-47	1.06	1.07	1.05	1.04	1.05	1.01	1.01	1.01	0.98	0.98	0.97	0.97	0.99	0.98	0.99	0.96	0.98	1.03	1.43	1.00	0.26
-53	1.09	1.10	1.09	1.08	1.09	1.05	1.07	1.08	1.09	1.09	1.11	1.09	1.11	1.10	1.13	1.05	0.95	1.03	1.27	1.00	0.24
-58	1.05	1.07	1.05	1.05	1.05	1.01	1.01	1.02	1.00	0.98	0.99	0.96	1.00	0.99	0.99	0.96	0.98	1.03	1.25	1.00	0.24
-64	1.00	1.01	1.00	0.99	0.99	0.97	0.99	1.01	1.01	1.03	1.05	1.07	1.07	1.07	1.05	1.05	0.95	0.99	0.95	1.00	0.21
-72	1.01	1.01	1.00	1.00	1.00	0.99	1.01	1.03	1.06	1.06	1.07	1.08	1.11	1.11	1.10	1.06	0.98	1.02	0.98	1.00	0.22
-77	1.02	1.02	1.01	1.01	1.01	0.99	0.98	0.99	0.98	0.98	0.97	0.97	0.97	0.97	1.00	1.08	0.97	0.99	1.06	1.00	0.22
-85	1.00	1.00	0.99	0.99	0.99	1.00	0.98	1.00	0.98	0.99	0.99	1.02	1.01	1.02	1.02	1.13	0.94	1.04	0.97	1.00	0.23
-93	1.02	1.02	1.01	1.01	1.01	0.99	1.00	1.01	1.01	1.02	1.05	1.08	1.06	1.05	1.04	1.02	0.93	0.97	0.82	1.00	0.21
-100	1.00	1.00	1.00	1.00	1.00	1.00	1.00	1.00	1.00	1.00	1.00	1.00	1.00	1.00	1.00	1.00	1.00	1.00	1.00	1.00	0.23

Table 3: Enrichment factors (normalization to Ti and the soil from 100cm depth, i.e. $[(X_i/Ti_i)/(X100/Ti100)]$)

Figure 3 represents the REE distribution pattern for different depths of the VP2 soil profile. The REE contents are normalized to the bedrock granite of the catchment (Aubert et al., 2001) (Fig. 3A) and to the deeper soil (DS) from the VP2 soil profile (Fig. 3B). The DS normalized REE distribution patterns show REE depletions from the surface to the depth with a more pronounced depletion for HREE compared to Light REE (LREE: La to Sm). At 30 cm depth, the soils REE distribution pattern is different than above and below. It presents a progressive enrichment from MREE to HREE compared to the deeper soil. Moreover, all REE distribution patterns of the different soils are slightly enriched in Ce and depleted in Eu compared to the deeper soil.

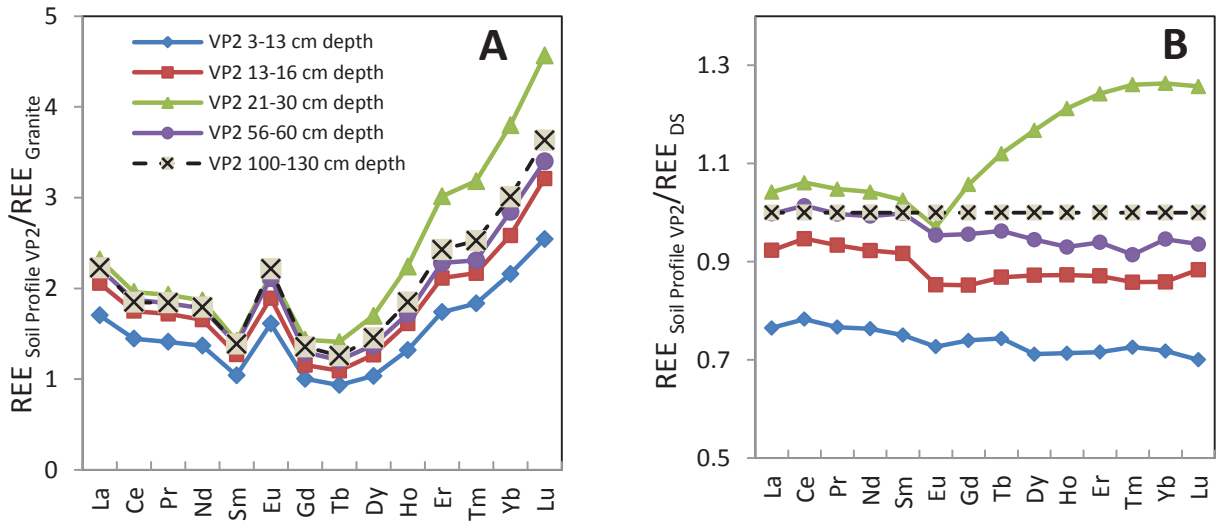

Figure 3: Rare Earth Element distribution patterns in the VP2 soil profile with Bedrock normalization (Granite in Aubert at al. 2001) (A) and deeper soil (DS) normalization (B)

4.2. Chemical composition and Rare Earth Elements (REE) distribution pattern in water extracts and soil solutions

Table 4 in (Gangloff et al., 2014b) compares the normalized rates of the different water extractable elements ($WECE_N$) with the rate of Water Extractable Organic Carbon ($WEOC_N$). It has been shown that Organic Carbon, Mn, Ca and P are especially extractable in the upper soil compartment and much less in the deeper horizons. The $WECE_N$ of Al, Fe, Y, Zr and REE progressively decreases with depth in the descending order as follow: Fe> Al> MREE>Y- HREE> LREE> Zr. The REE distribution patterns of the water extracts are compared to the corresponding soil solution at each depth (Fig.4).

The results concerning Al, Fe, Mn, Ca, P, OC concentrations and aromaticity of soil solutions filtered at 0.2µm and ultra-filtered are detailed in (Gangloff et al., 2016)(in review). The concentrations of REE, Y and Zr in soil solutions are given in the Table 1. These trace elements fluctuate seasonally in the organic horizon (0-30cm depth) in the same way as OC. Their contents decrease weakly until 30cm depth and strongly at 60 cm depth. The REE_{DS} distribution patterns of the soil solutions collected between 5 and 30cm depth are $MREE_{DS}$ enriched samples (Fig. 4A, 4B and 4C) whereas they are $LREE_{DS}$ depleted for the 60 cm depth soil solutions (Fig. 4D). Similar evolution from surface to depth has been observed by Stille et al. (2009) and Zhu et al. (2012) for soil solutions from other soil profiles.

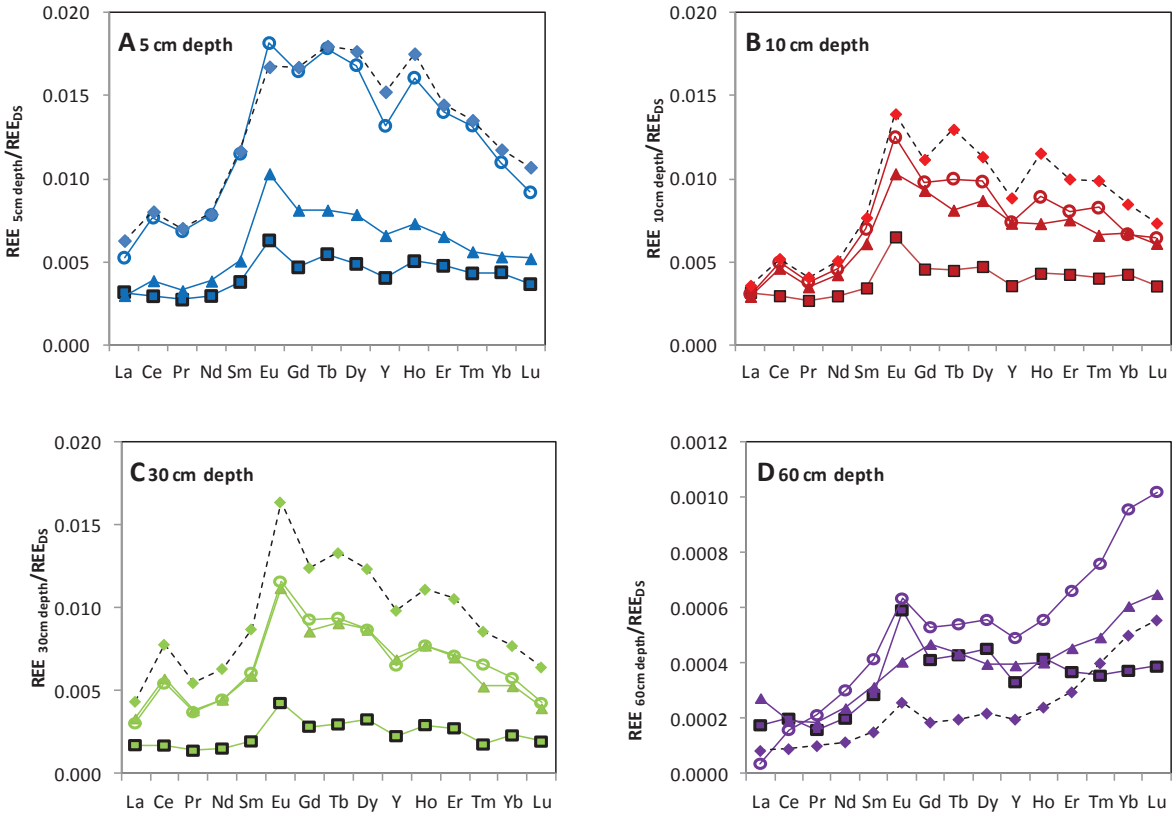

Figure 4: soil solutions <0.2µm (June 2010) ◆ , soil solutions <0.2 µm (November 2012) ▲, soil solutions <0.2µm (August 2013) ○ and water extracts □

The soil solutions (<0.2 µm) show weak Ce enrichments as indicated by positive $(Ce^*/Ce)_{DS}$ anomalies (Shields and Stille, 2001). The $(Ce^*/Ce)_{DS}$ anomalies increase with depth from 1.12 (± 0.15) at 5 cm depth to 1.49 (± 0.08) at 30 cm depth (Fig.5A). For the deepest 60 cm samples, $(Ce^*/Ce)_{DS}$ fluctuate (1.00 ± 0.24) with positive anomalies for samples collected during summer (1.31 and 1.27). The soil solutions (<0.2 µm) show weak Eu enrichments as indicated by positive $(Eu^*/Eu)_{DS}$ anomalies. Their values vary with depth from 1.32 (± 0.12) at 5 cm depth to 1.51 (± 0.04) at 30 cm depth (Fig.5B). For the deepest 60 cm samples, $(Eu^*/Eu)_{DS}$ fluctuate (1.35 ± 0.18). Concerning the water extracts, the $(Ce^*/Ce)_{DS}$ are lower and the $(Eu^*/Eu)_{DS}$ are higher than those of soil solutions (Fig. 5).

For the ultra-filtered samples, REE, Y and Zr are principally distributed in the different colloidal fractions (between 40% and 70% in the 300R and 5R colloidal fractions) and their distribution does not vary significantly between 5cm and 30cm depth. At 60 cm depth, REE, Y and Zr are principally found in the colloidal fraction for summer samples (70% for June 2010 and August 2013) and in the 5P dissolved fraction for the other months (Table1).

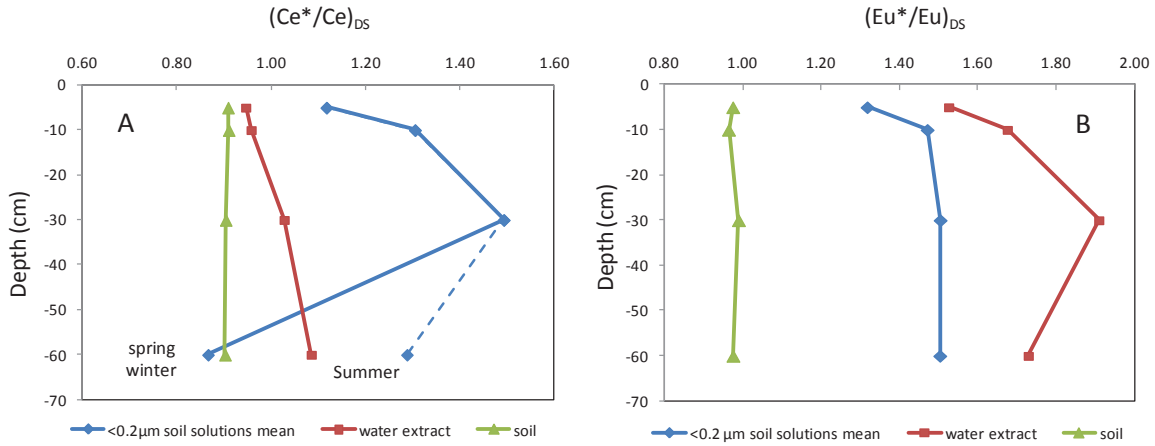

Figure 5: Comparison of $(Ce^*/Ce)_{DS}$ and $(Eu^*/Eu)_{DS}$ between the soil, water extracts and the mean of the soil solutions (<0.2 µm) along the profile

For all soil solutions filtered at 0.2 µm, Yb_{DS} ($HREE_{DS}$) is more enriched than Nd_{DS} ($LREE_{DS}$) (Fig.6A) and the 5R colloidal fraction is more depleted in YbDS ($HREE_{DS}$) rather than the 5P dissolved fraction (Fig. 6B). The distribution of these trace elements in colloidal fractions is of the same order of magnitude as found by Ingri et al. (2000), Pourret et al. (2007a), Åström et al. (2010) and Pokrovsky et al. (2010).

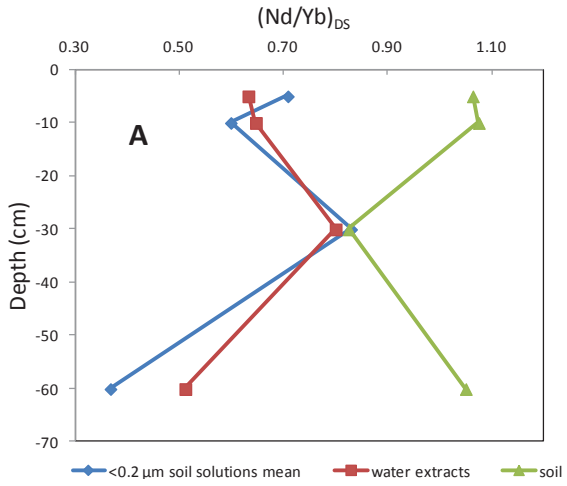

B

(Nd/Yb)DS (0.2µm)	(Nd/Yb)DS (5R) (1)	(Nd/Yb)DS (5P) (2)	(1)/(2)	Depth
0.71	0.75	0.64	1.17	5 cm
0.60	0.64	0.58	1.10	10 cm
0.83	0.89	0.79	1.12	30 cm
0.37	0.35	0.23	1.53	60 cm

Figure 6 : (A) Comparison of $(Nd/Yb)_{DS}$ between the soils, water extracts and soil solutions (<0.2 µm) and (B) enrichment rates of Yb in the 5P dissolved fraction along the profile

5. Discussion

5.1. **Weathering behavior of Y-REE in a granitic soil profile**

Previous studies have shown that zircon and primary and secondary phosphates are the most important mineral phases controlling the REE mobility in the soils of the Strengbach catchment during weathering (Aubert et al., 2001; Aubert et al., 2004; Stille et al., 2006; Stille et al., 2009). These studies have been performed on soil profiles from other parcels (HP and PP) of the catchment. The HP soil profile is situated on a different slope and covered with beeches whereas the PP soil profile is on the same slope as VP2 and also covered by spruces (Fig.1). The REE distribution pattern of the here studied VP2 soil profile, normalized to the fresh granite (fig.3A), is similar to that of the HP soil profile which is less altered than PP. The only difference between VP2 and HP is the depth of the observed HREE enrichment which is close to 130 cm for the HP while it is only 30 cm for the VP2 soil profile. In these two cases, the REE distribution patterns might be related to HREE enriched minerals such as zircon. Moreover, the PP profile is comparatively depleted especially in the upper 30 cm of the soil profile due to the presence of smaller amounts of zircon.

During granite weathering, gradual dissolution of primary minerals such as apatite occurs (Aubert et al., 2001). This causes the release of Ca, P and REE. Calcium is taken up by vegetation and PO_4 co-precipitates with REE in secondary minerals. The formation of secondary REE(PO_4), like rhabdophane or florencite, was observed in other studies of granite alteration (Stille et al., 2009; Sanematsu et al., 2015; Santana et al., 2015). In this study, Nd (LREE) is enriched in the surface horizons (Fig.2) probably due to atmospheric depositions and recycling by vegetation (Aubert et al., 2002; Stille et al., 2009). Moreover, LREE(PO_4) are less soluble than HREE(PO4) and are immobilized in the upper compartment of the soil (Liu and Byrne, 1997; Cidu et al., 2013; Gangloff et al., 2014b). In contrast, there is a progressive accumulation of the MREE and HREE (Dy to Lu) slightly above and below 30 cm depth which coincides with the PO_4 accumulations (Fig.2). Consequently, there is a formation of secondary phosphate phases such as Dy(PO_4) and Yb(PO_4) inducing a fractionation between Nd (HREE) and Yb (HREE) as a function of PO_4 concentration in the soil (Figures 3 and 7). The comparatively high HREE contents and their accumulation at 30 cm depth might be due to weathering of zircon in the upper soil profile which releases HREE according to its REE characteristics (Fujimaki, 1986; Fu et al., 2009; Flores et al., 2013; Nardi et al., 2013). Indeed, sequential leaching experiments of granite showed that very small amounts of Zr might be dissolved out of zircons. The results indicate that the released Zr is adsorbed by the organic carbon (Du et al., 2012). Consequently, during Zircon alteration, Y-HREE released might co-precipitate with PO_4 to form secondary mineral like xenotime. The accumulation of Y, HREE and PO4 at the same depth supports this suggestion. Moreover, the enrichment factor EF_{Ti} Zr is relatively constant along the soil profile, compared to Y-HREE, which confirms that the enrichment of HREE-Y does not match to zircon but neo-formed xenotime. Similarly, other studies dealing with granite alteration, also mention the neo-formation of xenotime or churchite (De Putter et al., 1999; Harlov and Forster, 2003; Santana et al., 2015). Similar to our study,

others also observed LREE enrichments in surface horizons and HREE enrichments at greater depths of the soil profile (Soyol-Erdene and Huh, 2013; Jaireth et al., 2014) .

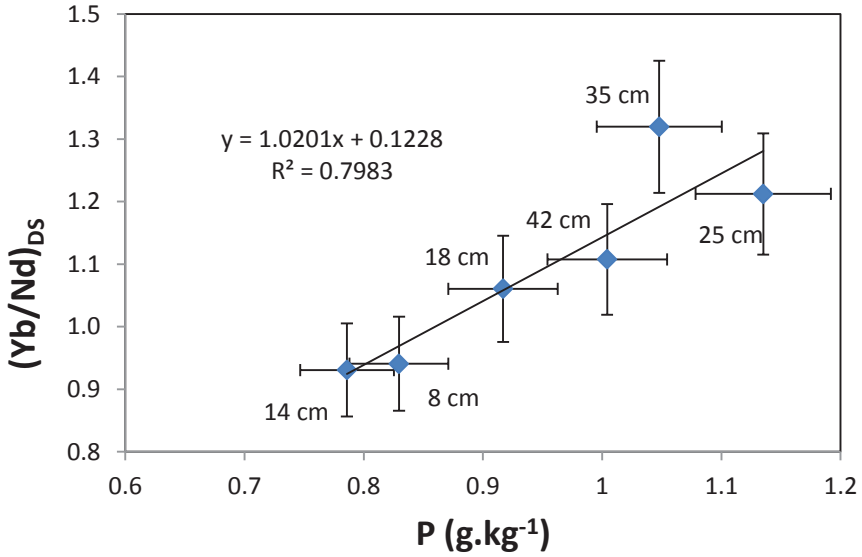

Figure 7: Correlation between the $(Yb/Nd)_{DS}$ and P soil contents

5.2. REE-Y behavior in the soil solutions circulating in the organic horizon at 0-30 cm depth

5.2.1. Comparison between soil water extracts and soil solutions

According to Zsolnay (1996) and Gangloff et al. (2014b), soil water extracts obtained by ultra-centrifugation contain the elements present in the micro and macro-pores of the soil whereas the soil solutions contain those from the macro-pores and gravity waters. Thus, their comparison permits to distinguish the factors impacting the REE-Y patterns of the soil solutions which can be influenced on the one hand by the soil and on the other hand by external factor transported by the gravity waters (Fig.4). More particularly, the REE-Y distribution patterns of the upper and summer soil solutions are different than those of the soil water extracts. Thus, their distribution patterns vary during the year especially due to the variable bacterial activity which impacts the OC content in soil solution. Moreover,

the REE-Y patterns approach those of soil water extracts with increasing depth indicating the decreased impact of surface factors such as litter decomposition. Also, the $(Ce^*/Ce)_{DS}$ values of the water extracts are lower than those of the soil solutions. This difference will be discussed below. The REE-Y pattern of the water extract is similar to that of the 5R colloidal fraction except for the upper summer sample (Fig.8). Consequently, the REE-Y transport by the 5R colloidal fraction might be influenced by the exchanges at the interface soil solutions/ micro-pores.

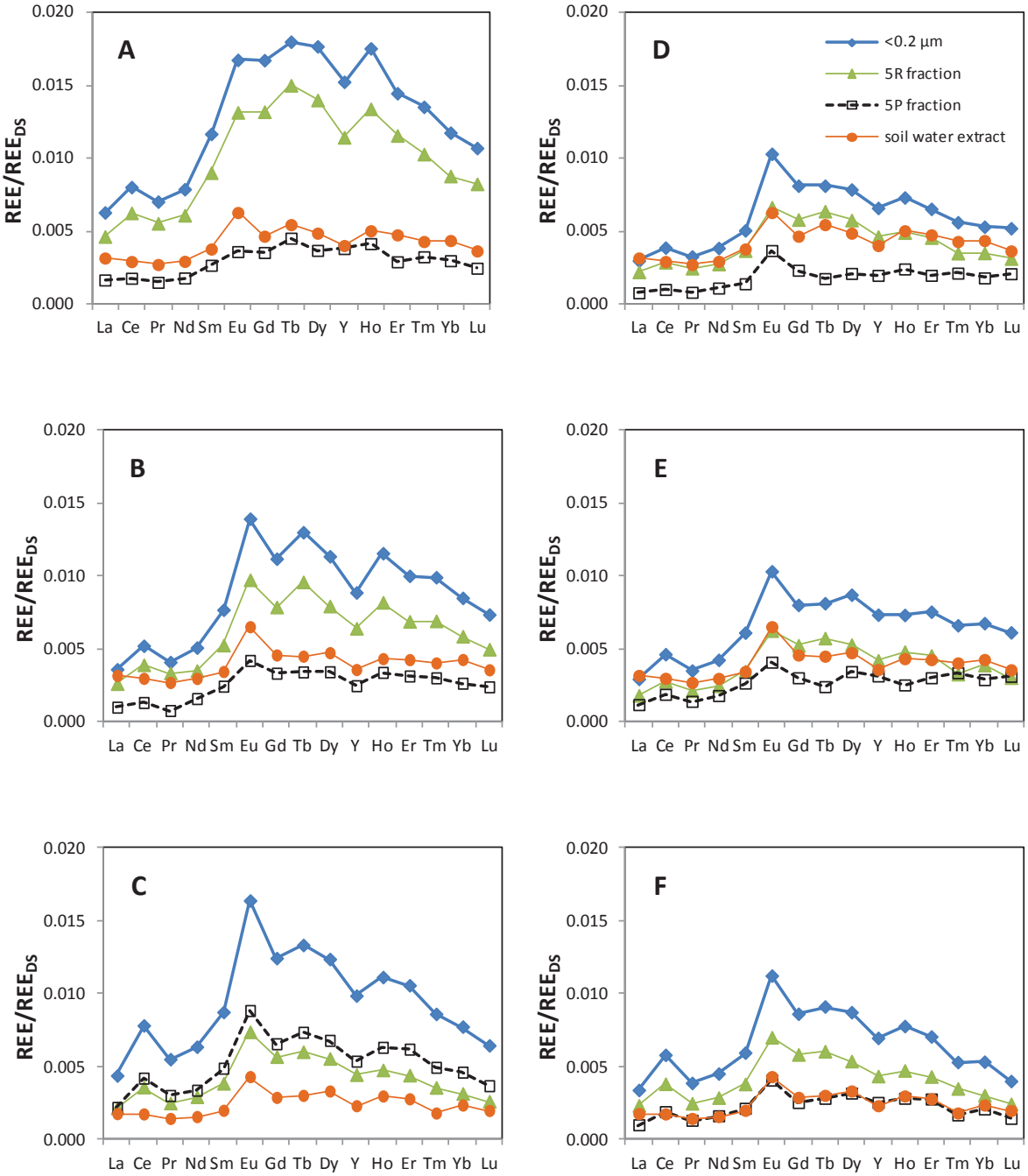

Figure 8: Comparison of REE-Y pattern between the soil water extract, the soil solutions filtered at 0.2 µm, the 5R colloidal and 5P dissolved fraction for the samples collected at 5, 10 and 30 cm depth, in June 2010 (A, B and C) and November 2012 (D, E and F).

5.2.2. Dissolution of REE-Y enriched minerals and precipitation of the REE-Y (PO_4)

During bio-weathering of phosphate minerals (rhabdophane, xenotime or apatite) or $P_{organic}$ originating from the degradation of litterfall (Rodríguez and Fraga, 1999; Chen et al., 2008; Courty et al., 2010), REE are released to soil solutions. The weathering and the reprecipitation of these phosphates govern a part of the REE dynamics between soil solutions and soil (Stille et al., 2009). Numerous leaching experiments on river sediments and soils yield MREE enrichments in the leachates while PO_4 was also released (Hannigan and Sholkovitz, 2001; Gangloff et al., 2014b). Rare earth element distribution patterns of the here studied soil solutions show a MREE enrichment in the different fractions and approve the PO_4 speciation of REE for the upper soil solutions (Fig 4). This enrichment is greater for samples collected during spring and summer when there is an increase of micro-organism activity needing more PO_4. The micro-organisms dissolve minerals through organic acids (Goyne et al., 2006, 2010). During bio-weathering and OC release, other minerals such as zircon might also be impacted (Du et al., 2012). Figure 9 confirms that dissolution of zircon increases the Yb (HREE) contents in the soil solution. Once dissolved, Yb (HREE) can co-precipitate with PO_4 in the soil solution. The variations of the Nd (LREE), Dy (MREE), Yb (HREE) and Y concentrations with those of PO_4 in the colloidal 5R fractions of soil solutions from the uppermost 10cm of the soil profile confirms dissolution of or/and precipitation of REE bearing phosphate (Fig. 10). The slopes of the correlation lines indicate that Nd is less released to the colloidal 5R fraction than Dy, Yb and Y which is in accordance with the solubility constants of REE-Y(PO_4) determined by Liu and Byrne (1997). In the colloidal 5R fraction, same orders of magnitude of Yb concentrations are correlated with those of P at 5cm and 10cm depth while there is a decrease for those of Nd, Dy and Y (Fig 10). This difference corresponds to an enrichment of Nd, Dy and Y in the upper soil solutions (filtered at 0.2µm as well as in the 5R colloidal and 5P dissolved fractions) collected between 5 and 10 cm depth while the water extract of the corresponding soil remains

constant (Fig 6A) (Gangloff et al. (2014b). Consequently, this enrichment in the soil solutions at close to the surface might be due to deposition of atmosphere derived LREE enriched dusts and cycling by vegetation (Aubert et al., 2002; Tyler, 2004; Stille et al., 2006).

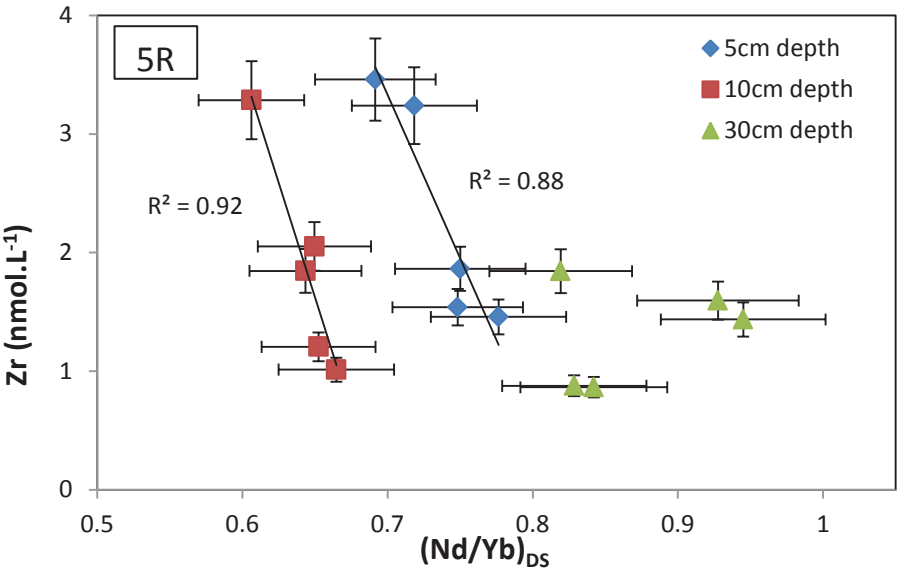

Figure 9: Correlation between Nd/Yb and Zr in the 5R colloidal fraction

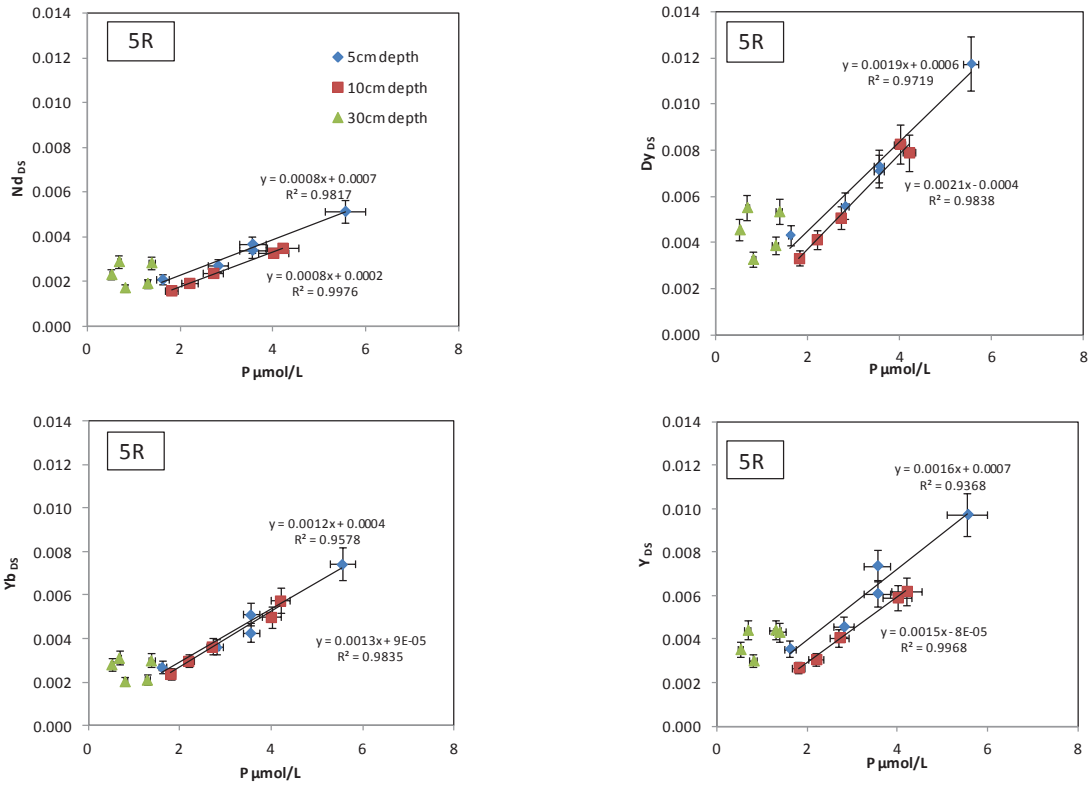

Figure 10: Correlation between Nd, Dy, Yb, Y and P in the 5R colloidal fraction

5.2.3. Complexation and transport by organic carbon

Alternatively, REE in soil solutions are also chelated by OC in the colloidal 5R fraction. These organic complexes are more stable than PO_4 or CO_3 (Byrne and Liu, 1996; Schijf and Byrne, 2001; Pourret et al., 2007a; Pédrot et al., 2010). Figure 11 shows the co-variations of DS normalized Nd, Dy, Yb and Y with OC in the colloidal 5R fractions. The slopes of the correlation lines point to significant enrichments of Y and Dy (MREE) compared to Nd (LREE) and Yb (HREE) in the shallower soil solutions. Moreover, the co-variation of Nd (LREE) with OC is similar while there are enrichments in Dy (MREE), Yb (HREE) and Y between 5 and 10 cm depth (Fig. 11). Consequently, this difference confirms that light and heavy REE have different affinities to OC in the colloidal fraction and, thus, for the different organic functions. More specifically, REE have a good affinity to carboxy-phenolic and phenolic groups of OC and the HREE compared to LREE are preferentially bound to the aromatic functional group (Marsac et al., 2010; Gangloff et al., 2014b). This affinity is confirmed by the co-variations between Nd/Yb and aromaticity (Fig 12). Therefore, Yb (HREE) can be transported by colloidal organic aromatic compounds over large distances and deeper than Nd (LREE). The study of the soil organic carbon of a neighboring soil profile of the same experimental parcel shows an accumulation of aromaticity between 30 and 36 cm depth (Gangloff et al., 2014b). This accumulation is due to the selective sorption of dissolved hydrophobic and aromatic organic compounds to soil particles which stabilize OC (Kalbitz et al., 2005; Gangloff et al., 2014b). Simultaneously, Yb (HREE) of the soil solutions is adsorbed to the soil through aromatic organic compounds. The soil enrichment profile of Yb (HREE) is similar to those of aromaticity and P (Fig. 2). Consequently, the mobility of Yb (HREE) in the soil profile is assumed conjointly by the dissolution of the zircon and phosphate minerals, the precipitation of the REE-Y(PO_4) and the evolution of OC with depth in the soil solutions, and more particularly in the colloidal 5R fraction. Thus, the REE-Y distribution patterns vary with depth in function

of the evolution of the organic functional groups of OC and the solubility of REE-Y(PO_4).

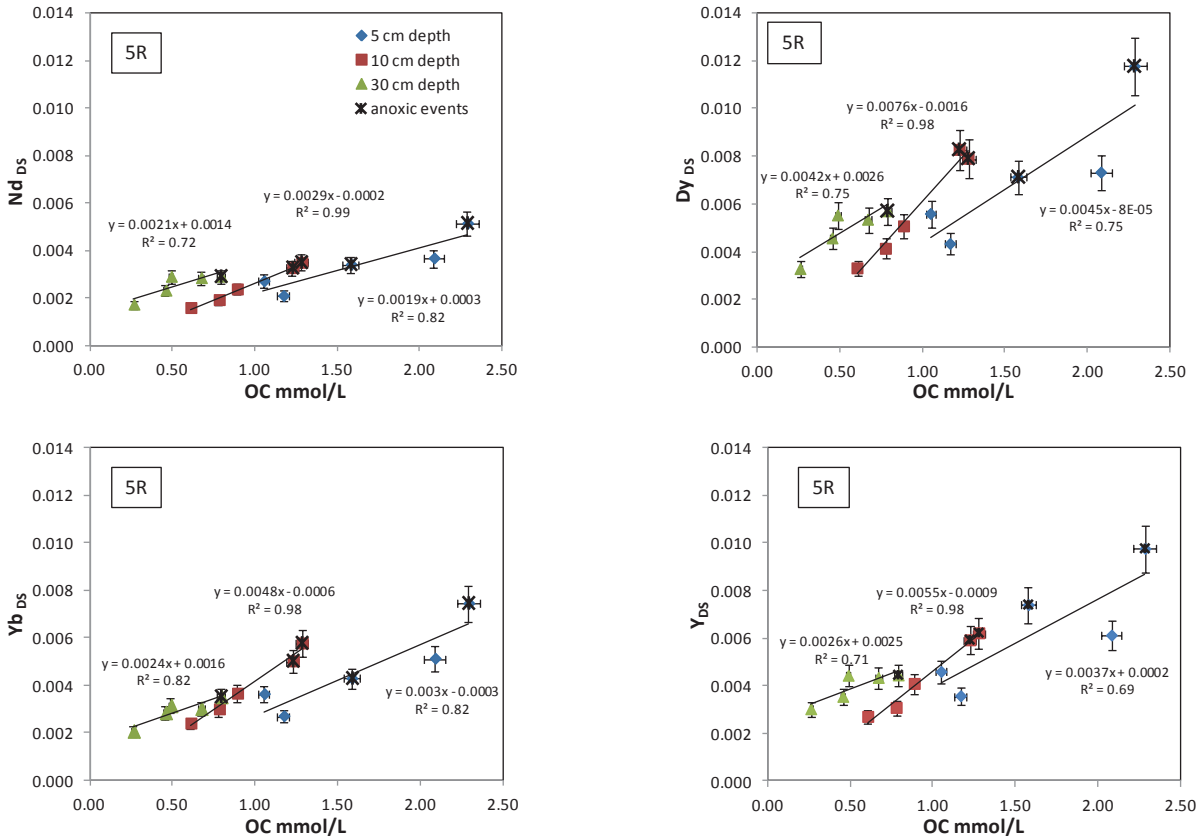

Figure 11: Correlation between Nd, Dy, Yb, Y and OC in the 5R colloidal fraction

5.2.4. Rare earth elements behavior in the dissolved fraction

The dissolved 5P fraction shows REE-Y distribution patterns similar to those of the colloidal 5R fraction. They present also a MREE enrichment. For this fraction, the correlations of REE-Y with other elements are less obvious than for the colloidal fraction. In the dissolved fraction, REE have different speciations and appear in complex forms like chloride, sulfate or organic with LMWOM (Wood, 1990; Johannesson et al., 1996; Goyne et al., 2010). The ratio $(Nd/Yb)_{5R}/(Nd/Yb)_{5P}$ is mainly below 1 and implies an enrichment of Yb (HREE) in the 5P dissolved fraction (Fig.6B). This might be due to competition between REE, Al and Fe for OC binding. Indeed, Al competes with Nd (LREE) and Fe with Yb (HREE) for acidic pH and low metal/OC ratio (Marsac et al., 2012; Marsac et al., 2013). Aluminum is present in the

dissolved 5P fraction in a larger proportion than Fe. This might be a reason why Yb (HREE) is enriched in the dissolved 5P fraction rather than Nd (LREE).

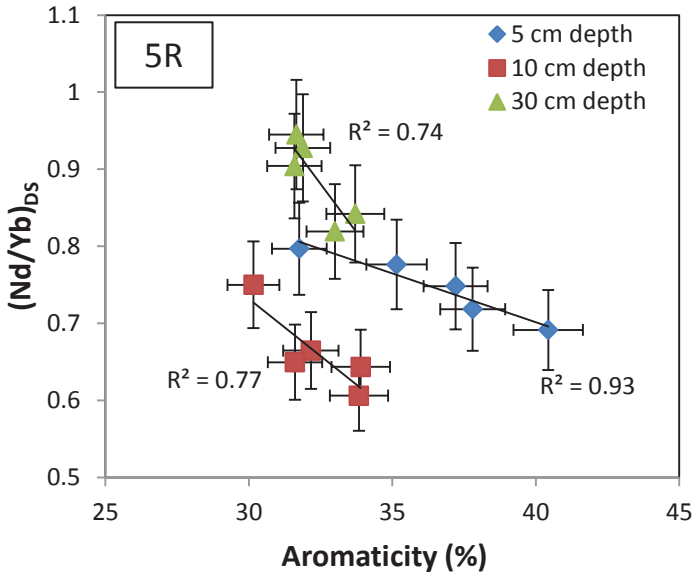

Figure 12: Correlation between Nd/Yb and aromaticity in the 5R colloidal fraction

5.3. Cerium and europium anomalies in the system soil/soil solutions

5.3.1. Cerium anomaly

Cerium shows always a positive anomaly $(Ce^*/Ce)_{DS}$ for the different fractions of all soil solutions originating from the humic horizon. The mean values of the 0.2 µm filtered soil solutions increase with depth from (1.12 ± 0.15) to (1.49 ± 0.08) between 5cm and 30cm depth. This is surprising since for oxidizing conditions negative anomalies are expected (Davranche et al., 2005; Prajith et al., 2015; Vázquez-Ortega et al., 2015). It is also important to note that $(Ce^*/Ce)_{DS}$ is not impacted by reductive conditions during anoxic events (November 2009 and June 2010) (Table 1). This implies that OC stabilizes Ce against redox processes (Dia et al., 2000; Davranche et al., 2005). Moreover, $(Ce^*/Ce)_{DS}$ in water extracts of the corresponding soils from 5cm to 30cm depth are relatively constant (0.92 to 1.08) (Fig. 5A). This indicates an enrichment of Ce (III) in soil solutions possibly due to

stabilization with Ce carrying OC. According to several authors, the electron shuttle of certain aromatic functional groups of OC like quinone can stabilize the reducer Ce (III) (Jiang and Kappler, 2008; Van der Zee and Cervantes, 2009). The correlations of $(Ce^*/Ce)_{DS}$ and aromaticity in the colloidal 5R fraction confirm this stabilization linked to the structure of OC (Fig. 13A). One observes also a covariation of $(Ce^*/Ce)_{DS}$ with the proportion of Mn in the 5R colloidal fraction for the deeper samples (Fig. 13B). At this depth, the $(Ce^*/Ce)_{DS}$ is season dependent with a positive anomaly for samples collected in summer and a negative for those collected in other seasons (Table 1). This reflects the redox conditions of the soil solutions which may be due to alternation of the wet and dry cycles of the soil and/or the micro-organism activity. Moreover, the OC of samples from deeper soil horizons has a different structure than the OC of the shallow soil solutions (Gangloff et al., 2016)(in review). Consequently, the reductive form of Ce (III) is not stabilized by humic acid and participates in the redox reactions.

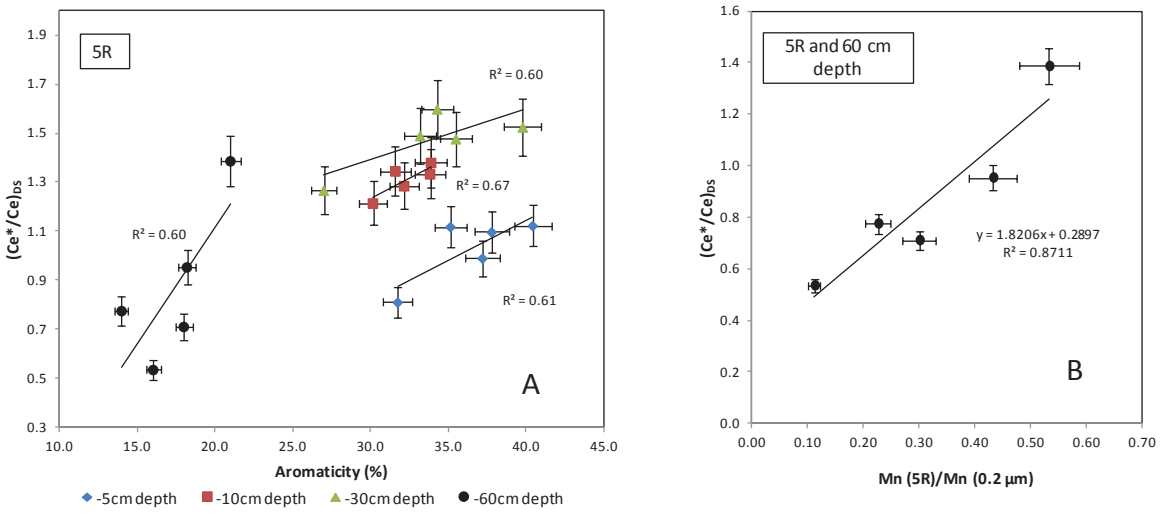

Figure 13: Correlation between $(Ce^*/Ce)_{DS}$ and aromaticity in the 5R colloidal fraction from different depths (A) and Mn proportion in the 5R colloidal fraction from 60 cm depth (B)

5.3.2. Europium anomaly

Europium shows always a positive anomaly $(Eu^*/Eu)_{DS}$ for the different fractions of all soil solutions (Table 1). The mean value of the 0.2 µm filtered soil solutions increases from 1.32 (± 0.12) at 5cm to 1.47 (± 0.08) at 10cm depth and is constant below (1.50 ± 0.05). The variation of the Eu anomaly $(Eu^*/Eu)_{DS}$ reflects progressive dissolution of different minerals during the granite weathering (Babechuk et al., 2014; Prajith et al., 2015; Vázquez-Ortega et al., 2015). Thus, the positive anomaly $(Eu^*/Eu)_{DS}$ of the soil solutions shows principally the alteration of the plagioclase (1.63) (Aubert et al., 2001). Moreover, the $(Eu^*/Eu)_{DS}$ values of the water extracts are larger than those of the soil solutions (Fig. 5B). Consequently, the positive anomaly $(Eu^*/Eu)_{DS}$ is more important in the micro-pores than in the macro-pores of the soil (Zsolnay, 1996). This enrichment might be due to the presence of plagioclase altered in the dissolution cavities of the soil and points out the evolution of alteration from micro-pores to macro-pores.

In the particular case of the upper soil solutions sampled in November 2009 and June 2010, $(Eu^*/Eu)_{DS}$ values are lower (1.23 and 1.18) than the others (Table 1). These samples are collected during anoxic events accompanied by a selective bacterial activity with an enrichment of the soil solution in Ca and PO_4^{3-} (Gangloff et al., 2016) (in review). Indeed, chemical and isotopic composition ($^{87}Sr/^{86}Sr$ versus $\delta^{44/40}Ca$) of the here studied soil solutions allowed to identify micro-organism activity and bio-weathering of apatite or phase with apatite as parent material (e.g. Ca and P recycled by the litter decomposition) in the soil solutions from uppermost (0-10 cm depth) soil horizons (Gangloff et al., 2014a). Consequently, these decreasing values of $(Eu^*/Eu)_{DS}$ indicate also a decreasing dissolution of plagioclase ($(Eu^*/Eu)_{DS}$ = 1.63) and increasing dissolution of apatite ($(Eu^*/Eu)_{DS}$ = 0.54) (values according to Aubert et al. (2001)) or litter decomposition ($(Eu^*/Eu)_{DS}$ = 1.07) (value according to Stille et al. (2009)).

5.4. **Geochemical characteristics of 60 cm depth samples**

The chemical composition of the 60 cm depth samples is different from that of the upper samples. The contents of OC, major and trace elements decrease strongly with increasing depth. The lower OC concentrations and aromaticities might originate from humic acid degradation in the upper soil horizons or rhizosphere (Pédrot et al., 2010). This OC has a different structure than that of the shallow soil solutions and interacts differently with trace elements like REE. Therefore, the REE distribution patterns in the colloidal 5R and dissolved 5P fractions of the 60 cm depth samples are different compared to those of the surface samples (Fig. 14).

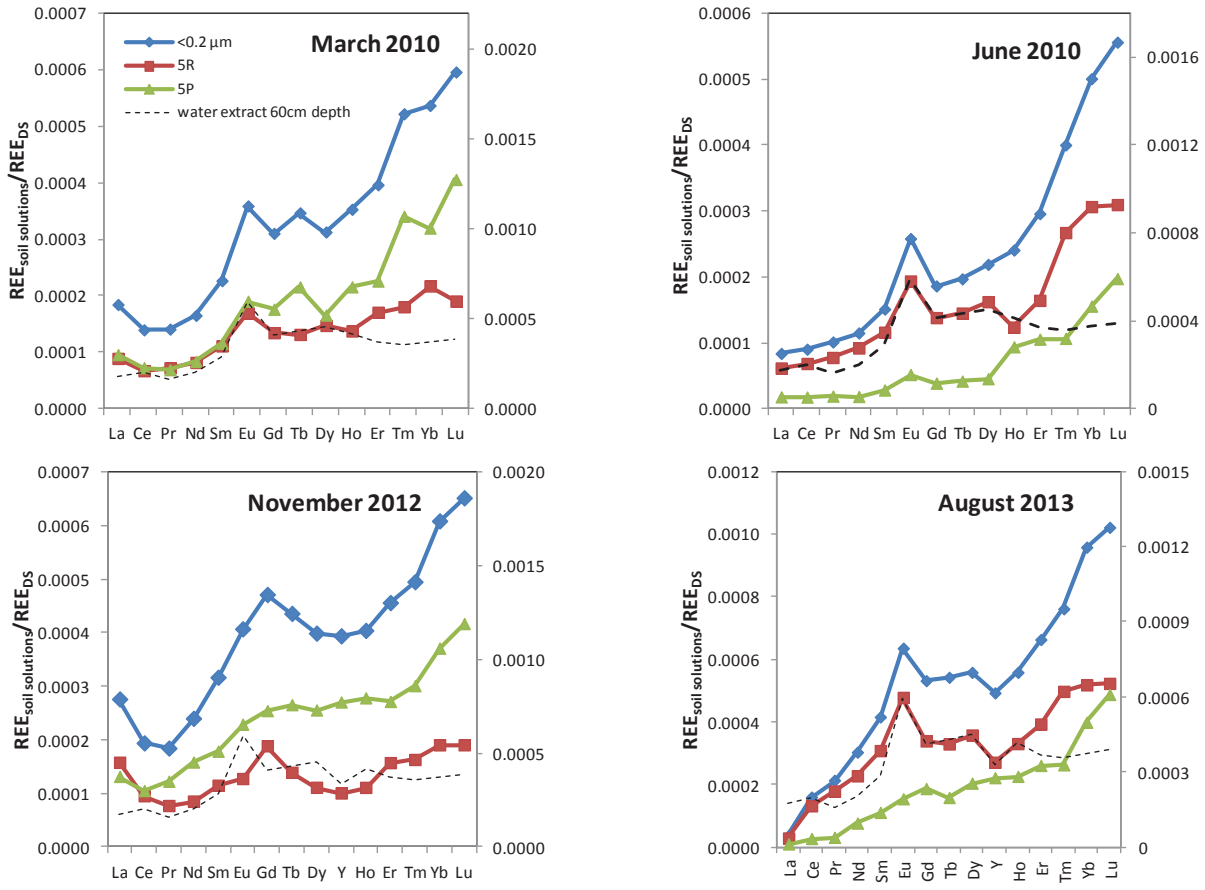

Figure 14: Comparson of REE-Y pattern between the soil water extract, the soil solutions filtered at 0.2 µm, the 5R colloidal and 5P dissolved fraction collected at 60 cm depth

5.4.1. Rare earth elements behavior in the dissolved fraction

The different REE-Y_{DS} patterns of the 5P dissolved fractions show similar distributions and concentrations. Observable is a progressive enrichment from La to Lu which may be the result of leaching process in the upper soil horizons. Indeed, at 30 cm depth, the soil is slightly enriched in heavy REE but not in Y and manifests low anomalies $(Eu/Eu^*)_{DS}$ (Fig. 14). This suggests that the REE in the 5P dissolved fraction are not derived from dissolution cavities of plagioclase but originate from soil macropores and are transported by gravity waters. Figure 15A shows the co-variation between $(Nd/Yb)_{DS}$ and Fe in the 5P dissolved fraction. This correlation might be due to a competition between Fe^{3+} and Yb (HREE) for the binding with OC (Marsac et al., 2013). Alternatively, it might be the result of leaching of Fe-oxy-hydroxides in the upper soil horizons which have a greater affinity for Nd (LREE) (Marmolejo-Rodríguez et al., 2007). This is also confirmed by the similar evolutions of the Fe and LREE enrichment factors throughout the soil profile Figure 15B.

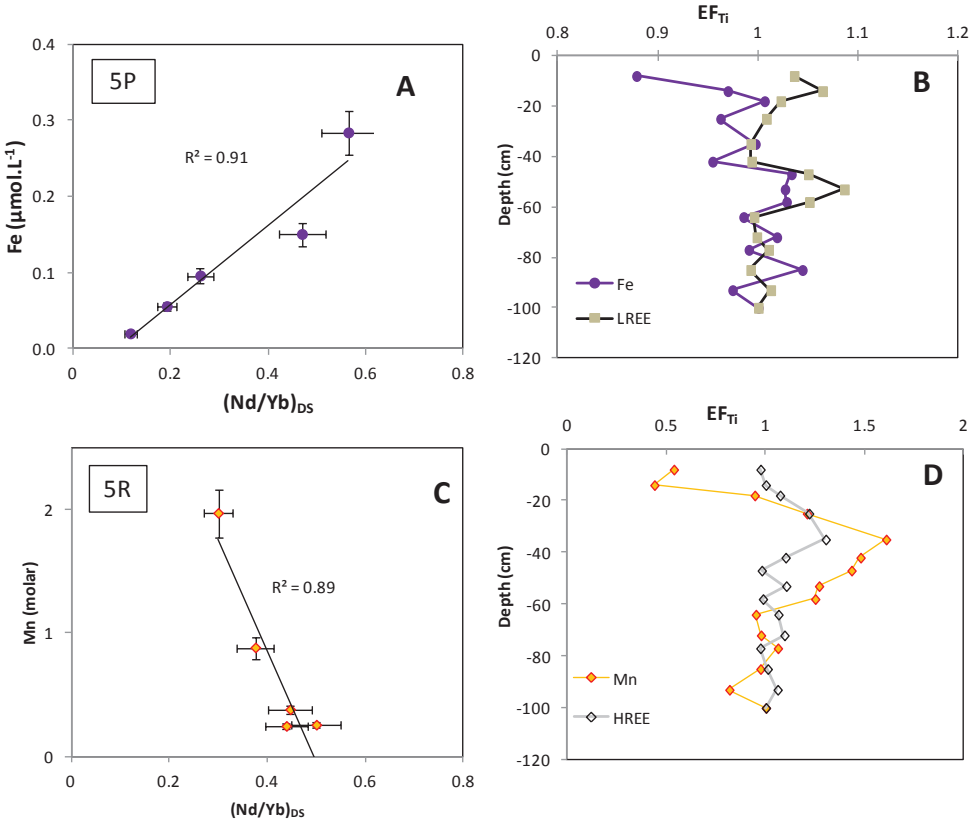

Figure 15: Correlation between Nd/Yb and (A) Fe in the 5P dissolved fraction and (C) Mn in the 5R colloidal fraction from 60 cm depth. Variation of EF_{Ti} for Fe, LREE (B) and Mn, HREE (D) (see caption Fig.2)

5.4.2. Rare earth elements behavior in the colloidal fraction

The REE-Y_{DS} patterns of the 5R colloidal fractions are different than those of the 5P dissolved fractions but similar to the REE-Y patterns of the 60 cm depth soil water extracts with Y anomaly and HREE enrichments (Fig. 14). Consequently, REE-Y in the colloidal fraction originate from micro-pores, macro-pores and gravity waters. The $(Eu/Eu^*)_{DS}$ anomalies point to plagioclase alteration which causes Eu enrichments in the colloidal fraction and prove the migration of the colloids from the its migration from the resulting dissolution cavities to the macro-pores. Moreover, the $(Nd/Yb)_{DS}$ fractionation in function of Mn in the colloidal fraction points to an enrichment in Yb (HREE) together with Mn (Fig. 15C). Consequently, the HREE enrichment in the colloidal fraction might be explained by the dissolution of Mn oxi-hydroxides in the upper soil horizons and their transport to lower soil horizons (Laveuf et al., 2012). Indeed, Mn has a similar EF_{Ti} than HREE along the soil profile (Fig. 15D). The REE-Y contents are more important in the 5R colloidal fraction than in the 5P dissolved fraction for June 2010 and August 2013 samples (Fig. 14). The reason might be the alternation of dry and wet flood periods which change the redox potential (E_H) and the pH (Shaheen et al., 2014). The formation of hydroxides like REE-$Y(OH)_3$ which are preferentially in the 5R colloidal fraction might be caused under least acidic conditions (Table1). The $(Ce^*/Ce)_{DS}$ values confirm the alternation of reductive or oxidative conditions in the soil system. It is interesting to note that Eu enrichments (Eu*/Eu) are more important during flooding periods

6. Conclusion

This study yield detailed information on alteration processes and pedogenesis in an acidic granite derived forest soil in the Strengbach catchment. The EF_{Ti} of the soil indicates that during alteration process, phosphate minerals and zircon might be dissolved and induce the formation of secondary mineral phase like xenotime in the deeper soil horizons. The ultra-filtered soil solutions from humic horizon show that (1) the REE-Y are principally enriched in the 5R colloidal fraction (5 kDa – 0.2 µm) controlling the REE-Y dynamic, (2) in the deeper soil solutions both, colloidal and dissolved fractions influence the REE-Y, (3) the mobility of REE-Y is controlled by the dissolution of the zircon and phosphate minerals, the precipitation of the REE-Y(PO_4) and the evolution of OC with depth in the colloidal 5R fraction. The comparative study of the soil profile, soil water extracts and soil solutions show that (1) the $(Eu^*/Eu)_{DS}$ anomaly reflects weathering of plagioclase in the micropores and the migration of the released Eu to the macropores, (2) the $(Ce^*/Ce)_{DS}$ anomaly, is stabilized by the electron shuttling of the humic acid (aromaticity) and provides information on the redox conditions only in the deeper soil horizons depleted in humic acid and finally (3) the HREE enrichment in the deeper soil solutions results from the partial dissolution of secondary minerals in the upper soil horizons (above 30 cm depth).

7. References

Aiuppa A., Allard P., D'alessandro W., Michel A., Parello F., Treuil M. and Valenza M., (2000). Mobility and fluxes of major, minor and trace metals during basalt weathering and groundwater transport at Mt. Etna volcano (Sicily). *Geochimica et Cosmochimica Acta*, **64** 1827-1841.

Andersson K., Dahlqvist R., Turner D., Stolpe B., Larsson T., Ingri J. and Andersson P., (2006). Colloidal rare earth elements in a boreal river: Changing sources and distributions during the spring flood. *Geochimica et Cosmochimica Acta*, **70** 3261-3274.

Aouad G., Stille P., Crovisier J.L., Geoffroy V.A., Meyer J.M. and Lahd-Geagea M., (2006). Influence of bacteria on lanthanide and actinide transfer from specific soil components (humus, soil minerals and vitrified municipal solid waste incinerator bottom ash) to corn plants: Sr-Nd isotope evidence. *The Science of the total environment*, **370** 545-551.

Åström M.E., Nystrand M., Gustafsson J.P., Österholm P., Nordmyr L., Reynolds J.K. and Peltola P., (2010). Lanthanoid behaviour in an acidic landscape. *Geochimica et Cosmochimica Acta*, **74** 829-845.

Aubert D., Stille P. and Probst A., (2001). REE fractionation during granite weathering and removal by waters and suspended loads: Sr and Nd isotopic evidence. *Geochimica et Cosmochimica Acta*, **65** 387-406.

Aubert D., Probst A. and Stille P., (2004). Distribution and origin of major and trace elements (particularly REE, U and Th) into labile and residual phases in an acid soil profile (Vosges Mountains, France). *Applied Geochemistry*, **19** 899-916.

Aubert D., Stille P., Probst A., Gauthier-Lafaye F., Pourcelot L. and Del Nero M., (2002). Characterization and migration of atmospheric REE in soils and surface waters. *Geochimica et Cosmochimica Acta*, **66** 3339-3350.

Babechuk M.G., Widdowson M. and Kamber B.S., (2014). Quantifying chemical weathering intensity and trace element release from two contrasting basalt profiles, Deccan Traps, India. *Chemical Geology*, **363** 56-75.

Bagard M.-L., Schmitt A.-D., Chabaux F., Pokrovsky O.S., Viers J., Stille P., Labolle F. and Prokushkin A.S., (2013). Biogeochemistry of stable Ca and radiogenic Sr isotopes in a larch-covered permafrost-dominated watershed of Central Siberia. *Geochimica et Cosmochimica Acta*, **114** 169-187.

Balan E., Trocellier P., Jupille J., Fritsch E., Muller J.-P. and Calas G., (2001). Surface chemistry of weathered zircons. *Chemical Geology*, **181** 13-22.

Bauer M., Fulda B. and Blodau C., (2008). Groundwater derived arsenic in high carbonate wetland soils: Sources, sinks, and mobility. *Science of The Total Environment*, **401** 109-120.

Blum J.D., Klaue A., Nezat C.A., Driscoll C.T., Johnson C.E., Siccama T.G., Eagar C., Fahey T.J. and Likens G.E., (2002). Mycorrhizal weathering of apatite as an important calcium source in base-poor forest ecosystems. *Nature*, **417** 729-731.

Bradl H.B., (2004). Adsorption of heavy metal ions on soils and soils constituents. *Journal of Colloid and Interface Science*, **277** 1-18.

Braun J.-J. and Pagel M., (1994). Geochemical and mineralogical behavior of REE, Th and U in the Akongo lateritic profile (SW Cameroon). *CATENA*, **21** 173-177.

Byrne R.H. and Liu X., (1996). Metal speciation assessments in natural waters: Comment on "Rare earth element complexation behavior in circumneutral pH ground waters: Assessing the role of carbonate and phosphate ions" by Kevin H. Johannesson, Klaus J. Stetzenbach, Vernon F. Hodge and W. Berry Lyons. *Earth and Planetary Science Letters*, **145** 135-137.

Cenki-Tok B., Chabaux F., Lemarchand D., Schmitt A.D., Pierret M.C., Viville D., Bagard M.L. and Stille P., (2009). The impact of water–rock interaction and vegetation on calcium isotope fractionation in soil- and stream waters of a small, forested catchment (the Strengbach case). *Geochimica et Cosmochimica Acta*, **73** 2215-2228.

Chen C.R., Condron L.M. and Xu Z.H., (2008). Impacts of grassland afforestation with coniferous trees on soil phosphorus dynamics and associated microbial processes: A review. *Forest Ecology and Management*, **255** 396-409.

Cidu R., Vittori Antisari L., Biddau R., Buscaroli A., Carbone S., Da Pelo S., Dinelli E., Vianello G. and Zannoni D., (2013). Dynamics of rare earth elements in water–soil systems: The case study of the Pineta San Vitale (Ravenna, Italy). *Geoderma*, **193–194** 52-67.

Clarholm M. and Skyllberg U., (2013). Translocation of metals by trees and fungi regulates pH, soil organic matter turnover and nitrogen availability in acidic forest soils. *Soil Biology and Biochemistry*, **63** 142-153.

Cobert F., Schmitt A.-D., Calvaruso C., Turpault M.-P., Lemarchand D., Collignon C., Chabaux F. and Stille P., (2011). Biotic and abiotic experimental identification of bacterial influence on calcium isotopic signatures. *Rapid Communications in Mass Spectrometry*, **25** 2760-2768.

Courty P.-E., Buée M., Diedhiou A.G., Frey-Klett P., Le Tacon F., Rineau F., Turpault M.-P., Uroz S. and Garbaye J., (2010). The role of ectomycorrhizal communities in forest ecosystem processes: New perspectives and emerging concepts. *Soil Biology and Biochemistry*, **42** 679-698.

Dahlqvist R., Andersson K., Ingri J., Larsson T., Stolpe B. and Turner D., (2007). Temporal variations of colloidal carrier phases and associated trace elements in a boreal river. *Geochimica et Cosmochimica Acta*, **71** 5339-5354.

Dahlqvist R., Benedetti M.F., Andersson K., Turner D., Larsson T., Stolpe B. and Ingri J., (2004). Association of calcium with colloidal particles and speciation of calcium in the Kalix and Amazon rivers. *Geochimica et Cosmochimica Acta*, **68** 4059-4075.

Dammshäuser A. and Croot P.L., (2012). Low colloidal associations of aluminium and titanium in surface waters of the tropical Atlantic. *Geochimica et Cosmochimica Acta*, **96** 304-318.

Davranche M., Pourret O., Gruau G., Dia A. and Le Coz-Bouhnik M., (2005). Adsorption of REE(III)-humate complexes onto MnO2: Experimental evidence for cerium anomaly and lanthanide tetrad effect suppression. *Geochimica et Cosmochimica Acta*, **69** 4825-4835.

Davranche M., Pourret O., Gruau G., Dia A., Jin D. and Gaertner D., (2008). Competitive binding of REE to humic acid and manganese oxide: Impact of reaction kinetics on development of cerium anomaly and REE adsorption. *Chemical Geology*, **247** 154-170.

Davranche M., Gruau G., Dia A., Marsac R., Pédrot M. and Pourret O., (2015). Biogeochemical Factors Affecting Rare Earth Element Distribution in Shallow Wetland Groundwater. *Aquatic Geochemistry*, **21** 197-215.

De Putter T., Charlet J.-M. and Quinif Y., (1999). REE, Y and U concentration at the fluid–iron oxide interface in late Cenozoic cryptodolines from Southern Belgium. *Chemical Geology*, **153** 139-150.

Deniel C. and Pin C., (2001). Single-stage method for the simultaneous isolation of lead and strontium from silicate samples for isotopic measurements. *Analytica Chimica Acta*, **426** 95-103.

Dia A., Gruau G., Olivié-Lauquet G., Riou C., Molénat J. and Curmi P., (2000). The distribution of rare earth elements in groundwaters: assessing the role of source-rock composition, redox changes and colloidal particles. *Geochimica et Cosmochimica Acta*, **64** 4131-4151.

Don A. and Kalbitz K., (2005). Amounts and degradability of dissolved organic carbon from foliar litter at different decomposition stages. *Soil Biol Biochem*, **37** 2171-2179.

Du X., Rate A.W. and Gee M.a.M., (2012). Redistribution and mobilization of titanium, zirconium and thorium in an intensely weathered lateritic profile in Western Australia. *Chemical Geology*, **330–331** 101-115.

Egli M., Sartori G., Mirabella A., Giaccai D., Favilli F., Scherrer D., Krebs R. and Delbos E., (2010). The influence of weathering and organic matter on heavy metals lability in silicatic, Alpine soils. *Science of The Total Environment*, **408** 931-946.

Fichter J., Turpault M.P., Dambrine E. and Ranger J., (1998). Mineral evolution of acid forest soils in the Strengbach catchment (Vosges mountains, N-E France). *Geoderma*, **82** 315-340.

Filella M. and Williams P.A., (2012). Antimony interactions with heterogeneous complexants in waters, sediments and soils: A review of binding data for homologous compounds. *Chem Erde-Geochem*, **72** 49-65.

Flores K.E., Martens U.C., Harlow G.E., Brueckner H.K. and Pearson N.J., (2013). Jadeitite formed during subduction: In situ zircon geochronology constraints from two different tectonic events within the Guatemala Suture Zone. *Earth and Planetary Science Letters*, **371–372** 67-81.

Francioso O., Sanchez-Cortes S., Tugnoli V., Ciavatta C., Sitti L. and Gessa C., (1996). Infrared, Raman, and Nuclear Magnetic Resonance (1H, 13C, and 31P) Spectroscopy in the Study of Fractions of Peat Humic Acids. *Appl. Spectrosc.*, **50** 1165-1174.

Fraysse F., Pokrovsky O.S. and Meunier J.D., (2010). Experimental study of terrestrial plant litter interaction with aqueous solutions. *Geochimica et Cosmochimica Acta*, **74** 70-84.

Fu B., Mernagh T.P., Kita N.T., Kemp A.I.S. and Valley J.W., (2009). Distinguishing magmatic zircon from hydrothermal zircon: A case study from the Gidginbung high-sulphidation Au–Ag–(Cu) deposit, SE Australia. *Chemical Geology*, **259** 131-142.

Fujimaki H., (1986). Partition coefficients of Hf, Zr, and REE between zircon, apatite, and liquid. *Contr. Mineral. and Petrol.*, **94** 42-45.

Fulda B., Voegelin A., Ehlert K. and Kretzschmar R., (2013). Redox transformation, solid phase speciation and solution dynamics of copper during soil reduction and reoxidation as affected by sulfate availability. *Geochimica et Cosmochimica Acta*, **123** 385-402.

Fuss C., Driscoll C., Johnson C., Petras R. and Fahey T., (2011). Dynamics of oxidized and reduced iron in a northern hardwood forest. *Biogeochemistry*, **104** 103-119.

Gabor R.S., Eilers K., Mcknight D.M., Fierer N. and Anderson S.P., (2014). From the litter layer to the saprolite: Chemical changes in water-soluble soil organic matter and their correlation to microbial community composition. *Soil Biology and Biochemistry*, **68** 166-176.

Gangloff S., Stille P., Schmitt A.-D. and Chabaux F., (2014a). Impact of Bacterial Activity on Sr and Ca Isotopic Compositions (87Sr/86Sr and δ44/40Ca) in Soil Solutions (the StrengbachCZO). *Procedia Earth and Planetary Science*, **10** 109-113.

Gangloff S., Stille P., Schmitt A.-D. and Chabaux F., (2016). Biotic and abiotic factors controlling the chemical composition of colloidal and dissolved fractions in soil solutions and the mobility of trace elements in soils. *Geochimica et Cosmochimica Acta* reviewed.

Gangloff S., Stille P., Pierret M.-C., Weber T. and Chabaux F., (2014b). Characterization and evolution of dissolved organic matter in acidic forest soil and its impact on the mobility of major and trace elements (case of the Strengbach watershed). *Geochimica et Cosmochimica Acta*, **130** 21-41.

Goyne K.W., Brantley S.L. and Chorover J., (2006). Effects of organic acids and dissolved oxygen on apatite and chalcopyrite dissolution: Implications for using elements as organomarkers and oxymarkers. *Chemical Geology*, **234** 28-45.

Goyne K.W., Brantley S.L. and Chorover J., (2010). Rare earth element release from phosphate minerals in the presence of organic acids. *Chemical Geology*, **278** 1-14.

Gustafsson J.P., Van Hees P., Starr M., Karltun E. and Lundström U., (2000). Partitioning of base cations and sulphate between solid and dissolved phases in three podzolised forest soils. *Geoderma*, **94** 311-333.

Hannigan R.E. and Sholkovitz E.R., (2001). The development of middle rare earth element enrichments in freshwaters: weathering of phosphate minerals. *Chemical Geology*, **175** 495-508.

Harlavan Y. and Erel Y., (2002). The release of Pb and REE from granitoids by the dissolution of accessory phases. *Geochimica et Cosmochimica Acta*, **66** 837-848.

Harlov D.E. and Forster H.J., (2003). Unraveling the history of high-grade rocks: What apatite may tell us? *Journal of the Czech Geological Society*, **48** 59-60.

Ingri J., Widerlund A., Land M., Gustafsson Ö., Andersson P. and Öhlander B., (2000). Temporal variations in the fractionation of the rare earth elements in a boreal river; the role of colloidal particles. *Chemical Geology*, **166** 23-45.

Jaireth S., Hoatson D.M. and Miezitis Y., (2014). Geological setting and resources of the major rare-earth-element deposits in Australia. *Ore Geology Reviews*, **62** 72-128.

Jiang J. and Kappler A., (2008). Kinetics of Microbial and Chemical Reduction of Humic Substances: Implications for Electron Shuttling. *Environmental Science & Technology*, **42** 3563-3569.

Johannesson K.H., Lyons W.B., Yelken M.A., Gaudette H.E. and Stetzenbach K.J., (1996). Geochemistry of the rare-earth elements in hypersaline and dilute acidic natural terrestrial waters: Complexation behavior and middle rare-earth element enrichments. *Chemical Geology*, **133** 125-144.

Kaiser K., Guggenberger G., Haumaier L. and Zech W., (2001). Seasonal variations in the chemical composition of dissolved organic matter in organic forest floor layer leachates of old-growth Scots pine (Pinus sylvestris L.) and European beech (Fagus sylvatica L.) stands in northeastern Bavaria, Germany. *Biogeochemistry*, **55** 103-143.

Kaiser K., Guggenberger G., Haumaier L. and Zech W., (2002). The composition of dissolved organic matter in forest soil solutions: changes induced by seasons and passage through the mineral soil. *Organic Geochemistry*, **33** 307-318.

Kalbitz K., Geyer W. and Geyer S., (1999). Spectroscopic properties of dissolved humic substances - a reflection of land use history in a fen area. *Biogeochemistry*, **47** 219-238.

Kalbitz K., Schmerwitz J., Schwesig D. and Matzner E., (2003). Biodegradation of soil-derived dissolved organic matter as related to its properties. *Geoderma*, **113** 273-291.

Kalbitz K., Schwesig D., Rethemeyer J. and Matzner E., (2005). Stabilization of dissolved organic matter by sorption to the mineral soil. *Soil Biol Biochem*, **37** 1319-1331.

Kleber M., Eusterhues K., Keiluweit M., Mikutta C., Mikutta R. and Nico P.S. (2015) Chapter One - Mineral–Organic Associations: Formation, Properties, and Relevance in Soil Environments, in: Donald L.S. (Ed.), Advances in Agronomy. Academic Press, pp. 1-140.

Lang S.Q., Bernasconi S. and Früh-Green G., (2012). Stable isotope analysis of organic carbon in small (µgC) samples and dissolved organic matter using a GasBench preparation device. *Rapid Communications in Mass Spectrometry*, **1** 9-16.

Laveuf C. and Cornu S., (2009). A review on the potentiality of Rare Earth Elements to trace pedogenetic processes. *Geoderma*, **154** 1-12.

Laveuf C., Cornu S., Guilherme L.R.G., Guerin A. and Juillot F., (2012). The impact of redox conditions on the rare earth element signature of redoximorphic features in a soil sequence developed from limestone. *Geoderma*, **170** 25-38.

Lemarchand D., Cividini D., Turpault M.P. and Chabaux F., (2012). Boron isotopes in different grain size fractions: Exploring past and present water–rock interactions from two soil profiles (Strengbach, Vosges Mountains). *Geochimica et Cosmochimica Acta*, **98** 78-93.

Lemarchand E., Chabaux F., Vigier N., Millot R. and Pierret M.-C., (2010). Lithium isotope systematics in a forested granitic catchment (Strengbach, Vosges Mountains, France). *Geochimica et Cosmochimica Acta*, **74** 4612-4628.

Liu R. and Lead J.R., (2006). Partial validation of cross flow ultrafiltration by atomic force microscopy. *Anal Chem*, **78** 8105-8112.

Liu R.X., Lead J.R. and Zhang H., (2013). Combining cross flow ultrafiltration and diffusion gradients in thin-films approaches to determine trace metal speciation in freshwaters. *Geochimica et Cosmochimica Acta*, **109** 14-26.

Liu X. and Byrne R.H., (1997). Rare earth and yttrium phosphate solubilities in aqueous solution. *Geochimica et Cosmochimica Acta*, **61** 1625-1633.

Lorenz K., Preston C.M., Raspe S., Morrison I.K. and Feger K.H., (2000). Litter decomposition and humus characteristics in Canadian and German spruce ecosystems: information from tannin analysis and 13C CPMAS NMR. *Soil Biology and Biochemistry*, **32** 779-792.

Lundström U.S., Van Breemen N. and Bain D., (2000). The podzolization process. A review. *Geoderma*, **94** 91-107.

Marmolejo-Rodríguez A.J., Prego R., Meyer-Willerer A., Shumilin E. and Sapozhnikov D., (2007). Rare earth elements in iron oxy−hydroxide rich sediments from the Marabasco River-Estuary System (pacific coast of Mexico). REE affinity with iron and aluminium. *Journal of Geochemical Exploration*, **94** 43-51.

Marsac R., Davranche M., Gruau G. and Dia A., (2010). Metal loading effect on rare earth element binding to humic acid: Experimental and modelling evidence. *Geochimica et Cosmochimica Acta*, **74** 1749-1761.

Marsac R., Davranche M., Gruau G., Dia A. and Bouhnik-Le Coz M., (2012). Aluminium competitive effect on rare earth elements binding to humic acid. *Geochimica et Cosmochimica Acta*, **89** 1-9.

Marsac R., Davranche M., Gruau G., Dia A., Pedrot M., Le Coz-Bouhnik M. and Briant N., (2013). Effects of Fe competition on REE binding to humic acid: Origin of REE pattern variability in organic waters. *Chemical Geology*, **342** 119-127.

Meng Y.-T., Zheng Y.-M., Zhang L.-M. and He J.-Z., (2009). Biogenic Mn oxides for effective adsorption of Cd from aquatic environment. *Environmental Pollution*, **157** 2577-2583.

Miller A.Z., Dionísio A., Sequeira Braga M.A., Hernández-Mariné M., Afonso M.J., Muralha V.S.F., Herrera L.K., Raabe J., Fernandez-Cortes A., Cuezva S., Hermosin B., Sanchez-Moral S., Chaminé H. and Saiz-Jimenez C., (2012). Biogenic Mn oxide minerals coating in a subsurface granite environment. *Chemical Geology*, **322–323** 181-191.

Nardi L.V.S., Formoso M.L.L., Müller I.F., Fontana E., Jarvis K. and Lamarão C., (2013). Zircon/rock partition coefficients of REEs, Y, Th, U, Nb, and Ta in granitic rocks: Uses for provenance and mineral exploration purposes. *Chemical Geology*, **335** 1-7.

Pédrot M., Dia A. and Davranche M., (2009). Double pH control on humic substance-borne trace elements distribution in soil waters as inferred from ultrafiltration. *Journal of Colloid and Interface Science*, **339** 390-403.

Pédrot M., Dia A. and Davranche M., (2010). Dynamic structure of humic substances: Rare earth elements as a fingerprint. *Journal of Colloid and Interface Science*, **345** 206-213.

Pierret M.C., Stille P., Prunier J., Viville D. and Chabaux F., (2014). Chemical and U–Sr isotopic variations in stream and source waters of the Strengbach watershed (Vosges mountains, France). *Hydrol. Earth Syst. Sci.*, **18** 3969-3985.

Pokrovsky O.S. and Schott J., (2002). Iron colloids/organic matter associated transport of major and trace elements in small boreal rivers and their estuaries (NW Russia). *Chemical Geology*, **190** 141-179.

Pokrovsky O.S., Dupré B. and Schott J., (2005). Fe–Al–organic Colloids Control of Trace Elements in Peat Soil Solutions: Results of Ultrafiltration and Dialysis. *Aquatic Geochemistry*, **11** 241-278.

Pokrovsky O.S., Viers J., Shirokova L.S., Shevchenko V.P., Filipov A.S. and Dupré B., (2010). Dissolved, suspended, and colloidal fluxes of organic carbon, major and trace elements in the Severnaya Dvina River and its tributary. *Chemical Geology*, **273** 136-149.

Pourret O., Davranche M., Gruau G. and Dia A., (2007a). Organic complexation of rare earth elements in natural waters: Evaluating model calculations from ultrafiltration data. *Geochimica et Cosmochimica Acta*, **71** 2718-2735.

Pourret O., Dia A., Gruau G., Davranche M. and Bouhnik-Le Coz M., (2012). Assessment of vanadium distribution in shallow groundwaters. *Chemical Geology*, **294** 89-102.

Pourret O., Dia A., Davranche M., Gruau G., Henin O. and Angee M., (2007b). Organo-colloidal control on major- and trace-element partitioning in shallow groundwaters: Confronting ultrafiltration and modelling. *Applied Geochemistry*, **22** 1568-1582.

Prajith A., Rao V.P. and Kessarkar P.M., (2015). Controls on the distribution and fractionation of yttrium and rare earth elements in core sediments from the Mandovi estuary, western India. *Continental Shelf Research*, **92** 59-71.

Probst A., El Gh'mari A., Aubert D., Fritz B. and Mcnutt R., (2000). Strontium as a tracer of weathering processes in a silicate catchment polluted by acid atmospheric inputs, Strengbach, France. *Chemical Geology*, **170** 203-219.

Prunier J., Chabaux F., Stille P., Gangloff S., Pierret M.C., Viville D. and Aubert A., (2015). Geochemical and isotopic (Sr, U) monitoring of soil solutions from the Strengbach catchment (Vosges mountains, France): Evidence for recent weathering evolution. *Chemical Geology*, **417** 289-305.

Rihs S., Prunier J., Thien B., Lemarchand D., Pierret M.-C. and Chabaux F., (2011). Using short-lived nuclides of the U- and Th-series to probe the kinetics of colloid migration in forested soils. *Geochimica et Cosmochimica Acta*, **75** 7707-7724.

Riotte J. and Chabaux F., (1999). (234U/238U) activity ratios in freshwaters as tracers of hydrological processes: the Strengbach watershed (Vosges, France). *Geochimica et Cosmochimica Acta*, **63** 1263-1275.

RodríGuez H. and Fraga R., (1999). Phosphate solubilizing bacteria and their role in plant growth promotion. *Biotechnology Advances*, **17** 319-339.

Said-Pullicino D., Erriquens F.G. and Gigliotti G., (2007). Changes in the chemical characteristics of water-extractable organic matter during composting and their influence on compost stability and maturity. *Bioresour Technol*, **98** 1822-1831.

Sanematsu K., Kon Y. and Imai A., (2015). Influence of phosphate on mobility and adsorption of REEs during weathering of granites in Thailand. *Journal of Asian Earth Sciences*, **111** 14-30.

Santana I.V., Wall F. and Botelho N.F., (2015). Occurrence and behavior of monazite-(Ce) and xenotime-(Y) in detrital and saprolitic environments related to the Serra Dourada granite, Goiás/Tocantins State, Brazil: Potential for REE deposits. *Journal of Geochemical Exploration*, **155** 1-13.

Schijf J. and Byrne R.H., (2001). Stability constants for mono- and dioxalato-complexes of Y and the REE, potentially important species in groundwaters and surface freshwaters. *Geochimica et Cosmochimica Acta*, **65** 1037-1046.

Schlosser C. and Croot P.L., (2008). Application of cross-flow filtration for determining the solubility of iron species in open ocean seawater. *Limnology and Oceanography: Methods*, **6** 630-642.

Schmitt A.-D., Chabaux F. and Stille P., (2003). The calcium riverine and hydrothermal isotopic fluxes and the oceanic calcium mass balance. *Earth and Planetary Science Letters*, **213** 503-518.

Schmitt A.D., Gangloff S., Cobert F., Lemarchand D., Stille P. and Chabaux F., (2009). High performance automated ion chromatography separation for Ca isotope measurements in geological and biological samples. *Journal of Analytical Atomic Spectrometry*, **24** 1089-1097.

Shaheen S.M., Rinklebe J., Rupp H. and Meissner R., (2014). Lysimeter trials to assess the impact of different flood–dry-cycles on the dynamics of pore water concentrations of As, Cr, Mo and V in a contaminated floodplain soil. *Geoderma*, **228–229** 5-13.

Shields G. and Stille P., (2001). Diagenetic constraints on the use of cerium anomalies as palaeoseawater redox proxies: an isotopic and REE study of Cambrian phosphorites. *Chemical Geology*, **175** 29-48.

Singhal R.K., Preetha J., Karpe R., Tirumalesh K., Kumar S.C. and Hegde A.G., (2006). The use of ultra filtration in trace metal speciation studies in sea water. *Environment International*, **32** 224-228.

Sipos P., Németh T., Mohai I. and Dódony I., (2005). Effect of soil composition on adsorption of lead as reflected by a study on a natural forest soil profile. *Geoderma*, **124** 363-374.

Sivry Y., Riotte J. and Dupré B., (2006). Study of exchangeable metal on colloidal humic acids and particulate matter by coupling ultrafiltration and isotopic tracers: Application to natural waters. *Journal of Geochemical Exploration*, **88** 144-147.

Soyol-Erdene T.-O. and Huh Y., (2013). Rare earth element cycling in the pore waters of the Bering Sea Slope (IODP Exp. 323). *Chemical Geology*, **358** 75-89.

Stille P., Pierret M.C., Steinmann M., Chabaux F., Boutin R., Aubert D., Pourcelot L. and Morvan G., (2009). Impact of atmospheric deposition, biogeochemical cycling and water–mineral interaction on REE fractionation in acidic surface soils and soil water (the Strengbach case). *Chemical Geology*, **264** 173-186.

Stille P., Pourcelot L., Granet M., Pierret M.C., Guéguen F., Perrone T., Morvan G. and Chabaux F., (2011). Deposition and migration of atmospheric Pb in soils from a forested silicate catchment today and in the past (Strengbach case): Evidence from 210Pb activities and Pb isotope ratios. *Chemical Geology*, **289** 140-153.

Stille P., Steinmann M., Pierret M.C., Gauthier-Lafaye F., Chabaux F., Viville D., Pourcelot L., Matera V., Aouad G. and Aubert D., (2006). The impact of vegetation on REE fractionation in stream waters of a small forested catchment (the Strengbach case). *Geochimica et Cosmochimica Acta*, **70** 3217-3230.

Taboada T., Cortizas A.M., García C. and García-Rodeja E., (2006). Particle-size fractionation of titanium and zirconium during weathering and pedogenesis of granitic rocks in NW Spain. *Geoderma*, **131** 218-236.

Tricca A., Stille P., Steinmann M., Kiefel B., Samuel J. and Eikenberg J., (1999). Rare earth elements and Sr and Nd isotopic compositions of dissolved and suspended loads from small river systems in the Vosges mountains (France), the river Rhine and groundwater. *Chemical Geology*, **160** 139-158.

Tyler G., (2004). Rare earth elements in soil and plant systems - A review. *Plant and Soil*, **267** 191-206.

Ussiri D.a.N. and Johnson C.E., (2003). Characterization of organic matter in a northern hardwood forest soil by 13C NMR spectroscopy and chemical methods. *Geoderma*, **111** 123-149.

Ussiri D.a.N. and Johnson C.E., (2007). Organic matter composition and dynamics in a northern hardwood forest ecosystem 15 years after clear-cutting. *Forest Ecology and Management*, **240** 131-142.

Van Der Zee F.P. and Cervantes F.J., (2009). Impact and application of electron shuttles on the redox (bio)transformation of contaminants: A review. *Biotechnology Advances*, **27** 256-277.

Van Hees P.a.W., Lundström U.S. and Giesler R., (2000). Low molecular weight organic acids and their Al-complexes in soil solution—composition, distribution and seasonal variation in three podzolized soils. *Geoderma*, **94** 173-200.

Van Hees P.a.W., Van Hees A.M.T. and Lundström U.S., (2001). Determination of aluminium complexes of low molecular organic acids in soil solution from forest soils using ultrafiltration. *Soil Biology and Biochemistry*, **33** 867-874.

Vázquez-Ortega A., Perdrial J., Harpold A., Zapata-Ríos X., Rasmussen C., Mcintosh J., Schaap M., Pelletier J.D., Brooks P.D., Amistadi M.K. and Chorover J., (2015). Rare earth elements as reactive tracers of biogeochemical weathering in forested rhyolitic terrain. *Chemical Geology*, **391** 19-32.

Verstraeten A., De Vos B., Neirynck J., Roskams P. and Hens M., (2014). Impact of air-borne or canopy-derived dissolved organic carbon (DOC) on forest soil solution DOC in Flanders, Belgium. *Atmospheric Environment*, **83** 155-165.

Viville D., Chabaux F., Stille P., Pierret M.C. and Gangloff S., (2012). Erosion and weathering fluxes in granitic basins: The example of the Strengbach catchment (Vosges massif, eastern France). *CATENA*, **92** 122-129.

Waeles M., Tanguy V., Lespes G. and Riso R.D., (2008). Behaviour of colloidal trace metals (Cu, Pb and Cd) in estuarine waters: An approach using frontal ultrafiltration (UF) and stripping chronopotentiometric methods (SCP). *Estuarine, Coastal and Shelf Science*, **80** 538-544.

Weishaar J.L., Aiken G.R., Bergamaschi B.A., Fram M.S., Fujii R. and Mopper K., (2003). Evaluation of Specific Ultraviolet Absorbance as an Indicator of the Chemical Composition and Reactivity of Dissolved Organic Carbon. *Environmental Science & Technology*, **37** 4702-4708.

White A.F., Blum A.E., Schulz M.S., Vivit D.V., Stonestrom D.A., Larsen M., Murphy S.F. and Eberl D., (1998). Chemical Weathering in a Tropical Watershed, Luquillo Mountains, Puerto Rico: I. Long-Term Versus Short-Term Weathering Fluxes. *Geochimica et Cosmochimica Acta*, **62** 209-226.

Wood S.A., (1990). The aqueous geochemistry of the rare-earth elements and yttrium: 1. Review of available low-temperature data for inorganic complexes and the inorganic REE speciation of natural waters. *Chemical Geology*, **82** 159-186.

Wu P., Zhang Q., Dai Y., Zhu N., Dang Z., Li P., Wu J. and Wang X., (2011). Adsorption of Cu(II), Cd(II) and Cr(III) ions from aqueous solutions on humic acid modified Ca-montmorillonite. *Geoderma*, **164** 215-219.

Zhu Z., Wang Z., Li J., Li Y., Zhang Z. and Zhang P., (2012). Distribution of rare earth elements in sewage-irrigated soil profiles in Tianjin, China. *Journal of Rare Earths*, **30** 609-613.

Zsolnay A. (1996) Chapter 4 - Dissolved Humus in Soil Waters, in: Alessandro P. (Ed.), Humic Substances in Terrestrial Ecosystems. Elsevier Science B.V., Amsterdam, pp. 171-223.

Chapitre 5

Identification des mécanismes de fractionnement isotopique du Ca dans les solutions d'un sol forestier: apport des ultrafiltrations et du couplage isotopique $\delta^{44/40}$Ca-δ^{13}C-^{87}Sr/^{86}Sr

1. Introduction

Le calcium (Ca) est un macronutriment essentiel à la croissance des végétaux et est impliqué dans de nombreux processus biologiques. C'est pourquoi il est impotant d'identifier et de caractériser les différents compartiments impliqués dans le cycle biogéochimique du Ca. L'étude de ce cycle dans la zone critique est complexe en raison d'une grande hétérogénéité spatiale et temporelle du milieu naturel. Il est donc nécessaire d'identifier les sources, les réservoirs ainsi que les mécanismes impliqués dans le stockage et la libération du Ca. Pour un écosystème forestier, il faut une réserve suffisante en nutriments dans le sol pour que les arbres puissent se développer. Les apports en Ca dans le sol se font par l'intermédiaire des pluies, des pluviolessivats et de l'altération des minéraux comme l'apatite ou le plagioclase (Likens et al., 1998; Chadwick et al., 1999; Aubert et al., 2001; Dijkstra and Smits, 2002; Dijkstra, 2003; Schmitt and Stille, 2005). Le Ca ainsi libéré peut être prélevé par la végétation, précipité sous forme de minéraux secondaires, adsorbé et/ou désorbé sur les particules organiques ou minérales du sol (minéraux argileux, oxydes-hydroxydes de Fe ou Al, complexe argilo-humique) ou complexés par les acides organiques. Les sols forestiers acidifiés par les pluies ont des réserves plus limitées, par conséquent, le recyclage par la végétation joue un rôle important (Likens et al., 1998). La quantité de Ca ainsi libérée est conditionnée par la dégradation de la litière. Ensuite, il migre vers les solutions de sol où il se répartit entre la fraction colloïdale et la fraction dissoute. Le prélèvement racinaire par la végétation se fait préférentiellement dans la fraction dissoute, ainsi la fraction colloïdale peut représenter un réservoir de Ca pour un écosystème forestier.

L'étude préliminaire de Cenki-Tok et al. (2009) a mis en évidence une variabilité isotopique en Ca des solutions de sol de surface de la parcelle couverte d'épicéas du bassin versant du Strengbach, observatoire hydrogéochimique de l'environnement (OHGE). Cette variabilité pourrait s'expliquer par une différence de l'intensité des différents flux de Ca au cours

des saisons ou par la présence de colloïdes plus ou moins importants en fonction des saisons.

Différentes études, principalement en milieu boréal ou tropical, ont identifié qu'entre 16 et 30% de Ca colloïdal pouvait contribuer au bilan en Ca des eaux de rivière (Dahlqvist et al., 2004; Pokrovsky et al., 2010; Bagard et al., 2011; Pokrovsky et al., 2012). Pokrovsky et al. (2010) ont pour leur part reporté des proportions de colloïdes plus importants en été qu'en hiver dans les eaux de rivières, lié au fait que la matière organique dissoute est plus importante au printemps qu'en hiver. Pour leur part Bagard et al. (2013) ont suggéré que le cycle biogéochimique du Ca en climat boréal soumis au permafrost est principalement contrôlé par la dégradation de la biomasse ainsi que par la présence de colloïdes organo-minéraux enrichis en ^{40}Ca. Ceci rejoint également la conclusion de l'étude de Stille et al. (2012) portant sur des cernes d'épicéas du bassin versant du Strengbach où les auteurs ont suggéré qu'un flux additionnel de Ca, fortement enrichi en ^{40}Ca est nécessaire pour équilibrer le bilan de masse du Ca. Les phases colloïdales ont notamment été invoquées pour représenter un tel flux.

Afin de vérifier cela, nous avons effectué des expérimentations d'ultrafiltrations sur les solutions de sol du bassin versant du Strengbach (OHGE), sur la parcelle expérimentale recouverte d'épicéas VP2, à différentes profondeurs (entre 5 et 60 cm) et saisons (entre 2009 et 2013). Ensuite, nous avons caractérisé les signatures isotopiques du Ca des phases dissoutes et colloïdales à l'aide de différentes tailles de filtres : filtration frontale (0,22 µm) et tangentielle (300 et 5 kDa). L'objectif de cette étude est d'identifier (1) une potentielle variabilité isotopique de ces différentes phases (dissoute et colloïdale) et (2) l'origine des phases colloïdales (organique ou minérale) à l'aide d'une approche isotopique couplée ($\delta^{40/44}Ca$, $^{87}Sr/^{86}Sr$, $\delta^{13}C_{orga}$).

2. Site de prélèvement et échantillonnage

Le Bassin Versant du Strengbach est un bassin versant forestier de 80 ha situé dans le massif Vosgien au Nord - Est de la France sur la commune d'Aubure à une altitude comprise entre 883 m et 1146 m (Figure 1). Ce bassin a été équipé à partir de 1986. En 2007, il a été labellisé en tant qu'Observatoire National par la CNRS sous le nom d'Observatoire Hydro-Géochimique de l'Environnement (OHGE, http://ohge.unistra.fr). Un suivi des paramètres climatologiques, hydrologiques et géochimiques est effectué de façon régulière et continue.

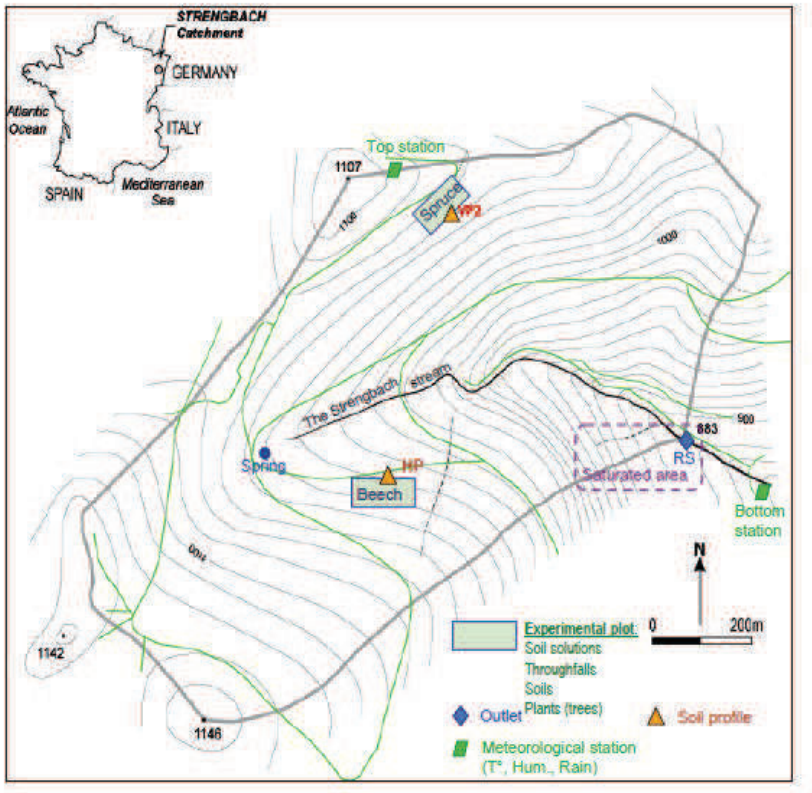

Figure 1: Carte du bassin versant du Strengbach avec les deux parcelles expérimentales (VP: Vieux peuplement sous conifères et HP: la hêtraie)

Le climat est de type océanique-montagnard. La précipitation annuelle est d'environ 1400 mm, 25% sont apportés par de la neige du mois de décembre au mois d'avril. La température moyenne annuelle est de 6°C. La forêt du bassin versant est dominée à 80% par des conifères et les 20%

restant correspondent à des hêtres. Des symptômes de dépérissement forestier ont été observés vers 1980, essentiellement dû à la carence en calcium et en magnésium dans le sol (Probst et al., 1990; Bonneau et al., 1991), phénomène observé encore aujourd'hui. Le bassin versant possède deux parcelles expérimentales. Une est située sur le versant sud sous couvert de hêtres (HP) et la seconde sur le versant nord sous couvert de conifères (VP) (Figure 1). Tous les échantillons étudiés dans ce chapitre proviennent de la parcelle VP sous conifères. Le sol situé à la parcelle VP est un sol brun acide dont le pH est compris entre 3.7 et 5 (Gangloff et al., 2014b). L'acidification du sol est dû d'une part à une acidification naturelle par le processus de podzolisation et d'autre part aux dépôts atmosphériques acides. Cette forte acidité accélère l'altération du sol et diminue son pouvoir tampon.

Seize solutions de sol ont été collectées par l'intermédiaire de plaques lysimétriques sans tension à 5, 10, 30 et 60 cm de profondeur entre le 9 septembre 2009 et le 9 septembre 2010; et 10 entre le 25 septembre 2012 et le 6 août 2013 (Tableau 1).

3. Méthodes de filtration et d'analyses

3.1. **Procédures de filtrations et ultra-filtrations**

Chaque solution de sol a été filtrée à 0,2 µm par des filtres Omnipore® (PTFE hydrophile) (Merck Millipore©). Ensuite, une partie de ces échantillons a été ultra-filtrée (UF) par flux de filtration tangentiel (TFF) par un appareil Labscale TFF de Millipore© dont le protocole est décrit de façon détaillée dans Gangloff et al. (2016) (soumis ou chapitre 3) . Les cassettes utilisées sont des PelliconXL® en cellulose régénérée. La partie de l'échantillon qui passe au travers de la membrane contient les composés plus petits que le seuil de coupure de la membrane, ils correspondent au perméat (P). La partie de l'échantillon qui reste dans le réservoir renferme principalement les composés plus grands que le seuil de coupure de la membrane et correspond au rétentat (R).

Les solutions de sol filtrées à 0,2 µm sont ultra-filtrées à 300 kDa afin d'obtenir le rétentat (300R) correspondant à la fraction colloïdale comprise entre 300 kDa et 0,2 µm (fraction gros colloïde) et le perméat (300P) correspondant à la fraction inférieure à 300 kDa. Ensuite, la fraction 300P est ultra-filtrée à 5 kDa pour obtenir le rétentat (5R) correspondant à la fraction colloïdale comprise entre 5 kDa et 300 kDa (fraction petit colloïde) et le perméat (5P) correspondant à la fraction dissoute dans notre étude. Par manque de volume, deux échantillons prélevés à 60 cm de profondeur ont été ultra-filtrés seulement à 5 kDa.

3.2. **Paramètres d'ultra-filtrations**

Différents paramètres dus à la procédure d'ultra-filtration tangentielle doivent être considérés pour déterminer correctement les concentrations de chaque fraction ultra-filtrée (Francioso et al. (1996) ; Ingri et al. (2000) ; Dahlqvist et al. (2004) ; Liu and Lead (2006) ; Schlosser and Croot (2008) ; Dammshäuser and Croot (2012) ; Liu et al. (2013)). Un des paramètres importants est le facteur de concentration volumique du rétentat (VCF_r). Il est déterminé comme suit:

$$VCF_r = (volume\ initial)/(\ volume\ du\ rétentat) \quad (1)$$

Dans cette étude, $VCF_{r(300kDa)}$ est égal à 5.0 ± 0.4 (N=20) et $VCF_{r(5kDa)}$ est égal à 3.6 ± 0.3 (N=20). C'est important d'avoir des valeurs de VCF_r similaires pour chaque seuil de coupure pour pouvoir ensuite comparer les différents échantillons. Les valeurs des concentrations des échantillons ultra-filtrés discutées dans ce chapitre correspondent aux concentrations entre les deux seuils de coupure et sont calculées par:

$$Ci = \frac{(Ci_{rétentat} - Ci_{perméat})}{VCF_{r_i}} \quad (2)$$

où Ci = concentration de l'élément i, VCF_{ri} = facteur de concentration volumique de l'élément i dans le rétentat.

Pour chaque ultra-filtration, il est important de calculer le rendement pour chaque élément pour vérifier qu'il n'y a pas de phénomène d'adsorption ou de contamination. Le rendement pour chaque composé i correspond à:

$$Rendement\ i = \frac{Quantité\ de\ i\ dans\ le\ rétentat + Quantité\ de\ i\ dans\ le\ perméat}{Quantité\ initiale\ de\ i\ dans\ l'échantillon} \quad (3)$$

Les rendements varient essentiellement entre 95% et 99%.

3.3. **Méthodes analytiques**

Le pH est mesuré avec une électrode combinée calibrée par des standards NIST (pH 4.00 et 7.00). Le carbone organique est mesuré par une méthode thermique avec une incertitude de 2% et une limite de détection de 0,3 mg $C.L^{-1}$ (Shimadzu TOC VPH - Shimadzu©). Les concentrations en Ca sont déterminées par sptectrométrie atomique à source plasma et couplage inductif (ICP/AES) (Thermo Scientific iCAP 6000 SERIES - Thermo Fisher Scientific©) et celles en Sr par spectrométrie de masse à source plasma et à couplage inductif (ICP/MS) (Thermo-Fisher X SerieII - Thermo Fisher Scientific©) par calibration traditionnelle et en utilisant l'Indium comme standard interne. La validité et la reproductibilité des différents paramètres analysés ont été vérifiées par des standards certifiés tels que SLRS5, Perade-20, Rain 97 et Big-Moose 02.

L'absorbance UV spécifique à 254 nm ($SUVA_{254}$) a été déterminée par l'absorbance UV à 254 nm normalisée par la concentration en carbone organique (Corga) en mg $C.L^{-1}$. Elle a été mesurée par un spectrophotomètre UV-Vis (SHIMADZU UV-1700). Weishaar et al. (2003) a montré qu'il y avait une relation entre le pourcentage d'aromaticité déterminé par ^{13}C-NMR et la valeur $SUVA_{254}$ (pourcentage d'aromaticité = 6,53 x $SUVA_{254}$ + 3,63).

3.4. **Séparations, purifications chimiques et mesures isotopiques**

3.4.1. Strontium ($^{87}Sr/^{86}Sr$)

La séparation et la purification du strontium (Sr) contenu dans les échantillons ont été menées au LHyGeS suivant une procédure mise au point par (Deniel and Pin, 2001). Ces étapes sont effectuées par chromatographie solide liquide en utilisant une résine échangeuse d'ions Sr-Spec Eichrom©, 50-100 mesh.

La mesure du rapport isotopique $^{87}Sr/^{86}Sr$ des solutions de sol filtrées à 0,2 µm et ultra-filtrées ont été réalisées sur un TIMS Triton (Spectromètre de masse à Thermo-ionisation) (Thermo Fisher Scientific©). Environ 100 ng de Sr sont déposés sur un filament en rhénium (Re) (pureté 99,995%) préalablement dégazé avec du Ta_2O_5 comme activateur. La valeur du rapport isotopique $^{87}Sr/^{86}Sr$ est évaluée par la moyenne statistique de 100 rapports mesurés. La validité et la reproductibilité des mesures sont vérifiées par le standard certifié NBS 987 à chaque séquence analytique ($^{87}Sr/^{86}Sr$ = 0.710250 ± 6 ; 2SD, N=10).

3.4.2. Calcium ($\delta^{44/40}Ca$)

La séparation chimique et la mesure isotopiques du Ca ont été réalisées au LHyGeS. Afin d'éviter tout fractionnement isotopique au cours de la séparation chimique ou de la mesure, 1µg de double spike $^{42}Ca/^{43}Ca$ est ajouté à une quantité d'échantillon contenant 5 µg de Ca avant d'effectuer la séparation, la purification en Ca et la mesure isotopique. Cette séparation est faite par une chromatographie ionique ICS-3000 (Dionex©) équipée d'un collecteur de fraction. La colonne utilisée est une colonne de type CS16 (Dionex©). Ce protocole expérimental est détaillé dans Schmitt et al. (2009). Une fois purifié, l'échantillon est évaporé à sec et le résidu est dissous dans 1µl d'HNO_3 0,25N pour être déposé sur un filament en Ta (pureté 99,995%) préalablement dégazé et oxydé. La composition isotopique en Ca est mesurée par un TIMS Triton (Thermo Fisher Scientific©) en mode multi-collection dynamique (Schmitt et al., 2009). Entre 150 et 200 cycles de mesures sont collectés. Les valeurs $\delta^{44/40}Ca$ sont corrigées du fractionnement instrumental hors ligne par l'intermédiaire du logiciel Matlab©. Les valeurs isotopiques en Ca sont exprimées en ‰ avec une valeur relative au standard NIST SRM 915a selon l'expression:

$$\delta^{44/40}Ca = (((^{44}Ca/^{40}Ca)_{échantillon}/(^{44}Ca/^{40}Ca)_{SRM\ 915a})-1)*1000$$

La différence de compositions isotopiques en Ca entre deux réservoirs est symbolisé par △ et est définie par: $\triangle_{i-j} = \delta^{44/40}Ca_i - \delta^{44/40}Ca_j$ où i et j sont les deux réservoirs à comparer.

Le facteur de fractionnement alpha (α) est défini par la proportion des deux isotopes dans le composé A divisé par la proportion des mêmes isotopes dans le composé B: $\alpha_{A-B} = R_A/R_B$

La justesse et la reproductibilité des mesures isotopiques sont vérifiées à chaque série analytique par des solutions de référence (Eau de mer : 1,80 ± 0,11 ‰ (2SD, N = 20); CaF_2 : 1,45 ± 0,12 ‰ (2SD, N=10)).

3.4.3. Carbone organique ($\delta^{13}C_{orga}$)

Les mesures de $\delta^{13}C_{orga}$ de certains échantillons filtrés et ultra-filtrés ont été faites selon le protocole de Lang et al. (2012) à l'Institut de Géologie de l'ETH à Zürich (Suisse). Tout d'abord, les échantillons sont acidifiés par de l'acide ortho-phosphorique et le carbone inorganique est éliminé par bullage avec de l'hélium. Ensuite, le C_{orga} est oxydé à chaud. La composition isotopique du CO_2 formé et dégagé est mesurée par un couplage d'équipements composé d'un système d'introduction en ligne GasBench II (Thermo Fisher Scientific©, Bremen, Allemagne), d'un passeur automatique CTC (CTC Analytics AG, Zwingen, Suisse) et d'un couplage de l'interface ConFlo IV avec un Delta V Plus mass spectrometer (les deux ThermoFisher Scientific©).

3.4.4. Validation du protocole d'ultrafiltration appliqué aux mesures isotopiques

Afin de vérifier que les isotopes de Ca ne sont pas fractionnés au cours de l'expérimentation d'ultra-filtration, une solution de Nitrate de Calcium ainsi qu'une eau minérale (Mont-Roucous) ont été ultra-filtrées. Ensuite, la composition isotopique en Ca de l'échantillon initial (filtré à 0,2 µm), des fractions colloïdales et dissoutes ont été mesurées suivant le même protocole que les échantillons. Nous observons que $\delta^{44/40}Ca_{SRM915a}$ = 0,85 ± 0,12 ‰

Table 1: Results for the different fractions (colloidal and dissolved)

(<D.L.: below to the detection limit)

sampling period	sample type	depth	Colloidal size		date	pH	Arom	DOC (mmol/L)	Ca (µmol/L)	Sr (nmol/L)	$\delta^{44/40}Ca_{SRM915a}$ (‰)	$^{87}Sr/^{86}Sr$	$\delta^{13}C_{orga}$ (‰)	OC (%)	Ca (%)	Sr (%)
09/09/2009 to 11/12/2009	**soil solution**	**5cm**	0.2µm	November 2009	11/12/2009		30.7	3.51	42.00	35.84	***0.58***	0.71855	-28.1	1.00	1.00	1.00
			0.2 µm to 300kDa				31.4	0.02	0.00	0.00				0.00	0.00	0.00
			300kDa to 5kDa				31.8	1.58	14.00	7.18	0.41			0.45	0.33	0.20
			<5kDa				24.3	1.85	28.00	29.12	0.77			0.53	0.67	0.81
11/12/2009 to 03/19/2010	**soil solution**	**5cm**	0.2µm	March 2010	03/19/2010	4.05	36.7	1.79	16.76	15.98	***0.66***	0.72001	-27.9	1.00	1.00	1.00
			0.2 µm to 300kDa			4	37.0	0.00	0.00	0.06	0.67			0.00	0.00	0.00
			300kDa to 5kDa			3.66	37.2	1.05	4.82	4.68	0.11	0.71983	-28.3	0.59	0.29	0.29
			<5kDa			4.21	31.9	0.74	11.99	11.24	0.97	0.71984	-27.8	0.41	0.72	0.70
03/19/2010 to 06/21/2010	**soil solution**	**5cm**	0.2µm	June 2010	06/21/2010	5.1	35.4	4.08	53.25	54.11	***0.42***	0.71729	-27.5	1.00	1.00	1.00
			0.2 µm to 300kDa			5.06	37.8	0.47	4.92	5.18	0.28			0.11	0.09	0.10
			300kDa to 5kDa			4.95	40.4	2.29	24.57	25.00	0.25	0.71731	-27.6	0.56	0.46	0.46
			<5kDa			5.3	30.2	1.32	23.75	23.93	0.70	0.71731	-27.1	0.32	0.45	0.44
06/21/2010 to 09/08/2010	**soil solution**	**5cm**	0.2µm	September 2010	08/09/2012	3.97	34.0	3.03	21.75	21.13	***0.69***	0.71952	-28.1	1.00	1.00	1.00
09/25/2012 to 11/20/2012	**soil solution**	**5cm**	0.2µm	November 2012	11/20/2012	4.4	38.3	2.17	10.30	10.81	***0.78***	0.71981	-27.8	1.00	1.00	1.00
			0.2µm to 300kDa			4.13	38.0	0.35	1.14	1.21	0.66			0.16	0.11	0.11
			300kDa to 5kDa			4.05	35.2	1.17	5.03	5.56	0.71	0.71992	-27.9	0.54	0.49	0.51
			<5kDa			4.6	27.0	0.65	4.13	4.04	1.15	0.71973	-27.7	0.30	0.40	0.37
11/20/2012 to 03/26/2013	**soil solution**	**5cm**	0.2µm	March 2013	03/26/2013	4.1	34.0	2.11	15.73	17.47	***0.77***	0.72077		1.00	1.00	1.00
05/22/2013 to 08/06/2013	**soil solution**	**5cm**	0.2µm	August 2013	08/06/2013	4	38.3	3.96	18.65	21.69	***0.65***	0.72062	-28.0	1.00	1.00	1.00
			0.2 µm to 300kDa			3.64	43.3	0.86	2.96	3.20	0.55			0.22	0.16	0.15
			300kDa to 5kDa			3.72	37.8	2.08	10.31	11.49	0.50	0.72063	-28.2	0.53	0.55	0.53
			<5kDa			4.5	31.3	1.01	5.38	7.00	0.94		-27.7	0.26	0.29	0.32

sampling period	sample type	depth	Colloidal size		date	pH	Arom	DOC (mmol/L)	Ca (µmol/L)	Sr (nmol/L)	$\delta^{44/40}Ca_{SRM915a}$ (‰)	$^{87}Sr/^{86}Sr$	$\delta^{13}C_{orga}$ (‰)	OC (%)	Ca (%)	Sr (%)
09/09/2009 to 11/12/2009	**soil solution**	**10cm**	0.2µm	November 2009	11/12/09	4.6	28.1	2.27	33.00	32.08	***0.84***	0.71964	-28.0	1.00	1.00	1.00
			0.2 µm to 300kDa				28.4	0.05	0.00	-0.13				0.02	0.00	0.00
			300kDa to 5kDa				30.2	1.23	9.50	8.05	0.73			0.54	0.29	0.25
			<5kDa				23.3	1.01	23.74	24.38	1.09			0.44	0.72	0.76
11/12/2009 to 03/19/2010	**soil solution**	**10cm**	0.2µm	March 2010	3/19/10	4.3	32.0	1.03	12.30	14.16	***0.83***	0.72202	-27.2	1.00	1.00	1.00
			0.2µm to 300kDa			4.25	32.9	0.00	0.00	0.02	0.74			0.00	0.00	0.00
			300kDa to 5kDa			4	32.2	0.61	3.69	3.95	0.52			0.59	0.30	0.28
			<5kDa			4.4	29.8	0.43	8.62	10.19	1.00			0.41	0.70	0.72
03/19/2010 to 06/21/2010	**soil solution**	**10cm**	0.2µm	June 2010	6/21/10	5.1	31.9	1.85	31.50	37.56	***0.42***	0.71888	-27.5	1.00	1.00	1.00
			0.2µm to 300kDa			5.1	31.1	0.02	0.05	-0.05	0.43			0.01	0.00	0.00
			300kDa to 5kDa			4.9	33.8	1.10	10.80	15.27	0.31	0.71890		0.59	0.34	0.41
			<5kDa			5.33	28.0	0.73	20.65	22.33	0.53			0.39	0.66	0.59
06/21/2010 to 09/08/2010	**soil solution**	**10cm**	0.2µm	September 2010	8/9/10	4.44	33.3	1.79	14.23	15.94	***0.71***	0.72106	-27.9	1.00	1.00	1.00
09/25/2012 to 11/20/2012	**soil solution**	**10cm**	0.2µm	November 2012	11/20/12	4.46	33.5	1.43	11.83	15.41	***1.03***	0.72308	-27.5	1.00	1.00	1.00
			0.2 µm to 300kDa			4.42	34.0	0.02	0.10	0.03	0.98	0.72289		0.01	0.01	0.00
			300kDa to 5kDa			4.17	31.6	0.81	3.60	4.97	0.72	0.72284	-27.8	0.57	0.66	0.32
			<5kDa			4.73	29.2	0.60	8.20	10.42	1.30	0.72285	-27.5	0.42	0.34	0.68
05/22/2013 to 08/06/2013	**soil solution**	**10cm**	0.2µm to 300kDa	August 2013	8/6/13	4.12	33.99	1.68	7.95	12.21	***0.76***	0.72412	-27.6	1.00	1.00	1.00
			0.2µm to 300kDa			3.94	34.01	0.34	0.96	1.38	0.57			0.21	0.12	0.11
			300kDa to 5kDa			3.92	33.90	0.78	3.84	5.32	0.65			0.46	0.48	0.44
			<5kDa			4.54	30.90	0.55	3.15	5.51	1.16			0.33	0.40	0.45

sampling period	sample type	depth	Colloidal size		date	pH	Arom	DOC (mmol/L)	Ca (µmol/L)	Sr (nmol/L)	$\delta^{44/40}Ca_{SRM915a}$ (‰)	$^{87}Sr/^{86}Sr$	$\delta^{13}C_{orga}$ (‰)	OC (%)	Ca (%)	Sr (%)
09/09/2009 to 11/12/2009	**soil solution**	**30cm**	0.2µm	November 2009	11/12/2009	4.30	28.8	2.22	33.00	38.81	***0.81***	0.72057	-28.1	1.00	1.00	1.00
			0.2 µm to 300kDa			n.d.	28.4	0.05	0.00	-0.15				0.02	0.00	0.00
			300kDa to 5kDa			n.d.	31.6	0.79	3.79	5.24	0.55			0.36	0.11	0.14
			<5kDa			n.d.	22.9	1.38	29.21	35.09	1.06			0.62	0.89	0.90
11/12/2009 to 03/19/2010	**soil solution**	**30cm**	0.2µm	March 2010	03/19/2010	4.80	33.7	0.55	8.50	13.93	***0.88***	0.72160	-27.2	1.00	1.00	1.00
			0.2 µm to 300kDa			4.72	34.9	0.01	0.03	0.19	0.70			0.01	0.00	0.01
			300kDa to 5kDa			4.30	33.7	0.26	1.73	4.28	0.25			0.48	0.20	0.31
			<5kDa			4.88	27.3	0.28	6.75	9.46	1.18			0.51	0.79	0.68
03/19/2010 to 06/21/2010	**soil solution**	**30cm**	0.2µm	June 2010	06/21/2010	4.43	31.7	0.92	9.75	20.89	***0.75***	0.72173	-27.2	1.00	1.00	1.00
			0.2 µm to 300kDa			4.40	30.7	0.02	0.09	0.06	0.83			0.03	0.01	0.00
			300kDa to 5kDa			4.13	31.9	0.49	2.55	6.00	0.40		-27.5	0.53	0.26	0.29
			<5kDa			4.55	26.5	0.40	7.10	14.82	1.02		-26.6	0.44	0.73	0.71
06/21/2010 to 09/08/2010	**soil solution**	**30cm**	0.2µm	September 2010	09/08/2010	4.59	30.6	1.25	13.80	20.39	***0.94***	0.72058	-27.9	1.00	1.00	1.00
09/25/2012 to 11/20/2012	**soil solution**	**30cm**	0.2µm	November 2012	11/20/2012	4.59	31.6	1.00	4.60	9.93	***1.22***	0.72140	-27.3	1.00	1.00	1.00
			0.2µm to 300kDa			4.54	30.3	0.03	0.06	0.06	0.87			0.03	0.01	0.01
			300kDa to 5kDa			4.20	31.7	0.44	1.61	5.51	0.90		-27.9	0.44	0.35	0.55
			<5kDa			4.92	26.9	0.54	2.99	4.37	1.70		-27.0	0.54	0.65	0.44
05/22/2013 to 08/06/2013	**soil solution**	**30cm**	0.2µm to 300kDa	August 2013	08/06/2013	4.70	34.3	0.83	2.90	6.62	***1.21***	0.7227	-27.1	1.00	1.00	1.00
			0.2µm to 300kDa			4.55	33.8	0.02	0.02	0.07	1.09			0.02	0.01	0.01
			300kDa to 5kDa			4.38	32.0	0.46	1.37	3.86	0.85		-27.4	0.55	0.47	0.58
			<5kDa			5.00	28.6	0.35	1.51	2.69	1.50		-27.0	0.42	0.52	0.41

sampling period	sample type	depth	Colloidal size		date	pH	Arom	DOC (mmol/L)	Ca (µmol/L)	Sr (nmol/L)	$\delta^{44/40}Ca_{SRM915a}$ (‰)	$^{87}Sr/^{86}Sr$	$\delta^{13}C_{orga}$ (‰)	OC (%)	Ca (%)	Sr (%)
09/09/2009 to 11/12/2009	**soil solution**	**60cm**	0.2µm	November 2009	11/12/2009	4.6	16.0	0.92	10.80	14.04				1.00	1.00	1.00
			0.2µm to 5kDa				16.0	0.41	1.42	2.42				0.44	0.13	0.17
			<5kDa				15.5	0.51	9.38	11.62				0.56	0.87	0.83
11/12/2009 to 03/19/2010	**soil solution**	**60cm**	0.2µm to 300kDa	March 2010	03/19/2010	4.80	15.5	0.20	9.10	22.83	***0.65***	0.72606	-26.6	1.00	1.00	1.00
			0.2µm to 300kDa			4.90	16	0.00	0.04	0.04		0.72605		0.02	0.00	0.00
			300kDa to 5kDa			4.34	14	0.05	2.82	6.13	0.36			0.27	0.31	0.27
			<5kDa			5.13	10.5	0.15	7.25	16.65	0.96	0.72606		0.71	0.80	0.73
03/19/2010 to 06/21/2010	**soil solution**	**60cm**	0.2µm	June 2010	06/21/2010	6.09	15.7	0.23	10.57	26.03	***0.98***	0.72651	-26.6	1.00	1.00	1.00
			0.2 µm to 300kDa			6.08	16.4	0.00	0.04	0.14	0.81			0.00	0.00	0.01
			300kDa to 5kDa			6.03	18.2	0.11	5.17	12.67	0.72	0.72628		0.49	0.49	0.49
			<5kDa			5.94	14.0	0.12	5.36	13.22	1.06			0.51	0.51	0.51
06/21/2010 to 09/08/2010	**soil solution**	**60cm**	0.2µm	September 2010	09/08/2010	4.90	18.1	0.42	9.08	24.79	***0.71***	0.724724	-26.2	1.00	1.00	1.00
09/25/2012 to 11/20/2012	**soil solution**	**60cm**	0.2µm	November 2012	11/20/2012	4.86	18.4	0.26	3.05	10.96	***0.80***	0.72650	-26.1	1.00	1.00	1.00
			0.2 µm to 300kDa			4.80	15.7	0.01	0.00	0.06	0.90			0.05	0.00	0.01
			300kDa to 5kDa			4.50	18	0.09	0.83	4.09	0.58		-26.5	0.34	0.27	0.37
			<5kDa			4.97	18.9	0.16	2.22	6.82	1.06		-26.0	0.61	0.73	0.62
11/20/2012 to 03/26/2014	**soil solution**	**60cm**	0.2µm	March 2013	03/26/2013	4.95	17.2	0.23	2.43	6.07	***0.96***	0.726035		1.00	1.00	1.00
05/22/2013 to 08/06/2013	**soil solution**	**60cm**	0.2µm	August 2013	08/06/2013	6.20	21.1	0.28	27.00	23.06	***0.09***	0.71747	-26.6	1.00	1.00	1.00
		60cm	0.2µm to 5kDa			6.47	21.0	0.18	15.89	14.27	-0.07			0.64	0.59	0.62
		60cm	<5kDa			6.30	22.0	0.10	11.11	8.79	0.48			0.36	0.41	0.38

(2SD, N=3) pour les différentes fractions filtrées et ultra-filtrées de la solution de nitrate de calcium et $\delta^{44/40}Ca_{SRM915a}$ = 1,10 ± 0,12 ‰ (2SD, N=5) pour les différentes fractions de l'eau minérale Mont-Roucous. Ainsi, les signatures isotopiques obtenues sont identiques et montrent que la méthode d'ultra-filtration ne fractionne pas les isotopes de Ca. Aucune variation du rapport isotopique $^{87}Sr/^{86}Sr$ n'a été observée entre les fractions ultra-filtrées et l'échantillon initial (Cf. paragraphe résultats), en accord avec les travaux antérieurs de Sivry et al. (2006) portant sur des eaux de source du Mengong et des eaux de la rivière Nyong . Ceci est également une preuve en faveur de l'absence de fractionnement des isotopes du Sr lors de l'expérimentation d'ultrafiltration.

4. Résultats

4.1. Variations chimiques du carbone organique, du calcium et strontium dans les solutions de sol

La concentration en carbone organique (C_{orga}) des solutions de sol filtrées à 0,2 µm est comprise entre 2,95 ± 0,4 mmol.L^{-1} (2SE, N=7) en surface et 0,36 ± 0,1 mmol.L^{-1} (2SE, N=7) à 60 cm de profondeur (Tableau 1). Les aromaticités correspondantes sont 35 ± 1 % (2SE, N=7) et 17 ± 1 % (2SE, N=7). Ces valeurs sont du même ordre de grandeur que celles observées par Kalbitz et al. (1999), Weishaar et al. (2003) et Gabor et al. (2014) pour des solutions de sol échantillonnées dans des sols forestiers de conifères. Elles fluctuent en fonction de la saison dans le compartiment de la couche supérieure du sol et diminuent avec la profondeur comme observé précédemment par Kaiser et al. (2001b) et Verstraeten et al. (2014). Quelle que soit la fraction considérée (5P ou 5R), les valeurs de C_{orga} et d'aromaticité montrent une forte variabilité dans les échantillons prélevés dans les horizons supérieurs du sol et une diminution avec la profondeur (Tableau 1). Pour presque toutes les solutions de sol, C_{orga} est fortement enrichi dans la fraction colloïdale 5R (40 à 70 %) alors que l'aromaticité est relativement constante jusqu'à 30 cm de profondeur (soit 36 % à 32 %) et diminue

significativement à 17 % à 60 cm de profondeur. La proportion de C_{orga} dans la fraction dissoute 5P augmente avec la profondeur et l'aromaticité est moins importante c'est-à-dire comprise entre 29 % et 26% en surface et 16 % pour les échantillons plus profonds.

Les concentrations en Ca et en Sr dans les solutions de sol filtrées à 0,2 µm varient de la même manière jusqu'à 10 cm de profondeur. Les échantillons prélevés en juin 2010 ont des concentrations jusqu'à cinq fois supérieures à celles correspondantes aux autres périodes de prélèvement. Leurs valeurs sont comprises entre 25,5 ± 5,6 $mmol.L^{-1}$ (2SE, N=7) et 7,5 ± 1 $mmol.L^{-1}$ (2SE, N=7) pour le Ca et entre 25,3 ± 5,2 $nmol.L^{-1}$ (2SE, N=7) et 17,5 ± 3 $nmol.L^{-1}$ (2SE, N=7) pour le Sr, respectivement à 5 cm et 60 cm de profondeur. A partir de 30 cm de profondeur, la teneur en Ca diminue plus que celle du Sr et ne montre plus de variation dépendante de la saison. Le Ca et le Sr ont une distribution identique entre les fractions colloïdales et dissoutes (Tableau 1). Cette répartition est du même ordre de grandeur que celles mentionnées par Pokrovsky and Schott (2002), Pourret et al. (2007) et Pokrovsky et al. (2010) (Ca et Sr sont entre 60 et 80 % dans la fraction dissoute).

4.2. **Signatures isotopiques des solutions de sol**

La signature isotopique $\delta^{13}C_{orga}$ des solutions de sol filtrées à 0,2µm varie de -27,9 ± 0,1 ‰ (2SE, N=6) en surface à -26,4 ± 0,1 ‰ (2SE, N=5) en profondeur. Ces valeurs correspondent à des valeurs précédemment observées lors de la dégradation de litière sous couvert forestier de conifères (Crow et al., 2006; Seki et al., 2010; Schulte et al., 2011). Nous observons également que la fraction colloïdale est enrichie en isotope léger ^{12}C et la fraction dissoute en isotope lourd ^{13}C, par rapport à la fraction filtrée à 0,2 µm (Tableau 1). La figure 2 représente la variation de $\delta^{13}C_{orga}$ en fonction du rapport $1/C_{orga}$ dans les différentes fractions (5R et 5P) et dans la solution filtrée à 0,2 µm. Elle met en évidence que la solution de sol est un mélange des deux fractions. Ces droites de mélanges sont significatives essentiellement pour les échantillons prélevés à 5 cm de profondeur. Il est

difficile de généraliser ce résultat pour les autres échantillons. En effet, la variabilité y est faible et ne se démarque pas significativement des incertitudes analytiques (± 0,15) ‰.

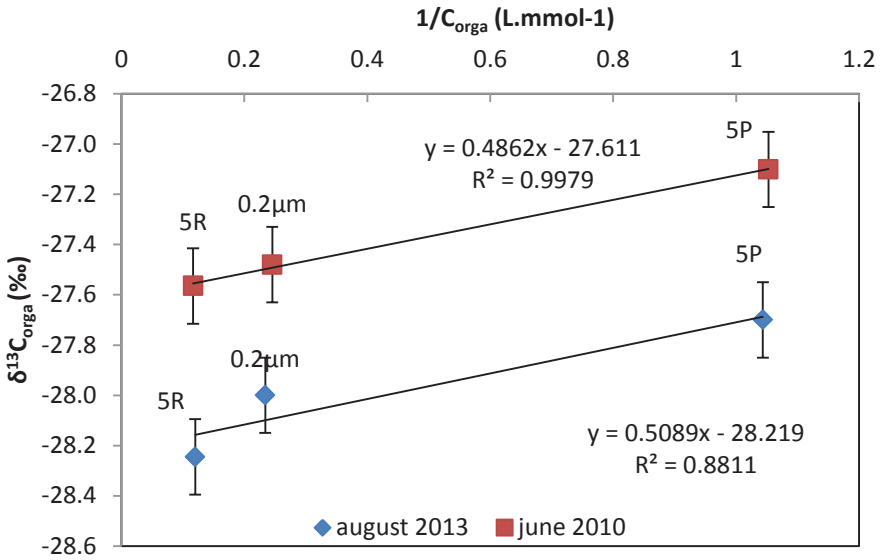

Figure 2 : Variation de la composition isotopique en C_{orga} colloïdal (5R), C_{orga} dissous (5P) et C_{orga} filtré à 0,2 µm (0,2 µm) des solutions de sol à 5 cm de profondeur prélevées en Juin 2010 et août 2013 en fonction de la concentration en C_{orga}

La signature isotopique $\delta^{44/40}Ca_{SRM915a}$ des solutions de sol filtrées à 0,2µm varie de 0,63 ± 0,05 ‰ (2SE, N=7) en surface à 0,64 ± 0,14 ‰ (2SE, N=6) en profondeur. Les valeurs intermédiaires sont plus importantes : 0,77 ± 0,08 ‰ (2SE, N=6) à 10 cm et 0,97 ± 0,08 ‰ (2SE, N=6) à 30 cm de profondeur. Ces valeurs sont du même ordre de grandeur que celles mesurées précédemment dans des échantillons prélevés en 2005 et 2006 sur le même bassin versant (Cenki-Tok et al., 2009). Tout comme pour les isotopes du C_{orga}, la fraction colloïdale 5R est enrichie en isotope léger ^{40}Ca alors que la fraction dissoute 5P est enrichie en isotope lourd ^{44}Ca par rapport à la fraction filtrée à 0,2 µm, qui correspond à un mélange de Ca colloïdal et de Ca dissous (Figure 3).

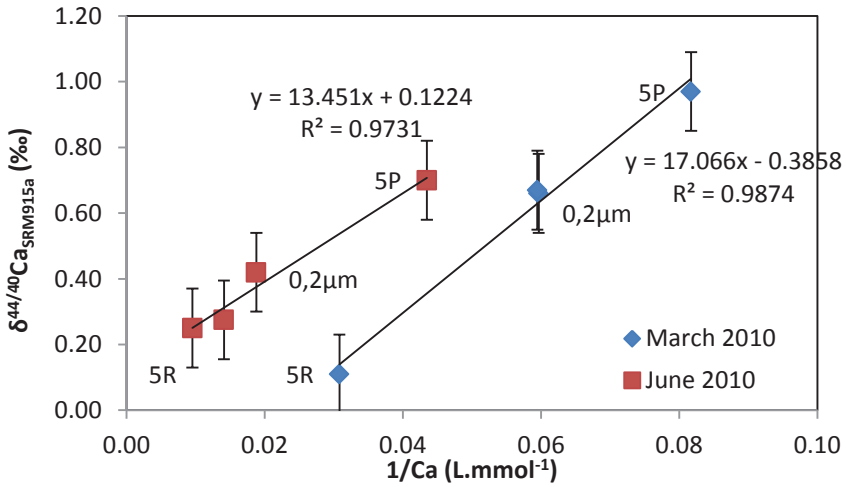

Figure 3 : Variation de la composition isotopique en Ca colloïdal (5R), Ca dissous (5P) et Ca filtré à 0,2 µm (0,2 µm) des solutions de sol à 5 cm de profondeur prélevées en Mars et Juin 2010 en fonction de la concentration en Ca

Le rapport isotopique $^{87}Sr/^{86}Sr$ des solutions de sol filtrées à 0,2 µm évolue en moyenne de 0,719510 ± 0,0005 (2SE, N=7) en surface à 0,72455 ± 0,001 (2SE, N=6) en profondeur. Ces valeurs sont du même ordre de grandeur que celles mesurées précédemment dans des échantillons prélevés entre 1997 et 1998 sur le même bassin versant (Aubert et al., 2001; 2002). Le rapport isotopique en $^{87}Sr/^{86}Sr$ ne varie pas entre la fraction colloïdale 5R et la fraction dissoute 5P (Figure 4). Il peut donc être utilisé pour déterminer la source du Sr ainsi que celle du Ca contenus dans les échantillons. En effet, ce rapport n'étant pas affecté par un fractionnement de masse lors des processus d'altération continentale ou des processus biologiques puisqu'un tel fractionnement est faible et circonvenu *via* une normalisation interne lors du processus de mesure, il a souvent été utilisé dans des études biogéochimiques dans des écosystèmes forestiers afin de déterminer les sources de Ca (et leurs mélanges) disponibles pour les forêts (Blum et al., 2002; Drouet et al., 2005; Bélanger et al., 2012; Bedel et al., 2016).

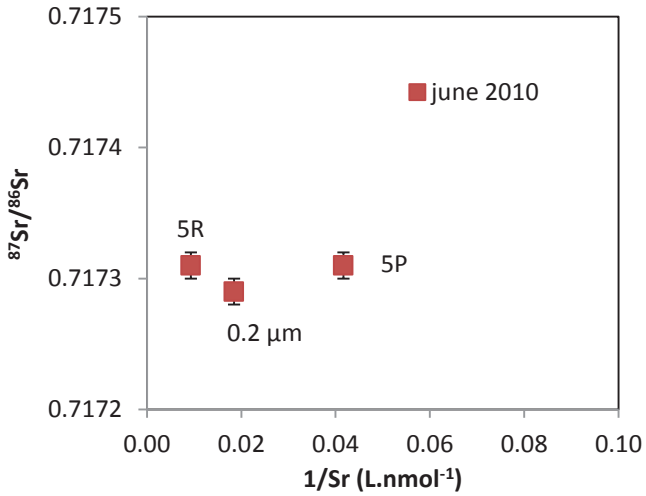

Figure 4 : Variation de la composition isotopique en Sr colloïdal (5R), Ca dissous (5P) et Ca filtré à 0,2 µm (0,2 µm) des solutions de sol à 5 cm de profondeur prélevées en Mars et Juin 2010 en fonction de la concentration en Sr

5. Discussion

5.1. Répartition du calcium et du strontium entre la fraction colloïdale et la fraction dissoute

Dans les chapitres 2 et 3, il a été montré que le sol de la parcelle VP2 est acide (pH ≈ 4) et très appauvri en Ca et qu'une des sources principales de Ca est le recyclage par la végétation. Ainsi, la dégradation de la litière conditionnera la quantité de Ca libéré qui peut être sous forme libre ou sous forme lié (Ca pecto-cellulosique ou oxalate de Ca) (Marschner, 1995). Parallèlement à la libération du Ca en solution, les molécules organiques hydrosolubles provenant de la dégradation de la litière migrent vers les solutions de sol. Le Ca est alors complexé par les molécules de C_{orga} en formant des ponts entre les différents groupements fonctionnels organiques. Il stabilise les charges négatives des molécules organiques et ralentit ainsi le phénomène de minéralisation de C_{orga} (chapitre 3).

En fonction de la nature et de la densité des groupements fonctionnels organiques, le Ca se répartit entre la fraction colloïdale et la fraction dissoute. La Figure 5 montre la variation des flux en Ca et en Sr en fonction de celui de C_{orga} dans la fraction colloïdale et la fraction dissoute. Ces

variations mettent en évidence le comportement similaire du Ca et du Sr avec les molécules organiques. En effet, le Ca et le Sr, qui sont tous deux des cations alcalins, se ressemblent chimiquement en raison de leur rayon ionique similaire (r_{Sr}=0.113 nm et r_{Ca}=0.099 nm) et de leur charge divalente et sont considérés avoir un comportement similaire dans les écosystèmes naturels (Poszwa et al., 2000; Probst et al., 2000; Dasch et al., 2006; Andrews et al., 2016; Bedel et al., 2016).

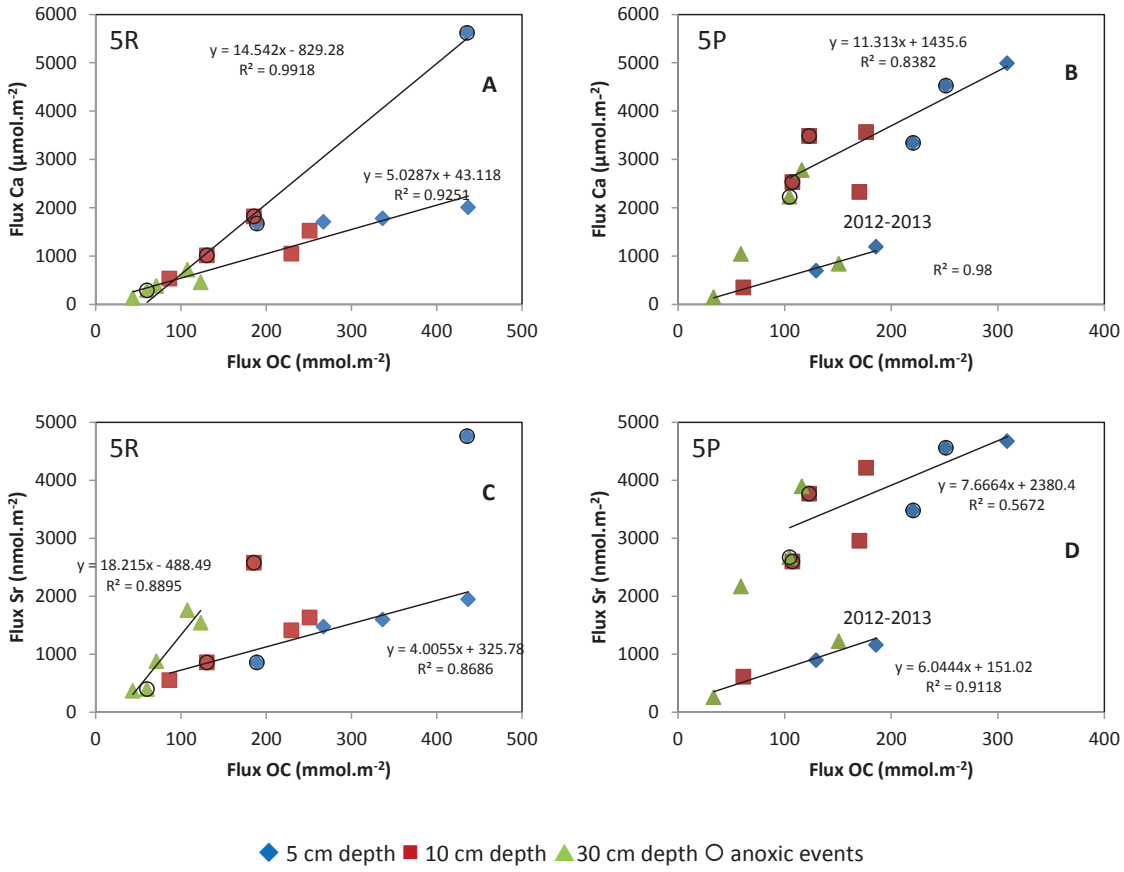

Figure 5 : Variations des flux en Ca et en Sr en fonction du flux en C_{orga} dans la fraction colloïdale 5R (A et C) et la fraction dissoute 5P (B et D).

En phase colloïdale, le Ca et le Sr sont complexés entièrement par C_{orga} (Figures 5A et 5C) alors qu'en fraction dissoute ce n'est pas le cas pour tous les échantillons (Figures 5B et 5D). Deux cas se présentent :

- Le Ca et le Sr sont complexés avec C_{orga} de la fraction dissoute (5P) et une partie restante est sous forme ionique Ca^{2+} et Sr^{2+}. Il s'agit des échantillons prélevés en 2009-2010. Ce cas de figure est dit non limitant en Ca et en Sr.
- Le Ca et le Sr sont complexés avec C_{orga} dans la fraction dissoute (5P) et ne sont pas sous forme ionique. Il s'agit des échantillons de 2012-2013 ayant une faible concentration en Ca et en Sr par rapport aux autres périodes. Ce cas de figure est dit limitant en Ca et en Sr.

Il en résulte que le Ca et le Sr vont d'abord se complexer à C_{orga} en fraction colloïdale. En effet, dans le cas des échantillons dit limitants en Ca et en Sr, la proportion de ces éléments que l'on retrouve en fraction colloïdale (5R) est plus importante qu'en phase dissoute (Tableau 1). Ce phénomène a également été observé par Pokrovsky et al. (2010) lors de l'étude de la fraction colloïdale de la rivière Severnaya Dvina. Plus l'échantillon était appauvri en Ca, plus la proportion de Ca présent dans la fraction colloïdale était importante. Ensuite, le Ca et le Sr non complexés en fraction colloïdale sont complexés par C_{orga} en fraction dissoute. Finalement, les cations excédentaires restent dans la fraction dissoute.

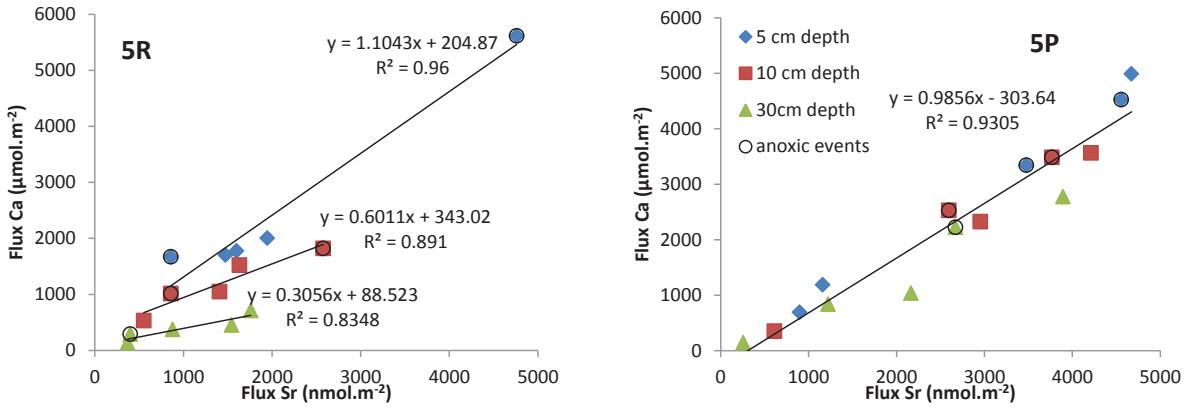

Figure 6 : Variations des flux en Ca en fonction de ceux en Sr dans la fraction colloïdale 5R et la fraction dissoute 5P

Il résulte également de cette étude que si Ca et Sr présentent des similitudes de comportement, dans le détail un fractionnement chimique est observé, en accord avec les travaux antérieurs (Chadwick et al., 1999; Poszwa et al., 2000; Blum et al., 2002; Poszwa et al., 2002; Wiegand et al., 2005; Dasch et al., 2006; Blum et al., 2008; Drouet and Herbauts, 2008). La figure 6 montre en effet que le Ca et le Sr ont un comportement similaire dans la fraction dissoute et que le Sr est préférentiellement retenu dans la fraction colloïdale par rapport au Ca. Deux mécanismes permettent d'expliquer cela : soit les forces de liaison Sr-C_{orga} sont plus fortes que celles Ca-C_{orga}, soit le Ca est davantage prélevé par la végétation. En effet, Blum et al. (2012) ont montré qu'il existait une discrimination lors du prélèvement par les racines entre le Ca et le Sr, variable en fonction des essences d'arbres et de la composition de la solution nutritive.

5.2. **Evolution spatiale et temporelle de la signature isotopique $\delta^{13}C_{orga}$ dans les solutions de sol**

Dans le chapitre 3, nous avons montré que l'augmentation de C_{orga} dans les solutions de sol est liée à une augmentation de l'activité des micro-organismes dans les sols. Cette variation est fonction des conditions environnementales comme la température, le taux d'humidité du sol ainsi que le taux d'O_2 dans l'espace poral (Chen et al., 2015; Ge et al., 2015). Pour que ces micro-organismes puissent se développer, ils ont besoin également de nutriments comme N, P ou C dont une des sources principales est la litière. Pour accéder à ces éléments, les micro-organismes la dégradent par l'intermédiaire de réactions d'hydrolyse et d'oxydo-réduction catalysées par des systèmes enzymatiques (Ussiri and Johnson, 2003; Klotzbücher et al., 2013). La dégradation de la litière commence par la décomposition de composés facilement minéralisables comme la cellulose puis continue par la recombinaison de composés plus récalcitrants comme la lignine (Berg, 2000; Walela et al., 2014). Ensuite, les composés hydrosolubles vont être lessivés par la pluie ou les pluviolessivats et vont migrer vers les solutions de

sol (Kalbitz et al., 2003; Gangloff et al., 2014b). Par conséquent, le C_{orga} présent dans les solutions de sol reflète le degré de décomposition de la litière et des processus impliqués.

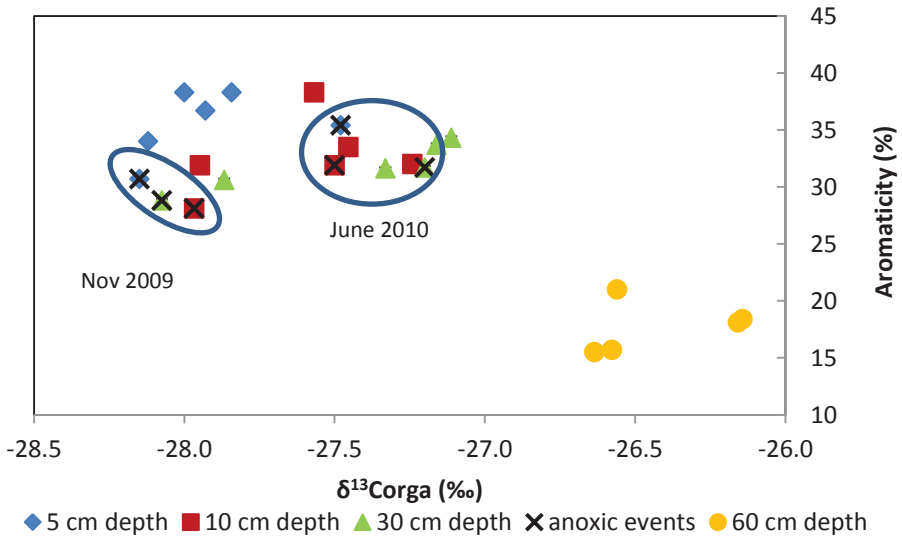

Figure 7 : Variations de la signature isotopique $\delta^{13}C_{orga}$ en fonction de l'aromaticité dans les différentes solutions de sol filtrées à 0,2 µm.

La figure 7 montre que le C_{orga} des échantillons prélevés a une aromaticité qui diminue et une signature isotopique $\delta^{13}C_{orga}$ qui augmente avec la profondeur. La figure 8 montre que la variation d'aromaticité entre la surface et la profondeur est corrélée avec $\Delta^{13}C$ des solutions de sol filtrées à 0,2 µm entre 5 et 60 cm avec une différence saisonnière. De façon générale, ces variations montrent que la structure des molécules organiques varie avec la profondeur et témoignent de leur minéralisation dans les horizons plus profonds du sol. Plus il y a une augmentation de la signature isotopique $\delta^{13}C_{orga}$ avec la profondeur, plus la variation en aromaticité est importante. Par conséquent, le processus de minéralisation du C_{orga} modifie sa structure moléculaire ainsi que sa signature isotopique $\delta^{13}C_{orga}$. Cette minéralisation est impactée soit par l'activité bactérienne qui utilise préférentiellement ^{12}C dans les processus, comme la respiration, soit par les conditions du milieu (Crow et al., 2006; Brunn et al., 2014), soit par les phénomènes d'adsorption sur le sol (Kaiser et al., 2001a). La variation d'aromaticité différente entre

l'hiver et l'été peut s'expliquer par une plus grande destruction des cycles aromatiques par photolyse pendant l'été (Austin and Ballaré, 2010).

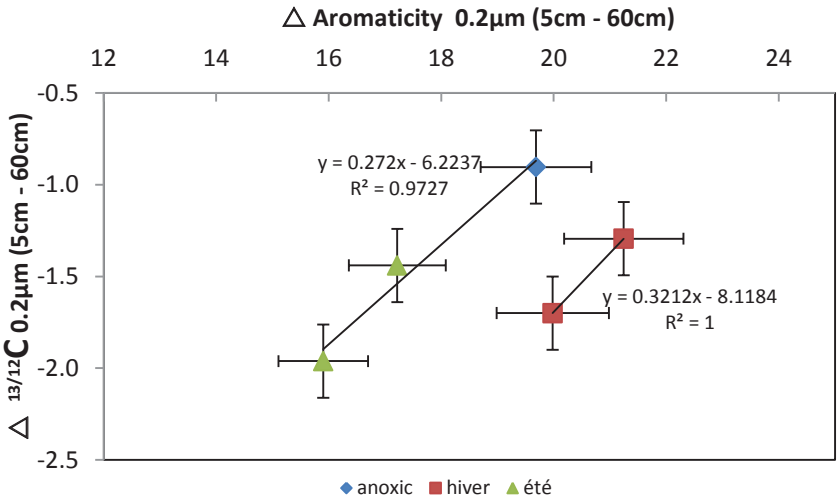

Figure 8 : Variations de la signature isotopique $\delta^{13}C_{orga}$ en fonction de la variation de l'aromaticité dans les différentes solutions de sol filtrées à 0,2 µm entre 5 et 60 cm.

Les échantillons correspondants aux conditions anoxiques font exception. Les échantillons de Novembre 2009 ont des aromaticités plus faibles avec une signature isotopique constante alors que les échantillons de Juin 2010 ont également des aromaticités un peu plus faibles avec des signatures isotopiques plus importantes (Tableau 1). Dans le cas particulier de ces échantillons, la figure 6 permet de distinguer deux processus différents qu'il n'avait pas été possible de discriminer avec les simples données physico-chimiques dans les chapitres 3 et 4. La différence de signature isotopique en C_{orga} entre les deux périodes montre qu'un processus faisant intervenir des micro-organismes est plus prononcé pour les échantillons de Juin 2010 que pour ceux de Novembre 2009. On peut donc supposer que l'activité bactérienne a été plus importante en Juin 2010 et qu'elle a décomposé de la matière organique plus récalcitrante par rapport aux échantillons de Novembre 2009 au vu de la variation d'aromaticité. La différence de processus entre les deux périodes d'échantillonnage est due à des conditions différentes dans l'espace poral du sol. En effet, les échantillons de Juin 2010 ont été prélevés après une période de fonte de

neige longue qui a saturée en eau l'espace poral développant ainsi des conditions anoxiques dans le sol. Tandis que les échantillons de Novembre 2009 ont été prélevés lors d'une remise en eau des pores du sol après une période sèche (Cf Figure 2 Chapitre 1). Il s'agit plutôt d'un flush d'eau entre deux périodes plus sèches, phénomène différent de la saturation en eau. Ces deux phénomènes de remise en eau sont différents et libèrent ainsi différemment le $C_{orga.}$ Dans le cas des échantillons de Novembre 2009, le flush d'eau va lessiver le sol libérant ainsi les molécules les plus hydrosolubles (chapitre 3 paragraphe 5.2) alors que pour les échantillons de Juin 2010, les molécules organiques ont une structure modifiée par l'activité des micro-organismes. D'autres études concernant l'alternance et la fréquence de cycles secs/humides sur des sols ont montré que dans tous les cas une forte quantité de C_{orga} est libérée dans les solutions de sol lors de la remise en eau, que ces phénomènes influencent le cycle de l'azote et que seul le processus de libération de C_{orga} pouvait être différent (Yao et al., 2011; Abel et al., 2014; Shaheen et al., 2014). Ces observations sont en accord avec notre étude.

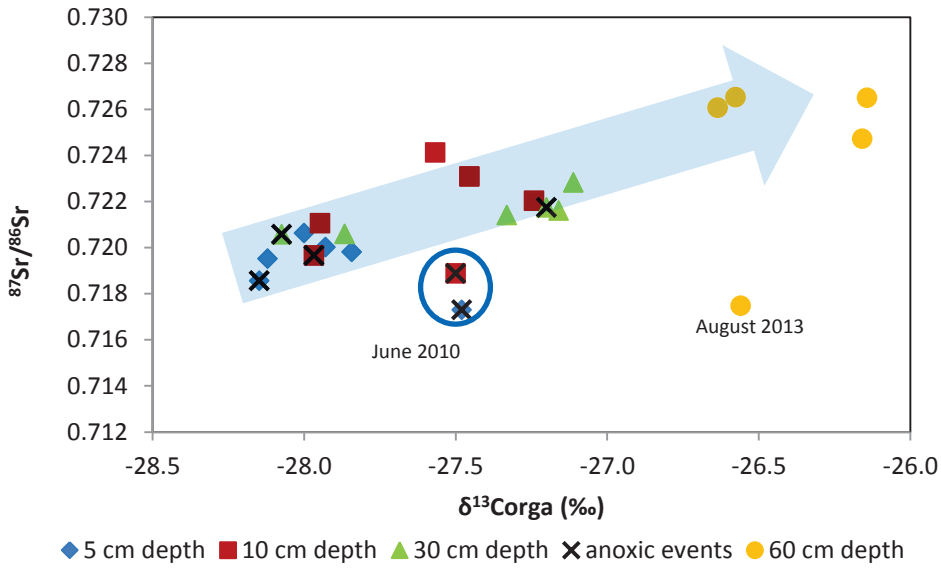

Figure 9 : Variations de la signature isotopique $\delta^{13}C_{orga}$ en fonction du rapport isotopique $^{87}Sr/^{86}Sr$ dans les différentes solutions de sol filtrées à 0,2 µm.

Lors du processus de minéralisation du C_{orga}, la proportion de groupements fonctionnels polaires diminue et celle des composés aliphatiques augmente avec la profondeur (Ussiri and Johnson, 2003; Gangloff et al., 2014b). Conjointement à cette évolution, des échanges d'éléments minéraux se font entre le sol et la solution de sol, plus particulièrement avec le C_{orga}. La figure 9 montre qu'en parallèle au phénomène d'évolution du C_{orga}, il y a une évolution des sources de Ca et Sr dans les solutions de sol. A la surface du sol, la source correspond au recyclage de la litière ($^{87}Sr/^{86}Sr$= 0.7189 selon Stille et al. (2009)) et elle évolue en profondeur vers une source plus radiogénique type feldspath (Prunier et al., 2015). Ainsi, cette figure permet de mettre en évidence les échanges qui existent entre le C_{orga}, le Ca et le Sr à l'interface eau-sol.

5.3. **Processus de fractionnement isotopique du calcium**

L'utilisation des isotopes du Ca appliqués aux solutions de sol filtrées à 0,2µm a montré leur potentiel en tant que traceur pour le prélèvement ou le recyclage de la végétation (Cenki-Tok et al., 2009; Holmden and Bélanger, 2010; Farkaš et al., 2011; Bagard et al., 2013; Schmitt et al., 2013). En particulier, Cenki-Tok et al. (2009) ont montré dans leur étude portant sur des solutions de sol du même bassin versant que les solutions de sol sont enrichies en ^{44}Ca, suite au prélèvement racinaire qui enrichit la plante en isotope léger ^{40}Ca. Ceci a été confirmé expérimentalement via l'étude de la croissance hydroponique de plants de haricots: les isotopes légers ^{40}Ca sont préférentiellement adsorbés par les groupements carboxylates ($R\text{-}COO^-$) situés sur les racines latérales, enrichissant ainsi la solution nutritive en isotope lourd ^{44}Ca (Cobert et al., 2011b; Schmitt et al., 2013). La présente étude le confirme également. Elle montre en plus que c'est à 30 cm de profondeur, zone de prélèvement racinaire maximal de Ca pour les épicéas, que l'amplitude de fractionnement est maximale entre les racines et les fractions 5P, et complémentaires par rapport à la source de Ca (Figure 10). Par ailleurs, le rapport isotopique $^{87}Sr/^{86}Sr$ d'une racine d'épicéas (Prunier, 2008) est identique à celui des solutions de sol collectées à 30 cm de

profondeur. Ces échantillons ont donc une source commune en Sr et donc en Ca. Cette source est probablement une source minérale du type « apatite » (apatite ou minéral secondaire dérivé de l'apatite), en accord avec les études antérieures (Aubert et al., 2001; Schmitt et al., 2003; Stille et al., 2009) ou le recyclage de la végétation, la litière ayant une signature isotopique en Sr proche de celle de l'apatite (Figure 10).

La fraction colloïdale 5R des échantillons de 2009/2010 n'est pas fractionnée isotopiquement par rapport à la source de Ca, alors que celle correspondant à la période 2012/2013 l'est (Figure 11). De même, les échantillons dissous (5P) collectés en 2009/2010 sont enrichis en ^{40}Ca par rapport à ceux collectés en 2012/2013. Par ailleurs, les échantillons de surface (5-10 cm) filtrés à 0,2 µm et collectés en Novembre 2009 et Juin 2010 sont enrichis en isotopes légers ^{40}Ca par rapport aux autres échantillons de la période 2009/2010 (Tableau 1). D'après l'étude des éléments majeurs et traces de ces mêmes échantillons, nous savons qu'ils correspondent à des périodes anoxiques (c.f. chapitres 3 et 6) (Gangloff et al., 2014a). Les solutions de sol correspondant à ces périodes sont enrichies en Ca et l'étude du C_{orga} témoigne d'une dégradation plus importante de la litière par rapport aux autres échantillons (chapitre 3). Le Ca ainsi libéré provient des différents constituants des cellules végétales. Au début, le Ca libéré correspond au Ca libre enrichi en isotopes lourds ^{44}Ca et le Ca libéré ensuite correspond au Ca lié sous forme d'oxalates de Ca ou lié aux molécules pecto-cellulosiques, fractions enrichies en isotopes légers ^{40}Ca. Cette seconde fraction est plus stable et libère plus difficilement le Ca (Cobert et al., 2011a; Bagard et al., 2013).

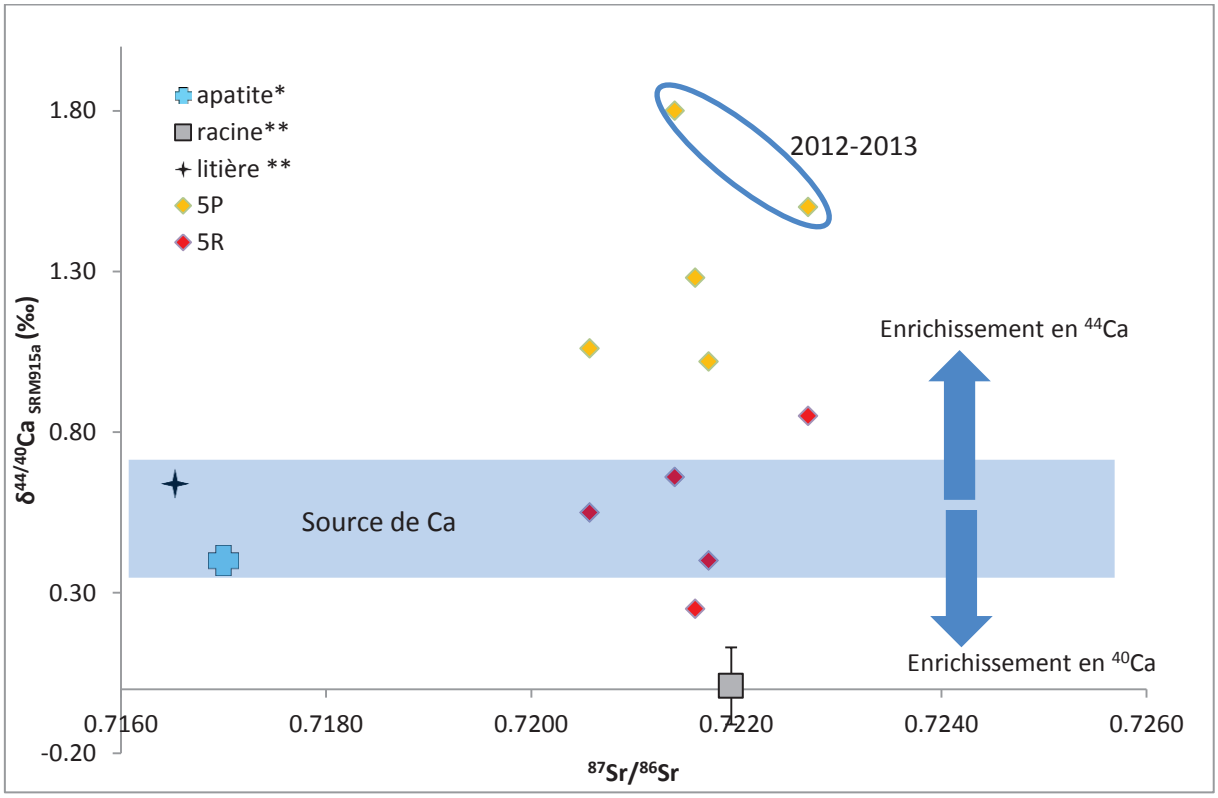

Figure 10 : Variations de la signature isotopique $\delta^{44/40}Ca_{SRM915a}$ dans les fractions 5R et 5P en fonction du rapport isotopique $^{87}Sr/^{86}Sr$ pour les échantillons prélevés à 30 cm de profondeur. (valeurs apatite* selon Aubert et al. (2001) et Schmitt et al. (2003), et valeurs racine et litière** selon Prunier (2008) et Cenki-Tok et al. (2009))

Une fois libéré, le Ca va se complexer avec le C_{orga} (Clarholm and Skyllberg, 2013; Clarholm et al., 2015). Dans le paragraphe 5.1., il a été montré que le Ca est d'abord complexé par le C_{orga} en fraction colloïdale 5R, puis en fraction dissoute 5P et que la quantité excédentaire est sous forme ionique Ca^{2+} hydratée. Ce processus est confirmé par le fait que les rapports isotopiques $^{87}Sr/^{86}Sr$ ne sont pas significativement différents entre les fractions colloïdales et les fractions dissoutes des solutions de sol (Tableau 1). Par conséquent, la répartition du Ca entre les différentes fractions est due à un processus mécanistique et non pas à des sources différentes. On peut ainsi distinguer deux cas de figure :

(1) La signature isotopique de la fraction colloïdale (5R) est peu variable (0,39 ± 0,06 ‰, 2SE, N=9) et la fraction dissoute associée (5P) est variable et enrichie en isotope lourd ^{44}Ca par rapport à la fraction colloïdale. On peut attribuer un facteur de fractionnement associé égal à $\alpha_{5R/5P}$ = 0.9991. Ces échantillons correspondent à ceux fortement enrichis en Ca (26,7 ± 5 mmol.L^{-1}, 2SE, N=9). On peut proposer que dans ce cas de figure le réservoir de Ca est non-limitant en Ca.

(2) La signature isotopique de la fraction colloïdale (5R) est variable et enrichie en isotope lourd ^{44}Ca par rapport à la source de Ca. La fraction dissoute (5P) associée est elle aussi variable et enrichie en isotope lourd ^{44}Ca. On peut attribuer un facteur de fractionnement associé égal à $\alpha_{5R/5P}$ =0.9980. Ces échantillons correspondent à ceux fortement appauvris en Ca (8,1 ± 2 mmol.L^{-1}, 2SE, N=6). Ceci implique que le facteur de fractionnement est d'autant plus important que le milieu est pauvre en Ca, ce qui est en accord avec une étude expérimentale antérieure (Schmitt et al., 2013). On peut proposer que dans ce cas de figure le réservoir est limitant en Ca.

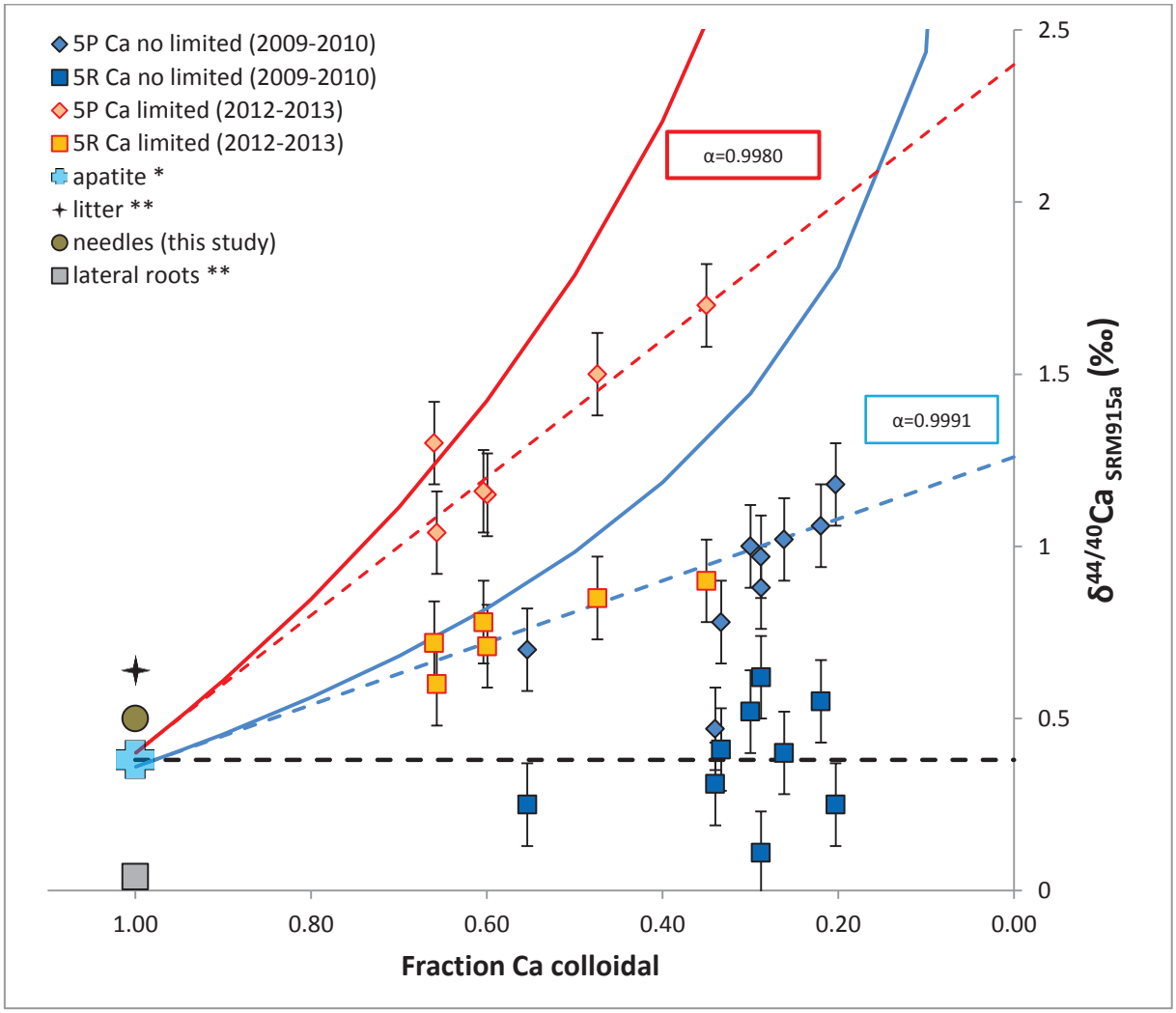

Figure 11: Variations de la signature isotopique $\delta^{44/40}Ca_{SRM915a}$ dans les fractions 5R et 5P en fonction de la proportion de Ca dans la fraction colloïdale (entre 5 et 30 cm de profondeur). La solution initiale a une composition isotopique similaire à celle de l'apatite ($\delta^{44/40}Ca$=0,40‰), supposée être la principale source en Ca du bassin versant du Strengbach (Aubert et al., 2001; Schmitt et al., 2003). Les droites et les courbes (bleues et rouges) représentent les modèles théoriques de fractionnement isotopique sous contrôle cinétique (traits pleins) et sous contrôle thermodynamique (traits en pointillés) pour les fractions dissoutes et colloïdales pour des facteurs de fractionnement α=0.9991 (courbes bleues) et α=0.9980 (courbes rouges). Elles ont été tracées avec les équations de lois thermodynamiques et cinétiques selon Ding et al. (2005), Black et al. (2008) et Schmitt et al. (2013). (* Schmitt et al. (2003) et ** Cenki-Tok et al. (2009)).

Le processus de fractionnement isotopique du Ca se fait donc selon un processus sous contrôle thermodynamique plutôt que cinétique. Ceci implique que les racines prélèvent préférentiellement les isotopes légers ^{40}Ca dans la fraction dissoute 5P selon une réaction d'équilibre entre les groupements carboxylates et ^{40}Ca. Ceci est en accord avec les résultats obtenus au cours d'expérimentations effectuées en conditions hydroponiques (Schmitt et al., 2013). Par conséquent, ce prélèvement crée un fractionnement isotopique dans la fraction dissoute qui s'enrichit en ^{44}Ca. La forme ionique hydratée Ca^{2+} est la plus accessible et sera la première espèce chimique concernée par le fractionnement isotopique. Dans les solutions de sol limitantes en Ca, il est entièrement complexé avec Corga (cf. paragraphe 5.1.). Le prélèvement racinaire va donc entrainer un déplacement des équilibres chimiques pour accéder au $^{40}Ca^{2+}$, tout d'abord dans la fraction dissoute 5P puis dans la fraction colloïdale 5R.

(1) Cas où le Ca est non limitant :

$Ca+C_{orga}$ (0,2 µm) → $Ca–C_{orga}$ (5R) → $Ca–C_{orga}$ (5P) + Ca^{2+} → Prélèvement racinaire ($^{40}Ca^{2+}$)

(2) Cas où le Ca est limitant :

$Ca+C_{orga}$ (0,2 µm) → $Ca–C_{orga}$ (5R) → $Ca–C_{orga}$ (5P)→ Prélèvement racinaire ($^{40}Ca^{2+}$)

Ce processus thermodynamique permet d'expliquer les signatures isotopiques en Ca des échantillons correspondant à la période d'échantillonnage 2012-2013 (Figure 11).

5.4. **Variabilité des sources dans les solutions de sol**

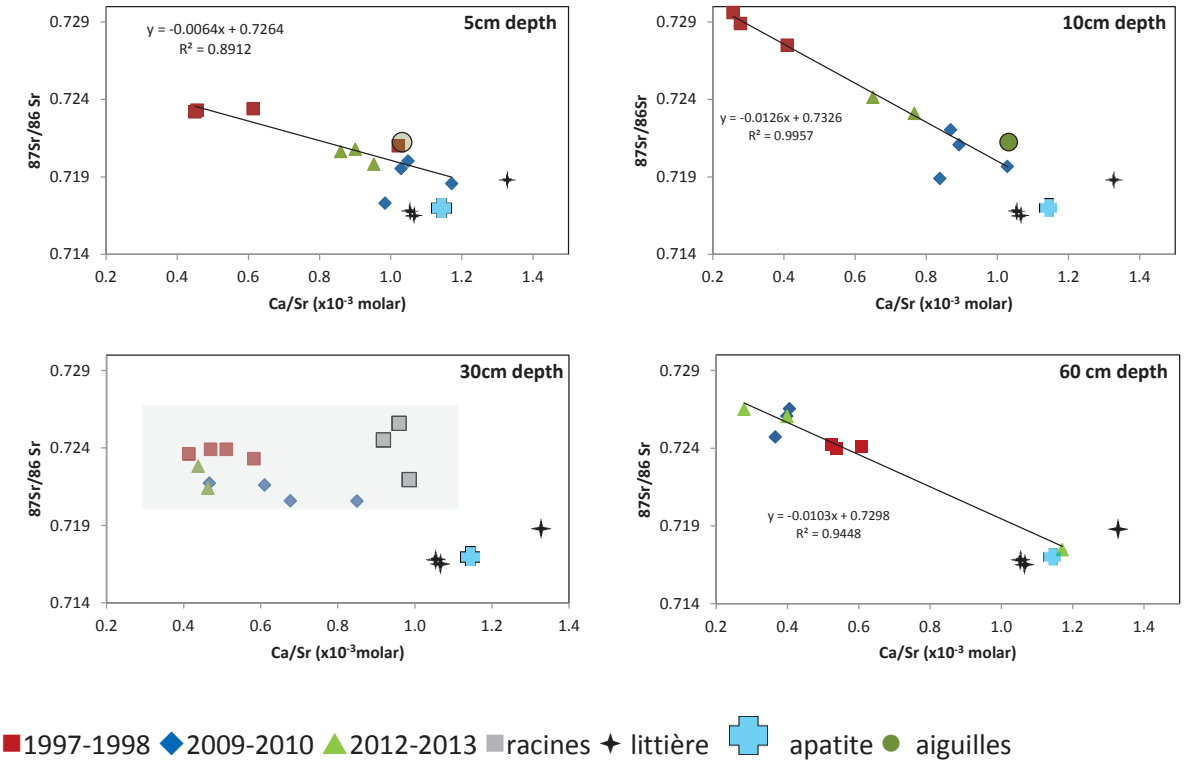

Figure 12: Variation du rapport isotopique $^{87}Sr/^{86}Sr$ en fonction du rapport Ca/Sr aux différentes profondeurs de prélèvement.

La source de Sr et donc de Ca des solutions de sol varie entre deux pôles sauf à 30 cm de profondeur (Figure 12). A 30 cm de profondeur, les différents rapports isotopiques sont homogènes avec un rapport Ca/Sr qui varie. Cela suggère qu'il y a une homogénéité de la source de Ca à cette profondeur. Cette profondeur correspond à la zone de la rhizosphère où les activités biologiques et végétales sont importantes. Ces activités entraînent une destruction des minéraux primaires avec la formation de minéraux néoformés et une homogénéité du milieu. C'est à cette profondeur que s'achève l'horizon organique, et que sont observées les plus importantes quantités d'argiles (Chapitres 3 et 4). On peut donc proposer, en accord avec les travaux de (Prunier et al., 2015) qu'à cette profondeur la signature isotopique en Sr est davantage influencée par la dissolution de l'apatite ou de minéraux secondaires qui en sont dérivés que par le flux d'altération des

autres horizons de sol. Comme cette signature est proche de celle de la litière (ce qui suggère que le Sr de la litière est certainement issu de minéraux ayant une signature similaire à celle de l'apatite ou à un mélange de différents flux aboutissant à cette signature), une variation de l'intensité des flux d'altération versus de dégradation de la végétation ne devrait pas affecter significativement la signature isotopique en Ca des solutions de sol provenant de 30 cm de profondeur.

Si l'on compare les rapports isotopiques $^{87}Sr/^{86}Sr$ de la fraction 0,2 µm des solutions de sol de la présente étude (période 2009 à 2013) à des données plus anciennes (1997-1998, Aubert et al. (2002)), on s'aperçoit qu'en surface, les échantillons de 1997-1998 ont un rapport isotopique $^{87}Sr/^{86}Sr$ plus radiogénique que les échantillons de 2009-2013. L'inverse est observé à 60 cm de profondeur. Cependant, la signature isotopique d'un des échantillons de surface de 1997-1998 a une signature isotopique $^{87}Sr/^{86}Sr$ (0,721) proche de celle des échantillons de 2009-2010. De plus, les échantillons de 2012-2013 ont une composition isotopique $^{87}Sr/^{86}Sr$ plus radiogénique que celle des échantillons de 2009-2010. Par conséquent, cette variation n'est pas temporelle. Elle correspond plutôt à la contribution variable de différentes sources de Sr, et par conséquent de Ca. Stille et al. (2009) ont proposé un schéma classique de mélange entre trois pôles définis par les dépôts atmosphériques, l'altération des minéraux et la dégradation de la litière. En effet, si toutes les compositions isotopiques sont rassemblées dans un même graphe (Figure 13), auxquelles sont ajoutées celles d'échantillons correspondant à la période 2004-2005 (Prunier et al., 2015), la variabilité du rapport isotopique $^{87}Sr/^{86}Sr$ s'explique par l'existence de trois pôles. Le pôle correspondant à la litière a comme source primaire de calcium l'apatite ou les minéraux secondaires qui en sont dérivés. Ceci implique qu'une des sources importantes de Ca est le recyclage de la végétation qui a prélevé il y a plusieurs années le Ca libéré lors de l'altération de l'apatite ou d'un minéral dérivé. Le second pôle a un rapport isotopique $^{87}Sr/^{86}Sr$ plus radiogénique et est plus enrichi en Sr (Figure 13). Il correspond à un autre minéral qui est moins riche en Ca comme l'albite ou

l'orthose (Prunier et al., 2015). Pour finir, le troisième pôle correspond aux dépôts atmosphériques avec une variabilité en Ca et en Sr.

Prunier et al. (2015) suggèrent que la variation de la composition isotopique $^{87}Sr/^{86}Sr$ dans les solutions de sol reflète des contributions différentes des flux résultants de l'altération des minéraux et du recyclage de la végétation avec une plus forte contribution lithologique en 2004-2005. Notre étude est complémentaire à cette dernière. En effet, elle confirme l'hypothèse qu'en 2004-2005 le recyclage par la végétation a très peu d'impact, certainement en raison de la sécheresse de 2003 qui a fortement ralenti la dégradation de la litière. Les échantillons de 1997-1998 et ceux de 2009-2013 ont des compositions isotopiques globalement moins radiogéniques que ceux de 2004-2005 (sauf à 30 cm de profondeur) (figure 13). Ceci montre une contribution plus importante des flux correspondants aux dépôts atmosphériques et à la dégradation de la litière dans l'apport de Sr et de Ca.

5.5. **Implications pour le cycle biogéochimique du Ca à l'échelle du bassin versant**

Les solutions de sol sont le résultat des sorption/désorption des éléments chimiques sur les fractions organiques et minérales des sols. L'étude systématique de la composition isotopique en Ca des solutions de sol d'un profil de sol sur une période de quatre ans réalisée au cours de la présente étude constitue la base de données la plus complète à ce jour. Si l'on compare la variabilité isotopique en Ca de la fraction 0,2 µm des solutions de sol sous épicéas obtenue dans la présente étude à celle obtenue dans l'étude préliminaire de Cenki-Tok et al. (2009) dans le même bassin versant, on s'aperçoit qu'elle est plus importante (0,45 ‰ contre 0,31 ‰, respectivement), même si les valeurs moyennes sont similaires (0,77 ± 0,10 ‰, 2SE, N=25 contre 0,82 ± 0,06 ‰, 2SE, N=9, respectivement) (Figure 14). Ceci implique qu'une étude en détail des solutions de sol permet d'identifier une variation des sources de Ca (recyclage de la végétation versus lithologie) et de préciser les mécanismes en jeu. Ainsi, on s'aperçoit que dans ce bassin

versant la source de Ca disponible pour la végétation se trouve dans la fraction dissoute 5P et que la fraction colloïdale 5R constitue un réservoir de Ca mobilisable lorsque le Ca devient limitant en phase dissoute. Plus généralement, ces résultats imposent de considérer les phases colloïdales et dissoutes lors de l'établissement de bilans de masse du Ca à l'échelle du bassin versant. Ceci est notamment essentiel dans des environnements tels que ceux soumis au permafrost. Bagard et al. (2013) ont en effet suggéré que les phases colloïdales étaient enrichies en isotope léger ^{40}Ca par rapport à la fraction dissoute (5P), ce que nous avons démontré dans ce travail et contribuaient de façon significative au bilan en Ca de leur bassin versant sibérien.

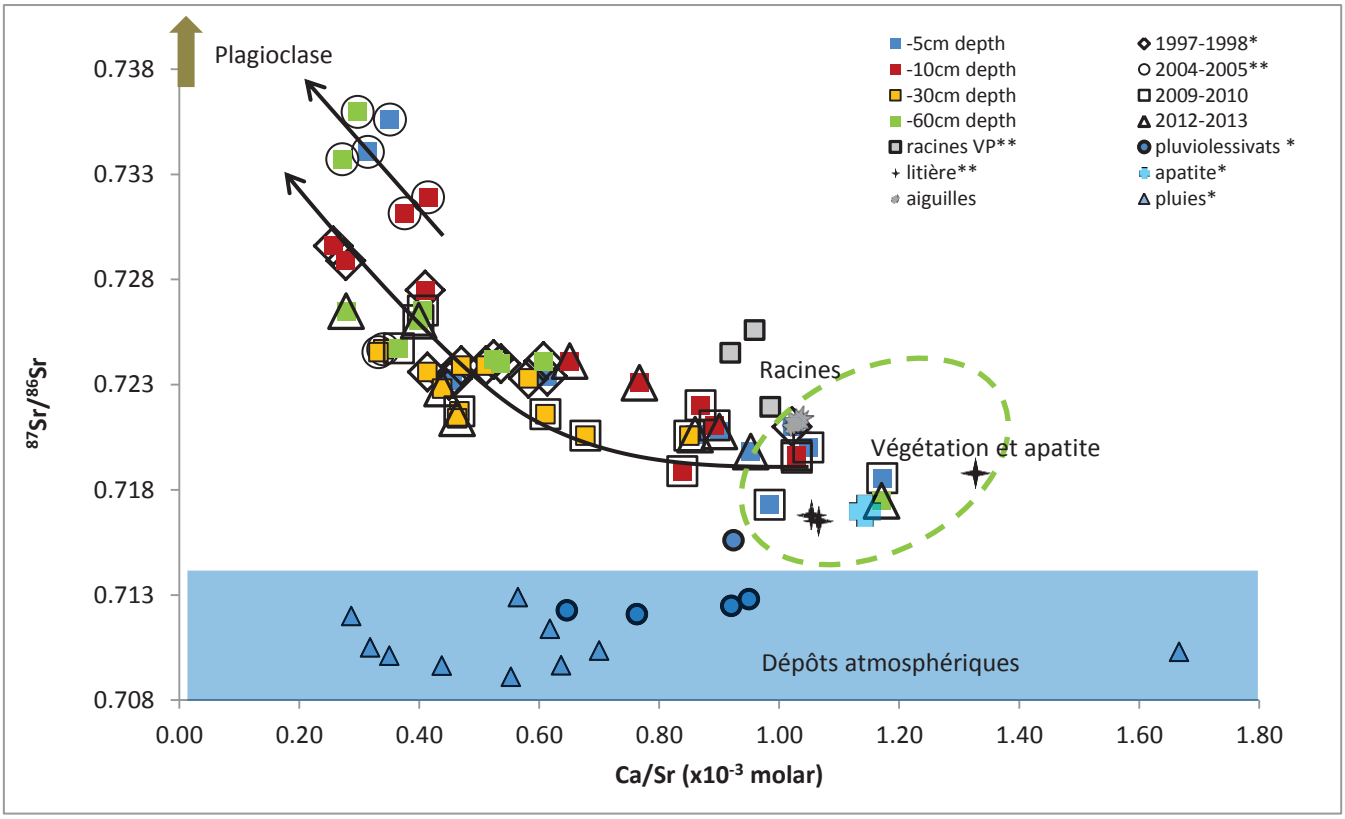

Figure 13: Variation du rapport isotopique $^{87}Sr/^{86}Sr$ en fonction du rapport Ca/Sr à différentes périodes de prélèvement (1997-1998 selon Aubert et al. (2002), 2004-2005 selon Prunier et al. (2015) et 2009-2013 cette étude. Les autres données sont selon Aubert (2001) et Prunier (2008)).

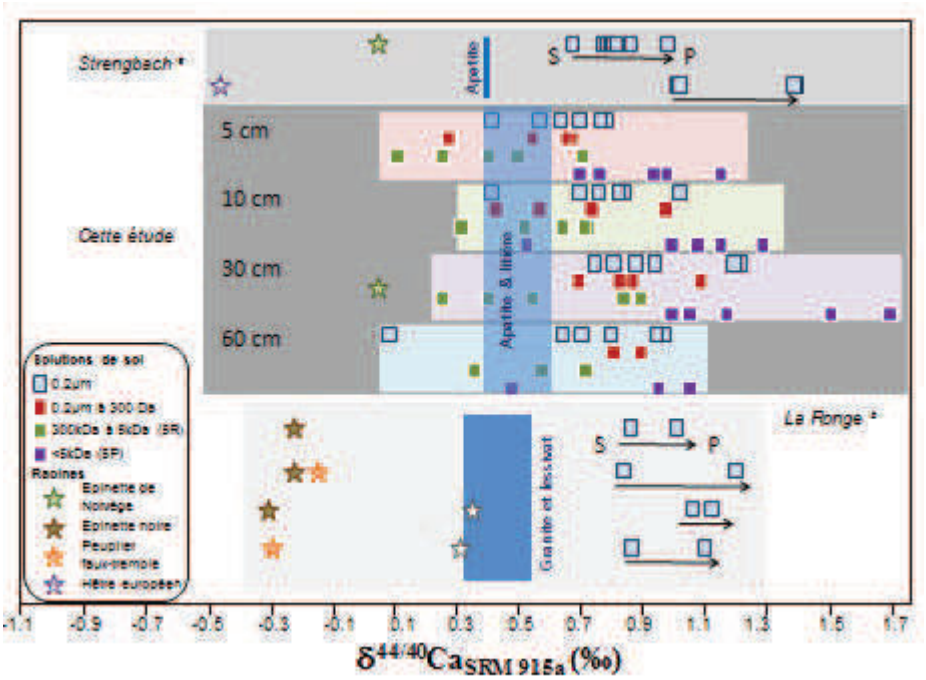

Figure 14 : Amplitude de fractionnement isotopique entre les différentes fractions de solutions de sol (0,2µm, 0,2 µm - 300 kDa, 300-5kDa et <5kDa) et les racines latérales pour le bassin versant du Strengbach (cette étude et [a] Cenki-Tok et al. (2009)) et le bassin versant de Saskatchewan ([b] Holmden and Bélanger (2010)). (S = surface et P = profond).

Si l'on compare les résultats de la présente étude avec ceux obtenus dans d'autres travaux, sur d'autres sites, il n'y a pas de réservoir de sol commun à l'ensemble des études (solutions de sol, extractions séquentielles, eaux porales ou sol brut), ce qui rend cet exercice difficile (Wiegand et al. (2005); Holmden and Bélanger (2010); Farkaš et al. (2011); Hindshaw et al. (2011); Bagard et al. (2013); Schmitt et al. (2013)) Il ressort néanmoins de l'ensemble de ces études que si les flux d'apport de Ca via l'altération des minéraux du sol, les apports atmosphériques ou la dégradation de la litière sont plus importants que les flux de prélèvement de Ca par la végétation, alors les réservoirs du sol peuvent être considérés comme étant infinis par rapport au Ca (Fantle and Tipper, 2014). Dans ce cas, le prélèvement de la végétation qui s'enrichit en ^{40}Ca par rapport à la solution de sol, sera sans effet sur la signature isotopique en Ca du réservoir de sol, tel que cela a été observé à Hawaii pour des sols jeunes (0,3 ka) ou au glacier Damma, sujet à

des processus récents d'altération (Wiegand et al., 2005; Hindshaw et al., 2011). Au contraire, à Hawaii pour des sols plus anciens (4100ka), appauvris en nutriments, les réservoirs du sol ne peuvent plus être considérés comme étant infini et l'augmentation en ^{44}Ca du réservoir échangeable peut être expliqué soit par le prélèvement de l'isotope léger ^{40}Ca par la végétation ou par des apports d'aérosols marins (Wiegand et al., 2005). Les travaux antérieurs ont proposé que pour les bassins versants granitiques où le Ca ne peut être considéré comme infini tels que les bassins versants du Strengbach ou de Saskatechewan, le mécanisme principal responsable du fractionnement isotopique est le prélèvement par la végétation, qui entraîne un enrichissement en ^{40}Ca dans les racines et en ^{44}Ca dans les solutions de sol comparé à la source de Ca (Cenki-Tok et al. (2009); Holmden and Bélanger (2010) ; figure 14). A la lumière des résultats de la présente étude, on peut proposer qu'en conditions non-limitantes le Ca est complexé par le C_{orga} en fraction colloïdale 5R sans fractionner, alors qu'il l'est en fraction dissoute 5P par le prélèvement de ^{40}Ca par la végétation. De même, en conditions limitantes, le prélèvement racinaire va entraîner un déplacement des équilibres chimiques pour accéder au $^{40}Ca^{2+}$, d'abord dans la fraction dissoute 5P, puis dans la fraction colloïdale 5R. Ceci entraîne un fractionnement isotopique en Ca à la fois dans la fraction dissoute 5P et colloïdale 5R avec, à chaque fois, un enrichissement en isotope lourd par rapport aux conditions non-limitantes. Par conséquent, $\delta^{44/40}Ca_{5P} > \delta^{44/40}Ca_{5R} > \delta^{44/40}Ca_{source}$. L'ensemble de ces cas de figure est synthétisé par la figure 15.

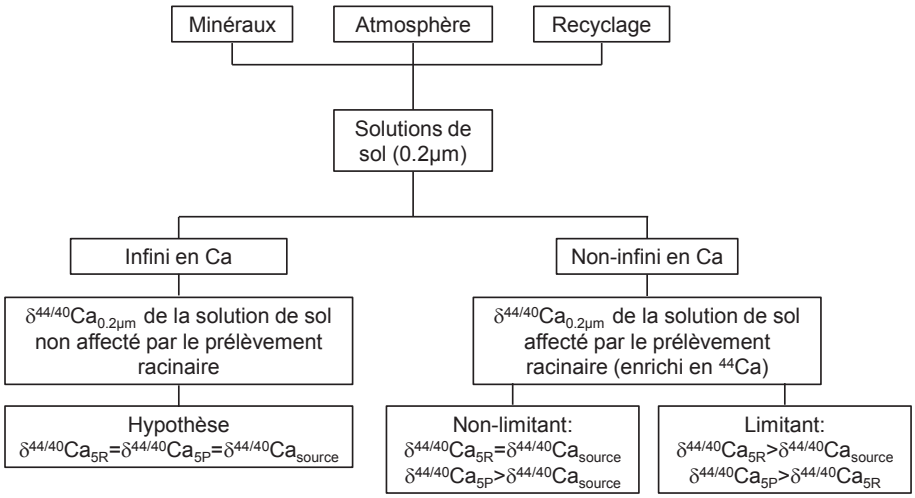

Figure 15: Schéma décrivant la variabilité de fractionnement isotopique en Ca induit par le prélèvement racinaire dans les fractions filtrées à 0.2%m, 5R et 5P en fonction de la quantité de Ca dans le réservoir du sol

6. Conclusion

Cette étude a permis d'apporter des précisions sur le fonctionnement du cycle biogéochimique du Ca dans un écosystème forestier. En effet, il a été mis en évidence que (1) le recyclage du Ca par la végétation et plus particulièrement par la dégradation de la litière est une source non négligeable de Ca, (2) le Ca se complexe avec C_{orga} dans les phases colloïdale et dissoute, (3) la phase colloïdale est un réservoir potentiel de Ca pour le prélèvement racinaire dans le sol lorsque les teneurs en Ca deviennent limitantes dans les solutions de sol; le Ca peut ainsi être libéré de la fraction colloïdale par des déplacements d'équilibre chimique sous contrôle thermodynamique, (4) les sources de Ca varient au cours du temps en fonction des conditions hydriques du sol (sécheresse ou non). Ce travail met en avant le potentiel des expérimentations d'ultra-filtrations accompagnées d'un couplage isotopique ($^{87}Sr/^{86}Sr$, $\delta^{44/40}Ca$) et confirme le contrôle biotique du fractionnement des isotopes du Ca dans des solutions de sol sous couvert forestier. Ce travail confirme également l'intérêt d'un suivi temporel des solutions de sol afin d'identifier des tendances sur le long terme et des épisodes ponctuels.

7. Références

Abel C.D.T., Sharma S.K., Mersha S.A. and Kennedy M.D., (2014). Influence of intermittent infiltration of primary effluent on removal of suspended solids, bulk organic matter, nitrogen and pathogens indicators in a simulated managed aquifer recharge system. *Ecological Engineering*, **64** 100-107.

Andrews M.G., Jacobson A.D., Lehn G.O., Horton T.W. and Craw D., (2016). Radiogenic and stable Sr isotope ratios (87Sr/86Sr, δ88/86Sr) as tracers of riverine cation sources and biogeochemical cycling in the Milford Sound region of Fiordland, New Zealand. *Geochimica et Cosmochimica Acta*, **173** 284-303.

Aubert A. (2001) Contribution de l'altération et des apports atmosphériques aux transferts de matières en milieu silicaté: traçage par le strontiulm et les Terres Rares. Cas du bassin versant du Strengbach (Vosges, France). Université Louis Pasteur, Strasbourg.

Aubert D., Stille P. and Probst A., (2001). REE fractionation during granite weathering and removal by waters and suspended loads: Sr and Nd isotopic evidence. *Geochimica et Cosmochimica Acta*, **65** 387-406.

Aubert D., Stille P., Probst A., Gauthier-Lafaye F., Pourcelot L. and Del Nero M., (2002). Characterization and migration of atmospheric REE in soils and surface waters. *Geochimica et Cosmochimica Acta*, **66** 3339-3350.

Austin A.T. and Ballaré C.L., (2010). Dual role of lignin in plant litter decomposition in terrestrial ecosystems. *Proceedings of the National Academy of Sciences of the United States of America*, **107** 4618-4622.

Bagard M.-L., Schmitt A.-D., Chabaux F., Pokrovsky O.S., Viers J., Stille P., Labolle F. and Prokushkin A.S., (2013). Biogeochemistry of stable Ca and radiogenic Sr isotopes in a larch-covered permafrost-dominated watershed of Central Siberia. *Geochimica et Cosmochimica Acta*, **114** 169-187.

Bagard M.-L., Chabaux F., Pokrovsky O.S., Viers J., Prokushkin A.S., Stille P., Rihs S., Schmitt A.-D. and Dupré B., (2011). Seasonal variability of element fluxes in two Central Siberian rivers draining high latitude permafrost dominated areas. *Geochimica et Cosmochimica Acta*, **75** 3335-3357.

Bedel L., Poszwa A., Van Der Heijden G., Legout A., Aquilina L. and Ranger J., (2016). Unexpected calcium sources in deep soil layers in low-fertility forest soils identified by strontium isotopes (Lorraine plateau, eastern France). *Geoderma*, **264, Part A** 103-116.

Bélanger N., Holmden C., Courchesne F., Côté B. and Hendershot W.H., (2012). Constraining soil mineral weathering 87Sr/86Sr for calcium apportionment studies of a deciduous forest growing on soils developed from granitoid igneous rocks. *Geoderma*, **185–186** 84-96.

Berg B., (2000). Litter decomposition and organic matter turnover in northern forest soils. *Forest Ecology and Management*, **133** 13-22.

Black J.R., Epstein E., Rains W.D., Yin Q.-Z. and Casey W.H., (2008). Magnesium-Isotope Fractionation During Plant Growth. *Environmental Science & Technology*, **42** 7831-7836.

Blum J., Hamburg S., Yanai R. and Arthur M., (2012). Determination of foliar Ca/Sr discrimination factors for six tree species and implications for Ca sources in northern hardwood forests. *Plant and Soil*, **356** 303-314.

Blum J., Dasch A., Hamburg S., Yanai R. and Arthur M., (2008). Use of foliar Ca/Sr discrimination and 87Sr/86Sr ratios to determine soil Ca sources to sugar maple foliage in a northern hardwood forest. *Biogeochemistry*, **87** 287-296.

Blum J.D., Klaue A., Nezat C.A., Driscoll C.T., Johnson C.E., Siccama T.G., Eagar C., Fahey T.J. and Likens G.E., (2002). Mycorrhizal weathering of apatite as an important calcium source in base-poor forest ecosystems. *Nature*, **417** 729-731.

Bonneau M., Dambrine E., Nys C. and Ranger J., (1991). Apports acides et cycles des cations dans les pessières du Nord-Est. Intérêt des bilans saisonniers. *Sc. du Sol*, **29** 125-145.

Brunn M., Spielvogel S., Sauer T. and Oelmann Y., (2014). Temperature and precipitation effects on δ13C depth profiles in SOM under temperate beech forests. *Geoderma*, **235–236** 146-153.

Cenki-Tok B., Chabaux F., Lemarchand D., Schmitt A.D., Pierret M.C., Viville D., Bagard M.L. and Stille P., (2009). The impact of water–rock interaction and vegetation on calcium isotope fractionation in soil- and stream waters of a small, forested catchment (the Strengbach case). *Geochimica et Cosmochimica Acta*, **73** 2215-2228.

Chadwick O.A., Derry L.A., Vitousek P.M., Huebert B.J. and Hedin L.O., (1999). Changing sources of nutrients during four million years of ecosystem development. *Nature*, **397** 491-497.

Chen Z., Ding W., Xu Y., Müller C., Rütting T., Yu H., Fan J., Zhang J. and Zhu T., (2015). Importance of heterotrophic nitrification and dissimilatory nitrate reduction to ammonium in a cropland soil: Evidences from a 15N tracing study to literature synthesis. *Soil Biology and Biochemistry*, **91** 65-75.

Clarholm M. and Skyllberg U., (2013). Translocation of metals by trees and fungi regulates pH, soil organic matter turnover and nitrogen availability in acidic forest soils. *Soil Biology and Biochemistry*, **63** 142-153.

Clarholm M., Skyllberg U. and Rosling A., (2015). Organic acid induced release of nutrients from metal-stabilized soil organic matter – The unbutton model. *Soil Biology and Biochemistry*, **84** 168-176.

Cobert F., Schmitt A.-D., Bourgeade P., Labolle F., Badot P.-M., Chabaux F. and Stille P., (2011a). Experimental identification of Ca isotopic fractionations in higher plants. *Geochimica et Cosmochimica Acta*, **75** 5467-5482.

Cobert F., Schmitt A.-D., Calvaruso C., Turpault M.-P., Lemarchand D., Collignon C., Chabaux F. and Stille P., (2011b). Biotic and abiotic experimental identification of bacterial influence on calcium isotopic signatures. *Rapid Communications in Mass Spectrometry*, **25** 2760-2768.

Crow S.E., Sulzman E.W., Rugh W.D., Bowden R.D. and Lajtha K., (2006). Isotopic analysis of respired CO2 during decomposition of separated soil organic matter pools. *Soil Biology and Biochemistry*, **38** 3279-3291.

Dahlqvist R., Benedetti M.F., Andersson K., Turner D., Larsson T., Stolpe B. and Ingri J., (2004). Association of calcium with colloidal particles and speciation of calcium in the Kalix and Amazon rivers. *Geochimica et Cosmochimica Acta*, **68** 4059-4075.

Dammshäuser A. and Croot P.L., (2012). Low colloidal associations of aluminium and titanium in surface waters of the tropical Atlantic. *Geochimica et Cosmochimica Acta*, **96** 304-318.

Dasch A., Blum J., Eagar C., Fahey T., Driscoll C. and Siccama T., (2006). The relative uptake of Ca and Sr into tree foliage using a whole-watershed calcium addition. *Biogeochemistry*, **80** 21-41.

Deniel C. and Pin C., (2001). Single-stage method for the simultaneous isolation of lead and strontium from silicate samples for isotopic measurements. *Analytica Chimica Acta*, **426** 95-103.

Dijkstra F.A., (2003). Calcium mineralization in the forest floor and surface soil beneath different tree species in the northeastern US. *Forest Ecology and Management*, **175** 185-194.

Dijkstra F.A. and Smits M.M., (2002). Tree Species Effects on Calcium Cycling: The Role of Calcium Uptake in Deep Soils. *Ecosystems*, **5** 385-398.

Ding T., Wan D., Bai R., Zhang Z., Shen Y. and Meng R., (2005). Silicon isotope abundance ratios and atomic weights of NBS-28 and other reference materials. *Geochimica et Cosmochimica Acta*, **69** 5487-5494.

Drouet T. and Herbauts J., (2008). Evaluation of the mobility and discrimination of Ca, Sr and Ba in forest ecosystems: consequence on the use of alkaline-earth element ratios as tracers of Ca. *Plant and Soil*, **302** 105-124.

Drouet T., Herbauts J., Gruber W. and Demaiffe D., (2005). Strontium isotope composition as a tracer of calcium sources in two forest ecosystems in Belgium. *Geoderma*, **126** 203-223.

Fantle M.S. and Tipper E.T., (2014). Calcium isotopes in the global biogeochemical Ca cycle: Implications for development of a Ca isotope proxy. *Earth-Science Reviews*, **129** 148-177.

Farkaš J., Déjeant A., Novák M. and Jacobsen S.B., (2011). Calcium isotope constraints on the uptake and sources of Ca2+ in a base-poor forest: A new concept of combining stable (δ44/42Ca) and radiogenic (εCa) signals. *Geochimica et Cosmochimica Acta*, **75** 7031-7046.

Francioso O., Sanchez-Cortes S., Tugnoli V., Ciavatta C., Sitti L. and Gessa C., (1996). Infrared, Raman, and Nuclear Magnetic Resonance (1H, 13C, and 31P) Spectroscopy in the Study of Fractions of Peat Humic Acids. *Appl. Spectrosc.*, **50** 1165-1174.

Gabor R.S., Eilers K., Mcknight D.M., Fierer N. and Anderson S.P., (2014). From the litter layer to the saprolite: Chemical changes in water-soluble soil organic matter and their correlation to microbial community composition. *Soil Biology and Biochemistry*, **68** 166-176.

Gangloff S., Stille P., Schmitt A.-D. and Chabaux F., (2014a). Impact of Bacterial Activity on Sr and Ca Isotopic Compositions (87Sr/86Sr and δ44/40Ca) in Soil Solutions (the StrengbachCZO). *Procedia Earth and Planetary Science*, **10** 109-113.

Gangloff S., Stille P., Schmitt A.-D. and Chabaux F., (2016). Biotic and abiotic factors controlling the chemical composition of colloidal and dissolved fractions in soil solutions and the mobility of trace elements in soils. *Geochimica et Cosmochimica Acta* reviewed.

Gangloff S., Stille P., Pierret M.-C., Weber T. and Chabaux F., (2014b). Characterization and evolution of dissolved organic matter in acidic forest soil and its impact on the mobility of major and trace elements (case of the Strengbach watershed). *Geochimica et Cosmochimica Acta*, **130** 21-41.

Ge S., Jiang Y. and Wei S., (2015). Gross Nitrification Rates and Nitrous Oxide Emissions in an Apple Orchard Soil in Northeast China. *Pedosphere*, **25** 622-630.

Hindshaw R.S., Reynolds B.C., Wiederhold J.G., Kretzschmar R. and Bourdon B., (2011). Calcium isotopes in a proglacial weathering environment: Damma glacier, Switzerland. *Geochimica et Cosmochimica Acta*, **75** 106-118.

Holmden C. and Bélanger N., (2010). Ca isotope cycling in a forested ecosystem. *Geochimica et Cosmochimica Acta*, **74** 995-1015.

Ingri J., Widerlund A., Land M., Gustafsson Ö., Andersson P. and Öhlander B., (2000). Temporal variations in the fractionation of the rare earth elements in a boreal river; the role of colloidal particles. *Chemical Geology*, **166** 23-45.

Kaiser K., Guggenberger G. and Zech W., (2001a). Isotopic fractionation of dissolved organic carbon in shallow forest soils as affected by sorption. *European Journal of Soil Science*, **52** 585-597.

Kaiser K., Guggenberger G., Haumaier L. and Zech W., (2001b). Seasonal variations in the chemical composition of dissolved organic matter in organic forest floor layer leachates of old-growth Scots pine (Pinus sylvestris L.) and European beech (Fagus sylvatica L.) stands in northeastern Bavaria, Germany. *Biogeochemistry*, **55** 103-143.

Kalbitz K., Geyer W. and Geyer S., (1999). Spectroscopic properties of dissolved humic substances - a reflection of land use history in a fen area. *Biogeochemistry*, **47** 219-238.

Kalbitz K., Schmerwitz J., Schwesig D. and Matzner E., (2003). Biodegradation of soil-derived dissolved organic matter as related to its properties. *Geoderma*, **113** 273-291.

Klotzbücher T., Kaiser K., Filley T.R. and Kalbitz K., (2013). Processes controlling the production of aromatic water-soluble organic matter during litter decomposition. *Soil Biology and Biochemistry*, **67** 133-139.

Lang S.Q., Bernasconi S. and Früh-Green G., (2012). Stable isotope analysis of organic carbon in small (μgC) samples and dissolved organic matter using a GasBench preparation device. *Rapid Communications in Mass Spectrometry*, **1** 9-16.

Likens G.E., Driscoll C.T., Buso D.C., Siccama T.G., Johnson C.E., Lovett G.M., Fahey T.J., Reiners W.A., Ryan D.F., Martin C.W. and Bailey S.W., (1998). The biogeochemistry of calcium at Hubbard Brook. *Biogeochemistry*, **41** 89-173.

Liu R. and Lead J.R., (2006). Partial validation of cross flow ultrafiltration by atomic force microscopy. *Anal Chem*, **78** 8105-8112.

Liu R.X., Lead J.R. and Zhang H., (2013). Combining cross flow ultrafiltration and diffusion gradients in thin-films approaches to determine trace metal speciation in freshwaters. *Geochimica et Cosmochimica Acta*, **109** 14-26.

Marschner H. (1995) Mineral nutrition of higher plants, second edition ed. Academic Press, London.

Pokrovsky O.S. and Schott J., (2002). Iron colloids/organic matter associated transport of major and trace elements in small boreal rivers and their estuaries (NW Russia). *Chemical Geology*, **190** 141-179.

Pokrovsky O.S., Viers J., Shirokova L.S., Shevchenko V.P., Filipov A.S. and Dupré B., (2010). Dissolved, suspended, and colloidal fluxes of organic carbon, major and trace elements in the Severnaya Dvina River and its tributary. *Chemical Geology*, **273** 136-149.

Pokrovsky O.S., Viers J., Dupré B., Chabaux F., Gaillardet J., Audry S., Prokushkin A.S., Shirokova L.S., Kirpotin S.N., Lapitsky S.A. and Shevchenko V.P., (2012). Biogeochemistry of carbon, major and trace elements in watersheds of northern Eurasia drained to the Arctic Ocean: The change of fluxes, sources and mechanisms under the climate warming prospective. *Comptes Rendus Geoscience*, **344** 663-677.

Poszwa A., Dambrine E., Pollier B. and Atteia O., (2000). A comparison between Ca and Sr cycling in forest ecosystems. *Plant and Soil*, **225** 299-310.

Poszwa A., Dambrine E., Ferry B., Pollier B. and Loubet M., (2002). Do deep tree roots provide nutrients to the tropical rainforest? *Biogeochemistry*, **60** 97-118.

Pourret O., Dia A., Davranche M., Gruau G., Henin O. and Angee M., (2007). Organo-colloidal control on major- and trace-element partitioning in shallow groundwaters: Confronting ultrafiltration and modelling. *Applied Geochemistry*, **22** 1568-1582.

Probst A., Dambrine E., Viville D. and Fritz B., (1990). Influence of Acid Atmospheric Inputs on Surface-Water Chemistry and Mineral Fluxes in a Declining Spruce Stand within a Small Granitic Catchment (Vosges Massif, France). *Journal of Hydrology*, **116** 101-124.

Probst A., El Gh'mari A., Aubert D., Fritz B. and Mcnutt R., (2000). Strontium as a tracer of weathering processes in a silicate catchment polluted by acid atmospheric inputs, Strengbach, France. *Chemical Geology*, **170** 203-219.

Prunier J. (2008) Étude du fonctionnement d'un écosystème forestier en climat tempéré, par l'apport de la géochimie élémentaire et isotopique (Sr, U-Th-Ra). Cas du bassin versant du Strengbach, Thèse. Université Louis Pasteur de Strasbourg.

Prunier J., Chabaux F., Stille P., Gangloff S., Pierret M.C., Viville D. and Aubert A., (2015). Geochemical and isotopic (Sr, U) monitoring of soil solutions from the Strengbach catchment (Vosges mountains, France): Evidence for recent weathering evolution. *Chemical Geology*, **417** 289-305.

Schlosser C. and Croot P.L., (2008). Application of cross-flow filtration for determining the solubility of iron species in open ocean seawater. *Limnology and Oceanography: Methods*, **6** 630-642.

Schmitt A.-D. and Stille P., (2005). The source of calcium in wet atmospheric deposits: Ca-Sr isotope evidence. *Geochimica et Cosmochimica Acta*, **69** 3463-3468.

Schmitt A.-D., Chabaux F. and Stille P., (2003). The calcium riverine and hydrothermal isotopic fluxes and the oceanic calcium mass balance. *Earth and Planetary Science Letters*, **213** 503-518.

Schmitt A.-D., Cobert F., Bourgeade P., Ertlen D., Labolle F., Gangloff S., Badot P.-M., Chabaux F. and Stille P., (2013). Calcium isotope fractionation during plant growth under a limited nutrient supply. *Geochimica et Cosmochimica Acta*, **110** 70-83.

Schmitt A.D., Gangloff S., Cobert F., Lemarchand D., Stille P. and Chabaux F., (2009). High performance automated ion chromatography separation for Ca isotope measurements in geological and biological samples. *Journal of Analytical Atomic Spectrometry*, **24** 1089-1097.

Schulte P., Van Geldern R., Freitag H., Karim A., Négrel P., Petelet-Giraud E., Probst A., Probst J.-L., Telmer K., Veizer J. and Barth J.a.C., (2011). Applications of stable water and carbon isotopes

in watershed research: Weathering, carbon cycling, and water balances. *Earth-Science Reviews*, **109** 20-31.

Seki O., Nakatsuka T., Shibata H. and Kawamura K., (2010). A compound-specific n-alkane δ13C and δD approach for assessing source and delivery processes of terrestrial organic matter within a forested watershed in northern Japan. *Geochimica et Cosmochimica Acta*, **74** 599-613.

Shaheen S.M., Rinklebe J., Rupp H. and Meissner R., (2014). Lysimeter trials to assess the impact of different flood–dry-cycles on the dynamics of pore water concentrations of As, Cr, Mo and V in a contaminated floodplain soil. *Geoderma*, **228–229** 5-13.

Sivry Y., Riotte J. and Dupré B., (2006). Study of exchangeable metal on colloidal humic acids and particulate matter by coupling ultrafiltration and isotopic tracers: Application to natural waters. *Journal of Geochemical Exploration*, **88** 144-147.

Stille P., Pierret M.C., Steinmann M., Chabaux F., Boutin R., Aubert D., Pourcelot L. and Morvan G., (2009). Impact of atmospheric deposition, biogeochemical cycling and water–mineral interaction on REE fractionation in acidic surface soils and soil water (the Strengbach case). *Chemical Geology*, **264** 173-186.

Stille P., Schmitt A.D., Labolle F., Pierret M.C., Gangloff S., Cobert F., Lucot E., Gueguen F., Brioschi L., Steinmann M. and Chabaux F., (2012). The suitability of annual tree growth rings as environmental archives: Evidence from Sr, Nd, Pb and Ca isotopes in spruce growth rings from the Strengbach watershed. *Comptes Rendus Geoscience*, **344** 297-311.

Ussiri D.a.N. and Johnson C.E., (2003). Characterization of organic matter in a northern hardwood forest soil by 13C NMR spectroscopy and chemical methods. *Geoderma*, **111** 123-149.

Verstraeten A., De Vos B., Neirynck J., Roskams P. and Hens M., (2014). Impact of air-borne or canopy-derived dissolved organic carbon (DOC) on forest soil solution DOC in Flanders, Belgium. *Atmospheric Environment*, **83** 155-165.

Walela C., Daniel H., Wilson B., Lockwood P., Cowie A. and Harden S., (2014). The initial lignin:nitrogen ratio of litter from above and below ground sources strongly and negatively influenced decay rates of slowly decomposing litter carbon pools. *Soil Biology and Biochemistry*, **77** 268-275.

Weishaar J.L., Aiken G.R., Bergamaschi B.A., Fram M.S., Fujii R. and Mopper K., (2003). Evaluation of Specific Ultraviolet Absorbance as an Indicator of the Chemical Composition and Reactivity of Dissolved Organic Carbon. *Environmental Science & Technology*, **37** 4702-4708.

Wiegand B.A., Chadwick O.A., Vitousek P.M. and Wooden J.L., (2005). Ca cycling and isotopic fluxes in forested ecosystems in Hawaii. *GEOPHYSICAL RESEARCH LETTERS*, **32** 1-4 L11404.

Yao S.-H., Zhang B. and Hu F., (2011). Soil biophysical controls over rice straw decomposition and sequestration in soil: The effects of drying intensity and frequency of drying and wetting cycles. *Soil Biology and Biochemistry*, **43** 590-599.

Chapitre 6

Impact of bacterial activity on Sr and Ca isotopic compositions (87Sr/86Sr and δ44/40Ca) in soil solutions (the Strengbach CZO)

Procedia Earth and Planetary Science 10 (2014) 109 – 113

Résumé

Il porte sur l'étude de mesures isotopiques effectuées sur des solutions de sol provenant du bassin versant du Strengbach (massif des Vosges, nord-est de la France), plus particulièrement de la parcelle expérimentale recouverte par des épicéas. Les échantillons ont été prélevés pendant l'hiver, le printemps et l'été 2010. Leurs compositions chimiques et isotopiques ($^{87}Sr/^{86}Sr$ et $\delta^{44/40}$ Ca) ont permis de mettre en évidence une augmentation de l'activité de certains micro-organismes et d'identifier la bio-altération de l'apatite (ou un matériel dont le parent est l'apatite) dans les solutions de sol des horizons de surface (0-10 cm de profondeur). Ainsi, les bactéries facilitent le prélèvement de Ca par la végétation. Cette étude met en évidence le potentiel des isotopes de Ca pour identifier l'activité des bactéries dans les sols.

Available online at www.sciencedirect.com

ScienceDirect

Procedia Earth and Planetary Science 10 (2014) 109–113

Procedia Earth and Planetary Science

www.elsevier.com/locate/procedia

Geochemistry of the Earth's Surface meeting, GES-10

Impact of bacterial activity on Sr and Ca isotopic compositions ($^{87}Sr/^{86}Sr$ and $\delta^{44/40}Ca$) in soil solutions (the Strengbach CZO)

Gangloff Sophie[a]1, Stille Peter[a], Schmitt Anne-Désirée[a], Chabaux François[a]

[a]*Université de Strasbourg, CNRS-UMR 7517, LHyGeS/EOST, 1 rue Blessig, F-67084 Strasbourg Cedex, France*

Abstract

This study deals with soil solutions originating from the spruce parcel of the Strengbach catchment (Vosges mountains, Northeastern France). Samples were collected during winter, spring and summer 2010. Their chemical and isotopic (87Sr/86Sr and δ44/40Ca) compositions allowed to identify micro-organism activity and bio-weathering of apatite in the soil solutions from uppermost (0-10 cm depth) soil horizons. Indeed, in presence of bacteria, any Ca isotopic fractionation due to vegetation uptake is ruled out and δ44/40Ca values reflect the signature of apatite. Thus, bacteria facilitate the Ca uptake from soil. This study highlights the potential of Ca isotopes to identify bacteria activity in soils.

Peer-review under responsibility of the Scientific Committee of GES-10.

Keywords: bio-weathering; bacteria; apatite; calcium and strontium isotopes; Strengbach.

Corresponding author. Tel.: +33 368850470; fax: +33 3688550402.
E-mail address: sgangloff@unistra.fr

Peer-review under responsibility of the Scientific Committee of GES-10.
Doi: 10.1016/j.proeps.2014.08.038

1. Introduction

Previous trace element and Sr-Nd isotope studies showed that both plants and bacteria recognize nutrient sources in soils and that bacteria allow the plants an even more important assimilation of nutrient elements (e.g. apatite) (Blum et al., 2002; Aouad et al., 2006). Calcium is an essential nutrient for plants and micro-organisms. Two recent studies, focused on different compartments of watersheds, have shown the potential of Ca isotopes to trace the impact of vegetation on soil solutions. The first was performed in the forested Strengbach catchment and showed that the uptake of vegetation impacts significantly on the Ca cycle by enriching the vegetation in the light 40Ca isotope and the soil solution in the heavy 44Ca one (Cenki-Tok et al., 2009). The second study performed in a small catchment from the Central Siberian plateau, showed the impact of the degradation of vegetation on the Ca isotopic composition of soil solutions (Bagard et al., 2013). It has also to be noted that in the Strengbach catchment an additional Ca flux into the soil solutions was proposed, associated with water-rock interactions strongly controlled by prevailing hydrologic conditions (Cenki-Tok et al., 2009). Biotic experiments realized on Scots pines in the presence of apatite and bacteria suggested that bacterial activity influences the Ca isotope compositions of soil solutions by dissolving efficiently Ca from apatite (Cobert et al., 2011). In the present study, we check a similar impact of bacteria induced apatite bio-weathering on the chemical and isotopic compositions ($^{87}Sr/^{86}Sr$ and $\delta^{44/40}Ca$) of soil solutions from the field. This bacteria induced weathering is a supplementary factor to be considered in the Ca cycle.

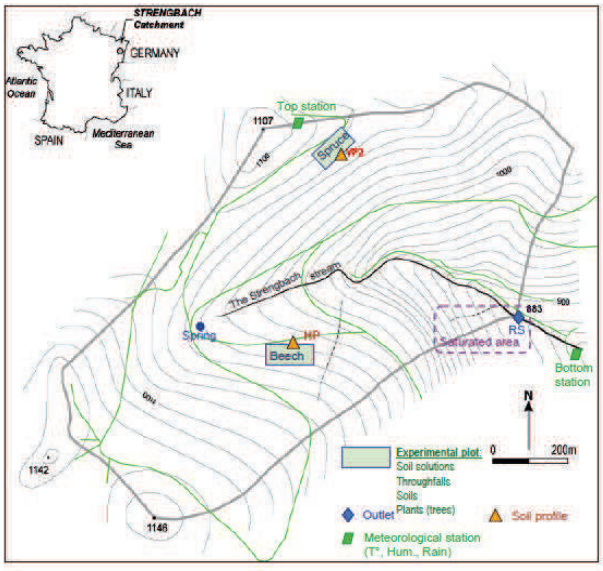

Fig. 1: Map of the Strengbach catchment showing the spruce sampling site to the north of the basin

2. Samples and sampling site

The Strengbach catchment is located in the eastern part of the Vosges mountains (Northeastern France) at altitudes ranging from 883m to 1146m. This watershed has a surface of 80 ha and is covered by spruces (80%) and beech trees (20%). It has become a completely equipped environmental observatory with permanent sampling and measuring stations (http://ohge.u-strasbg.fr). The spruce parcel (VP2) (figure 1) is equipped with lysimeter plates situated at 5, 10, 30 and 60 cm depth which permit to collect soil solutions. This study focuses on soil solutions removed in the VP2 parcel during winter 2010 (from november 2009 to march 2010), spring 2010 (from april to june) and summer 2010 (from july to september). The soil profile and the water extractable organic matter from this parcel have been previously characterized (Gangloff et al., 2014b).

3. Experiments and results

The 12 collected soil solutions have been filtered at 0.2 µm. Major and trace elements, dissolved organic carbon (DOC) and isotopic compositions ($^{87}Sr/^{86}Sr$ and $\delta^{44/40}Ca$) have been determined on aliquots of these samples. The different analytical methods are described in (Schmitt et al., 2009; Bagard et al., 2013; Gangloff et al., 2014b).

Table 1 gives Sr and Ca isotopic compositions, major and trace elements concentrations of the soil solutions collected at different depths. There are important differences between the spring and other samples for the upper soil solutions (0-10 cm). The spring samples are especially enriched in NH_4^+, Cu, Sr, Ca and P. $^{87}Sr/^{86}Sr$ and $\delta^{44/40}Ca$ ratios are also different for these spring samples. Aluminum, Si and DOC are less concentrated for the winter samples but similar for spring and summer samples.

Figure 2 shows the variations of the isotopic compositions for the different soil solutions.

Sample references	NH_4 (µmol/L)	DOC (µmol/L)	Al (µmol/L)	Si (µmol/L)	P (µmol/L)	Ca (µmol/L)	Cu (nmol/L)	Sr (nmol/L	$^{87}Sr/^{86}Sr$	$\delta^{44/40}Ca$
VP -5cm w	15	1792	19	84	20.7	17	33	16	0.7200	0.66
VP -10cm w	3	1033	21	66	9.4	12	18	14	0.7220	0.83
VP -30cm w	11	550	17	26	3.2	9	17	12	0.7216	0.88
VP -60cm w	4	203	11	46	4.7	9	4	23	0.7261	0.65
VP -5cm s	444	4075	30	159	57.1	53	297	54	0.7173	0.42
VP -10cm s	320	1850	24	74	34.5	32	173	38	0.7188	0.42
VP -30cm s	12	917	22	60	4.3	10	18	21	0.7217	0.75
VP -60cm s	19	225	1	47	0.4	11	8	26	0.7265	0.98
VP -5cm su	43	3033	36	136	18.8	22	43	21	0.7195	0.69
VP -10cm su	45	1792	24	70	18.4	14	28	16	0.7211	0.71
VP -30cm su	25	1250	19	45	5.0	14	17	20	0.7206	0.94
VP -60cm su	11	417	3	39	1.2	9	13	25	0.7247	0.71

Table1:Isotopic compositions, major and trace element concentrations of soil solutions collected at 5, 10, 30 and 60 cm depth (w: winter samples, s: spring samples, su: summer samples)

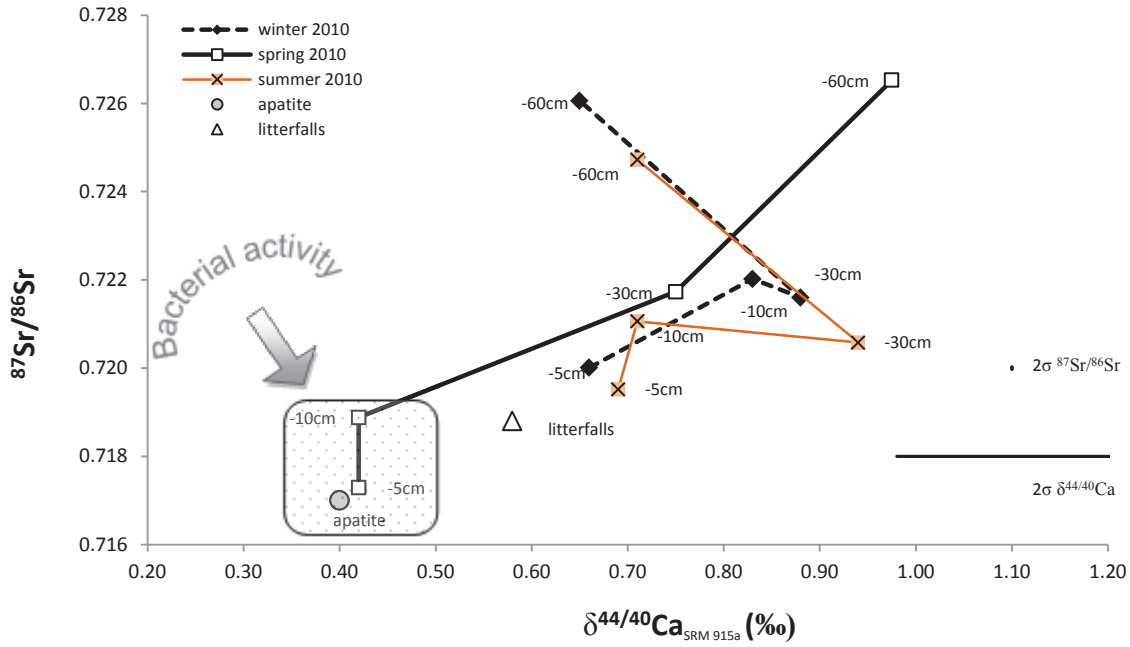

Fig.2: Variations of the isotopic compositions for the different soil solutions. The isotopic compositions of the apatite are given in (Aubert et al., 2001) for $^{87}Sr/^{86}Sr$ and in (Schmitt et al., 2003) for $\delta^{44/40}Ca$ (values are expressed against the NIST SRM 915a standard.)

4. Discussion

Winter and spring 2010 were characterized by heavy rainfall. Therefore, the upper soil horizons became strongly saturated with water. This soil moisture has fostered anoxic conditions which caused increased bacterial activity as also indicated by increasing major and trace element concentrations for the upper soil solutions collected in spring. These concentration increases are the result of ammonification and nitrification processes (444µmol/L NH_4^+ for the spring samples; 15 and 44µmol/L respectively for winter and summer samples). This increasing bacterial activity also explains the important concentration of Cu (297nmol/L) which is necessary for the enzymatic reactions. At the same time, one observes increased concentrations of Sr, Ca and P in the upper soil solutions collected

in spring. This points to bio-weathering and dissolution of apatite leaving behind Ca and P which are nutrient elements for the micro-organisms.

The Sr and Ca isotopic composition of the soil solutions collected in spring confirms the process of apatite weathering. Their $\delta^{44/40}Ca$ and $^{87}Sr/^{86}Sr$ are similar to those of apatite ($\delta^{44/40}Ca$ = 0.40‰ (Schmitt et al., 2003) and $^{87}Sr/^{86}Sr$ = 0.7161 (Aubert et al., 2001)). However, the winter and summer samples have isotopic compositions closer to those of needle litter ($\delta^{44/40}Ca$ = 0.58‰ and $^{87}Sr/^{86}Sr$ = 0.7185- this study and (Stille et al., 2009)) (figure 2).This interpretation is in accord with recently performed bio-weathering experiments using Ca isotopes, apatite and Scots pines in inoculated and bacteria-free environments which showed that bacteria influence the Ca isotopic signature of the soil solution by dissolving Ca from apatite more efficiently than Scots pines growing in a bacteria- free apatite solution (Cobert et al., 2011). From our previous laboratory experiments and this field study it results that in presence of bacterial activity any Ca isotopic fractionation can be ruled out and $\delta^{44/40}Ca$ rather reflects the signature of the main Ca contributing mineral from the soil: apatite. The presence of bacteria might indeed facilitate the access of nutrient to the plants suppressing a possible reservoir effect of the nutritive medium (e.g. it becomes non-Ca limited) (Cobert et al., 2011).

5. Conclusion

This study elucidates the impact of bacteria-induced apatite bio-weathering on chemical and isotopic compositions of soil solutions collected in the Strengbach catchment during spring 2010 compared to those collected during winter and summer 2010. The bacterial activity in soils increases the availability of Ca for the plants and contributes significantly to the Ca cycle. Consequently this bacteria-induced weathering is a supplementary factor to be considered when studying the Ca biogeochemical cycle. This study also emphasizes the potential of Ca isotopes to identify bacterial activity in soils.

6. References

1. Blum JD, Klaue A, Nezat CA, Driscoll CT, Johnson CE, Siccama TG, Eagar C, Fahey TJ, and Likens GE, Mycorrhizal weathering of apatite as an important calcium source in base-poor forest ecosystems. *Nature*, 2002; **417**(6890): p. 729-731.
2. Aouad G, Stille P, Crovisier J-L, Geoffroy VA, Meyer J-M, and Lahd-Geagea M, Influence of bacteria on lanthanide and actinide transfer from specific soil components (humus, soil minerals and vitrified municipal solid waste incinerator bottom ash) to corn plants: Sr–Nd isotope evidence. *Science of The Total Environment*, 2006; **370**(2–3): p. 545-551.
3. Cenki-Tok B, Chabaux F, Lemarchand D, Schmitt AD, Pierret MC, Viville D, Bagard ML, and Stille P, The impact of water–rock interaction and vegetation on calcium isotope fractionation in soil- and stream waters of a small, forested catchment (the Strengbach case). *Geochimica et Cosmochimica Acta*, 2009; **73**(8): p. 2215-2228.
4. Bagard M-L, Schmitt A-D, Chabaux F, Pokrovsky OS, Viers J, Stille P, Labolle F, and Prokushkin AS, Biogeochemistry of stable Ca and radiogenic Sr isotopes in a larch-covered permafrost-dominated watershed of Central Siberia. *Geochimica et Cosmochimica Acta*, 2013; **114**(0): p. 169-187.
5. Cobert F, Schmitt A-D, Calvaruso C, Turpault M-P, Lemarchand D, Collignon C, Chabaux F, and Stille P, Biotic and abiotic experimental identification of bacterial influence on calcium isotopic signatures. *Rapid Communications in Mass Spectrometry*, 2011; **25**(19): p. 2760-2768.
6. Gangloff S, Stille P, Pierret M-C, Weber T, and Chabaux F, Characterization and evolution of dissolved organic matter in acidic forest soil and its impact on the mobility of major and trace elements (case of the Strengbach watershed). *Geochimica et Cosmochimica Acta*, 2014; **130**(0): p. 21-41.
7. Schmitt AD, Gangloff S, Cobert F, Lemarchand D, Stille P, and Chabaux F, High performance automated ion chromatography separation for Ca isotope measurements in geological and biological samples. *Journal of Analytical Atomic Spectrometry*, 2009; **24**(8): p. 1089-1097.
8. Aubert D, Stille P, and Probst A, REE fractionation during granite weathering and removal by waters and suspended loads: Sr and Nd isotopic evidence. *Geochimica et Cosmochimica Acta*, 2001; **65**(3): p. 387-406.
9. Schmitt A-D, Chabaux F, and Stille P, The calcium riverine and hydrothermal isotopic fluxes and the oceanic calcium mass balance. *Earth and Planetary Science Letters*, 2003; **213**(3–4): p. 503-518.
10. Stille P, Pierret MC, Steinmann M, Chabaux F, Boutin R, Aubert D, Pourcelot L, and Morvan G, Impact of atmospheric deposition, biogeochemical cycling and water–mineral interaction on REE fractionation in acidic surface soils and soil water (the Strengbach case). *Chemical Geology*, 2009; **264**(1–4): p. 173-186.

Conclusion Générale

Le but de cette thèse était d'apporter des éléments d'information sur l'impact de la fraction colloïdale sur le transport des éléments majeurs et traces au sein des solutions de sol du bassin versant du Strengbach. Ce travail était essentiellement axé sur l'étude d'un profil de sol et des solutions de sol prélevés sur une même parcelle expérimentale sous épicéas. Les solutions de sol ont été collectées à différentes profondeurs (5, 10, 30 et 60 cm) et sur la période allant de 2009 à 2013. Ceci a permis d'étudier le système eau-sol dans sa globalité ainsi que ses variations spatiales et temporelles.

Un des constituants majeur de la fraction colloïdale est le carbone organique. C'est pourquoi les expérimentations ainsi que les chapitres de cette thèse sont souvent axés sur son étude ainsi que sur le rôle qu'il joue dans le sol. Tout d'abord, le carbone organique extrait du sol a été caractérisé par des spectres infra-rouge. Ils ont permis de montrer que sa structure moléculaire est modifiée avec la profondeur du sol avec une diminution des groupements fonctionnels polaires et une augmentation relative des moins polaires accompagnée d'une aromaticité maximale vers 30 cm de profondeur où se termine l'horizon enrichi en carbone organique. Des expérimentations complémentaires ont également mis en évidence qu'une forte proportion des groupements, type carboxylate, sont sous forme ionique en surface et que cette proportion diminue avec la profondeur. Les ultra-filtrations des solutions de sol ont permis de montrer une variabilité de structure (macromoléculaire) entre la surface et la profondeur ainsi qu'en fonction des conditions environnementales (température, saturation en eau ou non de l'espace poral du sol, activité des micro-organismes…). Des mesures isotopiques de $\delta^{13}C$ ont confirmé cette variabilité temporelle.

Ces différents changements structurels des molécules de carbone organique ont une incidence sur la complexation des cations et par conséquent sur le comportement des éléments traces. En effet, dans l'horizon du sol enrichi en carbone organique, il y a une relation entre les éléments traces et la variation des groupements fonctionnels organiques. Par exemple, Pb est fortement lié à la fonction acide carboxylique alors que Fe, V

et Cr ont plus d'affinité avec les groupements carboxy-phénoliques et phénoliques. Ainsi, une partie de l'évolution de ces cations sera fonction de l'évolution de ces fonctions organiques.

Ces changements structurels des molécules de carbone organique ont également une incidence sur les processus d'échange d'ions, et par conséquent sur la biodisponibilité des éléments nutritifs comme le calcium ou le magnésium. L'étude des fractions colloïdales et dissoutes a montré que les cations majoritaires échangés avec les molécules organiques sont H^+, Ca^{2+} et Al^{3+}. L'aluminium est plus présent dans la fraction colloïdale et le calcium dans la fraction dissoute. Une constatation importante est que Al dans la fraction colloïdale peut devenir un risque de phyto-toxique lorsqu'il passe dans la fraction dissoute pour remplacer les cations nutritifs comme Ca dans les sols appauvris.

Cette étude a permis d'apporter des précisions sur le fonctionnement du cycle biogéochimique du Ca dans un écosystème forestier. En effet, il a été mis en évidence que le recyclage du Ca par la végétation et plus particulièrement par la dégradation de la litière est une source non négligeable de Ca, que le Ca se complexe avec le carbone organique dans les phases colloïdale et dissoute, que la phase colloïdale est un réservoir potentiel de Ca pour le prélèvement racinaire dans le sol lorsque les teneurs en Ca deviennent limitantes dans les solutions de sol; le Ca peut ainsi être libéré de la fraction colloïdale par des déplacements d'équilibre chimique sous contrôle thermodynamique, que les sources de Ca varient au cours du temps en fonction des conditions hydriques du sol (sécheresse ou non). Ce travail met en avant le potentiel des expérimentations d'ultra-filtrations accompagnées d'un couplage isotopique ($^{87}Sr/^{86}Sr$, $\delta^{44/40}Ca$) et confirme le contrôle biotique du fractionnement des isotopes du Ca dans des solutions de sol sous couvert forestier.

Les Terres Rares sont souvent utilisés en tant que traceurs pour les processus d'altération. Leur comportement en phase colloïdale ainsi qu'avec les molécules organiques a donc été étudié plus en détail. Il en ressort qu'ils ont un comportement semblable à Fe, V et Cr avec une affinité pour les

groupements carboxy-phénoliques et phénoliques avec une différence de comportement entre les terres rares lourdes et les terres rares légères pour les groupements aromatiques. Ceci entraîne un fractionnement du spectre des terres rares des solutions de sol à 30cm de profondeur en raison de l'enrichissement en aromaticité observé à cette profondeur. Les solutions de sol ultra-filtrées de l'horizon organique montrent que les terres rares sont principalement enrichis dans la fraction colloïdale (5 kDa – 0,2 µm) qui contrôle leur dynamique. Dans les horizons plus profonds (60 cm), les deux fractions colloïdales et dissoutes contrôlent la dynamique des terres rares. La mobilité des terres rares par la fraction colloïdale est contrôlée par la dissolution de zircon et des minéraux de phosphate, la précipitation de minéraux secondaire, type xénotime, et l'évolution des molécules organiques dans la fraction colloïdale.

Parallèlement, cette étude a donné des informations détaillées sur les processus d'altération et de pédogenèse dans un sol acide forestier provenant du bassin versant du Strengbach. Ainsi, au cours du processus d'altération, le zircon et des minéraux de phosphates pourraient être dissous et entraîner la formation de phases minérales secondaires comme le xénotime dans des horizons du sol plus profonds. L'étude comparative du profil du sol, de ses extraits aqueux et des solutions de sol montrent que l'anomalie $(Eu^*/Eu)_{DS}$ reflète l'altération du plagioclase dans les micropores et la migration de Eu vers les macropores, l'anomalie $(Ce^*/Ce)_{DS}$ est stabilisée par le transfert d'électron de l'acide humique (aromaticité) et fournit des informations sur les conditions d'oxydo-réduction uniquement dans les horizons du sol plus profonds appauvris en acides humiques et enfin l'enrichissement en terres rares lourdes dans les solutions de sol les plus profondes résulte de la dissolution partielle des minéraux secondaires situés dans les horizons supérieurs du sol (au-dessus de 30 cm de profondeur).

Le suivi temporel des solutions de sol a mis en évidence que l'alternance des saisons sèches et humides provoque des changements importants au niveau de l'activité des micro-organismes du sol. En fonction

de leur besoin nutritif, la litière est plus ou moins dégradée. Ce stade de dégradation conditionne la nature des molécules organiques ainsi que celle des cations libérés. Ensuite, une fois dissous, les éléments majeurs et traces sont transportés par le carbone organique dans la solution du sol et sont réparties entre les fractions colloïdales et dissoutes. Les expériences d'ultra-filtration font ressortir cette répartition dans les différentes fractions et leur évolution saisonnière avec la profondeur. Elles permettent ainsi une meilleure précision dans les bilans de matières et donne des informations différentes par rapport aux solutions de sol filtrées à 0,2 µm.

Une des originalités de cette thèse est d'avoir pu affiner la composition des solutions de sol et d'étudier en parallèle le comportement des molécules organiques associé aux variations des éléments majeurs et traces. Ce travail a également montré qu'il était important de bien connaitre les conditions environnementales de l'échantillon. En effet, cela permet de connaitre les épisodes ponctuels atypiques et d'éviter de faire une généralisation d'un cas particulier. Elle confirme également l'intérêt d'un suivi temporel des solutions de sol afin d'identifier des tendances sur le long terme et de savoir reconnaitre ces épisodes ponctuels. Ceci est possible grâce à l'existence d'un site comme le bassin versant du Strengbach où de nombreux travaux ont déjà été réalisés permettant ainsi une comparaison des différentes études.

UNIVERSITÉ DE STRASBOURG

Ecole et Observatoire des Sciences de la Terre

Evaluation des mécanismes de transport des éléments traces (Pb, REE, …) et du fractionnement des rapports élémentaires et isotopiques (Ca et Sr) à l'interface eau, sol, plante.

Résumé

Ce travail est axé sur l'étude d'un profil de sol et des solutions de sol prélevés sur une parcelle expérimentale couvertes d'épicéas. Tous ces échantillons proviennent du Bassin Versant du Strengbach (Observatoire HydroGéochimique de l'Environnement – OHGE), ont été échantillonnés à différentes profondeurs (5, 10, 30 et 60 cm) et durant la période comprise entre 2009 et 2013.
Les caractérisations des extraits des sols par spectroscopie Infra-Rouge ont permis de mettre en évidence les modifications des groupements fonctionnels organiques avec la profondeur et que ces modifications ont une forte incidence sur le comportement des cations (majeurs et traces) dans le sol. Des expérimentations d'ultra-filtration ont permis d'identifier les flux colloïdaux et dissous du carbone organique ainsi que ceux des éléments majeurs et traces présents dans les solutions de sol. L'utilisation conjointe des traceurs isotopiques ($^{87}Sr/^{86}Sr$ et $\delta^{44/40}Ca$) et chimiques (Terres Rares) ont mis en évidence des processus ayant lieu aux interfaces eau-sol-plante, comme le prélèvement racinaire ou l'altération des sols.

Mots clés : Carbone et fonction organique, ultra-filtration, flux chimiques colloïdaux et dissous, géochimie isotopique, Calcium et Strontium, Terres Rares, prélèvement racinaire, activité bactérienne, altération du sol

This work is focused on the study of a profile of soil and soil solutions collected on an experimental plot covered with spruce. All these samples come from the watershed of the Strengbach (environment - OHGE Hydrogeochimique Observatory), were sampled at different depths (5, 10, 30 and 60 cm) and during the period between 2009 and 2013.
Characterizations of soil extracts by infrared spectroscopy allowed to highlight changes in the organic functional groups with depth and that these changes have a significant impact on the behaviour of the cations (major and trace) in the soil. Ultrafiltration experiments helped to identify flows of colloidal and dissolved organic carbon as well as those of the major and trace-element present in soil solutions. The joint use of isotope tracers (^{87}Sr / ^{86}Sr and $\delta^{44/40}Ca$) and chemical (Rare Earth Elements) have highlighted processes taking place at the water-soil-plant interface, as the uptake by root or soil alteration.

Key words: Organic carbon, organic functional groups, ultrafiltration, colloidal and dissolved chemical fluxes, isotope geochemistry, Calcium and Strontium, REE, uptake by root, bacterial activity, soil alteration